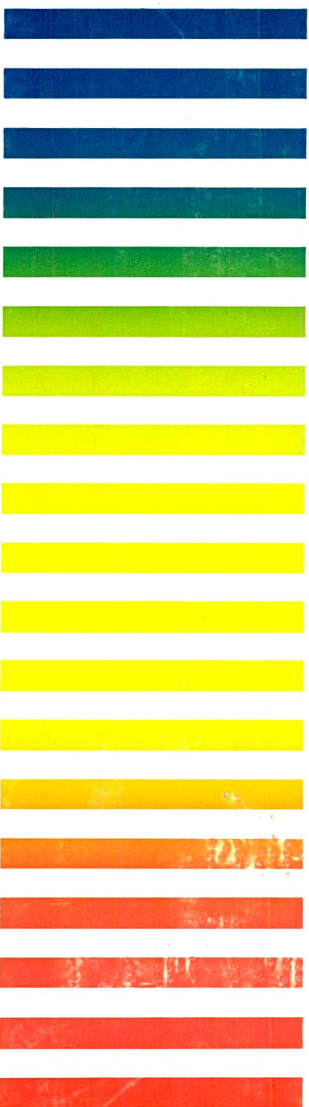




JOURNAL OF

CHROMATOGRAPHY

INTERNATIONAL JOURNAL ON CHROMATOGRAPHY, ELECTROPHORESIS AND RELATED METHODS

**EDITORS**

R. W. Giese (Boston, MA)
 J. K. Haken (Kensington, N.S.W.)
 K. Macek (Prague)
 L. R. Snyder (Orinda, CA)

EDITOR, SYMPOSIUM VOLUMES, E. Heftmann (Orinda, CA)

EDITORIAL BOARD

D. W. Armstrong (Rolla, MO)
 W. A. Aue (Halifax)
 P. Boček (Brno)
 A. A. Boulton (Saskatoon)
 P. W. Carr (Minneapolis, MN)
 N. H. C. Cooke (San Ramon, CA)
 V. A. Davankov (Moscow)
 Z. Deyl (Prague)
 S. Dilli (Kensington, N.S.W.)
 H. Engelhardt (Saarbrücken)
 F. Erni (Basle)
 M. B. Evans (Hatfield)
 J. L. Glajch (N. Billerica, MA)
 G. A. Guiochon (Knoxville, TN)
 P. R. Haddad (Kensington, N.S.W.)
 I. M. Hais (Hradec Králové)
 W. S. Hancock (San Francisco, CA)
 S. Hjertén (Uppsala)
 Cs. Horváth (New Haven, CT)
 J. F. K. Huber (Vienna)
 K.-P. Hupe (Waldbronn)
 T. W. Hutchens (Houston, TX)
 J. Janák (Brno)
 P. Jandera (Pardubice)
 B. L. Karger (Boston, MA)
 E. sz. Kováts (Lausanne)
 A. J. P. Martin (Cambridge)
 L. W. McLaughlin (Chestnut Hill, MA)
 R. P. Patience (Sunbury-on-Thames)
 J. D. Pearson (Kalamazoo, MI)
 H. Poppe (Amsterdam)
 F. E. Regnier (West Lafayette, IN)
 P. G. Righetti (Milan)
 P. Schoenmakers (Eindhoven)
 G. Schomburg (Mülheim/Ruhr)
 R. Schwarzenbach (Dübendorf)
 R. E. Shoup (West Lafayette, IN)
 A. A. Siouffi (Marseille)
 D. J. Strydom (Boston, MA)
 K. K. Unger (Mainz)
 Gy. Vigh (College Station, TX)
 J. T. Watson (East Lansing, MI)
 B. D. Westerlund (Uppsala)

EDITORS, BIBLIOGRAPHY SECTION

Z. Deyl (Prague), J. Janák (Brno), V. Schwarz (Prague), K. Macek (Prague)

ELSEVIER

Scope. The *Journal of Chromatography* publishes papers on all aspects of chromatography, electrophoresis and related methods. Contributions consist mainly of research papers dealing with chromatographic theory, instrumental development and their applications. The section *Biomedical Applications*, which is under separate editorship, deals with the following aspects: developments in and applications of chromatographic and electrophoretic techniques related to clinical diagnosis or alterations during medical treatment; screening and profiling of body fluids or tissues with special reference to metabolic disorders; results from basic medical research with direct consequences in clinical practice; drug level monitoring and pharmacokinetic studies; clinical toxicology; analytical studies in occupational medicine.

Submission of Papers. Papers in English, French and German may be submitted, in three copies. Manuscripts should be submitted to: The Editor of *Journal of Chromatography*, P.O. Box 681, 1000 AR Amsterdam, The Netherlands, or to: The Editor of *Journal of Chromatography, Biomedical Applications*, P.O. Box 681, 1000 AR Amsterdam, The Netherlands. Review articles are invited or proposed by letter to the Editors. An outline of the proposed review should first be forwarded to the Editors for preliminary discussion prior to preparation. Submission of an article is understood to imply that the article is original and unpublished and is not being considered for publication elsewhere. For copyright regulations, see below.

Subscription Orders. Subscription orders should be sent to: Elsevier Science Publishers B.V., P.O. Box 211, 1000 AE Amsterdam, The Netherlands, Tel. 5803 911, Telex 18582 ESPA NL. The *Journal of Chromatography* and the *Biomedical Applications* section can be subscribed to separately.

Publication. The *Journal of Chromatography* (incl. *Biomedical Applications*) has 37 volumes in 1990. The subscription prices for 1990 are:

J. Chromatogr. (incl. *Cum. Indexes, Vols. 451-500*) + *Biomed. Appl.* (Vols. 498-534):

Dfl. 6734.00 plus Dfl. 1036.00 (p.p.h.) (total ca. US\$ 3564.25)

J. Chromatogr. (incl. *Cum. Indexes, Vols. 451-500*) only (Vols. 498-524):

Dfl. 5616.00 plus Dfl. 756.00 (p.p.h.) (total ca. US\$ 2923.00)

Biomed. Appl. only (Vols. 525-534):

Dfl. 2080.00 plus Dfl. 280.00 (p.p.h.) (total ca. US\$ 1082.50).

Our p.p.h. (postage, package and handling) charge includes surface delivery of all issues, except to subscribers in Argentina, Australia, Brasil, Canada, China, Hong Kong, India, Israel, Malaysia, Mexico, New Zealand, Pakistan, Singapore, South Africa, South Korea, Taiwan, Thailand and the U.S.A. who receive all issues by air delivery (S.A.L. — Surface Air Lifted) at no extra cost. For Japan, air delivery requires 50% additional charge; for all other countries airmail and S.A.L. charges are available upon request. Back volumes of the *Journal of Chromatography* (Vols. 1-497) are available at Dfl. 195.00 (plus postage). Claims for missing issues will be honoured, free of charge, within three months after publication of the issue. Customers in the U.S.A. and Canada wishing information on this and other Elsevier journals, please contact Journal Information Center, Elsevier Science Publishing Co. Inc., 655 Avenue of the Americas, New York, NY 10010, Tel. (212) 633-3750.

Abstracts/Contents Lists published in Analytical Abstracts, ASCA, Biochemical Abstracts, Biological Abstracts, Chemical Abstracts, Chemical Titles, Chromatography Abstracts, Clinical Chemistry Lookout, Current Contents/Physical, Chemical & Earth Sciences, Current Contents/Life Sciences, Deep-Sea Research/Part B: Oceanographic Literature Review, Excerpta Medica, Index Medicus, Mass Spectrometry Bulletin, PASCAL-CNRS, Pharmaceutical Abstracts, Referativnyi Zhurnal, Science Citation Index and Trends in Biotechnology.

See inside back cover for Publication Schedule, Information for Authors and information on Advertisements.

All rights reserved. No part of this publication may be reproduced, stored in a retrieval system or transmitted in any form or by any means, electronic, mechanical, photocopying, recording or otherwise, without the prior written permission of the publisher, Elsevier Science Publishers B.V., P.O. Box 330, 1000 AH Amsterdam, The Netherlands.

Upon acceptance of an article by the journal, the author(s) will be asked to transfer copyright of the article to the publisher. The transfer will ensure the widest possible dissemination of information.

Submission of an article for publication entails the authors' irrevocable and exclusive authorization of the publisher to collect any sums or considerations for copying or reproduction payable by third parties (as mentioned in article 17 paragraph 2 of the Dutch Copyright Act of 1912 and the Royal Decree of June 20, 1974 (S. 351) pursuant to article 16 b of the Dutch Copyright Act of 1912) and/or to act in or out of Court in connection therewith.

Special regulations for readers in the U.S.A. This journal has been registered with the Copyright Clearance Center, Inc. Consent is given for copying of articles for personal or internal use, or for the personal use of specific clients. This consent is given on the condition that the copier pays through the Center the per-copy fee stated in the code on the first page of each article for copying beyond that permitted by Sections 107 or 108 of the U.S. Copyright Law. The appropriate fee should be forwarded with a copy of the first page of the article to the Copyright Clearance Center, Inc., 27 Congress Street, Salem, MA 01970, U.S.A. If no code appears in an article, the author has not given broad consent to copy and permission to copy must be obtained directly from the author. All articles published prior to 1990 may be copied for a per-copy fee of US\$ 2.25, also payable through the Center. This consent does not extend to other kinds of copying, such as for general distribution, resale, advertising and promotion purposes, or for creating new collective works. Special written permission must be obtained from the publisher for such copying.

No responsibility is assumed by the Publisher for any injury and/or damage to persons or property as a matter of products liability, negligence or otherwise, or from any use or operation of any methods, products, instructions or ideas contained in the materials herein. Because of rapid advances in the medical sciences, the Publisher recommends that independent verification of diagnoses and drug dosages should be made.

Although all advertising material is expected to conform to ethical (medical) standards, inclusion in this publication does not constitute a guarantee or endorsement of the quality or value of such product or of the claims made of it by its manufacturer.

This issue is printed on acid-free paper.

CONTENTS

(Abstracts/Contents Lists published in Analytical Abstracts, ASCA, Biochemical Abstracts, Biological Abstracts, Chemical Abstracts, Chemical Titles, Chromatography Abstracts, Current Contents/Physical, Chemical & Earth Sciences, Current Contents/Life Sciences, Deep Sea Research/Part B: Oceanographic Literature Review, Excerpta Medica, Index Medicus, Mass Spectrometry Bulletin, PASCAL-CNRS, Referativnyi Zhurnal and Science Citation Index)

Gas chromatographic retention indices of monoterpenes and sesquiterpenes on methyl silicone and Carbowax 20M phases (Review) by N. W. Davies (Hobart, Australia) (Received November 3rd, 1989)	1
Adsorption effect on the retention volume of hydrocarbons and dialkyl ethers in gas-liquid chromatography using a polar stationary phase and silica gel support by K. Naito, T. Sagara and S. Takei (Hitachi, Japan) (Received October 24th, 1989)	25
Improvement of activated carbon for air sampling by J. Rudling (Solna, Sweden) (Received November 10th, 1989)	33
Studies on the selectivity of porous polymers based on polyaromatic esters by B. Gawdzik (Lublin, Poland) (Received November 3rd, 1989)	41
Determination of individual hydrocarbons in automobile exhaust from gasoline-, methanol- and variable-fueled vehicles by F. Lipari (Warren, MI, U.S.A.) (Received November 7th, 1989)	51
Confirmation and application of transmission near infrared absorption technique for absolute quantitation of functional groups on silica gel by S. G. Bush and J. W. Jorgenson (Chapel Hill, NC, U.S.A.) (Received October 6th, 1989)	69
Preparative affinity chromatography of proteins. Influence of the physical properties of the base matrix by S. R. Narayanan, S. Knochs, Jr. and L. J. Crane (Phillipsburg, NJ, U.S.A.) (Received October 31st, 1989)	93
Large-scale purification of factor VIII by affinity chromatography: optimization of process parameters by M. P. W. M. te Booy, A. Faber, E. de Jonge and E. P. Wolterink (Amsterdam, The Netherlands), W. Riethorst, T. Beugeling and A. Bantjes (Enschede, The Netherlands) and J. Over and B. W. König (Amsterdam, The Netherlands) (Received October 27th, 1989)	103
Reversed-phase high-performance liquid chromatographic separation of the enantiomers of N-[4,4-di(3-methylthien-2-yl)-but-3-enyl] nipecotic acid on a Pirkle-type phenylglycine stationary phase by A. M. Rustum and L. Gutierrez (North-Chicago, IL, U.S.A.) (Received November 22nd, 1989)	115
Evaluation of refractive index artifacts in liquid chromatographic absorbance detection. Extension to non-ideal injection and gradient elution by C. E. Evans and V. L. McGuffin (East Lansing, MI, U.S.A.) (Received November 23rd, 1989)	127
Post-column adjustment of conditions for peroxyoxalate chemiluminescence detection for high-performance liquid chromatography by N. Hanaoka (Lawrence, KS, U.S.A.) (Received October 17th, 1989)	155
Development of an automated high-performance liquid chromatographic method for the on-line pre-concentration and determination of trace concentrations of pesticides in drinking water by C. H. Marvin and I. D. Brindle (St. Catharines, Canada), C. D. Hall (Rexdale, Canada) and M. Chiba (Vineland Station, Canada) (Received November 8th, 1989)	167

(Continued overleaf)

Contents (continued)

High-performance liquid chromatographic determination of selected amino acids in rat brain by precolumn derivatization with phenylisothiocyanate by S. Gunawan, N. Y. Walton and D. M. Treiman (Los Angeles, CA, U.S.A.) (Received October 4th, 1989)	177
Studies on the uptake of N-methylisoquinolinium ion into rat striatal slices using high-performance liquid chromatography with fluorimetric detection by Y. Hirata and M. Minami (Tokyo, Japan) and M. Naoi and T. Nagatsu (Nagoya, Japan) (Received August 22nd, 1989)	189
Chromatographic purification of glucose-6-phosphate dehydrogenase and lactate dehydrogenase from <i>Leuconostoc mesenteroides</i> by Z. Glatz, J. Tomandl, O. Janiczek and A. Marek (Brno, Czechoslovakia) (Received November 2nd, 1989)	197
High-performance liquid chromatography of levomepromazine (methotrimeprazine) and its main metabolites by T. Loennechen and S. G. Dahl (Tromsø, Norway) (Received October 16th, 1989)	205
High-performance liquid chromatography of clindamycin and clindamycin phosphate with electrochemical detection by A. Hornedo-Nuñez, T. A. Getek and W. A. Korfmacher (Jefferson, AR, U.S.A.) and F. Simenthal (Washington, DC, U.S.A.) (Received November 28th, 1989)	217
High-pH ion-exchange separation and electrochemical detection of alditols, carbohydrates and acidic sugars by S. V. Prabhu and R. P. Baldwin (Louisville, KY, U.S.A.) (Received November 14th, 1989)	227
Determination of iron(III) ion using ion chromatography with electrochemical detection and its application to the assay of the ferroxidase activity of ceruloplasmin by N. Kawasaki, A. Ishigami, T. Tanimoto and A. Tanaka (Tokyo, Japan) (Received October 2nd, 1989)	237
Feasibility of capillary zone electrophoresis with suppression of electroosmotic flow in completely closed systems by Th. P. E. M. Verheggen, A. C. Schoots and F. M. Everaerts (Eindhoven, The Netherlands) (Received October 31st, 1989)	245
<i>Notes</i>	
Enantiomer separation of chiral barbiturates and of α -lipoic acid by capillary gas chromatography with modified cyclodextrins as chiral stationary phases by W. A. König, S. Lutz and P. Evers (Hamburg, F.R.G.) and J. Knabe (Saarbrücken, F.R.G.) (Received October 26th, 1989)	256
Capillary gas chromatographic determination of sulphadimidine in pork tissues by S. Kmošák and M. Dvořák (Jílové near Prague, Czechoslovakia) (Received October 27th, 1989)	260
Direct liquid chromatographic separation of enantiomeric diastereomeric terpenic alcohols as β -cyclodextrin inclusion complexes by A. Italia, M. Schiavi and P. Ventura (Piacenza, Italy) (Received October 26th, 1989)	266
Immobilized mucin: an affinity matrix for the isolation of winged bean acidic and basic lectins by S. Y. Sawhney and S. V. Bhide (Pune, India) (Received October 26th, 1989)	272
Purification of mammalian tyrosyl-tRNA synthetase by high-performance liquid chromatography by A. D. Wolfson, Yu. A. Motorin, T. I. Ribkinska and S. F. Beresten (Moscow, U.S.S.R.) (Received September 12th, 1989)	277

High-performance liquid chromatographic determination of alterporriol D and E in fermentation of <i>Alternaria porri</i> (Ellis) Ciferri by R. Suemitsu, K. Horiuchi, K. Ohnishi and M. Kubota (Kyoto, Japan) (Received October 20th, 1989)	282
Analysis of peramine in fungal endophyte-infected grasses by reversed-phase thin-layer chromato- graphy by F. F. Fannin, L. P. Bush and M. R. Siegel (Lexington, KY, U.S.A.) and D. D. Rowan (Palmerston North, New Zealand) (Received November 28th, 1989)	288

*
* In articles with more than one author, the name of the author to whom correspondence should be addressed is indicated in the *
* article heading by a 6-pointed asterisk (*). *
*

Announcing a new journal!

Vibrational Spectroscopy

—Section of *Analytica Chimica Acta*

AN INTERNATIONAL JOURNAL DEVOTED TO APPLICATIONS OF
INFRARED AND RAMAN SPECTROSCOPY

Editors:

J.G. Grasselli, *Dept. of Chemistry,
Ohio University, Athens, OH, USA*

J.H. van der Maas, *Dept. of Analytical
Chemistry, University of Utrecht, The
Netherlands*

Vibrational Spectroscopy is a section of **Analytica Chimica Acta** which, while forming part of a subscription to the latter, is also available separately. Providing a vehicle for the publication of original research in vibrational spectroscopy, it will cover infrared, near infrared and Raman spectroscopy and will publish papers dealing with developments in applications, theory, techniques and instrumentation.

The journal will serve a useful role in bringing together the papers published on vibrational spectroscopy which are currently scattered throughout the literature. It will thus provide its readership with a concise picture of the "state of the art" of the field on a regular basis. In order to achieve this goal the journal will publish review articles, news, and book reviews, as well as original research papers and short communications.

Subscription Information:

1990: Volume 1 (4 issues)
US\$ 164.00 / Dfl. 328.00 incl. postage
ISSN 0924-2031

Topics covered will include:

- Sampling techniques - including attenuated total reflection, diffuse and specular reflection, reflection-absorption, and photoacoustic spectroscopy
- Vibrational spectroscopy coupled with separation techniques
- Instrumentation (Fourier transform, conventional and laser based)
- Data manipulation
- Expert systems for identification and structure elucidation
- Spectra-structure correlation and group frequencies

Application areas will include:

- Analytical chemistry
- Bio-organic and bio-inorganic chemistry
- Catalysis
- Environmental science
- Industrial chemistry
- Inorganic chemistry
- Materials science
- Organic chemistry
- Physical chemistry
- Polymer science
- Process control
- Specialized problem solving

*A free sample copy is
available on request from the
publisher.*

Elsevier Science Publishers

P.O. Box 211, 1000 AE Amsterdam, The Netherlands.
P.O. Box 882, Madison Square Station, New York, NY 10159, USA.

JOURNAL OF CHROMATOGRAPHY

VOL. 503 (1990)

JOURNAL *of* CHROMATOGRAPHY

INTERNATIONAL JOURNAL ON CHROMATOGRAPHY,
ELECTROPHORESIS AND RELATED METHODS

EDITORS

R. W. GIESE (Boston, MA), J. K. HAKEN (Kensington, N.S.W.), K. MACEK (Prague),
L. R. SNYDER (Orinda, CA)

EDITOR, SYMPOSIUM VOLUMES

E. HEFTMANN (Orinda, CA)

EDITORIAL BOARD

D. W. Armstrong (Rolla, MO), W. A. Aue (Halifax), P. Boček (Brno), A. A. Boulton (Saskatoon), P. W. Carr (Minneapolis, MN), N. H. C. Cooke (San Ramon, CA), V. A. Davankov (Moscow), Z. Deyl (Prague), S. Dilli (Kensington, N.S.W.), H. Engelhardt (Saarbrücken), F. Erni (Basle), M. B. Evans (Hatfield), J. L. Glajch (N. Billerica, MA), G. A. Guiochon (Knoxville, TN), P. R. Haddad (Kensington, N.S.W.), I. M. Hais (Hradec Králové), W. S. Hancock (San Francisco, CA), S. Hjertén (Uppsala), Cs. Horváth (New Haven, CT), J. F. K. Huber (Vienna), K.-P. Hupe (Waldbronn), T. W. Hutchens (Houston, TX), J. Janák (Brno), P. Jandera (Pardubice), B. L. Karger (Boston, MA), E. sz. Kováts (Lausanne), A. J. P. Martin (Cambridge), L. W. McLaughlin (Chestnut Hill, MA), R. P. Patience (Sunbury-on-Thames), J. D. Pearson (Kalamazoo, MI), H. Poppe (Amsterdam), F. E. Regnier (West Lafayette, IN), P. G. Righetti (Milan), P. Schoenmakers (Eindhoven), G. Schomburg (Mülheim/Ruhr), R. Schwarzenbach (Düben-dorf), R. E. Shoup (West Lafayette, IN), A. M. Siouffi (Marseille), D. J. Strydom (Boston, MA), K. K. Unger (Mainz), Gy. Vigh (College Station, TX), J. T. Watson (East Lansing, MI), B. D. Westerlund (Uppsala)

EDITORS, BIBLIOGRAPHY SECTION

Z. Deyl (Prague), J. Janák (Brno), V. Schwarz (Prague), K. Macek (Prague)



ELSEVIER
AMSTERDAM — OXFORD — NEW YORK — TOKYO

J. Chromatogr., Vol. 503 (1990)

All rights reserved. No part of this publication may be reproduced, stored in a retrieval system or transmitted in any form or by any means, electronic, mechanical, photocopying, recording or otherwise, without the prior written permission of the publisher, Elsevier Science Publishers B.V., P.O. Box 330, 1000 AH Amsterdam, The Netherlands.

Upon acceptance of an article by the journal, the author(s) will be asked to transfer copyright of the article to the publisher. The transfer will ensure the widest possible dissemination of information.

Submission of an article for publication entails the authors' irrevocable and exclusive authorization of the publisher to collect any sums or considerations for copying or reproduction payable by third parties (as mentioned in article 17 paragraph 2 of the Dutch Copyright Act of 1912 and the Royal Decree of June 20, 1974 (S. 351) pursuant to article 16 b of the Dutch Copyright Act of 1912) and/or to act in or out of Court in connection therewith.

Special regulations for readers in the U.S.A. This journal has been registered with the Copyright Clearance Center, Inc. Consent is given for copying of articles for personal or internal use, or for the personal use of specific clients. This consent is given on the condition that the copier pays through the Center the per-copy fee stated in the code on the first page of each article for copying beyond that permitted by Sections 107 or 108 of the U.S. Copyright Law. The appropriate fee should be forwarded with a copy of the first page of the article to the Copyright Clearance Center, Inc., 27 Congress Street, Salem, MA 01970, U.S.A. If no code appears in an article, the author has not given broad consent to copy and permission to copy must be obtained directly from the author. All articles published prior to 1980 may be copied for a per-copy fee of US\$ 2.25, also payable through the Center. This consent does not extend to other kinds of copying, such as for general distribution, resale, advertising and promotion purposes, or for creating new collective works. Special written permission must be obtained from the publisher for such copying.

No responsibility is assumed by the Publisher for any injury and/or damage to persons or property as a matter of products liability, negligence or otherwise, or from any use or operation of any methods, products, instructions or ideas contained in the materials herein. Because of rapid advances in the medical sciences, the Publisher recommends that independent verification of diagnoses and drug dosages should be made.

Although all advertising material is expected to conform to ethical (medical) standards, inclusion in this publication does not constitute a guarantee or endorsement of the quality or value of such product or of the claims made of it by its manufacturer.

This issue is printed on acid-free paper.

Review

Gas chromatographic retention indices of monoterpenes and sesquiterpenes on methyl silicone and Carbowax 20M phases

N. W. DAVIES

Central Science Laboratory, University of Tasmania P.O. Box 252C, Hobart, Tasmania 7001 (Australia)

(Received November 3rd, 1989)

CONTENTS

1. Introduction	1
2. Kováts retention indices	2
3. Acknowledgements	23
4. Summary	23
References	23

INTRODUCTION

The separation and identification of monoterpenes and sesquiterpenes in plant essential oils and other natural and synthetic sources relies heavily on gas chromatography. In some cases gas chromatography may be the sole means of identification, in which case at least two columns of substantially different polarity are required for any confidence in assignments based on direct comparison of retention times with standards or precise knowledge of Kováts' retention indices¹. Even where combined gas chromatography–mass spectrometry is used for the analysis, assignments often cannot be made on the basis of mass spectrometric data only. As has been noted by Jennings and Shibamoto², many terpenes have essentially identical mass spectra. This can be due to the initial similarity of structures, or due to various fragmentations and rearrangements after ionization. Hence some knowledge of retention characteristics is often required to complement mass spectral data.

Much of the relevant literature is concerned with retention data on the many different types of stationary phase that have been used for terpene separations. However, most work now is carried out on capillary columns with “standard” dimethyl polysiloxane (methyl silicone) non-polar and Carbowax 20M polar phases. Indices on these phases have been reported in the literature over many years, but no single source to date has provided a comprehensive summary. Jennings and Shibamoto² have published a substantial set of retention indices for flavour and fragrance compounds on these phases, including some 150 terpenes. Andersen and

co-workers³⁻⁸ have provided a significant amount of information on sesquiterpene hydrocarbons. A general discussion on the use of retention indices in essential oil analyses has been presented by Shibamoto⁹.

The following tables list Kováts' retention indices for some 400 monoterpenes and sesquiterpenes (including some hydrogenation products) on either or both of these two types of stationary phase from various literature sources. Carbowax 20M (CW20M) phases include DB-Wax, BP20, PEG 20M and HP20, while methyl silicone phases include SE-30, SF-96, OV-1, OV-101, BP1, CPSIL5CB, SP2100, DB1 and HP1. There will be slight differences between the McReynold's constants on these various "equivalent" phases. The age of a column and amount of use it has had also have a slight influence on polarity of the liquid phase.

The dependence of retention index on temperature has been extensively described, including specific reference to terpenes¹⁰⁻¹³. In the temperature programmed mode variables such as carrier gas flow-rate and programme rate affect the measurement, since they determine the temperature range that the sample is exposed to prior to elution. Several articles have described the relationships between isothermal and temperature programmed retention indices¹⁴⁻¹⁸.

Temperature has a relatively small effect on Kováts' indices of terpenes on methyl silicone phases, but can have quite marked effects on the indices on CW20M. Differences of over 50 units can readily occur in indices determined under widely different conditions on CW20M. Multiple entries occur in the tables for many compounds to enable comparisons between different references and to give an indication of the dependence of the retention index on temperature. Some indices have been specifically excluded from the tables where there is a clear discrepancy between different sources.

This summary is primarily intended as a guide to aid the analysis of essential oils and related natural and synthetic products by gas chromatography combined with mass spectrometry or other spectroscopic detection. Data on the majority of commonly occurring monoterpenes and sesquiterpenes are listed here, as well as data on some that are relatively obscure. The tables are listed in alphabetical order, and also in order of reported Kováts' indices on CW20M and methyl silicone phases. These naturally do not represent elution sequences since the data include indices obtained under various isothermal and temperature programmed conditions, as well as multiple entries. Where possible generally accepted common names have been used. Isomer identification symbols (α , β , γ , δ , ϵ , *cis*, *trans*, *p*, *epi*, etc.) have been added at the end of the parent compound name.

2. KOVÁTS' RETENTION INDICES

The Kováts' retention indices are listed in Tables 1-3.

TABLE I

ALPHABETICAL LIST OF REPORTED KOVÁTS' INDICES OF MONOTERPENES AND SESQUITERPENES ON CW20M AND METHYL SILICONE PHASES

I = Kováts' index; *T* = isothermal temperature (°C) at which the index was determined, or "prog" if the index was determined using temperature programming.

Compound	CW20M			Methyl silicone		
	<i>I</i>	<i>T</i>	Ref.	<i>I</i>	<i>T</i>	Ref.
Aequilobene	1702	150	4	1483	170	4
Agarofuran α -	1907	prog	19			
Alaskene α -	1763	165	5			
Alaskene β -	1738	165	5			
Alloaromadendrene	1660	130	20	1475	150	20
	1662	prog	2	1478	prog	2
	1683	prog	21 ^a			
Allo-ocimene <i>cis</i> -	1373	70	13	1132	110	13
Allo-ocimene <i>trans</i> -	1392	70	13	1120	110	13
Amorphene α -	1691	prog	22	1451	prog	22
	1724	165	3	1492	170	3
Anastreptene	1568	150	4	1391	170	4
Aromadendrene	1650	prog	21 ^a			
Ascaridole				1278	110	23
Ascaridole epoxide				1215	110	23
Barbatene α -	1627	150	4	1440	170	4
Barbatene β -	1690	150	4	1473	170	4
Bergamotene α -	1590	prog	24	1436	prog	24
Bergamotene <i>trans</i> - β -	1586	prog	22	1427	prog	22
Bicycloelemene	1482	prog	24			
Bicyclogermacrene	1744	prog	22	1490	prog	22
	1738	130	20			
	1768	prog	21 ^a			
Bisabolane a	1492	130	25	1448	150	25
Bisabolane b	1510	130	25	1458	150	25
Bisabolene α -	1766	165	3	1505	170	3
Bisabolene <i>cis</i> - α -	1740	prog	22	1496	prog	22
Bisabolene β -	1745	165	3	1496	130	3
Bisabolol α -	2022	160	26	1595	175	26
Bisabolol β -				1666	175	27
Borneol	1698	prog	2	1164	prog	2
	1735	prog	21 ^a	1154	110	23
				1177	175	27
Bornyl acetate	1599	135	28	1278	135	28
	1615	150	29			
Bornyl benzoate				1749	prog	2
Bornyl butyrate	1760	prog	2	1473	prog	2
Bornyl formate	1610	prog	2	1239	prog	2
Bornyl isopentanoate	1774	prog	2	1512	prog	2
Bourbonene β -	1586	165	3	1386	130	3
	1546	prog	2	1406	prog	2
	1526	prog	22			
Bulnesene α -	1729	prog	22	1502	prog	22
Cadalene	2203	prog	30	1646	prog	22
Cadina-1,4-diene	1786	prog	22	1518	prog	22

(Continued on p. 4)

TABLE 1 (continued)

Compound	CW20M			Methyl silicone		
	<i>I</i>	<i>T</i>	Ref.	<i>I</i>	<i>T</i>	Ref.
Cadinene δ -	1784	165	3	1504	130	3
	1761	prog	2	1524	prog	2
	1785	prog	21 ^a			
Cadinene γ -	1792	165	3	1507	130	3
	1766	prog	2	1227	prog	2
Cadinol α -	2224	prog	24			
Cadinol δ -	2150	prog	31			
Cadinol T-	2136	prog	31			
Calacorene α -	1926	165	6			
	1916	prog	22			
Calamenene	1837	prog	22	1502	prog	22
	1839	150	4	1524	170	4
	1842	prog	2	1518	prog	2
Camphane	1021	65	32	953	100	32
Camphene	1066	75	5	952	100	5
	1078	75	28	956	100	28
	1083	prog	2	954	prog	2
Camphor	1518	prog	2	1136	prog	2
				1126	110	23
Carane <i>cis</i> -	1064	65	32	986	100	32
Carene 3-	1141	75	5	1009	100	5
	1156	75	28	1013	100	28
Carvacrol	2159	prog	2	1297	prog	2
Carveol <i>cis</i> -	1820	prog	2	1215	120	23
				1222	prog	2
Carveol <i>trans</i> -	1790	prog	2	1209	prog	2
				1200	120	23
Carveyl acetate <i>cis</i> -	1795	150	29			
Carveyl acetate <i>trans</i> -	1759	150	29			
Carvomenthone				1181	110	23
Carvomenthyl acetate	1641	150	29			
Carvone	1715	prog	2	1228	prog	2
				1223	125	23
Carvone oxide	1805	prog	2	1261	prog	2
Carvyl propionate	1833	prog	2	1440	prog	2
Caryolan-1-ol	2019	prog	31			
Caryophyllane <i>a</i>	1522	130	25	1425	150	25
Caryophyllane <i>b</i>	1533	130	25	1432	150	25
Caryophyllane <i>c</i>	1555	130	25	1450	150	25
Caryophyllane <i>d</i>	1562	130	25	1450	150	25
Caryophyllene	1617	prog	2	1428	prog	2
	1618	130	20	1436	150	20
	1655	165	3	1417	130	3
Caryophyllene alcohol	2033	prog	31	1559	prog	24
Caryophyllene oxide	2000	prog	24	1576	prog	24
	1966	prog	31			
Cedrane 8 β H-	1617	130	25	1458	150	25
Cedrane 8 α H-	1627	130	25	1465	150	25
Cedrene epoxide α -	1961	prog	2	1585	prog	2
Cedrene α -	1640	165	3	1414	130	3
	1578	prog	22	1411	prog	22
	1600	prog	2	1436	prog	2

TABLE 1 (continued)

Compound	CW20M			Methyl silicone		
	I	T	Ref.	I	T	Ref.
Cedrene β -	1670	165	3	1421	130	3
	1633	prog	2	1446	prog	2
	1605	prog	22			
Cedrol	2100	prog	2	1609	prog	2
				1616	175	27
Chamigrene α -	1765	150	4	1523	170	4
Chamigrene β -	1737	150	4	1550	170	4
Chrysanthenone				1100	100	23
Cineole 1,4-	1185	prog	2	1010	prog	2
				1000	80	23
Cineole 1,8-	1223	70	20	1025	100	20
	1228	prog	2	1017	prog	2
Citronellal	1465	prog	2	1137	prog	2
	1491	135	28	1143	135	28
				1146	160	33
Citronellic acid				1300	125	23
Citronellol β -	1722	prog	2	1215	prog	2
	1765	150	34	1216	100	23
				1224	175	27
Citronellol α -	1760	150	34			
Citronellyl acetate	1645	prog	2	1335	prog	2
	1662	135	28	1335	135	28
	1671	150	29	1335	140	23
Citronellyl butyrate	1786	prog	2	1511	prog	2
	1811	150	29			
Citronellyl ethyl acetal	1626	prog	2	1423	prog	2
Citronellyl formate	1600	prog	2	1261	prog	2
	1638	150	29			
Citronellyl isobutyrate	1705	prog	2	1469	prog	2
	1739	150	29			
Citronellyl pentanoate	1880	prog	2	1608	prog	2
Citronellyl propionate	1700	prog	2	1427	prog	2
	1738	150	29			
Clovane	1621	175	35			
Clovene	1601	175	35			
Copaene α -	1551	165	3	1378	130	3
	1493	prog	22	1369	prog	22
	1519	prog	2	1398	prog	2
Copaene β -	1626	prog	2	1445	prog	2
Cubebene α -	1481	130	20	1362	150	20
	1458	prog	22	1381	prog	22
Cubebene β -	1560	130	20	1400	150	20
	1541	prog	22	1381	prog	22
Cubenol <i>epi</i> -	2037	prog	30			
Cuparene	1811	130	20	1506	150	20
	1838	150	4	1516	170	4
	1831	prog	22			
Curcumene α - (ar-)	1777	prog	22			
	1787	165	3	1475	130	3
Curcumene β -	1756	165	3	1510	170	3

(Continued on p. 6)

TABLE 1 (continued)

Compound	CW20M			Methyl silicone		
	I	T	Ref.	I	T	Ref.
Cyclocitral α -				1100	110	23
Cyclocitral β -				1200	125	23
Cyclosativene	1549	165	3	1400	170	3
Cymene p -	1250	75	5	1016	100	5
	1272	prog	2	1020	prog	2
	1275	70	20	1018	100	20
Cymene-7-ol p -				1270	115	23
Cymene-8-ol p -	1846	prog	24	1167	115	23
Cymenene				1277	100	23
Cyperene	1606	165	3	1398	130	3
	1535	prog	22	1398	prog	22
Damascenone	1801	prog	31			
Dihydrocurcumene	1696	130	25	1448	150	25
Dihydroagarofuran β -	1737	prog	19			
Dihydrocarveol	1713	prog	2	1188	prog	2
Dihydrocarvone	1600	prog	2	1183	prog	2
Dihydrocarvyl acetate	1670	prog	2	1319	prog	2
	1700	150	29			
Dihydrogeraniol	1759	150	34			
Dihydrohumulene	1655	175	35			
Dihydrolinalool 1,2-	1512	prog	2	1122	prog	2
	1537	150	34			
Dihydrolinalool 6,7-	1449	150	34			
Dihydromyrcenol 6,10-	1438	prog	2	1063	prog	2
	1473	150	34	1056	80	23
Dihydromyrcenyl acetate	1431	prog	2	1202	prog	2
Dihydroneerol	1725	150	34			
Dihydroterpinyl acetate	1561	prog	2	1282	prog	2
Dimethyl-1,6-octadiene 3,7-				946	90	23
Dimethyloctane 2,6-	922	65	32	938	100	32
Dimethyl-2-octene 2,6-				966	80	23
Drimenol	2525	prog	19			
Elemene	1460	130	25	1403	150	25
Elemene β -	1608	130	20	1400	150	20
	1591	prog	22			
Elemene δ -	1469	prog	22	1381	prog	22
Elemene γ -	1642	prog	22	1425	prog	22
Elemol	2078	prog	24	1540	prog	24
Eudesmane 4 α H,5 α H-	1636	130	25	1497	150	25
Eudesmane 4 β H,5 α H-	1582	130	25	1405	150	25
Eudesmol α -	2237	prog	19			
	2249	prog	21 ^a			
Eudesmol β -	2248	prog	19			
	2258	prog	21 ^a			
Eudesmol γ -	2182	prog	19			
Eudesmol 7- <i>epi</i> - α -	2244	prog	19			
Eudesmol 10- <i>epi</i> - γ -	2121	prog	19			
Farnesene <i>cis,cis</i> - α -	1697	prog	22			
Farnesene <i>cis,trans</i> - α -	1727	prog	22			
Farnesene <i>trans,cis</i> - α -	1722	prog	22			

TABLE I (continued)

Compound	CW20M			Methyl silicone		
	I	T	Ref.	I	T	Ref.
Farnesene <i>trans,trans</i> - α -	1756	130	20	1501	150	20
	1735	prog	22	1494	prog	22
Farnesene <i>cis</i> - β -	1636	prog	22			
Farnesene <i>trans</i> - β -	1671	130	20	1426	150	20
	1668	165	3	1449	170	4
	1668	prog	22	1448	prog	36
Farnesol <i>trans,trans</i> -				1745	175	27
Farnesyl acetate	2225	200	28	1787	200	28
Fenchene α -	1071	70	13	957	110	13
Fenchene β -	1057	70	13	949	110	13
Fenchol	1574	prog	2	1110	prog	2
Fenchone	1580	135	28	1125	135	28
	1410	prog	2	1080	prog	2
				1077	105	23
Fenchyl acetate	1473	prog	2	1220	prog	2
Geranial	1730	prog	2	1252	prog	2
				1260	120	23
Geranic acid				1347	140	23
Geraniol	1842	150	34	1234	175	27
	1797	prog	2	1243	prog	2
				1237	120	23
Geranyl acetate	1754	135	28	1363	135	28
Geranyl butyrate	1872	prog	2	1532	prog	2
	1904	150	29			
Geranyl formate	1684	prog	2	1282	prog	2
	1717	150	29			
Geranyl isobutyrate	1795	prog	2	1493	prog	2
	1821	150	29			
Geranyl isopentanoate	1895	prog	2	1593	prog	2
Geranyl pentanoate	1960	prog	2	1632	prog	2
Geranyl propionate	1834	150	29			
Germacrane <i>b</i>	1572	130	25	1477	150	25
Germacrane <i>c</i>	1585	130	25	1482	150	25
Germacrane <i>d</i>	1593	130	25	1489	150	25
Germacrene D	1712	prog	22	1468	prog	22
	1718	130	20	1488	150	20
Globulol	2104	prog	21 ^a			
Grandisol				1200	110	23
Guaierie α -	1651	prog	22	1454	prog	22
Guaierie β -	1667	prog	22	1482	prog	22
Guaierie δ -	1729	prog	22	1502	prog	22
Gurjunene α -	1591	165	3	1413	130	3
	1529	prog	22	1400	prog	22
Gurjunene β - (calarene)	1656	165	3	1435	130	3
	1593	prog	22			
Helmiscapene α -	1683	150	4	1467	170	4
Helmiscapene β -	1686	150	4	1466	170	4
Himachalene ar-	1873	150	4	1542	170	4
Himachalene α -	1704	165	3	1444	130	3
	1649	prog	22	1442	prog	22
Himachalene β -	1736	150	4	1517	170	4
	1718	prog	22	1494	prog	22

(Continued on p. 8)

TABLE 1 (continued)

Compound	CW20M			Methyl silicone		
	I	T	Ref.	I	T	Ref.
Himachalene γ -	1723	150	4	1499	170	4
Hop ether	1360	prog	31			
Humuladienone	1952	prog	31			
Humulane	1609	175	35			
Humulene	1672	prog	22	1437	prog	22
	1707	prog	21 ^a	1465	prog	2
	1719	165	3	1447	130	3
Humulene epoxide I	1972	prog	31			
Humulene epoxide II	2011	prog	31			
Humulenol II	2234	prog	31			
Humulol	2124	prog	31			
Ipsdienol				1128	100	23
Ipsenol				1087	90	23
Iridomyrmecin				1400	135	23
Isoborneol	1660	prog	2	1157	prog	2
				1149	110	23
Isobornyl acetate	1584	prog	2	1279	prog	2
	1623	150	29			
Isobornyl formate	1596	prog	2	1228	prog	2
Isobornyl propionate	1676	prog	2	1376	prog	2
Isocamphane <i>trans</i> -	1056	65	32	975	100	32
Isocamphane <i>cis</i> -	1065	65	32	980	100	32
Isogeraniol <i>cis</i> -	1812	150	2			
Isogeraniol <i>trans</i> -	1812	150	2			
Isogeraniol γ -	1800	150	2			
Isogeranyl acetate γ -	1726	150	29			
Isoiridomyrmecin				1422	150	23
Isomenthol	1667	130	20	1182	130	20
				1174	100	23
Isomenthone	1528	130	20	1156	130	20
	1468	prog	39	1151	prog	39
Isomenthyl acetate	1579	130	20	1283	130	20
	1599	150	29			
Isopinocampheol				1170	115	23
Isopinocamphone				1157	110	23
Isopulegol	1574	prog	2	1145	prog	2
				1133	110	23
Isopulegyl acetate	1585	prog	2	1258	prog	2
	1608	150	29			
Isosativene	1639	165	3	1441	170	3
Junenol	2028	prog	31			
Karahana ether	1368	prog	31			
Lavandulol	1662	prog	2	1154	prog	2
	1707	150	34	1153	110	23
Lavandulyl acetate	1597	prog	2	1274	prog	2
	1609	150	29			
Limone	1187	75	5	1025	100	5
	1206	prog	2	1030	prog	2
	1210	70	20	1024	100	20
Limone epoxide <i>cis</i> -				1119	100	23
Limone epoxide <i>trans</i> -				1122	100	23

TABLE 1 (continued)

Compound	CW20M			Methyl silicone		
	I	T	Ref.	I	T	Ref.
Linalool	1506	prog	2	1092	prog	2
	1533	135	28	1097	135	28
	1555	150	34	1086	90	23
Linalool oxide <i>cis</i> - (furan)	1423	prog	2 ^b	1068	prog	2 ^b
	1461	prog	30 ^b			
Linalool oxide <i>trans</i> - (furan)	1451	prog	2 ^b	1082	prog	2 ^b
	1432	prog	30 ^b			
Linalool oxide I (pyran)				1063	100	23
Linalool oxide II (pyran)				1077	100	23
Linalyl acetate	1538	prog	2	1246	prog	2
	1569	150	29	1240	130	23
Linalyl butyrate	1680	prog	2	1420	prog	2
	1698	150	29			
Linalyl formate	1570	prog	2	1206	prog	2
Linalyl isobutyrate	1597	prog	2	1366	prog	2
	1622	150	29			
Linalyl isopentanoate	1698	prog	2	1461	prog	2
Linalyl 2-methylbutyrate	1695	prog	2	1450	prog	2
Linalyl pentanoate	1765	prog	2	1500	prog	2
Linalyl propionate	1596	prog	2	1324	prog	2
	1624	150	29			
Longicyclene	1554	165	3	1371	130	3
Longifolane 7 α H-	1627	130	25	1460	150	25
Longifolane 7 β H-	1633	130	25	1467	150	25
Longifolene	1574	prog	22	1398	prog	22
	1643	165	3	1404	130	3
Longipinene α -	1541	165	37	1359	130	3
Longipinene β -	1612	150	4	1432	170	4
Mentha-2,8-dien-1-ol <i>cis-p</i> -				1120	95	23
Menthane <i>trans-p</i> -	1022	65	32	981	100	32
Menthane <i>cis-p</i> -	1045	65	32	995	100	32
Menthan-1-ol <i>p</i> -				1156	160	33
Menthan-2-ol <i>p</i> -				1205	160	33
Menthan-7-ol <i>cis-p</i> -	1823	120	12			
Menthan-7-ol <i>trans-p</i> -	1800	120	12			
Menthan-8-ol <i>p</i> -				1162	160	33
Menthan-9-ol <i>cis-p</i> -	1806	120	12			
Menthan-9-ol <i>trans-p</i> -	1777	120	12			
Menthan-8-yl acetate <i>cis-p</i> -	1598	150	29			
Menthan-8-yl acetate <i>trans-p</i> -	1623	150	29			
Menth-1-ene <i>p</i> -				985	160	33
Menth-4(8)-ene <i>p</i> -				998	160	33
Menth-1-en-9-ol <i>p</i> -	1904	120	12			
Menth-1(7)-en-9-ol <i>p</i> -	1881	120	12			
Menth-2-en-1-ol <i>cis-p</i> -	1560	prog	38 ^c	1111	prog	38 ^c
	1662	prog	21 ^{a,c}			
Menth-2-en-1-ol <i>trans-p</i> -	1628	prog	38 ^c	1128	prog	38 ^c
	1597	prog	21 ^{a,c}			
Menth-2-en-7-ol <i>cis-p</i> -	1839	120	12			
Menth-2-en-7-ol <i>trans-p</i> -	1842	120	12			
Menth-3-en-9-ol <i>p</i> -	1736	120	12			

(Continued on p. 10)

TABLE 1 (continued)

Compound	CW20M			Methyl silicone		
	I	T	Ref.	I	T	Ref.
Menth-8-en-1-ol <i>p</i> -				1156	160	33
Menth-8-en-2-ol <i>p</i> -				1208	160	33
Menthofuran	1503	130	20	1147	130	20
	1460	prog	39	1155	prog	39
Menthol	1612	prog	2	1171	prog	2
	1640	130	20	1168	130	20
	1600	prog	39	1171	prog	39
Menthone	1478	prog	2	1143	prog	2
	1518	130	20	1158	130	20
	1444	prog	39	1142	prog	39
Menthyl acetate	1600	150	29			
	1541	prog	39	1281	prog	39
Muurolene α -	1753	165	3	1495	130	3
	1727	prog	22			
	1730	prog	2	1500	prog	2
Muurolene γ -	1695	130	20	1486	150	20
	1725	165	3	1486	150	20
	1692	prog	22			
Muurolene ε -	1714	165	3	1445	130	3
Myrcene	1156	prog	2	986	prog	2
	1166	75	28	988	100	28
	1168	70	20	984	100	20
Myrcene-8-ol	1919	150	34			
Myrcenol	1585	prog	2	1103	prog	2
	1631	150	34			
Myrcenyl acetate	1574	prog	2	1247	prog	2
	1595	150	29			
Myrcenyl propionate	1625	prog	2	1327	prog	2
Myrtanol <i>cis</i> -				1245	120	23
Myrtenal				1173	120	23
Myrtenol				1281	120	23
Myrtenyl acetate	1720	150	29			
Neocarvomenthyl acetate	1604	150	29			
Neoisocarvomenthyl acetate	1672	150	29			
Neoisomenthol	1634	130	20	1180	130	20
Neoisomenthyl acetate	1602	130	20	1297	130	20
	1623	150	29			
Neomenthol	1559	prog	39	1159	prog	39
				1159	120	23
Neomenthyl acetate	1569	150	29			
Neral	1680	prog	2	1227	prog	2
				1220	120	23
Nerol	1757	prog	2	1218	prog	2
	1808	150	34	1218	120	23
Nerolic acid				1316	140	23
Nerolidol <i>cis</i> -	1961	prog	2	1524	prog	2
				1540	175	27
Nerolidol <i>trans</i> -	2000	prog	2	1553	prog	2
	2044	prog	19			
Neryl acetate	1699	prog	2	1345	prog	2
	1735	150	29	1343	135	23

TABLE I (continued)

Compound	CW20M			Methyl silicone		
	I	T	Ref.	I	T	Ref.
Neryl butyrate	1868	150	29			
Neryl formate	1663	prog	2	1267	prog	2
	1700	150	29			
Neryl isobutyrate	1764	prog	2	1474	prog	2
	1790	150	29			
Neryl isopentanoate	1864	prog	2	1574	prog	2
Neryl propionate	1771	prog	2	1436	prog	2
	1794	150	29			
Nootkatone	2250	prog	2	1802	prog	2
Norbornyl acetate	1476	prog	2	1112	prog	2
Ocimene <i>cis</i> - β -	1238	70	20	1027	100	20
	1228	prog	2	1025	prog	2
				1027	90	23
Ocimene <i>trans</i> - β -	1257	70	20	1042	100	20
	1250	prog	2	1038	prog	2
Ocimenol <i>cis</i> -	1660	150	34			
Ocimenol <i>trans</i> -	1685	150	34			
Patchoulene β -	1488	prog	22	1378	prog	22
Perilla aldehyde				1253	120	23
Perillyl acetate	1791	150	29			
Perillyl alcohol				1281	115	23
Phellandrene α -	1177	prog	2	1002	prog	2
	1173	70	13	1007	110	13
				1000	90	23
Phellandrene β -	1216	prog	2	1025	prog	2
	1213	70	13	1032	110	13
Phellandrol	1896	120	12			
Pinane <i>cis</i> -	1075	prog	2	987	prog	2
	1061	65	32	977	80	23
				1002	160	33
Pinane <i>trans</i> -	1062	prog	2	981	prog	2
	1049	65	32	973	100	32
Pinene α -	1036	75	28	942	100	28
	1038	70	20	939	100	20
				942	prog	2
Pinene oxide α -				1100	112	23
Pinene β -	1120	70	20	978	100	20
	1120	75	28	983	100	28
	1124	prog	2	981	prog	2
Pinocamphone				1152	110	23
Pinocarveol <i>trans</i> -				1132	110	23
Pinocarveyl acetate <i>trans</i> -	1682	150	29			
Pinonic acid <i>cis</i> -				1427	165	23
Piperitenone				1315	125	23
Piperitenone oxide	1997	prog	21 ^a			
Piperitone	1739	prog	2	1247	prog	2
				1231	125	23
Pulegone	1662	prog	2	1230	prog	2
Pyrovetivene α -	1817	165	3	1522	170	3
Rose oxide <i>cis</i> -	1354	prog	2	1087	prog	2
				1100	95	23

(Continued on p. 12)

TABLE 1 (continued)

Compound	CW20M			Methyl silicone		
	I	T	Ref.	I	T	Ref.
Rose oxide <i>trans</i> -	1370	prog	2	1100	prog	2
				1114	95	23
Sabinene	1130	70	20	972	100	20
	1130	prog	2	976	prog	2
Sabinene hydrate <i>cis</i> -				1092	prog	38
Sabinene hydrate <i>trans</i> -	1463	prog	38	1060	prog	38
Sabinol (<i>cis</i> -)	1683	prog	2	1135	prog	2
				1130	115	23
Sabinyl acetate (<i>cis</i> -)	1651	prog	2	1262	prog	2
	1677	150	29			
Safranal				1167	120	23
Santalene <i>epi</i> - β -	1638	prog	22	1437	prog	22
Santalene α -	1574	prog	22	1412	prog	22
Santalene β -	1653	prog	22	1450	prog	22
Santalol α -				1660	175	27
Sativene	1595	165	3	1421	170	3
Scapanene	1664	150	4	1465	170	4
Selina-3,7(11)-diene	1791	prog	19			
Selina-4(14), 7(11)-diene	1816	165	3			
Selina-4(14), 7-diene	1694	165	3	1476	170	3
Selina-4,11-diene	1702	150	4			
Selinene α -	1751	150	4	1513	170	3
	1729	prog	22	1484	prog	22
	1759	prog	21 ^a			
Selinene β -	1767	165	3	1506	170	3
	1727	prog	22	1477	prog	22
	1756	prog	21 ^a			
Selinene δ -	1728	165	3			
Selinene 7- <i>epi</i> - α -	1775	prog	19			
Selinene 10- <i>epi</i> - α -	1803	165	37			
Sesquiphellandrene β -	1776	prog	22	1512	prog	22
Seychellene	1669	prog	22			
Shisool				1248	130	23
Sibirene	1594	150	4	1427	170	4
Sinuene	1646	150	4	1451	170	4
Spathulenol	2153	prog	21 ^a			
Tagetone <i>cis</i> -				1136	110	23
Tagetone <i>trans</i> -				1125	110	23
Terpinene α -	1189	70	20	1016	100	20
	1188	70	13	1018	110	13
Terpinene γ -	1247	75	28	1056	100	28
	1251	prog	2	1057	prog	2
Terpinene-1-ol	1576	prog	24			
Terpinene-4-ol	1601	135	28	1129	135	28
	1628	prog	2	1175	prog	2
	1637	prog	21 ^a	1170	115	23
				1160	175	27
Terpinene-4-yl acetate	1640	150	29	1282	120	23
Terpineol α -	1731	prog	21 ^a	1185	prog	2
	1685	135	28	1178	135	28
				1205	160	33
Terpineol β -	1616	prog	2	1137	prog	2
Terpineol δ -	1655	prog	2	1160	prog	2

TABLE 1 (continued)

Compound	CW20M			Methyl silicone		
	<i>I</i>	<i>T</i>	Ref.	<i>I</i>	<i>T</i>	Ref.
Terpinolene	1279	75	28	1074	100	28
	1289	70	20	1081	100	20
	1287	prog	2			
Terpinyl acetate	1687	prog	2	1333	prog	2
	1722	150	29	1337	140	23
Terpinyl acetate <i>cis</i> - β -	1622	150	29			
Terpinyl butyrate	1828	prog	2	1514	prog	2
Terpinyl formate	1666	prog	2	1333	prog	2
Terpinyl isobutyrate	1748	prog	2	1467	prog	2
Terpinyl isopentanoate	1858	prog	2	1565	prog	2
Terpinyl pentanoate	1928	prog	2	1614	prog	2
Terpinyl propionate	1747	prog	2	1426	prog	2
Tetrahydrogeraniol	1626	prog	2	1185	prog	2
	1675	150	34			
Tetrahydrogeranyl acetate	1582	150	29			
Tetrahydrohumulene	1653	175	35			
Tetrahydrolavandulol	1600	150	34			
Tetrahydrolinalool	1397	prog	2	1087	prog	2
	1431	150	34	1088	90	23
Tetrahydrolinalyl acetate	1422	150	29			
Tetrahydromyrcenol	1414	prog	2	1090	prog	34
	1449	150	34			
Tetrahydrothujopsane <i>a</i>	1668	130	25	1496	150	25
Tetrahydrothujopsane <i>b</i>	1678	130	25	1508	150	25
Thuj-2-en-4-ol <i>cis</i> -	1551	100	40	1053	140	40
Thuj-2-en-4-ol <i>trans</i> -	1468	100	40	1035	140	40
Thujene α -	1038	70	20	931	100	20
	1023	70	13	935	110	13
Thujone α -				938	prog	2
				1100	110	23
Thujopsene	1626	prog	22	1425	prog	22
	1660	prog	2	1451	prog	2
	1684	165	3	1430	130	3
Thujyl acetate	1626	150	29			
Thymol				1270	130	23
Tricyclene	1009	75	5	928	100	5
Undulatene	1812	150	4	1557	170	4
Valencane (nootkatane)	1624	130	25	1493	150	25
Valencene	1722	prog	22	1482	prog	22
	1751	prog	34	1487	prog	2
	1760	165	3	1457	130	3
Valerianol	2231	prog	19			
Verbenol <i>cis</i> -				1165	100	23
Verbenol <i>trans</i> -				1140	120	23
Verbenone	1733	prog	2	1195	prog	2
				1185	110	23
Vetivenene β -	1885	165	3	1563	170	3
	1868	prog	22	1544	prog	22
Viridiflorene	1697	prog	22	1484	prog	22
Viridiflorol	2103	180	20	1588	150	20
	2112	prog	21 ^a			

(Continued on p. 14)

TABLE 1 (continued)

Compound	CW20M			Methyl silicone		
	I	T	Ref.	I	T	Ref.
Ylangene α -	1539	165	3	1396	170	3
	1491	prog	22	1368	prog	22
Zingiberene	1728	prog	22	1486	prog	22
	1738	165	3	1480	170	3
Zizaene	1706	165	3	1482	170	3
Zonarene	1781	165	8			

^a Indices reported from this laboratory were determined on a 50 m \times 0.33 mm I.D. BP20 column with a 0.5- μ m film thickness (S.G.E.), temperature programmed from 100 to 220°C at 3°C/min with helium as carrier gas.

^b Refs. 2 and 30 have conflicting orders of elution for *cis*- and *trans*-linalool oxides.

^c Refs. 21 and 38 have conflicting orders of elution for *cis*- and *trans*-*p*-menth-2-en-1-ols.

TABLE 2
KOVÁTS' INDICES LISTED IN ORDER ON CW20M

Column headings and footnotes as for Table 1.

Compound	I	T	Ref.	Compound	I	T	Ref.
Dimethyloctane 2,6-	922	65	32	Myrcene	1156	prog	2
Tricyclene	1009	75	5	Myrcene	1166	75	28
Camphane	1021	65	32	Myrcene	1168	70	20
Menthane <i>trans-p</i> -	1022	65	32	Phellandrene α -	1173	70	13
Thujene α -	1023	70	13	Phellandrene α -	1177	prog	2
Pinene α -	1036	75	28	Cineole 1,4-	1185	prog	2
Pinene α -	1038	70	20	Limonene	1187	75	5
Thujene α -	1038	70	20	Terpinene α -	1188	70	13
Menthane <i>cis-p</i> -	1045	65	32	Terpinene α -	1189	70	20
Pinane <i>trans</i> -	1049	65	32	Limonene	1206	prog	2
Isocamphane <i>trans</i> -	1056	65	32	Limonene	1210	70	20
Fenchene β -	1057	70	13	Phellandrene β -	1213	70	13
Pinane <i>cis</i> -	1061	65	32	Phellandrene β -	1216	prog	2
Pinane <i>trans</i> -	1062	prog	2	Cineole 1,8-	1223	70	20
Carane <i>cis</i> -	1064	65	32	Cineole 1,8-	1228	prog	2
Isocamphane <i>cis</i> -	1065	65	32	Ocimene <i>cis</i> - β -	1228	prog	2
Camphene	1066	75	5	Ocimene <i>cis</i> - β -	1238	70	20
Fenchene α -	1071	70	13	Terpinene γ -	1247	75	28
Pinane <i>cis</i> -	1075	prog	2	Cymene <i>p</i> -	1250	75	5
Camphene	1078	75	28	Ocimene <i>trans</i> - β -	1250	prog	2
Camphene	1083	prog	2	Terpinene γ -	1251	prog	2
Pinene β -	1120	70	20	Ocimene <i>trans</i> - β -	1257	70	20
Pinene β -	1120	75	28	Cymene <i>p</i> -	1272	prog	2
Pinene β -	1124	prog	2	Cymene <i>p</i> -	1275	70	20
Sabinene	1130	70	20	Terpinolene	1279	75	28
Sabinene	1130	prog	2	Terpinolene	1287	prog	2
Carene 3-	1141	75	5	Terpinolene	1289	70	20
Carene 3-	1156	75	28	Rose oxide <i>cis</i> -	1354	prog	2

TABLE 2 (continued)

Compound	I	T	Ref.	Compound	I	T	Ref.
Hop ether	1360	prog	31	Linalyl acetate	1538	prog	2
Karahana ether	1368	prog	31	Ylangene α -	1539	165	3
Rose oxide <i>trans</i> -	1370	prog	2	Cubebene β -	1541	prog	22
Allo-ocimene <i>cis</i> -	1373	70	13	Longipinene α -	1541	165	37
Allo-ocimene <i>trans</i> -	1392	70	13	Menthyl acetate	1541	prog	39
Tetrahydrolinalool	1397	prog	2	Bourbonene β -	1546	prog	2
Fenchone	1410	prog	2	Cyclosativene	1549	165	3
Tetrahydromyrcenol	1414	prog	2	Copaene α -	1551	165	3
Tetrahydrolinalyl acetate	1422	150	29	Thuj-2-en-4-ol <i>cis</i> -	1551	100	40
Linalool oxide <i>cis</i> - (furan)	1423	prog	2 ^b	Longicyclene	1554	165	3
Dihydromyrcenyl acetate	1431	prog	2	Caryophyllane <i>c</i>	1555	130	25
Tetrahydrolinalool	1431	150	34	Linalool	1555	150	34
Linalool oxide <i>trans</i> - (furan)	1432	prog	30 ^b	Neomenthol	1559	prog	39
Dihydromyrcenol 6,10-	1438	prog	2	Cubebene β -	1560	130	20
Menthone	1444	prog	39	Menth-2-en-1-ol <i>cis-p</i> -	1560	prog	38 ^c
Dihydrolinalool 6,7-	1449	150	34	Dihydroterpinyl acetate	1561	prog	2
Tetrahydromyrcenol	1449	150	34	Caryophyllane <i>d</i>	1562	130	25
Linalool oxide <i>trans</i> - (furan)	1451	prog	2 ^b	Anastreptene	1568	150	4
Cubebene α -	1458	prog	22	Linalyl acetate	1569	150	29
Elemene	1460	130	25	Neomenthyl acetate	1569	150	29
Menthofuran	1460	prog	39	Linalyl formate	1570	prog	2
Linalool oxide <i>cis</i> - (furan)	1461	prog	30 ^b	Germacrane <i>b</i>	1572	130	25
Sabinene hydrate <i>trans</i> -	1463	prog	38	Fenchol	1574	prog	2
Citronellal	1465	prog	2	Isopulegol	1574	prog	2
Isomenthone	1468	prog	39	Longifolene	1574	prog	22
Thuj-2-en-4-ol <i>trans</i> -	1468	100	40	Myrcenyl acetate	1574	prog	2
Elemene δ -	1469	prog	22	Santalene α -	1574	prog	22
Dihydromyrcenol 6,10-	1473	150	34	Terpinene-1-ol	1576	prog	24
Fenchyl acetate	1473	prog	2	Cedrene α -	1578	prog	22
Norbornyl acetate	1476	prog	2	Isomenthyl acetate	1579	130	20
Menthone	1478	prog	2	Fenchol	1580	135	28
Cubebene α -	1481	130	20	Eudesmane 4 β H, 5 α H-	1582	130	25
Bicycloelemene	1482	prog	24	Tetrahydrogeranyl acetate	1582	150	29
Patchoulene β -	1488	prog	22	Isobornyl acetate	1584	prog	2
Citronellal	1491	135	28	Germacrane <i>c</i>	1585	130	25
Ylangene α -	1491	prog	22	Isopulegyl acetate	1585	prog	2
Bisabolane <i>a</i>	1492	130	25	Myrcenol	1585	prog	2
Copaene α -	1493	prog	22	Bergamotene <i>trans</i> - β -	1586	prog	22
Menthofuran	1503	130	20	Bourbonene β -	1586	165	3
Linalool	1506	prog	2	Bergamotene α -	1590	prog	24
Bisabolane <i>b</i>	1510	130	25	Elemene β -	1591	prog	22
Dihydrolinalool 1,2-	1512	prog	2	Gurjunene α -	1591	165	3
Camphor	1518	prog	2	Germacrane <i>d</i>	1593	130	25
Menthone	1518	130	20	Gurjunene β - (calarene)	1593	prog	22
Copaene α -	1519	prog	2	Sibirene	1594	150	4
Caryophyllane <i>a</i>	1522	130	25	Myrcenyl acetate	1595	150	29
Bourbonene β -	1526	prog	22	Sativene	1595	165	3
Isomenthone	1528	130	20	Isobornyl formate	1596	prog	2
Gurjunene α -	1529	prog	22	Linalyl propionate	1596	prog	2
Caryophyllane <i>b</i>	1533	130	25	Lavandulyl acetate	1597	prog	2
Linalool	1533	135	28	Linalyl isobutyrate	1597	prog	2
Cyperene	1535	prog	22	Menth-2-en-1-ol <i>trans-p</i> -	1597	prog	21 ^{ac}
Dihydrolinalool 1,2-	1537	150	34	Menthan-8-yl acetate <i>cis-p</i> -	1598	150	29

(Continued on p. 16)

TABLE 2 (continued)

Compound	I	T	Ref.	Compound	I	T	Ref.
Bornyl acetate	1599	135	28	Santalene <i>epi-β</i> -	1638	prog	22
Isomenthyl acetate	1599	150	29	Isosativene	1639	165	3
Cedrene α -	1600	prog	2	Cedrene α -	1640	165	3
Citronellyl formate	1600	prog	2	Menthol	1640	130	20
Dihydrocarvone	1600	prog	2	Terpinene-4-yl acetate	1640	150	29
Menthol	1600	prog	39	Carvomenthyl acetate	1641	150	29
Menthyl acetate	1600	150	29	Elemene γ -	1642	prog	22
Tetrahydrolavandulol	1600	150	34	Longifolene	1643	165	3
Clovone	1601	175	35	Citronellyl acetate	1645	prog	2
Terpinene-4-ol	1601	135	28	Sinuene	1646	150	4
Neoisomenthyl acetate	1602	130	20	Himachalene α -	1649	prog	22
Neocarvomenthyl acetate	1604	150	29	Aromadendrene	1650	prog	21 ^a
Cedrene β -	1605	prog	22	Guaiene α -	1651	prog	22
Cyperene	1606	165	3	Sabinyl acetate (<i>cis</i> -)	1651	prog	2
Elemene β -	1608	130	20	Santalene β -	1653	prog	22
Isopulegyl acetate	1608	150	29	Tetrahydrohumulene	1653	175	35
Humulane	1609	175	35	Caryophyllene	1655	165	3
Lavandulyl acetate	1609	150	29	Dihydrohumulene	1655	175	35
Bornyl formate	1610	prog	2	Terpineol δ -	1655	prog	2
Longipinene β -	1612	150	4	Gurjunene β - (calarene)	1656	165	3
Menthol	1612	prog	2	Alloaromadendrene	1660	130	20
Bornyl acetate	1615	150	29	Isoborneol	1660	prog	2
Terpineol β -	1616	prog	2	Ocimenol <i>cis</i> -	1660	150	34
Caryophyllene	1617	prog	2	Thujopsene	1660	prog	2
Cedrane 8 β H-	1617	130	25	Alloaromadendrene	1662	prog	2
Caryophyllene	1618	130	20	Citronellyl acetate	1662	135	28
Clovane	1621	175	35	Lavandulol	1662	prog	2
Linalyl isobutyrate	1622	150	29	Menth-2-en-1-ol <i>cis-p</i> -	1662	prog	21 ^{a,c}
Terpinyl acetate <i>cis-β</i> -	1622	150	29	Pulegone	1662	prog	2
Isobornyl acetate	1623	150	29	Neryl formate	1663	prog	2
Menthan-8-yl acetate				Scapanene	1664	150	4
<i>trans-p</i> -	1623	150	29	Terpinyl formate	1666	prog	2
Neoisomenthyl acetate	1623	150	29	Guaiene β -	1667	prog	22
Linalyl propionate	1624	150	29	Isomenthol	1667	130	20
Valencane (nootkatane)	1624	130	25	Farnesene <i>trans-β</i> -	1668	165	3
Myrcenyl propionate	1625	prog	2	Farnesene <i>trans-β</i> -	1668	prog	22
Citronellyl ethyl acetal	1626	prog	2	Tetrahydrothujopsane <i>a</i>	1668	130	25
Copaene β -	1626	prog	2	Seychellene	1669	prog	22
Tetrahydrogeraniol	1626	prog	2	Cedrene β -	1670	165	3
Thujopsene	1626	prog	22	Dihydrocarvyl acetate	1670	prog	2
Thujyl acetate	1626	150	29	Citronellyl acetate	1671	150	29
Barbatene α -	1627	150	4	Farnesene <i>trans-β</i> -	1671	130	20
Cedrane 8 α H-	1627	130	25	Humulene	1672	prog	22
Longifolane 7 α H-	1627	130	25	Neoisocarvomenthyl acetate	1672	150	29
Menth-2-en-1-ol <i>trans-p</i> -	1628	prog	38 ^c	Tetrahydrogeraniol	1675	150	34
Terpinene-4-ol	1628	prog	2	Isobornyl propionate	1676	prog	2
Myrcenol	1631	150	34	Sabinyl acetate (<i>cis</i> -)	1677	150	29
Cedrene β -	1633	prog	2	Tetrahydrothujopsane <i>b</i>	1678	130	25
Longifolane 7 β H-	1633	130	25	Linalyl butyrate	1680	prog	2
Neoisomenthol	1634	130	20	Neral	1680	prog	2
Eudesmane 4 α H-, 5 α H-	1636	130	25	Pinocarveyl acetate <i>trans</i> -	1682	150	29
Farnesene <i>cis-β</i> -	1636	prog	22	Alloaromadendrene	1683	prog	21 ^a
Citronellyl formate	1638	150	29	Helmiscapene α -	1683	150	4

TABLE 2 (continued)

<i>Compound</i>	<i>I</i>	<i>T</i>	<i>Ref.</i>	<i>Compound</i>	<i>I</i>	<i>T</i>	<i>Ref.</i>
Sabinol (<i>cis</i> -)	1683	prog	2	Bulnesene α -	1729	prog	22
Geranyl formate	1684	prog	2	Guaiene δ -	1729	prog	22
Thujopsene	1684	165	3	Selinene α -	1729	prog	22
Ocimenol <i>trans</i> -	1685	150	34	Geranial	1730	prog	2
Terpineol α -	1685	135	28	Muurolene α -	1730	prog	2
Helmiscapene β -	1686	150	4	Verbenone	1733	prog	2
Terpinyl acetate	1687	prog	2	Borneol	1735	prog	21 ^a
Barbatene β -	1690	150	4	Farnesene <i>trans,trans</i> - α -	1735	prog	22
Amorphene α -	1691	prog	22	Neryl acetate	1735	150	29
Muurolene γ -	1692	prog	22	Himachalene β -	1736	150	4
Selina-4(14), 7-diene	1694	165	3	Menth-3-en-9-ol <i>p</i> -	1736	120	12
Linalyl 2-methylbutyrate	1695	prog	2	Chamigrene β -	1737	150	4
Muurolene γ -	1695	130	20	Dihydroagarofuran β -	1737	prog	19
Dihydrocurcumene	1696	130	25	Alaskene β -	1738	165	5
Farnesene <i>cis,cis</i> - α -	1697	prog	22	Bicyclogermacrene	1738	130	20
Viridiflorene	1697	prog	22	Citronellyl propionate	1738	150	29
Borneol	1698	prog	2	Zingiberene	1738	165	3
Linalyl butyrate	1698	150	29	Citronellyl isobutyrate	1739	150	29
Linalyl isopentanoate	1698	prog	2	Piperitone	1739	prog	2
Neryl acetate	1699	prog	2	Bisabolene <i>cis</i> - α -	1740	prog	22
Citronellyl propionate	1700	prog	2	Bicyclogermacrene	1744	prog	22
Dihydrocarvyl acetate	1700	150	29	Bisabolene β -	1745	165	3
Neryl formate	1700	150	29	Terpinyl propionate	1747	prog	2
Aequilobene	1702	150	4	Terpinyl isobutyrate	1748	prog	2
Selina-4-,11-diene	1702	150	4	Selinene α -	1751	150	4
Himachalene α -	1704	165	3	Valencene	1751	prog	34
Citronellyl isobutyrate	1705	prog	2	Muurolene α -	1753	165	3
Zizaene	1706	165	3	Geranyl acetate	1754	135	28
Humulene	1707	prog	21 ^a	Curcumene β -	1756	165	3
Lavandulol	1707	150	34	Farnesene <i>trans,trans</i> - α -	1756	130	20
Germacrene D	1712	prog	22	Selinene β -	1756	prog	21 ^a
Dihydrocarveol	1713	prog	2	Nerol	1757	prog	2
Muurolene ϵ -	1714	165	3	Carveyl acetate <i>trans</i> -	1759	150	29
Carvone	1715	prog	2	Dihydrogeraniol	1759	150	34
Geranyl formate	1717	150	29	Selinene α -	1759	prog	21 ^a
Germacrene D	1718	130	20	Bornyl butyrate	1760	prog	2
Himachalene β -	1718	prog	22	Citronellol α -	1760	150	34
Humulene	1719	165	3	Valencene	1760	165	3
Myrtenyl acetate	1720	150	29	Cadinene δ -	1761	prog	2
Citronellol (β -)	1722	prog	2	Alaskene α -	1763	165	5
Farnesene <i>trans,cis</i> - α -	1722	prog	22	Neryl isobutyrate	1764	prog	2
Terpinyl acetate	1722	150	29	Chamigrene α -	1765	150	4
Valencene	1722	prog	22	Citronellol (β -)	1765	150	34
Himachalene γ -	1723	150	4	Linalyl pentanoate	1765	prog	2
Amorphene α -	1724	165	3	Bisabolene	1766	165	3
Dihydronerol	1725	150	34	Cadinene γ -	1766	prog	2
Muurolene γ -	1725	165	3	Selinene β -	1767	165	3
Isogeranyl acetate γ -	1726	150	29	Bicyclogermacrene	1768	prog	21 ^a
Farnesene <i>cis,trans</i> - α -	1727	prog	22	Neryl propionate	1771	prog	2
Muurolene α -	1727	prog	22	Bornyl isopentanoate	1774	prog	2
Selinene β -	1727	prog	22	Selinene 7- <i>epi</i> - α -	1775	prog	19
Selinene δ -	1728	165	3	Sesquiphellandrene β -	1776	prog	22
Zingiberene	1728	prog	22	Curcumene α - (ar-)	1777	prog	22

(Continued on p. 18)

TABLE 2 (continued)

<i>Compound</i>	<i>I</i>	<i>T</i>	<i>Ref.</i>	<i>Compound</i>	<i>I</i>	<i>T</i>	<i>Ref.</i>
Menthan-9-ol <i>trans-p</i> -	1777	120	12	Citronellyl pentanoate	1880	prog	2
Zonarene	1781	165	8	Menth-1(7)-en-9-ol <i>p</i> -	1881	120	12
Cadinene δ -	1784	165	3	Vetivenene β -	1885	165	3
Cadinene δ -	1785	prog	21 ^a	Geranyl isopentanoate	1895	prog	2
Cadina-1,4-diene	1786	prog	22	Phellandrol	1896	120	12
Citronellyl butyrate	1786	prog	2	Geranyl butyrate	1904	150	29
Curcumene α - (ar-)	1787	165	3	Menth-1-en-9-ol <i>p</i> -	1904	120	12
Carveol <i>trans</i> -	1790	prog	2	Agarofuran α -	1907	prog	19
Neryl isobutyrate	1790	150	29	Calacorene α -	1916	prog	22
Perillyl acetate	1791	150	29	Myrcene-8-ol	1919	150	34
Selina-3,7(11)-diene	1791	prog	19	Calacorene α -	1926	165	6
Cadinene γ -	1792	165	3	Terpinyl pentanoate	1928	prog	2
Neryl propionate	1794	150	29	Humuladienone	1952	prog	31
Carveyl acetate <i>cis</i> -	1795	150	29	Geranyl pentanoate	1960	prog	2
Geranyl isobutyrate	1795	prog	2	Cedrene epoxide α -	1961	prog	2
Geraniol	1797	prog	2	Nerolidol <i>cis</i> -	1961	prog	2
Isogeraniol γ -	1800	150	2	Caryophyllene oxide	1966	prog	31
Menthan-7-ol <i>trans-p</i> -	1800	120	12	Humulene epoxide I	1972	prog	31
Damascenone	1801	prog	31	Caryophyllene oxide	2000	prog	24
Selinene 10- <i>epi</i> - α -	1803	165	37	Nerolidol <i>trans</i> -	2000	prog	2
Carvone oxide	1805	prog	2	Humulene epoxide II	2011	prog	31
Menthan-9-ol <i>cis-p</i> -	1806	120	12	Caryolan-1-ol	2019	prog	31
Nerol	1808	150	34	Bisabolol α -	2022	160	26
Citronellyl butyrate	1811	150	29	Junenol	2028	prog	31
Cuparene	1811	130	20	Caryophyllene alcohol	2033	prog	31
Isogeraniol <i>cis</i> -	1812	150	2	Cubenol <i>epi</i> -	2037	prog	30
Isogeraniol <i>trans</i> -	1812	150	2	Nerolidol <i>trans</i> -	2044	prog	19
Undulatene	1812	150	4	Elemol	2078	prog	24
Selina-4(14),7(11)-diene	1816	165	3	Cedrol	2100	prog	2
Pyrovetivene α -	1817	165	3	Viridiflorol	2103	180	20
Carveol <i>cis</i> -	1820	prog	2	Globulol	2104	prog	21 ^a
Geranyl isobutyrate	1821	150	29	Viridiflorol	2112	prog	21 ^a
Menthan-7-ol <i>cis-p</i> -	1823	120	12	Eudesmol 10- <i>epi</i> - γ -	2121	prog	19
Terpinyl butyrate	1828	prog	2	Humulol	2124	prog	31
Cuparene	1831	prog	22	Cadinol T-	2136	prog	31
Carvyl propionate	1833	prog	2	Cadinol δ -	2150	prog	31
Geranyl propionate	1834	150	29	Spathulenol	2153	prog	21 ^a
Calamenene	1837	prog	22	Carvacrol	2159	prog	2
Cuparene	1838	150	4	Eudesmol γ -	2182	prog	19
Calamenene	1839	150	4	Cadalene	2203	prog	30
Menth-2-en-7-ol <i>cis-p</i> -	1839	120	12	Cadinol α -	2224	prog	24
Calamenene	1842	prog	2	Farnesyl acetate	2225	200	28
Geraniol	1842	150	34	Valerianol	2231	prog	19
Menth-2-en-7-ol <i>trans-p</i> -	1842	120	12	Humulenol II	2234	prog	31
Cymene-8-ol <i>p</i> -	1846	prog	24	Eudesmol α -	2237	prog	19
Terpinyl isopentanoate	1858	prog	2	Eudesmol 7- <i>epi</i> - α -	2244	prog	19
Neryl isopentanoate	1864	prog	2	Eudesmol α -	2248	prog	19
Neryl butyrate	1868	150	29	Eudesmol α -	2249	prog	21 ^a
Vetivenene β -	1868	prog	22	Nootkatone	2250	prog	2
Geranyl butyrate	1872	prog	2	Eudesmol β -	2258	prog	21 ^a
Himachalene ar-	1873	150	4	Drimenol	2525	prog	19

TABLE 3

KOVÁTS' INDICES LISTED IN ORDER ON METHYL SILICONE

Column headings and footnotes as for Table 1.

<i>Compound</i>	<i>I</i>	<i>T</i>	<i>Ref.</i>	<i>Compound</i>	<i>I</i>	<i>T</i>	<i>Ref.</i>
Tricyclene	928	100	5	Cineole 1,8-	1025	100	20
Thujene α -	931	100	20	Limonene	1025	100	5
Thujene α -	935	110	13	Ocimene <i>cis</i> - β -	1025	prog	2
Dimethyloctane 2,6-	938	100	32	Phellandrene β -	1025	prog	2
Thujene α -	938	prog	2	Ocimene <i>cis</i> - β -	1027	100	20
Pinene α -	939	100	20	Ocimene <i>cis</i> - β -	1027	90	23
Pinene α -	942	100	28	Limonene	1030	prog	2
Pinene α -	942	prog	2	Phellandrene β -	1032	110	13
Dimethyl-1,6-octadiene 3,7-	946	90	23	Thuj-2-en-4-ol <i>trans</i> -	1035	140	40
Fenchene β -	949	110	13	Ocimene <i>trans</i> - β -	1038	prog	2
Camphene	952	100	5	Ocimene <i>trans</i> - β -	1042	100	20
Camphane	953	100	32	Thuj-2-en-4-ol <i>cis</i> -	1053	140	40
Camphene	954	prog	2	Dihydromyrcenol 6,10-	1056	80	23
Camphene	956	100	28	Terpinene γ -	1056	100	28
Fenchene α -	957	110	13	Terpinene γ -	1057	prog	2
Dimethyl-2-octene 2,6-	966	80	23	Sabinene hydrate <i>trans</i> -	1060	prog	38
Sabinene	972	100	20	Dihydromyrcenol 6,10-	1063	prog	2
Pinane <i>trans</i> -	973	100	32	Linalool oxide I (pyran)	1063	100	23
Isocamphane <i>trans</i> -	975	100	32	Linalool oxide <i>cis</i> - (furan)	1068	prog	2 ^b
Sabinene	976	prog	2	Terpinolene	1074	100	28
Pinane <i>cis</i> -	977	80	23	Fenchone	1077	105	23
Pinene β -	978	100	20	Linalool oxide II (pyran)	1077	100	23
Isocamphane <i>cis</i> -	980	100	32	Fenchone	1080	prog	2
Menthane <i>trans-p</i> -	981	100	32	Terpinolene	1081	100	20
Pinane <i>trans</i> -	981	prog	2	Linalool oxide <i>trans</i> - (furan)	1082	prog	2 ^b
Pinene β -	981	prog	2	Linalool	1086	90	23
Pinene β -	983	100	28	Ipsenol	1087	90	23
Myrcene	984	100	20	Rose oxide <i>cis</i> -	1087	prog	2
Menth-1-ene <i>p</i> -	985	160	33	Tetrahydrolinalool	1087	prog	2
Carane <i>cis</i> -	986	100	32	Tetrahydrolinalool	1088	90	23
Myrcene	986	prog	2	Tetrahydromyrcenol	1090	prog	34
Pinane <i>cis</i> -	987	prog	2	Linalool	1092	prog	2
Myrcene	988	100	28	Sabinene hydrate <i>cis</i> -	1092	prog	38
Menthane <i>cis-p</i>	995	100	32	Linalool	1097	135	28
Menth-4(8)-ene- <i>p</i> -	998	160	33	Chrysanthenone	1100	100	23
Cineole 1,4-	1000	80	23	Cyclocitral α -	1100	110	23
Phellandrene α -	1000	90	23	Pinene oxide α -	1100	112	23
Phellandrene α -	1002	prog	2	Rose oxide <i>cis</i> -	1100	95	23
Pinane <i>cis</i> -	1002	160	33	Rose oxide <i>trans</i> -	1100	prog	2
Phellandrene α -	1007	110	13	Thujone α -	1100	110	23
Carene 3-	1009	100	5	Myrcenol	1103	prog	2
Cineole 1,4-	1010	prog	2	Fenchol	1110	prog	2
Carene 3-	1013	100	28	Menth-2-en-1-ol <i>cis-p</i> -	1111	prog	38 ^c
Cymene <i>p</i> -	1016	100	5	Norbornyl acetate	1112	prog	2
Terpinene α -	1016	100	20	Rose oxide <i>trans</i> -	1114	95	23
Cineole 1,8-	1017	prog	2	Limonene epoxide <i>cis</i> -	1119	100	23
Cymene <i>p</i> -	1018	100	20	Allo-ocimene <i>trans</i> -	1120	110	13
Terpinene α -	1018	110	13	Mentha-2,8-dien-1-ol <i>cis-p</i> -	1120	95	23
Cymene <i>p</i> -	1020	prog	2	Dihydrolinalool 1,2-	1122	prog	2
Limonene	1024	100	20	Limonene epoxide <i>trans</i> -	1122	100	23

(Continued on p. 20)

TABLE 3 (continued)

<i>Compound</i>	<i>I</i>	<i>T</i>	<i>Ref.</i>	<i>Compound</i>	<i>I</i>	<i>T</i>	<i>Ref.</i>
Fenchol	1125	135	28	Borneol	1177	175	27
Tagetone <i>trans</i> -	1125	110	23	Terpineol α -	1178	135	28
Camphor	1126	110	23	Neoisomenthol	1180	130	20
Ipsdienol	1128	100	23	Carvomenthone	1181	110	23
Menth-2-en-1-ol <i>trans-p</i> -	1128	prog	38 ^c	Isomenthol	1182	130	20
Terpinene-4-ol	1129	135	28	Dihydrocarvone	1183	prog	2
Sabinol (<i>cis</i> -)	1130	115	23	Terpineol α -	1185	prog	2
Allo-ocimene <i>cis</i> -	1132	110	13	Tetrahydrogeraniol	1185	prog	2
Pinocarveol <i>trans</i> -	1132	110	23	Verbenone	1185	110	23
Isopulegol	1133	110	23	Dihydrocarveol	1188	prog	2
Sabinol (<i>cis</i> -)	1135	prog	2	Verbenone	1195	prog	2
Camphor	1136	prog	2	Carveol <i>trans</i> -	1200	120	23
Tagetone <i>cis</i> -	1136	110	23	Cyclocitral β -	1200	125	23
Citronellal	1137	prog	2	Grandisol	1200	110	23
Terpineol β -	1137	prog	2	Dihydromyrcenyl acetate	1202	prog	2
Verbenol <i>trans</i> -	1140	120	23	Menthan-2-ol <i>p</i> -	1205	160	33
Menthone	1142	prog	39	Terpineol α -	1205	160	33
Citronellal	1143	135	28	Linalyl formate	1206	prog	2
Menthone	1143	prog	2	Menth-8-en-2-ol <i>p</i> -	1208	160	33
Isopulegol	1145	prog	2	Carveol <i>trans</i> -	1209	prog	2
Citronellal	1146	160	33	Ascaridole epoxide	1215	110	23
Menthofuran	1147	130	20	Carveol <i>cis</i> -	1215	120	23
Isoborneol	1149	110	23	Citronellol (β -)	1215	prog	2
Isomenthone	1151	prog	39	Citronellol (β -)	1216	100	23
Pinocamphone	1152	110	23	Nerol	1218	prog	2
Lavandulol	1153	110	23	Nerol	1218	120	23
Borneol	1154	110	23	Fenchyl acetate	1220	prog	2
Lavandulol	1154	prog	2	Neral	1220	120	23
Menthofuran	1155	prog	39	Carveol <i>cis</i> -	1222	prog	2
Isomenthone	1156	130	20	Carvone	1223	125	23
Menth-8-en-1-ol <i>p</i> -	1156	160	33	Citronellol (β -)	1224	175	27
Menthan-1-ol <i>p</i> -	1156	160	33	Cadinene γ -	1227	prog	2
Isoborneol	1157	prog	2	Neral	1227	prog	2
Isopinocampheol	1157	110	23	Carvone	1228	prog	2
Menthone	1158	130	20	Isobornyl formate	1228	prog	2
Neomenthol	1159	prog	39	Pulegone	1230	prog	2
Neomenthol	1159	120	23	Piperitone	1231	125	23
Terpinene-4-ol	1160	175	27	Geraniol	1234	175	27
Terpineol δ -	1160	prog	2	Geraniol	1237	120	23
Menthan-8-ol <i>p</i> -	1162	160	33	Bornyl formate	1239	prog	2
Borneol	1164	prog	2	Linalyl acetate	1240	130	23
Verbenol <i>cis</i> -	1165	100	23	Geraniol	1243	prog	2
Cymene-8-ol <i>p</i> -	1167	115	23	Myrtenol <i>cis</i> -	1245	120	23
Safranal	1167	120	23	Linalyl acetate	1246	prog	2
Menthol	1168	130	20	Myrcenyl acetate	1247	prog	2
Isopinocampheol	1170	115	23	Piperitone	1247	prog	2
Terpinene-4-ol	1170	115	23	Shisool	1248	130	23
Menthol	1171	prog	2	Geranial	1252	prog	2
Menthol	1171	prog	39	Perilla aldehyde	1253	120	23
Menthol	1173	175	27	Isopulegyl acetate	1258	prog	2
Myrtenal	1173	120	23	Geranial	1260	120	23
Isomenthol	1174	100	23	Carvone oxide	1261	prog	2
Terpinene-4-ol	1175	prog	2	Citronellyl formate	1261	prog	2

TABLE 3 (continued)

Compound	I	T	Ref.	Compound	I	T	Ref.
Sabinyl acetate (<i>cis</i> -)	1262	prog	2	Cubebene β -	1400	150	20
Neryl formate	1267	prog	2	Cyclosativene	1400	170	3
Cymene-7-ol <i>p</i> -	1270	115	23	Elemene β -	1400	150	20
Thymol	1270	130	23	Gurjunene α -	1400	prog	22
Lavandulyl acetate	1274	prog	2	Iridomyrmecin	1400	135	23
Cymenene	1277	100	23	Elemene	1403	150	25
Ascaridole	1278	110	23	Longifolene	1404	130	3
Bornyl acetate	1278	135	28	Eudesmane 4 β H,5 α H-	1405	150	25
Isobornyl acetate	1279	prog	2	Bourbonene β -	1406	prog	2
Menthyl acetate	1281	prog	39	Cedrene α -	1411	prog	22
Myrtenol	1281	120	23	Santalene α -	1412	prog	22
Perillyl alcohol	1281	115	23	Gurjunene α -	1413	130	3
Dihydroterpinyl acetate	1282	prog	2	Cedrene α -	1414	130	3
Geranyl formate	1282	prog	2	Caryophyllene	1417	130	3
Terpinene-4-yl acetate	1282	120	23	Linalyl butyrate	1420	prog	2
Isomenthyl acetate	1283	130	20	Cedrene β -	1421	130	3
Carvacrol	1297	prog	2	Sativene	1421	170	3
Neoisomenthyl acetate	1297	130	20	Isoiridomyrmecin	1422	150	23
Citronellic acid	1300	125	23	Citronellyl ethyl acetal	1423	prog	2
Piperitenone	1315	125	23	Caryophyllane <i>a</i>	1425	150	25
Nerolic acid	1316	140	23	Elemene γ -	1425	prog	22
Dihydrocarvyl acetate	1319	prog	2	Thujopsene	1425	prog	22
Linalyl propionate	1324	prog	2	Farnesene <i>trans</i> - β -	1426	150	20
Myrcenyl propionate	1327	prog	2	Terpinyl propionate	1426	prog	2
Terpinyl acetate	1333	prog	2	Bergamotene <i>trans</i> - β -	1427	prog	22
Terpinyl formate	1333	prog	2	Citronellyl propionate	1427	prog	2
Citronellyl acetate	1335	prog	2	Pinonic acid <i>cis</i> -	1427	165	23
Citronellyl acetate	1335	135	28	Sibirene	1427	170	4
Citronellyl acetate	1335	140	23	Caryophyllene	1428	prog	2
Terpinyl acetate	1337	140	23	Thujopsene	1430	130	3
Neryl acetate	1343	135	23	Caryophyllane <i>b</i>	1432	150	25
Neryl acetate	1345	prog	2	Longipinene β -	1432	170	4
Geranic acid	1347	140	23	Gurjunene β - (calarene)	1435	130	3
Longipinene α -	1359	130	3	Bergamotene α -	1436	prog	24
Cubebene α -	1362	150	20	Caryophyllene	1436	150	20
Geranyl acetate	1363	135	28	Cedrene α -	1436	prog	2
Linalyl isobutyrate	1366	prog	2	Neryl propionate	1436	prog	2
Ylangene α -	1368	prog	22	Humulene	1437	prog	22
Copaene α -	1369	prog	22	Santalene <i>epi</i> - β -	1437	prog	22
Longicyclene	1371	130	3	Barbatene α -	1440	170	4
Isobornyl propionate	1376	prog	2	Carvyl propionate	1440	prog	2
Copaene α -	1378	130	3	Isosativene	1441	170	3
Patchoulene β -	1378	prog	22	Himachalene α -	1442	prog	22
Cubebene α -	1381	prog	22	Himachalene α -	1444	130	3
Cubebene β -	1381	prog	22	Copaene β -	1445	prog	2
Elemene δ -	1381	prog	22	Muurolene ϵ -	1445	130	3
Bourbonene β -	1386	130	3	Cedrene β -	1446	prog	2
Anastreptene	1391	170	4	Humulene	1447	130	3
Ylangene α -	1396	170	3	Bisabolane <i>a</i>	1448	150	25
Copaene α -	1398	prog	2	Dihydrocurcumene	1448	150	25
Cyperene	1398	130	3	Farnesene <i>trans</i> - β -	1448	prog	36
Cyperene	1398	prog	22	Farnesene <i>trans</i> - β -	1449	170	4
Longifolene	1398	prog	22	Caryophyllane <i>c</i>	1450	150	25

(Continued on p. 22)

TABLE 3 (continued)

<i>Compound</i>	<i>I</i>	<i>T</i>	<i>Ref.</i>	<i>Compound</i>	<i>I</i>	<i>T</i>	<i>Ref.</i>
Caryophyllane <i>d</i>	1450	150	25	Linalyl pentanoate	1500	prog	2
Linalyl 2-methylbutyrate	1450	prog	2	Murolene α -	1500	prog	2
Santalene β -	1450	prog	22	Farnesene <i>trans,trans</i> - α -	1501	150	20
Amorphene α -	1451	prog	22	Bulnesene α -	1502	prog	22
Sinuene	1451	170	4	Calamenene	1502	prog	22
Thujopsene	1451	prog	2	Guaiene δ -	1502	prog	22
Guaiene α -	1454	prog	22	Cadinene δ -	1504	130	3
Valencene	1457	130	3	Bisabolene	1505	170	3
Bisabolane <i>b</i>	1458	150	25	Cuparene	1506	150	20
Cedrane 8 β H-	1458	150	25	Selinene β -	1506	170	3
Longifolane 7 α H-	1460	150	25	Cadinene γ -	1507	130	3
Linalyl isopentanoate	1461	prog	2	Tetrahydrothujopsane <i>b</i>	1508	150	25
Cedrane 8 α H-	1465	150	25	Curcumene β -	1510	170	3
Humulene	1465	prog	2	Citronellyl butyrate	1511	prog	2
Scapanene	1465	170	4	Bornyl isopentanoate	1512	prog	2
Helmiscapene β -	1466	170	4	Sesquiphellandrene β -	1512	prog	22
Helmiscapene α -	1467	170	4	Selinene α -	1513	170	3
Longifolane 7 β H-	1467	150	25	Terpinyl butyrate	1514	prog	2
Terpinyl isobutyrate	1467	prog	2	Cuparene	1516	170	4
Germacrene D	1468	prog	22	Himachalene β -	1517	170	4
Citronellyl isobutyrate	1469	prog	2	Cadina-1,4-diene	1518	prog	22
Barbatene β -	1473	170	4	Calamenene	1518	prog	2
Bornyl butyrate	1473	prog	2	Pyrovetivene α -	1522	170	3
Neryl isobutyrate	1474	prog	2	Chamigrene α	1523	170	4
Alloaromadendrene	1475	150	20	Cadinene δ -	1524	prog	2
Curcumene α - (ar-)	1475	130	3	Calamenene	1524	170	4
Selina-4(14),7-diene	1476	170	3	Nerolidol <i>cis</i> -	1524	prog	2
Germacrene <i>b</i>	1477	150	25	Geranyl butyrate	1532	prog	2
Selinene β -	1477	prog	22	Elemol	1540	prog	24
Alloaromadendrene	1478	prog	2	Nerolidol <i>cis</i> -	1540	175	27
Zingiberene	1480	170	3	Himachalene ar-	1542	170	4
Germacrene <i>c</i>	1482	150	25	Vetivenene β -	1544	prog	22
Guaiene β -	1482	prog	22	Chamigrene β -	1550	170	4
Valencene	1482	prog	22	Nerolidol <i>trans</i> -	1553	prog	2
Zizaene	1482	170	3	Undulatene	1557	170	4
Aequilobene	1483	170	4	Caryophyllene alcohol	1559	prog	24
Selinene α -	1484	prog	22	Vetivenene β -	1563	170	3
Viridiflorene	1484	prog	22	Terpinyl isopentanoate	1565	prog	2
Murolene γ -	1486	150	20	Neryl isopentanoate	1574	prog	2
Zingiberene	1486	prog	22	Caryophyllene oxide	1576	prog	24
Valencene	1487	prog	2	Cedrene epoxide α -	1585	prog	2
Germacrene D	1488	150	20	Viridiflorol	1588	150	20
Germacrene <i>d</i>	1489	150	25	Geranyl isopentanoate	1593	prog	2
Bicyclogermacrene	1490	prog	22	Citronellyl pentanoate	1608	prog	2
Amorphene α -	1492	170	3	Cedrol	1609	prog	2
Geranyl isobutyrate	1493	prog	2	Terpinyl pentanoate	1614	prog	2
Valencane (nootkatane)	1493	150	25	Cedrol	1616	175	27
Farnesene <i>trans,trans</i> - α -	1494	prog	22	Geranyl pentanoate	1632	prog	2
Himachalene β -	1494	prog	22	Cadalene	1646	prog	22
Murolene α -	1495	130	3	Santalol α -	1660	175	27
Bisabolene <i>cis</i> - α -	1496	prog	22	Bisabolol β -	1666	175	27
Bisabolene β -	1496	130	3	Farnesol <i>trans,trans</i> -	1745	175	27
Tetrahydrothujopsane <i>a</i>	1496	150	25	Bornyl benzoate	1749	prog	2
Eudesmane 4 α H,5 α H-	1497	150	25	Farnesyl acetate	1787	200	28
Himachalene γ -	1499	170	4	Nootkatone	1802	prog	2

3. ACKNOWLEDGEMENTS

Drs. J. Brophy and M. Ridd are thanked for their comments and provision of some of the references.

4. SUMMARY

Gas chromatographic retention indices (Kováts' indices) are a valuable aid in the identification of monoterpenes and sesquiterpenes in essential oils and related natural and synthetic products. Some 900 Kováts' indices of 400 individual compounds on methyl silicone (dimethyl polysiloxane) and/or Carbowax 20M liquid phases are summarized from the general literature.

REFERENCES

- 1 E. sz. Kováts, *Helv. Chim. Acta*, 41 (1958) 1915.
- 2 W. Jennings and T. Shibamoto, *Qualitative Analysis of Flavor and Fragrance Volatiles by Glass Capillary Column Gas Chromatography*, Academic Press, New York, 1980.
- 3 N. H. Andersen and M. S. Falcone, *J. Chromatogr.*, 44 (1969) 52.
- 4 N. H. Andersen, P. Bissonette, C.-B. Liu, B. Shunk, Y. Ohta, C.-L. W. Tseng, B. Moore and S. Huneck, *Phytochemistry*, 16 (1977) 1731.
- 5 N. H. Andersen and D. D. Syrdal, *Phytochemistry*, 9 (1970) 1325.
- 6 N. H. Andersen, Y. Ohta, C.-B. Liu, C. M. Kramer, K. Allison and S. Huneck, *Phytochemistry*, 16 (1977) 1727.
- 7 N. H. Andersen, C. R. Costin, C. M. Kramer Jr., Y. Ohta and S. Huneck, *Phytochemistry*, 12 (1973) 2709.
- 8 N. H. Andersen, D. D. Syrdal, B. M. Lawrence, S. J. Terhune and J. W. Hogg, *Phytochemistry*, 12 (1973) 827.
- 9 T. Shibamoto, in P. Sandra and C. Bicchi (Editors), *Capillary Gas Chromatography in Essential Oil Analysis*, Hüthig, Heidelberg, 1987, p. 259.
- 10 P. N. Breckler and T. J. Betts, *J. Chromatogr.*, 53 (1970) 163.
- 11 J. Karlsen and H. Siwon, *J. Chromatogr.*, 110 (1975) 187.
- 12 J. Albaiges and X. Guardino, *J. High Resolut. Chromatogr. Chromatogr. Commun.*, 8 (1985) 301.
- 13 T. Saeed, G. Redant and P. Sandra, *J. High Resolut. Chromatogr. Chromatogr. Commun.*, 2 (1979) 75.
- 14 H. W. Habgood and W. E. Harris, *Anal. Chem.*, 32 (1960) 450.
- 15 H. van den Dool and P. D. Kratz, *J. Chromatogr.*, 11 (1963) 463.
- 16 G. Guiochon, *Anal. Chem.*, 36 (1964) 661.
- 17 R. B. Watts and R. G. O. Kekwick, *J. Chromatogr.*, 88 (1974) 165.
- 18 Y. Guan, J. Kiraly and J. A. Rijks, *J. Chromatogr.*, 472 (1989) 129.
- 19 T. A. van Beek, R. Kleis, M. A. Posthumus and A. van Veldhuizen, *Phytochemistry*, 28 (1989) 1909.
- 20 T. M. Malingre and H. Maarse, *Phytochemistry*, 13 (1974) 1531.
- 21 N. W. Davies, unpublished results.
- 22 S. K. Ramaswami, P. Briscese, R. J. Gargiullo and T. von Geldern, in B. M. Lawrence, B. D. Mookherjee and B. J. Willis (Editors), *Flavors and Fragrances: A World Perspective (Proceedings of the 10th International Congress of Essential Oils, Flavors and Fragrances, Washington, DC, 1986)*, (Developments in Food Science, Vol. 18), Elsevier, Amsterdam, 1988, p. 951.
- 23 A. A. Swigar and R. M. Silverstein, *Monoterpenes*, Aldrich, Milwaukee, WI, 1981.
- 24 Analytical Methods Committee, *Analyst (London)*, 109 (1984) 1343.
- 25 H. Maarse, *J. Chromatogr.*, 106 (1975) 369.
- 26 P. A. Hedin, A. C. Thompson and R. C. Gueldner, *Phytochemistry*, 10 (1971) 1693.
- 27 P. A. Hedin, R. C. Gueldner and A. C. Thompson, *Anal. Chem.*, 42 (1970) 403.
- 28 T. Sakai, H. Maarse, R. E. Kepner, W. G. Jennings and W. M. Longhurst, *J. Agric. Food Chem.*, 15 (1967) 1070.
- 29 R. Ter Heide, *Z. Anal. Chem.*, 236 (1968) 215.
- 30 R. Tressl, L. Friese, F. Fendesack and H. Köppler, *J. Agric. Food Chem.*, 26 (1978) 1426.

- 31 R. Tressl, L. Friese, F. Fendesack and H. Köppler, *J. Agric. Food Chem.*, 26 (1978) 1422.
- 32 R. E. Kepner and H. Maarse, *J. Chromatogr.*, 66 (1972) 229.
- 33 P. A. Hedin, A. C. Thompson and R. C. Gueldner, *Anal. Chem.*, 44 (1972) 1254.
- 34 R. Ter Heide, *J. Chromatogr.*, 129 (1976) 143.
- 35 R. U. Luisetti and R. A. Yunes, *J. Chromatogr. Sci.*, 9 (1971) 624.
- 36 L. Schreyen, P. Dirinck, P. Sandra and N. Schamp, *J. Agric. Food Chem.*, 27 (1979) 872.
- 37 Y. Ohta, *Tetrahedron*, 33 (1977) 617.
- 38 Analytical Methods Committee, *Analyst (London)*, 113 (1988) 1125.
- 39 T. Shibamoto, in *Applications of Glass Capillary Gas Chromatography*, Marcel Dekker, New York, 1981.
- 40 M. Novak, *Phytochemistry*, 24 (1985) 858.

Adsorption effect on the retention volume of hydrocarbons and dialkyl ethers in gas–liquid chromatography using a polar stationary phase and silica gel support

KUNISHIGE NAITO*, TAKASHI SAGARA and SHINSUKE TAKEI

Department of Industrial Chemistry, Faculty of Engineering, Ibaraki University, Hitachi 316 (Japan)

(First received September 27th, 1989; revised manuscript received October 24th, 1989)

SUMMARY

The mechanism of solute retention in gas–liquid chromatography was studied by using silica gel coated with different amounts of polyethylene glycol 20 000 (PEG 20M). The retention volumes of aliphatic hydrocarbons, aromatic hydrocarbons and dialkyl ethers were determined as a function of liquid phase loading. The silica gel surface showed homogeneous characteristics on adsorption of saturated hydrocarbons and a heterogeneous nature on adsorption of the other solutes. The experimental data could be interpreted on the basis of a model in which the silica gel surface was covered first with a monolayer and then with a double layer of PEG 20M. Distribution constants of adsorption on the silica gel, on the monolayer and on the double layer were calculated.

INTRODUCTION

For the quantitative interpretation of the effect of interfacial adsorption on solute retention in gas–liquid chromatography, several workers have proposed the following equation^{1–7}:

$$V_R = K_L V_L + K_A A_L + K_S A_S$$

where V_R is the retention volume of a given solute and K_L , K_A and K_S are distribution constants of bulk solution partitioning into a bulk liquid layer (volume V_L) and adsorption equilibria on the liquid layer (surface area A_L) and the solid surface (surface area A_S), respectively. For practical use of the above equation, a reasonable relationship must be established between the surface areas, A_L and A_S , and the liquid phase loading.

In previous studies using modified alumina as a solid support^{8–12}, we found that the experimental plot of the retention volume of a given solute against liquid phase loading could be divided into four or five regions and each part of the plot could be

fitted to a straight line. From this result, we proposed a model in which the modified alumina surface, involving two subsurfaces with low and high adsorption capacities, was incrementally covered with three different types of the liquid layer, a monolayer, a double layer and a bulk liquid layer, as the liquid phase loading was increased. On the basis of this model, the retention volume of a given solute and the specific surface area of the liquid-coated, modified alumina could be written as a linear function of liquid phase loading in each region. These relationships allowed the distribution constants to be determined for bulk solution partitioning and adsorption equilibria.

In this study, we used silica gel, which had milder and more homogeneous surface characteristics than modified alumina, as a solid support and polyethylene glycol 20 000 (PEG 20M) as a liquid stationary phase. On the basis of the previous model, we tried to interpret the effect of interfacial adsorption on the retention volumes of some hydrocarbons and dialkyl ethers which were determined as a function of liquid phase loading.

EXPERIMENTAL

Fujigel KC-3 silica gel for preparative column chromatography was used as a solid support after sizing into a 60–80-mesh fraction. Chromosorb P was used as a reference support. A 10-g amount of silica gel or 7 g of Chromosorb P were dried at 120°C for 3 h, weighed accurately and suspended in a dichloromethane solution containing the desired amount of PEG 20M. The stationary phase was deposited on the solid support as evenly as possible by evaporating the solvent with occasional stirring. These column packings were packed into stainless-steel tubes (100 × 0.3 cm I.D.) after drying under vacuum at room temperature to remove any volatile components. The newly packed columns were conditioned at 120°C for 15 h in a stream of nitrogen and then for 3 h in a stream of helium.

A Hitachi Model 263-30 gas chromatograph equipped with a thermal conductivity detector was used in conjunction with a Hitachi Model 561 recorder. Gas chromatographic measurements were made at a column temperature of 120°C and with helium as carrier gas at a flow-rate of 40 cm³ min⁻¹. The reduced retention volume, $V_{N,R}$, and liquid phase loading, X_L , were also calculated as described previously⁸.

RESULTS AND DISCUSSION

When Chromosorb P was coated with different amounts of PEG 20M, the reduced retention volume of each solute increased linearly with increasing liquid phase loading. Fig. 1 shows linear plots of $V_{N,R}$ against X_L for some hydrocarbons. These linear plots indicate the dominance of bulk solution partitioning in solute retention. In this instance, the slope of the $V_{N,R}$ vs. X_L line corresponds to the distribution constant of bulk solution partitioning, K'_L , which was defined previously¹². The K'_L values of solutes are listed in Table I. The presence of a small positive intercept for the $V_{N,R}$ vs. X_L curve suggests the concurrent contribution of the interfacial adsorption equilibrium to solute retention. This intercept is probably caused by the effect of adsorption at the gas-liquid interface of the bulk liquid layer of PEG 20M, because the surface of Chromosorb P is completely covered with a liquid layer even at low liquid phase loadings.

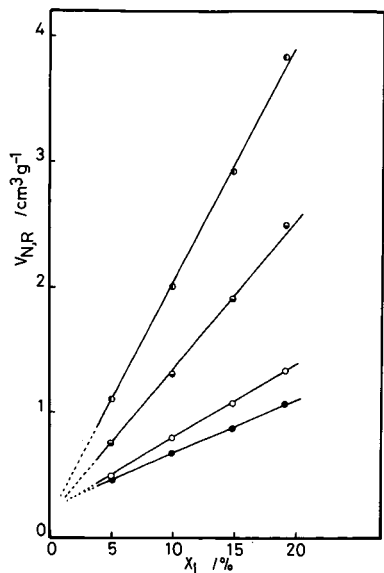


Fig. 1. Dependence of reduced retention volume on liquid loading. Solutes: ●, *n*-hexane; ○, 1-hexene; ◐, cyclohexane; ◑, cyclohexene. Solid support: Chromosorb P.

When silica gel was coated with PEG 20M, the reduced retention volume of unsaturated aliphatic hydrocarbons, aromatic hydrocarbons and dialkyl ethers decreased, first rapidly and then slowly, with increasing X_L . The profile of this curve is similar to those of the $V_{N,R}$ vs. X_L curves observed in previously studies⁸⁻¹². The decrease in $V_{N,R}$ vs. X_L suggests that interfacial adsorption dominates solute retention and does not always correspond to a monotonous decrease in the specific surface area of column packings (Fig. 2). According to the previous view, the rapid decrease in $V_{N,R}$ with increasing X_L up to 11% is due to the deactivation of original solid surface by occupying active sites with molecules of PEG 20M. The slow decrease in $V_{N,R}$ with

TABLE I

DISTRIBUTION CONSTANT FOR THE BULK SOLUTION PARTITION, K'_L

Solute	K'_L ($\text{cm}^3 \text{g}^{-1}$)	Solute	K'_L ($\text{cm}^3 \text{g}^{-1}$)
2-Methylpentane	3.0	Ethylbenzene	104
<i>n</i> -Hexane	4.3	<i>o</i> -Xylene	139
Cyclohexane	12.3	<i>m</i> -Xylene	111
1-Hexene	6.1	<i>p</i> -Xylene	107
2-Hexene	6.7	<i>tert.</i> -Butyl methyl ether	7.4
Cyclohexene	19.2	Methyl <i>n</i> -propyl ether	7.2
<i>n</i> -Heptane	8.3	Ethyl <i>n</i> -propyl ether	8.0
1-Heptene	10.8	Di- <i>n</i> -propyl ether	12.7
2-Heptene	13.1	Diisopropyl ether	6.4
Benzene	38.7	Diethyl ether	4.6
Toluene	65.9		

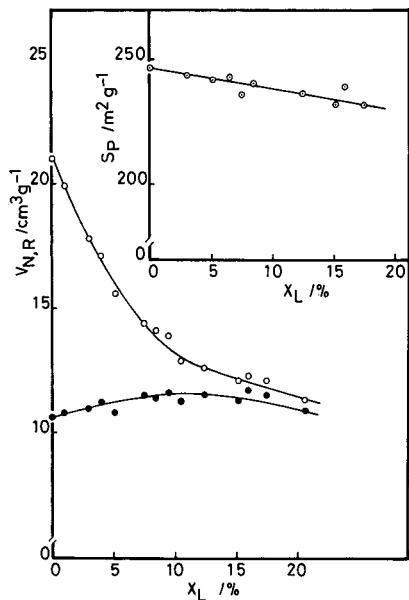


Fig. 2. Dependence of the specific surface area of the column packings and the reduced retention volume on the liquid loading. Solutes: ●, *n*-hexane, ○, 1-hexene. Solid support: silica gel.

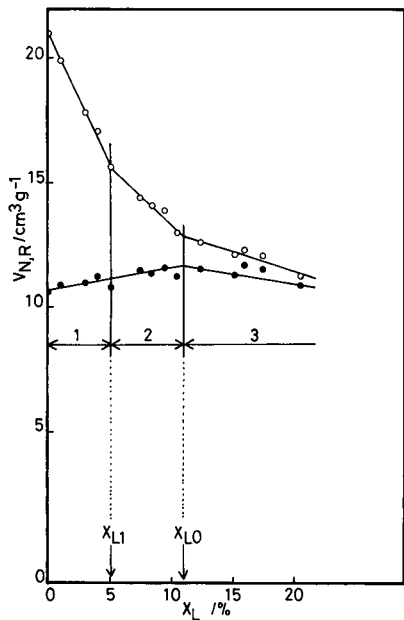


Fig. 3. Linear approximation of the $V_{N,R}$ vs. X_L curve. Solutes: ●, *n*-hexane; ○, 1-hexene. X_{L1} is the liquid loading at which the subsurface 1 is completely covered with a monolayer of PEG 20M.

further increase in X_L is caused by a gradual decrease in the specific surface area of the liquid-coated silica gel.

For saturated hydrocarbons, $V_{N,R}$ increased to a maximum and then decreased with increasing X_L . The almost linear increase in $V_{N,R}$ with X_L up to 11% suggests that bulk solution partitioning is important for solute retention, but the slope is inconsistent with the K'_L value of the corresponding solute listed in Table I. In this range of X_L , molecules of PEG 20M are fixed at active sites on the silica gel surface, so that a bulk liquid layer is not yet formed; there is only a thin liquid film like a monolayer or a double layer on the solid surface. Therefore, interfacial adsorption equilibria must dominate solute retention. From the evidence, we believe that saturated hydrocarbons can interact more strongly with the thin liquid film than with the solid surface, whereas the reverse is true for more polar solutes.

The experimental plot of $V_{N,R}$ against X_L can be approximated by two straight lines for saturated hydrocarbons and three for unsaturated aliphatic hydrocarbons, aromatic hydrocarbons and dialkyl ethers (Fig. 3). Two adjacent lines intersect at the same liquid phase loading (about 11%) for every solute. We took this liquid phase loading as X_{L0} , the liquid phase loading at which the silica gel surface is completely covered with a monolayer of PEG 20M. At liquid phase loadings lower than 11%, the $V_{N,R}$ vs. X_L curve can be approximated by only one straight line for saturated hydrocarbons and with two lines for the other solutes. This result indicates that the original surface of silica gel shows homogeneous characteristics on adsorption of saturated hydrocarbons but a heterogeneous nature on adsorption of the other solutes. The original surface of silica gel essentially involves two subsurfaces with low and high adsorption capacities towards unsaturated aliphatic hydrocarbons, aromatic hydrocarbons and dialkyl ethers. The subsurface with a high adsorption capacity (subsurface 1) corresponds to a part of the silica gel surface containing the surface hydroxyl groups which interact strongly with polar groups such as π -bonds and oxygen atoms of solute molecules. The subsurface with a low adsorption capacity (subsurface 2) corresponds to a different part of the silica gel surface.

Taking this model of the solid surface into account, first the subsurface 1 and then the subsurface 2 should be predominantly covered with a monolayer of PEG 20M in regions 1 and 2, respectively. X_{L1} (about 5%) is the liquid phase loading at which the subsurface 1 is completely covered with a monolayer of PEG 20M. In region 3, the silica gel surface covered completely with a PEG 20M monolayer is further covered with another type of liquid layer of PEG 20M. An apparent adsorption constant, K_{ad} , calculated by dividing the reduced retention volume by the specific surface area of the column packings, was given as a constant value for each hydrocarbon solute regardless of the liquid phase loadings in region 3. This result suggests that the liquid layer formed on the PEG 20M monolayer in this region has the same surface characteristics as the monolayer. Thus, we regarded this liquid layer as a double layer of PEG 20M.

In regions 1 and 2, the specific surface area of the column packing, S_p , is equal to the sum of the surface area of the uncoated part of the solid surface and of the PEG 20M monolayer. S_p can be formulated in the same form as described in a previous paper⁸:

$$S_p = S_s^0 - (\alpha - \beta)X_L \quad (1)$$

where S_S^0 is the specific surface area of the liquid-free silica gel and α and β are proportionality constants for relating X_L with the occupied area and the surface area of the PEG 20M monolayer. Taking K_S and K_A as distribution constants of adsorption equilibria on the uncoated part of the solid surface and on the monolayer, $V_{N,R}$ can be expressed for saturated hydrocarbons as follows:

$$V_{N,R} = K_S S_S^0 + (\beta K_A - \alpha K_S) X_L \quad (2)$$

For the other solutes, $V_{N,R}$ can be described with the same equations as described in the previous paper⁸:

$$V_{N,R} = K_{ad}^0 S_S^0 - (\alpha K_1 - \beta K_A) X_L \quad (3)$$

and

$$V_{N,R} = K_2 S_S^0 - (\alpha K_2 - \beta K_A) X_L \quad (4)$$

in regions 1 and 2, respectively. K_{ad}^0 is the apparent distribution constant of adsorption on the solid surface and is defined by $K_{ad}^0 S_S^0 = K_1 S_1 + K_2 S_2$, where K_1 and K_2 are distribution constants of adsorption equilibria on subsurface 1 (surface area S_1) and subsurface 2 (surface area S_2). These equations can be fitted to the experimental data if $K_A > K_S$ for saturated hydrocarbons, $K_1 > K_2 > K_A$ for the other solutes and $\alpha > \beta$.

In region 3, the silica gel surface has been completely covered with a monolayer of PEG 20M and partly with a double layer of PEG 20M. The specific surface area of column packings is the sum of the surface areas of the double layer and the uncoated part of the monolayer. The following equation can be written for S_P :

$$S_P = S_{LM}^0 + (\alpha' - \beta') X_{L0} - (\alpha' - \beta') X_L \quad (5)$$

where S_{LM}^0 is the specific surface area of column packings at a liquid phase loading of X_{L0} and α' and β' are proportionality constants to relate $X_L - X_{L0}$ with the occupied area and the surface area of the double layer of PEG 20M. In this case, $V_{N,R}$ can be written as

$$V_{N,R} = K_A S_{LM}^0 + K''_{exp} X_{L0} - K'''_{exp} X_L \quad (6)$$

where

$$K''_{exp} = \alpha' K_A - \beta' K'_A - K'_L \quad (7)$$

K'_A and K'_L are distribution constants of adsorption on the double layer and solution partitioning into the double layer.

In this study, we could not find regions 4 and 5 on the experimental plot of $V_{N,R}$ vs. X_L , in which a bulk liquid layer was formed on the solid surface, because we failed in uniformly loading such large an amount of PEG 20M on silica gel. The liquid phase loading, X'_{L0} , at which the silica gel surface was completely covered with a double layer of PEG 20M could not be directly determined from the experimental data. The

TABLE II
DISTRIBUTION CONSTANTS (10^{-5} cm) FOR ADSORPTION EQUILIBRIA

Solute	K_S		K_A			K'_A
			Regions 1 and 2		Region 3	
2-Methylpentane	0.39		0.44		0.43	0.44
<i>n</i> -Hexane	0.43		0.49		0.49	0.49
Cyclohexane	0.43		0.51		0.51	0.50
2-Methylhexane	0.73		0.81		0.79	0.80
<i>n</i> -Heptane	0.80		0.91		0.91	0.95
	K_1	K_2	K_A			K'_A
			Region 1	Region 2	Region 3	
1-Hexene	0.99	0.73	0.55	0.54	0.54	0.51
2-Hexene	1.18	0.84	0.56	0.55	0.56	0.56
Cyclohexene	1.51	0.94	0.61	0.62	0.61	0.60
1-Heptene	1.84	1.39	0.98	0.99	1.01	0.96
2-Heptene	2.48	1.63	1.06	1.05	1.03	0.99
Benzene	2.87	1.68	0.82	0.83	0.85	0.80
Toluene	7.85	3.65	1.49	1.63	1.64	1.50
Ethylbenzene	14.7	6.74	2.61	2.90	3.06	2.46
<i>o</i> -Xylene	21.9	8.23	3.88	3.58	3.50	3.19
<i>m</i> -Xylene	21.2	7.62	2.82	3.20	3.20	2.79
<i>p</i> -Xylene	21.1	7.36	2.81	3.24	3.18	2.76
<i>tert.</i> -Butyl methyl ether	—	32.0	—	2.77	2.16	0.61
Methyl <i>n</i> -propyl ether	32.4	12.6	1.47	1.48	1.07	0.37
Ethyl <i>n</i> -propyl ether	—	24.0	—	2.00	1.75	0.62
Di- <i>n</i> -propyl ether	—	33.9	—	3.52	2.85	1.10
Diisopropyl ether	—	28.5	—	1.88	1.90	0.73
Diethyl ether	34.1	14.0	1.74	1.28	1.01	0.32

proportionality constants α' and β' were calculated by using the relationships $\alpha' = S_{LM}^0/(X_{L0}^0 - X_{L0})$ and $\beta' = S_{LD}^0/(X_{L0}^0 - X_{L0})$, by assuming that $X_{L0}^0 = 2X_{L0}$. S_{LD}^0 is the specific surface area of column packings at X_{L0}^0 and is obtained by extrapolating the experimental relationship between S_p and X_L .

By fitting the equations to the experimental data in the respective regions, distribution constants of adsorption equilibria were determined as listed in Table II. The results show that $K_A > K_S$ for saturated hydrocarbons and $K_1 > K_2 > K_A$ for the other solutes. Similar values of K_A were determined for each solute in two or three different regions. The relatively large fluctuation in the K_A values of dialkyl ethers is due to poor reproducibility of the retention data of the skewed peaks.

The K_L'' value of each hydrocarbon was calculated from the slope of the $V_{N,R}$ vs. X_L plot in region 3 by assuming that $K_A' = K_A$ and that K_A' was equal to K_{ad} in region 3. The two values of K_L'' were different and inconsistent with the K_L' value of the corresponding solute listed in Table I. Negative values of K_L'' were obtained for unsaturated aliphatic hydrocarbons and aromatic hydrocarbons. From these results, we considered that solution partitioning into a double layer of PEG 20M did not take

part in solute retention in this instance. By neglecting the effect of solution partitioning, eqn. 7 can be rewritten as

$$K''_{\text{exp}} = \alpha' K_A - \beta' K'_A \quad (8)$$

The K'_A value of each hydrocarbon solute is in good agreement with the K_A value of the corresponding solute. That $K_A > K'_A$ for dialkyl ether implies that the surface of the PEG 20M monolayer still has polar adsorptive characteristics, which can be effectively suppressed by coverage with a thin liquid film of PEG 20M. In other words, the original surface activity of silica gel is significantly reduced with a monolayer of PEG 20M with respect to adsorption of hydrocarbons but a double layer is required for similar reduction with adsorption of dialkyl ethers. In this study, adsorption dominated the retention of all solutes used.

REFERENCES

- 1 J. R. Conder, D. C. Locke and J. H. Purnell, *J. Phys. Chem.*, 73 (1972) 700.
- 2 V. G. Berezkin, *J. Chromatogr.*, 65 (1972) 227.
- 3 V. G. Berezkin, *J. Chromatogr.*, 159 (1978) 358.
- 4 Z. Suprynowicz, A. Waksmunzki and W. Rudzinski, *J. Chromatogr.*, 67 (1972) 21.
- 5 A. Waksmunzki, W. Rudzinski and Z. Suprynowicz, *J. Chromatogr.*, 74 (1972) 3.
- 6 J. A. Jönsson and L. Mathiasson, *J. Chromatogr.*, 179 (1979) 1.
- 7 D. F. Fritz, A. Sahil and E. Sz. Kováts, *J. Chromatogr.*, 186 (1978) 63.
- 8 K. Naito, H. Ogawa, S. Igarashi and S. Takei, *Anal. Sci.*, 4 (1988) 185.
- 9 K. Naito, S. Wada and S. Takei, *Anal. Sci.*, 4 (1988) 105.
- 10 K. Naito, N. Ohwada, S. Moriguchi and S. Takei, *J. Chromatogr.*, 330 (1985) 193.
- 11 K. Naito, H. Ogawa, S. Moriguchi and S. Takei, *J. Chromatogr.*, 229 (1984) 73.
- 12 K. Naito and S. Takei, *J. Chromatogr.*, 190 (1980) 21.

Improvement of activated carbon for air sampling

JAN RUDLING

National Institute of Occupational Health, 171 84 Solna (Sweden)

(First received July 28th, 1989; revised manuscript received November 10th, 1989)

SUMMARY

In order to improve the charcoal tube method, activated carbon was treated with benzyl chloride (5 and 20%) in methylene chloride and heated (300°C). The carbons were evaluated with regards to water uptake, adsorption of toluene and carbon tetrachloride, desorption characteristics for polar compounds and storage stability of ketones. Carbons treated with benzyl chloride picked up less moisture, showed higher desorption efficiencies for polar compounds and lower catalytic activity compared with untreated carbons and those heat-treated with helium at 800°C. The best results were obtained with 20% benzyl chloride.

INTRODUCTION

The charcoal tube method^{1,2} has for many years been the standard method for the determination of solvent vapours in workplace air. The method is easy to use and, for many industrial hygiene applications, the sensitivity of liquid desorption is sufficient. However, there are factors that limit the general applicability of the method. In humid atmospheres, water vapour is adsorbed and this often significantly reduces the capacity of the carbon for volatile vapours³. Adsorbed water also influences the desorption efficiency (recovery) for polar compounds⁴. Carbon disulphide (CS₂) is a powerful desorbing agent for non-polar compounds, having a low response on a flame ionization detector and short retention time on most gas chromatographic (GC) columns. However, CS₂ does not give quantitative recoveries for many polar compounds^{5,6}. Moreover, the desorption efficiency (DE) depends on the sample load and the ratio of carbon to desorbing agent. Even though it is possible to overcome this problem by the use of polar solvents, *e.g.*, dimethylformamide⁵, or additions to CS₂ such as alcohols, chromatographic problems due to peak overlap can arise. Another problem with activated carbon is decomposition of the sample (especially for ketones) during storage due to catalytic action or chemisorption⁷.

Although the charcoal tube method is being challenged by other, more sensitive techniques employing “weak adsorbents” such as Tenax⁸ and graphitized carbon black⁹ followed by thermal desorption, the advantage of using activated carbon is that it has a superior sampling capacity, particularly for volatile vapours. A method

that is to be used routinely should allow the collection of samples over several hours at a sampling rate that can be achieved with ordinary sampling equipment. A conclusion from our previous studies¹⁰ was that a possible way to improve the charcoal tube method could be to improve the carbon itself. The carbon commonly used, SKC 120, and other carbons, are probably not the optimum choice.

Activated carbons originating from less well defined sources such as peat, wood and coal often contains mineral impurities (metal oxides), generally referred to as ash and oxygen complexes (surface oxides⁴), that constitute the polar sites of the carbon. To decrease the water uptake of the carbon and to raise the DE for polar compounds, these impurities should be removed. An efficient method to reduce the ash content is leaching with hydrofluoric and hydrochloric acid¹¹. A common way to eliminate many oxygen complexes is heat treatment of the carbon with inert gases¹² or hydrogen^{13,14} at 600–1000°C.

At our institution, we have evaluated a number of activated carbons and treatment procedures¹⁵. Seventeen untreated carbons were tested and the best results were obtained with Sorbonorit 3. The procedures studied were acid leaching, heat treatment with reactive gases (air, carbon dioxide, chlorine and hydrogen) and inert gases (helium and nitrogen at 800 and 1000°C). We found that the most efficient procedure was acid leaching followed by heat treatment with helium or a mixture of helium and hydrogen at 800°C for a period exceeding 10 h.

Another approach to make a carbon more homogenous is the deposition of pyrolytic carbon on the surface. This can be done with, *e.g.*, methylene chloride¹⁶ and benzene¹⁷. In a prestudy, we recently found that benzyl chloride in methylene chloride could be used and that 300°C was a useful temperature for this treatment. To eliminate impurities (mostly polyaromatic hydrocarbons) formed in this process, desorption at 500°C was carried out.

The purpose of this study was to evaluate two carbons (based on Sorbonorit 3) treated with benzyl chloride and to compare them with (i) Sorbonorit 3, (ii) SKC 120, which is the most commonly used carbon, (iii) helium-treated Sorbonorit 3, which yielded the best result in a previous study¹⁵, and (iv) Carboxen, a modern carbon prepared from a well defined polymer, porous beads of polystyrene–divinylbenzene.

EXPERIMENTAL

Description of carbons

Three carbons purchased in bulk were used, SKC 120 (SKC, Eighty-Four, PA, U.S.A.), Sorbonorit 3 (Norit, Amersfoort, The Netherlands) and Carboxen 563 (Supelco, Bellefonte, PA, U.S.A.). Sorbonorit 3 was crushed and sieved to the same fraction (20–40 mesh) as the other carbons. Before use, untreated SKC and Sorbonorit 3 were dried at 100°C until constant weight.

Treatments

Acid treatment was effected by leaching the carbons (1 g per 10 ml of solution) with 15% hydrofluoric acid (1 day) and 4 *M* hydrochloric acid (1 day). The carbons were thoroughly rinsed with distilled water until the chloride ions had been removed (pH about neutral) and dried at 100°C.

Benzyl chloride treatment was performed in an erlenmeyer flask by soaking the

carbon (7–8 g) with 25 ml of benzyl chloride (5 and 20%) dissolved in methylene chloride. After 2 days, the methylene chloride was evaporated and the carbon residue was transferred to a furnace. The carbon was conditioned 1.5 h at room temperature before heat treatment (1 l/min nitrogen for 5 h at 300°C followed by 3 h at 500°C).

For thermal treatment a tube furnace was used. The heated zone was *ca.* 30 cm and the sample (7–8 g) was spread out in the centre (about 15 cm) of a quartz tube (diameter 35 mm). Gases were added from a cylinder and the flow-rate was controlled with a rotometer. The heating rate up to the final temperature was 10°C/min. Samples were cooled in an inert atmosphere until a temperature below 100°C was reached. The helium treatment was carried out at 800°C for 20 h (0.5 l/min), preceded by conditioning for 0.5 h at room temperature and 1 h at 200°C.

Treatments of the carbons are summarized in Table I.

Uptake of water

The water uptake was determined by static measurements. Saturated salt solutions giving a constant relative humidity (RH) were placed in 100-ml erlenmeyer flasks and the carbon (50–60 mg) was contained in a threaded basket that was attached to the rubber stopper of the flask. After equilibration for 2 days, the weight increase was recorded and recalculated as microlitres of water per gram of carbon

Uptake of toluene and carbon tetrachloride

Solutions of 0.36 mole fraction of toluene and carbon tetrachloride in hexadecane were used to generate vapours with a relative vapour pressure (vapour pressure/saturated vapour pressure) of 0.36. The solution, contained in a beaker, was placed in the bottom of a vacuum desiccator. The carbon (100 mg), contained in small cups, was weighed and placed in the desiccator. After evacuation and 2 days of equilibration, the weight gain was recorded and recalculated as microlitres of liquid per gram of carbon.

Desorption experiments

Samples (duplicates) were prepared by charging 100 mg of carbon in 3-ml screw-cap vials. The analyte was added to the carbon with a microlitre syringe. Samples were set aside for 1 day (20°C) before desorption and analysis. When the added

TABLE I
TREATMENT OF CARBONS

<i>Designation of carbon^a</i>	<i>Treatment^b</i>
SKC	Conditioned at 100°C before use
Cx	None
Sn	Conditioned at 100°C before use
Sn He	AT + helium 800°C for 20 h
Sn Bc-5%	AT + 5% Bc, 300°C for 5 h + 500°C for 3 h
Sn Bc-20%	AT + 20% Bc, 300°C for 5 h + 500°C for 3 h

^a SKC = SKC 120; Cx = Carboxen 563; Sn = Sorbonorit 3.

^b AT = acid treatment; Bc = benzyl chloride.

amount was 1 μl or less, samples were prepared as mixtures with hexane. The coefficient of variation for these experiments was *ca.* 2% (ref. 10).

Humidified carbon was prepared by the use of saturated salt solutions as described above. The sample addition was then made to the wet carbon.

Samples were desorbed with 1.0 ml of desorbing agent and shaken for a minimum of 1 h. Analyses were made with a Varian 3400 gas chromatograph equipped with a flame ionization detector with the use of standard techniques.

RESULTS AND DISCUSSION

Adsorption of carbon tetrachloride and toluene, at a relative vapour pressure of 0.36, was initially determined (Fig. 1). These experiments give an estimate of the maximum capacity of a microporous adsorbent and they also reveal possible "pore discrimination" effects due to the different critical dimensions of carbon tetrachloride (6.4 Å) and toluene (3.7 Å)¹⁸.

Compared with SKC, the adsorption capacity of untreated Sorbonorit 3 is higher. There is almost no change in capacity after the helium heat treatment (Sn He). Heat treatment removes oxygen but, on the other hand, also decreases the pore diameters. A significant decrease in capacity (carbon tetrachloride) is seen for the carbons treated with benzyl chloride. Deposition of carbon and reactions with surface groups are possible explanations. However, compared with Carboxen, the capacities of the treated carbons are still high.

Adsorption of water vapour was determined at six levels between 45 and 90% RH. These results are presented in Fig. 2. There is a significant difference in the water adsorption pattern between the untreated carbons. SKC shows a poor performance; its water uptake is high at the lowest RH levels (45 and 56%), in contrast to the other carbons. For the Sorbonorit carbon, there is a sharp rise in water uptake between 56 and 66% RH. Helium treatment did not improve this carbon. In fact, there is a

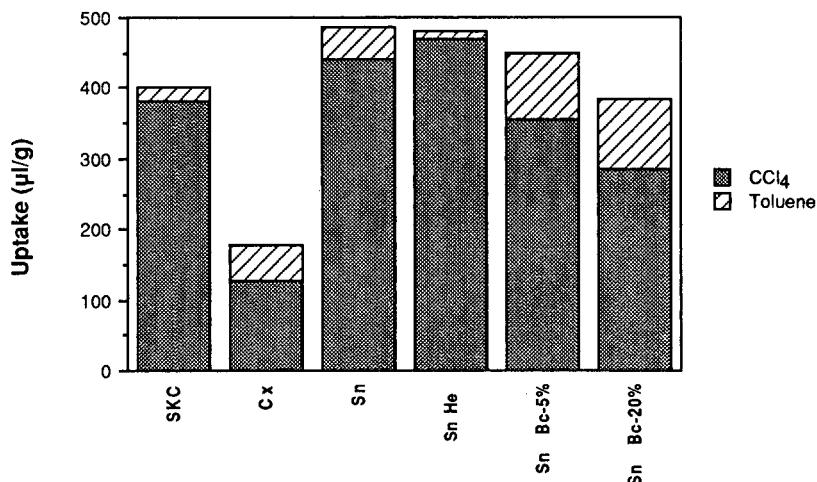


Fig. 1. Adsorption of carbon tetrachloride and toluene at a relative vapour pressure of 0.36. Results given as adsorbed volume (liquid) per gram of carbon.

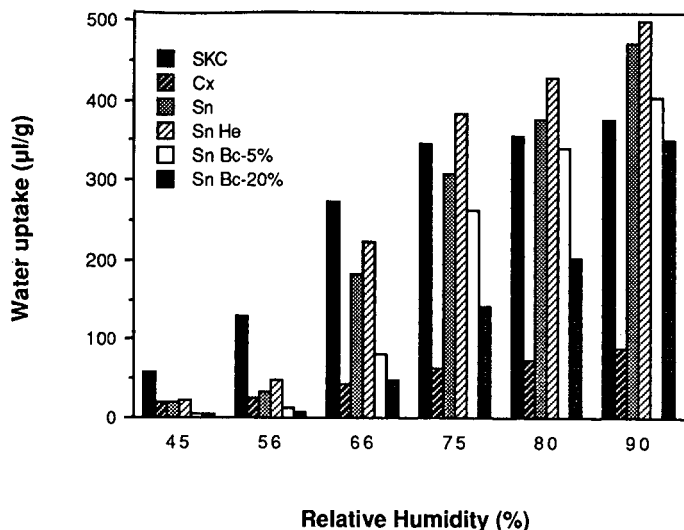


Fig. 2. Uptake of water in microlitres per gram of carbon at different levels of relative humidity.

tendency for increased water uptake that is probably due to a change in the pore structure. The benzyl chloride treatment causes a favourable shift in the water adsorption pattern, especially for the carbon that was treated with a 20% solution (Sn Bc-20%). In this instance, the drastic increase in water uptake commences above 70% RH. Carboxen shows excellent water adsorption characteristics; even at 90% RH the water uptake is small compared with its pore volume.

In a previous study on two carbons (SKC and Merck), we found that the DE for 2-ethoxyethanol (ethyl cellosolve) was extremely dependent on the sample load, whereas for butanol this dependence was not so pronounced¹⁹. Therefore, to evaluate the desorption characteristics for polar compounds, two test series with various amounts of butanol and 2-ethoxyethanol were examined using carbon disulphide as desorbing agent (Tables II and III).

TABLE II

DESORPTION EFFICIENCIES FOR BUTANOL

Experiments (duplicates) made with various amounts of butanol adsorbed on 100 mg of carbon. Desorption made with 1.0 ml of carbon disulphide. DE denotes desorption efficiency.

Carbon	DE (%) for added amount (μ l) of butanol					
	0.03	0.10	0.30	1.0	3.0	10
SKC	50	54	57	65	75	80
Cx	64	69	75	78	84	93
Sn	73	77	82	90	95	98
Sn He	83	88	93	95	98	101
Sn Bc-5%	83	89	94	95	96	98
Sn Bc-20%	89	92	95	96	96	100

TABLE III
DESORPTION EFFICIENCIES FOR 2-ETHOXYETHANOL

Experiments (duplicates) made with various amounts of 2-ethoxyethanol adsorbed on 100 mg of carbon. Desorption made with 1.0 ml of carbon disulphide. DE denotes desorption efficiency.

Carbon	DE (%) for added amount (μ l) of 2-ethoxyethanol				
	0.1	0.3	1	3	10
SKC	< 10	15	33	62	77
Cx	60	63	72	88	91
Sn	48	69	86	94	97
Sn He	78	88	93	97	99
Sn Bc-5%	84	93	97	95	100
Sn Bc-20%	86	93	96	98	99

It is clear that Sorbonorit 3 shows better results than SKC. For both carbons, the DEs for butanol are higher than those of 2-ethoxyethanol (corresponding amounts). For Carboxen, the recoveries (lower range) are also far from quantitative. The effect of the treatments is obvious. Helium treatment, which decreases the amount of oxygen complexes, renders the surface more hydrophobic, which results in a significant improvement in the DE in the lower sample range. The benzyl chloride treatment means a further improvement in the desorption characteristics of the carbon. The variations in DE with sample load for Sn Bc-20% are rather small, and linearity in DE is approached.

A serious problem with solvent desorption when a non-polar solvent such as carbon disulphide is used, is the impact of water on the DE of polar compounds⁴. To study the influence of water, tests were made with a mixture of 0.5 μ l of butanol and 0.5 μ l of 2-ethoxyethanol added to dry carbon and to carbons previously saturated with water vapour at 60 and 75% RH. The results were compared and the RH level giving a decrease in DE of 10% was calculated (Table IV). As expected from previous work⁴, the water uptake pattern (Fig. 1) is reflected in the results.

TABLE IV
INFLUENCE OF WATER ON DESORPTION EFFICIENCY

Calculation of RH level that causes the desorption efficiency to decrease by 10% compared with the desorption efficiency for dry carbon. Experiments (duplicates) done with a mixture of 0.5 μ l of butanol and 0.5 μ l of 2-ethoxyethanol adsorbed on 100 mg of dry carbon and carbons saturated with 60 and 75% RH. As desorbing agent 1.0 ml of carbon disulphide was used.

Carbon	Approximate RH (%)	
	Butanol	2-Ethoxyethanol
SKC	50	< 50
Cx	90	75
Sn	60	50
Sn He	60	50
Sn Bc-5%	70	60
Sn Bc-20%	75	65

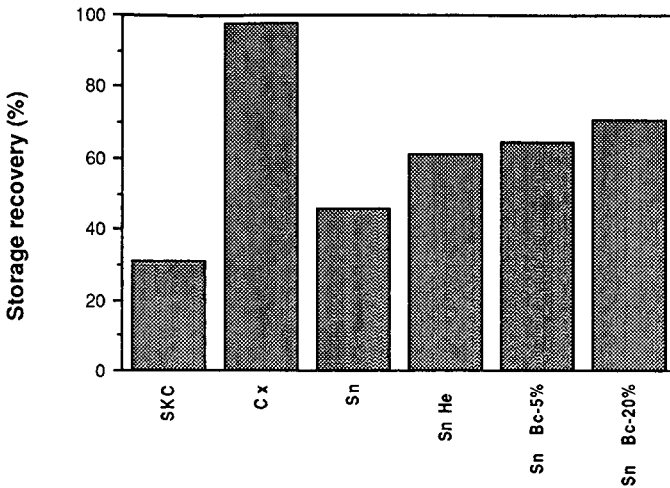


Fig. 3. Recoveries (desorption efficiencies) for samples (duplicates) of cyclohexanone ($3.0 \mu\text{l}$ on 100 mg of carbon) stored for 2 weeks (20°C). Desorption with 1.0 ml of carbon disulphide-acetone (1:1).

To check storage loss of ketones due to chemisorption or catalytic action⁷, storage stability tests (2 weeks at 20°C) with samples of cyclohexanone ($3 \mu\text{l}$ on 100 mg of carbon) were performed. To ensure complete desorption, a mixture of carbon disulphide and acetone was used⁷. The results are presented in Fig. 3. As can be seen, there is no storage loss for Carboxen. Thermal treatment and benzyl chloride treatment reduces the catalytic activity, which is seen as an increase in sample recovery. The test conditions were rough; cold storage is often used to minimize storage losses. When the experiment was repeated with storage for 1 day at room temperature followed by 2 weeks at 0°C ; the sample recoveries for the treated carbons exceeded 90%.

As a conclusion, it can be stated that the treatment with benzyl chloride improves activated carbon in several respects: the water uptake decreases, the DE for polar compounds is significantly increased and the catalytic activity is reduced. However, a slight reduction in capacity is seen. It also appears that treatment with a 20% solution of benzyl chloride yields better results than that with a 5% solution. If a comparison is made with Carboxen, the carbon Sn Bc-20% has a significantly higher adsorption capacity and DEs for polar compounds whereas its water adsorption characteristics above 70% RH and storage stability for ketones are poorer.

It is believed that further improvements will be possible by using other concentrations of benzyl chloride and treatment conditions. The use of a rotating furnace or fluidized bed is a possibility. Possibly benzyl chloride should be fed as a vapour directly to the carbon contained in a heated furnace.

ACKNOWLEDGEMENT

Thanks are due to Mrs Anne-Marie Nilsson-Hagelroth for skilful gas chromatographic analyses.

REFERENCES

- 1 L. D. White, D. G. Taylor, P. A. Mauer and R. E. Kupel, *Am. Ind. Hyg. Assoc. J.*, 31 (1970) 225.
- 2 R. G. Kupel and L. D. White, *Am. Ind. Hyg. Assoc. J.*, 32 (1971) 456.
- 3 A. T. Saalwechter, C. S. McCammon, C. P. Roper and K. S. Carlberg, *Am. Ind. Hyg. Assoc. J.*, 38 (1977) 476.
- 4 J. Rudling and E. Björkholm, *Am. Ind. Hyg. Assoc. J.*, 47 (1986) 615.
- 5 I. Johansen and J. F. Wendelboe, *J. Chromatogr.*, 217 (1981) 317.
- 6 J. C. Posner and J. R. Okenfuss, *Am. Ind. Hyg. Assoc. J.*, 42 (1981) 643.
- 7 J. Rudling, E. Björkholm and B.-O. Lundmark, *Ann. Occup. Hyg.*, 30 (1986) 319.
- 8 R. H. Brown and C. J. Purnell, *J. Chromatogr.*, 178 (1979) 79.
- 9 G. Ciccioli, E. Brancaleoni, R. Fratarcangelli and F. Bruner, *J. Chromatogr.*, 126 (1976) 757.
- 10 J. Rudling, *Thesis*, Royal Institute of Technology, Stockholm, 1987.
- 11 P. L. Walker, Jr., O. C. Caraiso and I. M. K. Ismail, *Carbon*, 18 (1980) 375.
- 12 B. W. R. Puri, in P. L. Walker, Jr. (Editor), *Chemistry and Physics of Carbon*, Vol. 6, Marcel Dekker, New York, 1970, p. 204.
- 13 H. L. McDermot and J. C. Arnell, *J. Phys. Chem.*, 58 (1954) 492.
- 14 Y. Matsumura, K. Yamabe and H. Takahashi, *Carbon*, 23 (1985) 263.
- 15 J. Rudling, *Undersökningsrapport 1989:3*, National Institute of Occupational Health, Solna, 1989.
- 16 R. Leboda, *Chromatographia*, 14 (1981) 524.
- 17 H. Colin, C. Eon and G. Guiochon, *J. Chromatogr.*, 119 (1976) 41.
- 18 J. W. Neely, *Carbon*, 19 (1981) 27.
- 19 J. Rudling, *Appl. Ind. Hyg.*, 2 (1987) 170.

Studies on the selectivity of porous polymers based on polyaromatic esters

B. GAWDZIK

Institute of Chemistry, Maria Curie-Skłodowska University, plac M. Curie-Skłodowskiej 3, 20031 Lublin (Poland)

(First received July 31st, 1989; revised manuscript received November 3rd, 1989)

SUMMARY

Four types of porous polymers containing ester groups were synthesized as stationary phases for gas chromatography using the monomers 1,4-di(methacryloyloxymethyl)naphthalene or 9,10-di(methacryloyloxymethyl)anthracene and styrene or divinylbenzene. The influence of the ester groups in the copolymer skeletons on their selectivities was studied. To determine the selectivities of these copolymers, two procedures were applied: the selectivity triangle and the general selectivity.

INTRODUCTION

Porous polymers are known under various tradenames and differ in their chemical and porous structures. The chemical structure of porous polymers depends on the chemical structure of the monomers used, whereas the porous structure is mainly dependent on the copolymerization conditions. The chemical structure is responsible for the chromatographic properties of porous polymers, in particular the selectivity.

Among various schemes for describing the selectivity of stationary phases, that of Rohrschneider¹, modified by McReynolds², is the most successful. Using this scheme, the selectivity of the phase is characterized by five constants represented by the differences in the Kováts retention indices of test substances (benzene, *n*-butanol, 2-pentanone, 1-nitropropane and pyridine) on the phase under study and on a reference column prepared from squalane, at the same temperature.

In order to determine the selectivity of porous polymers, Smith *et al.*³ adopted the McReynolds method using graphitized thermal carbon black (GTCB), a non-polar sorbent with the same retention mechanism as porous polymers, as a reference phase.

In order to distinguish the contribution of the common retention mechanism (hydrogen-bond donor, acceptor and dipole interaction) in the selectivity of porous polymers, Hepp and Klee⁴ introduced the selectivity triangle, developed earlier by Snyder⁵ for liquid stationary phases in liquid chromatography. In this method, *n*-butanol (hydrogen-bond donor) is used to measure hydrogen-bond acceptor

characteristics, 1,4-dioxane (hydrogen-bond acceptor) to measure hydrogen-bond donor characteristics and nitropropane to measure the dipole characteristics of porous polymers. As retention is governed by the total energy of interaction, the extent to which any selectivity is exhibited depends on the amount of polar interaction relative to non-polar interaction. In order to determine the solute-sorbent dispersive interaction, in this method GTCB was also used as a reference phase.

The aim of this work was to study the influence of the ester groups present in the copolymer skeletons, coming from the monomers of different chemical structure, on their selectivities. In addition to earlier copolymers based on 1,4-di(methacryloyloxymethyl)naphthalene (DMN) and divinylbenzene (DVB)⁶⁻⁸ some new porous copolymers containing ester groups were synthesized. They were formed from constant molar fractions of the following monomers: 1,4-di(methacryloyloxymethyl)naphthalene and styrene; 9,10-di(methacryloyloxymethyl)anthracene and divinylbenzene; and 9,10-di(methacryloyloxymethyl)anthracene and styrene. Their structures are shown in Fig. 1.

In order to determine the selectivities of these copolymers, two procedures were applied: the selectivity triangle^{4,5} and the general selectivity³.

EXPERIMENTAL

Preparation of copolymers

The preparation of porous copolymers was carried out by suspension copolymerization of the following monomers: 1,4-di(methacryloyloxymethyl)naphthalene with divinylbenzene (DMN-DVB), 1,4-di(methacryloyloxymethyl)naphthalene with styrene (DMN-ST), 9,10-di(methacryloyloxymethyl)anthracene with divinylbenzene (DMA-DVB) and 9,10-di(methacryloyloxymethyl)anthracene with styrene (DMA-ST).

Mixtures of the monomers containing 0.5 mole fractions of each monomer with α, α' -azobisisobutyronitrile as an initiator in the presence of a mixture of toluene and *n*-decanol (20:80, v/v) were suspended in an aqueous solution of poly(vinyl alcohol) and polymerized at 80°C for 16 h. The copolymers in the form of beads were washed

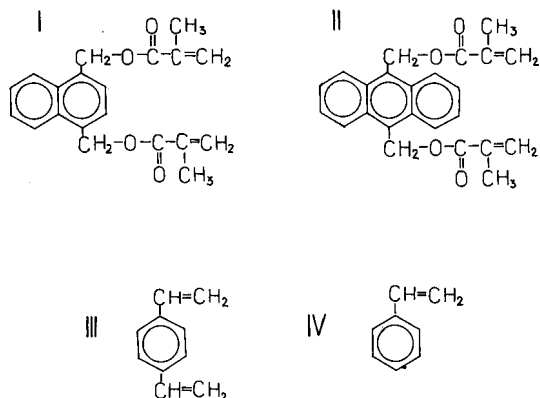


Fig. 1. Structure of the monomers used: I = 1,4-di(methacryloyloxymethyl)naphthalene; II = 9,10-di(methacryloyloxymethyl)anthracene; III = 1,4-divinylbenzene; IV = styrene.

with distilled water, filtered off, dried and extracted in a Soxhlet apparatus with boiling acetone, benzene and methanol. Then the polymer beads were separated on sieves.

For DMN-DVB and DMN-ST copolymers, the volume ratio of diluents to monomers was 1.8:1 but with DMA-DVB and DMA-ST copolymers, the volume ratio of diluents to monomers was increased to 2.8:1 because of their weak solubility in the diluent mixture.

The properties of the synthesized copolymers are summarized in Table I.

Column preparation

The columns were packed with porous polymers in the form of spherical beads. The shape of the beads was confirmed by microscopic examination. The diameter of the sorbent beads was always 0.15–0.20 mm.

Before use, all the columns were conditioned in a stream of hydrogen. The columns (DMN-DVB, DMN-ST and DMA-DVB) were conditioned with temperature programming from 60 to 250°C at 4°C/min and then overnight isothermally at the final temperature. The column packed with DMA-ST copolymer was heated from 60 to 230°C in the same way. Subsequently, the columns were filled and conditioned until the retention times for *n*-alkanes were constant.

Chromatographic measurements

Chromatographic measurements were carried out on a GCHF-18.3 gas chromatograph (Chromatron, Berlin, G.D.R.) equipped with a thermal conductivity detector, using stainless-steel columns (100 cm × 4 mm I.D.), sieve fraction of the copolymers beads 0.15–0.20 mm and hydrogen as carrier gas at a flow-rate of 50 ml/min.

The measurements of retention indices for McReynolds substances (benzene, *n*-butanol, 2-pentanone, nitropropane and pyridine) were carried out at 140°C³ and those of the selectivity parameters (*n*-butanol, nitropropane and 1,4-dioxane) at 200°C⁴. For all the porous copolymers, the relationships between log V_R and carbon number of *n*-alkanes (C₅–C₁₂) were linear at 140 and 200°C; hence the retention indices could be applied for selectivity measurements. The retention time of the peak of air was considered to be the dead time⁹.

TABLE I
PROPERTIES OF COPOLYMERS USED

The specific surface areas were measured on a Sorptomatic 1800 apparatus (Carlo Erba, Milan, Italy) using a standard nitrogen adsorption method; the initial decomposition temperature was determined from the course of the thermogravimetric curve. The thermogravimetric measurements were carried out on a MOM (Budapest, Hungary) derivatograph at a heating rate of 5°C/min in the range 20–500°C in air.

Sorbent	Mole fraction of monomers				Volume ratio of diluents to monomers	Specific surface area, S (m ² /g)	Initial decomposition temperature, T (°C)
	DMN	ST	DMA	DVB			
DMN-DVB	0.5			0.5	1.8	265.0	300
DMN-ST	0.5	0.5			1.8	144.0	280
DMA-DVB			0.5	0.5	2.8	263.0	265
DMA-ST		0.5	0.5		2.8	72.5	250

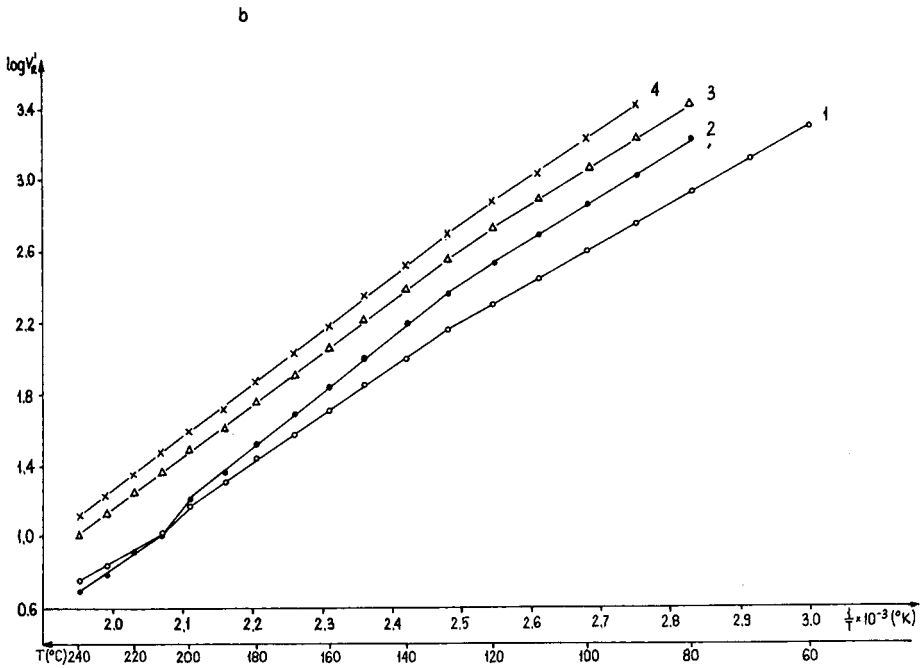
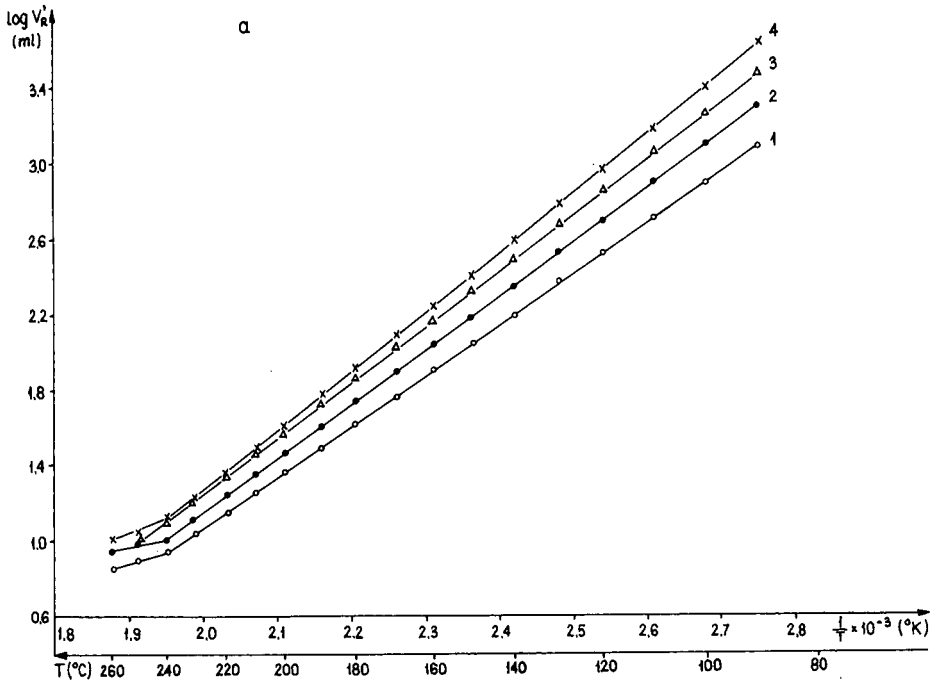


Fig. 2.

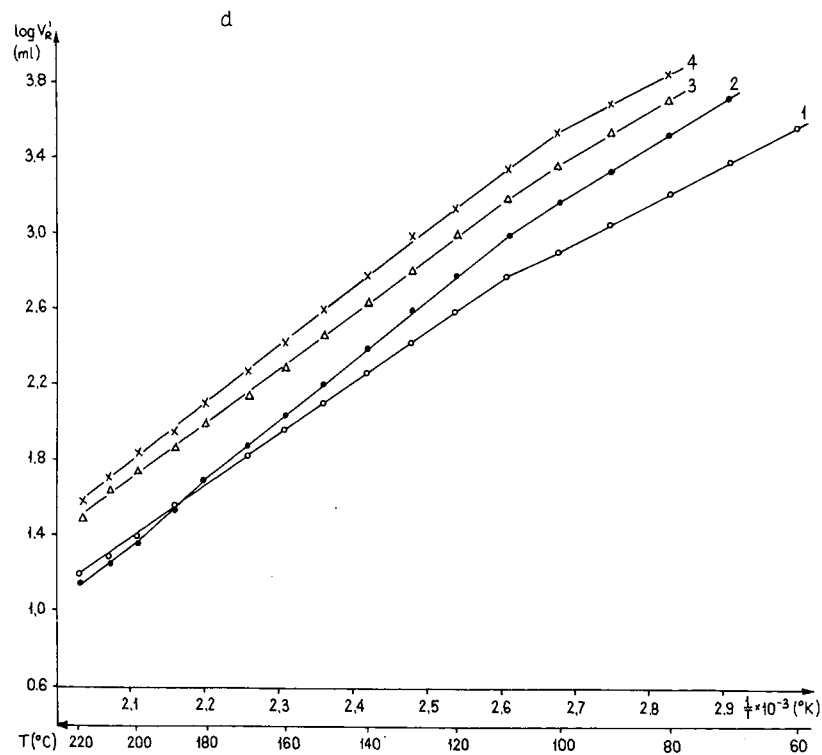
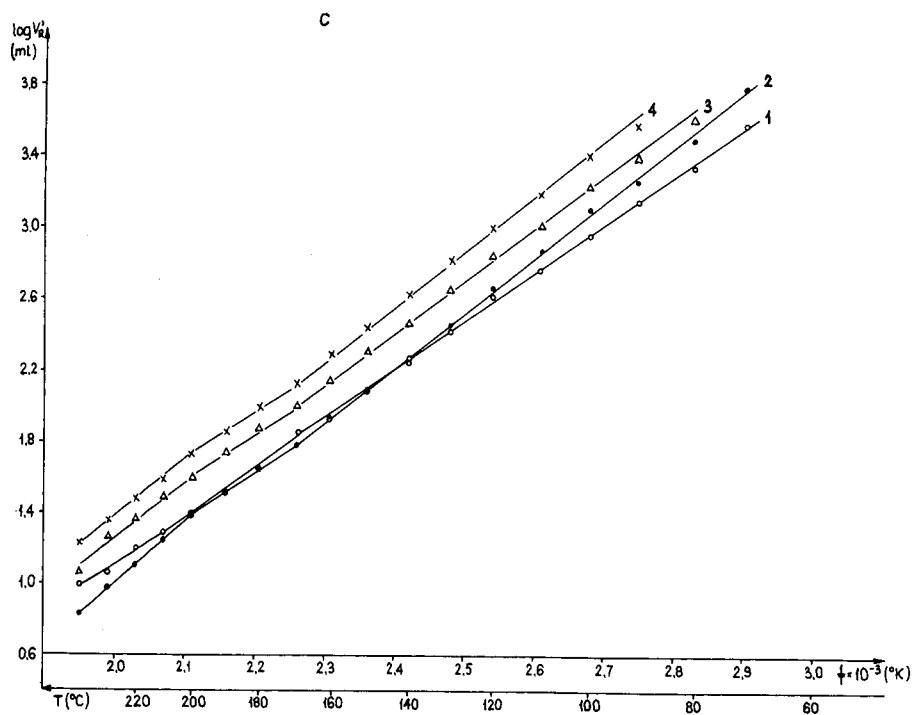


Fig. 2. Specific retention volume as a function of reciprocal of absolute temperature for the copolymers (a) DMN-DVB, (b) DMN-ST, (c) DMA-DVB and (d) DMA-ST. Curves: 1 = Acetone; 2 = hexane; 3 = chloroform; 4 = benzene.

The samples were injected by means of a 1- μ l syringe (SGE, North Melbourne, Australia). Each probe was injected separately, dipping the needle (at the zero position of the piston) into the sample for 1 s³. At least three injections were made for each substance and averaged. The mixture of polar test solutes (acetonitrile, 2-propanol, triethylamine, 1,2-dichloroethane and octane)¹⁰ was also injected at 200°C in an amount of 0.2 μ l.

To determine the phase transition curves of the copolymers, the retention volumes of acetone, *n*-hexane, benzene and chloroform were studied in the range 60–240°C at 10°C intervals. Only for DMA–ST copolymer was the range shortened to 220°C.

Selectivity calculations

The selectivity parameters (x_i) were calculated and plotted on the face of the selectivity triangle by using the equation⁴

$$x_i = \frac{\Delta I_i}{\Delta I_b + \Delta I_n + \Delta I_d}$$

where ΔI_b , ΔI_n and ΔI_d are the McReynolds constants for *n*-butanol, nitropropane and 1,4-dioxane, respectively. The McReynolds' constants (ΔI_i) were calculated by subtracting the average retention indices of the probe solute on GTCB from those on each of the porous copolymers. The values of the retention indices of *n*-butanol, nitropropane and 1,4-dioxane on GTCB were taken from the paper by Hepp and Klee⁴.

The general selectivity ($\Sigma I = x + y + z$) was calculated using the reported retention data of GTCB for benzene (x), *n*-butanol (y) and 2-pentanone (z)¹¹.

RESULTS AND DISCUSSION

It is generally accepted that below the glass transition temperature (T_g), retention on porous polymers is mainly governed by adsorption, whereas at temperatures higher than T_g the contribution due to bulk absorption may be significant, especially with good solvents for copolymer^{12,13}.

In Fig. 2 the phase transition curves are presented. For the highly cross-linked copolymers (DMN–DVB and DMA–DVB) the plots depart only slightly from linearity, but for DMN–ST and DMA–ST copolymers significant deviations from linearity in $\log V'_R$ versus $1/T$ plots occur¹⁴. It should be noted that only for DMN–DVB copolymer were the selectivity measurements carried out below the glass transition temperature. For the others, dissolution can disturb the adsorptive mechanism for some solutes.

In Table II, modified McReynolds constants and the general selectivities (ΣI) for the porous copolymers containing ester groups are presented. Independently of the chemical structure of the monomers used in the copolymerization, the retention indices for McReynolds substances have similar values. The general selectivity indices ΣI , defined as a measure of the polarity of the polymers, indicate that all the studied polyaromatic porous copolymers containing ester groups possess a polar character. Comparing ΣI , it can be seen that polymers obtained by copolymerization of two cross-linking agents (DMN–DVB and DMA–DVB) are slightly more polar than the other two.

TABLE II

KOVÁTS RETENTION INDICES FOR THE McREYNOLDS' TEST SUBSTANCES AND GENERAL SELECTIVITIES (ΣI) FOR THE POROUS COPOLYMERS (140°C)

Copolymer	I					x	y	z	$\Sigma I = x + y + z$
	Benzene	n-Butanol	2-Pentanone	1-Nitropropane	Pyridine				
DMN-DVB	702	745	790	822	831	128	256	225	609
DMN-ST	694	722	749	804	799	120	231	184	537
DMA-DVB	686	751	773	810	857	112	262	208	582
DMA-ST	707	729	757	822	828	133	240	192	565

The retention indices of *n*-butanol (hydrogen-bond donor), 1,4-dioxane (hydrogen-bond acceptor) and nitropropane (dipole) and $\Sigma \Delta I_i$ are given in Table III. It can be seen that for all the copolymers the retention indices for each kind of probe show only small differences. $\Sigma \Delta I_i$, describing the relative polar contributions to retention, are greater than 1000. According to Hepp and Klee⁴, phases with $\Sigma \Delta I_i$ values close to or exceeding 1000 exhibit inherent selectivity. On comparing the selectivity parameters (x_i) for the studied copolymers, one can see that they are more selective for molecules with large dipole moments and hydrogen-bond acceptors.

The location of these copolymers on the selectivity triangle is presented in Fig. 3. As all the copolymers are situated further away from the hydrogen-acceptor corner of the triangle, they would be expected to show little affinity towards hydrogen-donor compounds.

The elution order of the test mixture containing 2-propanol (hydrogen-bond donor), triethylamine (hydrogen-bond acceptor), 1,2-dichloroethane (weak dipole), acetonitrile (strong dipole) and octane (which has no polar interactions) is shown in Fig. 4. The retention of these substances on GTCB is due almost solely to dispersive interactions, hence the solutes elute in order of their boiling points and molar volumes (Table IV)¹⁰.

On all the copolymers, acetonitrile (dipole) is retained longer than 2-propanol (hydrogen-bond donor). Additionally, on DMN-ST and DMA-ST copolymers, 1,2-dichloroethane (dipole) is eluted (co-eluted) after octane. This means that the

TABLE III

KOVÁTS RETENTION INDICES FOR *n*-BUTANOL, NITROPROPANE AND 1,4-DIOXANE AND POROUS COPOLYMERS SELECTIVITY PARAMETERS (200°C)

Copolymer	I			ΔI_b	ΔI_n	ΔI_d	$\Sigma \Delta I_i$	x_{acc}	x_{dip}	x_{don}
	n-Butanol	Nitropropane	1,4-Dioxane							
DMN-DVB	779	894	836	293	388	352	1033	0.284	0.375	0.341
DMN-ST	768	897	830	282	391	346	1019	0.277	0.383	0.340
DMA-DVB	777	887	850	291	381	366	1038	0.280	0.367	0.353
DMA-ST	766	902	838	280	396	354	1030	0.272	0.384	0.344

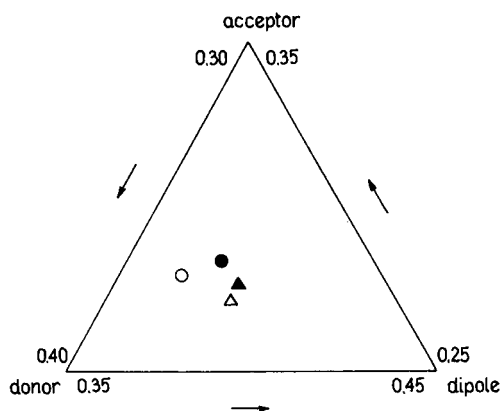


Fig. 3. Selectivity triangle showing relative selectivities of the porous polymers: ● = DMN-DVB; ▲ = DMN-ST; ○ = DMA-DVB; △ = DMA-ST.

selectivities of the copolymers containing ester groups are mainly based on dipole interactions.

DMA-DVB copolymer, with better hydrogen-donating properties than the others, retains triethylamine (hydrogen-bond acceptor) even longer than *n*-octane, but the peak of triethylamine is not symmetrical.

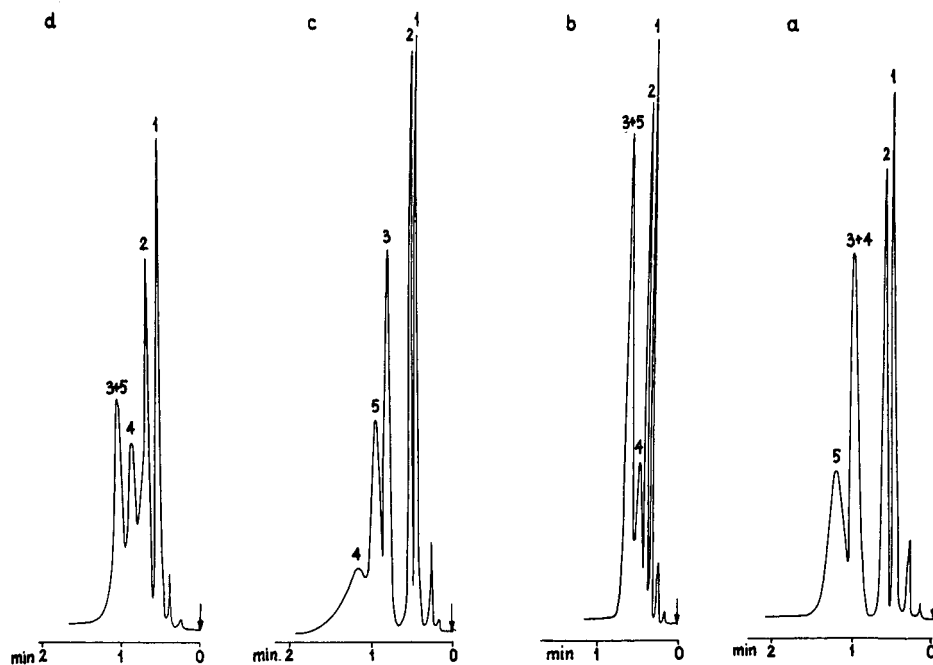


Fig. 4. Chromatograms of the test mixture obtained on copolymers (a) DMN-DVB; (b) DMN-ST, (c) DMA-DVB and (d) DMA-ST. Peaks: 1 = 2-propanol; 2 = acetonitrile; 3 = 1,2-dichloroethane; 4 = triethylamine; 5 = octane.

TABLE IV
 PROPERTIES OF TEST MIXTURE PROBES¹⁰

<i>Solute</i>	<i>Boiling point (°C)</i>	<i>Molar volume (ml/mol)</i>	<i>Dipole moment (Debye)</i>
Acetonitrile	81.6	52.6	3.44
2-Propanol	82.4	76.5	1.66
1,2-Dichloroethane	83.5	79.0	1.86
Triethylamine	89.3	139.1	0.66
Octane	125.7	162.6	0.00

The above results indicate that in spite of the presence of ester groups in the copolymer skeletons, suggesting the same type of interaction between the solute molecules and the sorbents, the polyaromatic copolymers studied show different selectivities. The selectivity of the porous copolymer is a result of the overall chemical structure of the monomers used in the copolymerization.

The important parameters determining the selectivity of the porous polymer towards various compounds are the relative position of the sorbent on the selectivity triangle and the elution order of the test mixture containing a proton donor, proton acceptor, dipole and non-polar probes.

ACKNOWLEDGEMENTS

I express my thanks to Mark A. Hepp and Matthew S. Klee for help and fruitful discussions on this subject.

REFERENCES

- 1 L. Rohrschneider, *J. Chromatogr.*, 22 (1966) 6.
- 2 W. O. McReynolds, *J. Chromatogr. Sci.*, 8 (1970) 685.
- 3 J. R. L. Smith, A. H. H. Tameesh and D. J. Waddington, *J. Chromatogr.*, 151 (1978) 21.
- 4 M. A. Hepp and M. S. Klee, *J. Chromatogr.*, 404 (1987) 145.
- 5 L. R. Snyder, *J. Chromatogr.*, 92 (1974) 223.
- 6 A. Patrykiewicz and B. Gawdzik, *J. Chromatogr.*, 365 (1986) 251.
- 7 A. Patrykiewicz and B. Gawdzik, *J. Chromatogr.*, 369 (1986) 182.
- 8 B. Gawdzik and A. Patrykiewicz, *J. Chromatogr.*, 448 (1988) 233.
- 9 A. Voelkel, *J. Chromatogr.*, 457 (1988) 73.
- 10 M. S. Klee, M. A. Kaiser and K. B. Laughlin, *J. Chromatogr.*, 279 (1983) 681.
- 11 E. V. Kalashnikova, A. V. Kiselev, D. P. Poshkus and K. D. Shcherbakova, *J. Chromatogr.*, 119 (1976) 233.
- 12 J. R. Conder and C. L. Young, *Physicochemical Measurement by Gas Chromatography*, Part I, Wiley-Interscience, New York, 1979, p. 275.
- 13 J. M. Braun and J. E. Guilled, *Macromolecules*, 9 (1976) 340.
- 14 B. Gawdzik and T. Matynia, *React. Polym.*, 5 (1987) 197.

CHROM 22 140

Determination of individual hydrocarbons in automobile exhaust from gasoline-, methanol- and variable-fueled vehicles

FRANK LIPARI

Environmental Science Department, General Motors Research Laboratories, 30500 Mound Road, Warren, MI 48090-9055 (U.S.A.)

(First received August 2nd, 1989; revised manuscript received November 7th, 1989)

SUMMARY

A method was developed for determining individual hydrocarbon (HC) emissions from gasoline-, methanol- and variable-fueled vehicles. The exhaust samples are collected in Tedlar® bags, and a portion of the sample is injected into a gas chromatograph, equipped with a DB-1 60 m × 0.32 mm I.D. (1.0 μm) fused-silica column. Methanol was well resolved from the gasoline HC species and did not interfere in the analysis. Validation, stability and intercomparison studies for total HC are also reported in this paper. In addition, an impinger-gas chromatography (GC) technique for determining unburned methanol emissions is also described. The detection limits of the GC methods for individual HCs and methanol was about 50 and 250 parts per billion (10⁹) C, respectively. This corresponds to a vehicular mass emission rate of 0.1 mg/mile HC and 1.3 mg/mile methanol, respectively, for the Federal Test Procedure emissions test.

INTRODUCTION

Recent reports show that many areas of the country are not in compliance with the National Ambient Air Quality Standard for ozone¹⁻⁴. Consequently, one of the strategies that states and the federal government are considering for meeting the standards is the mandatory introduction of methanol-fueled vehicles. The rationale for this decision is that methanol-fueled vehicles have the potential for improving air quality because of the potentially lower photochemical reactivity of their exhaust emissions. Conversion from gasoline to methanol would replace a large portion of the reactive hydrocarbons (HCs) in gasoline exhaust with less reactive methanol, and thus lower the ozone-forming potential of the exhaust^{5,6}.

Currently, the South Coast Air Quality Management District of California is adopting plans mandating methanol-fueled vehicles as an ozone-control strategy. Additionally, the California Energy Commission will purchase up to 5000 variable-fueled vehicles by 1993 for evaluation and demonstration purposes⁷.

In the past few years, General Motors has been involved in methanol technology development⁸⁻¹¹ and has assembled a fleet of prototype light-duty methanol vehicles^{12,13}. More recently, General Motors has developed a variable-fueled vehicle capable of operating on any combination of methanol or gasoline fuels. In support of these developing technologies, General Motors Research Laboratories needs to identify and measure the emissions of exhaust components from these vehicles that can contribute to air pollution. These components include individual HCs, unburned methanol, and aldehyde emissions that are produced by burning gasoline, methanol, and methanol-gasoline blends in these vehicles. This detailed data then can be incorporated into photochemical models so that air quality benefits of methanol vehicles as compared to gasoline vehicles can be calculated.

The problem that the chromatographer faces is the separation of the unburned methanol from other HC species such as methane, ethylene, acetylene, butane, 1,3-butadiene, pentane, benzene, toluene and many other HCs which are present in the exhaust. Many of the previous gas chromatography (GC) methods developed for measuring individual HCs in exhaust utilized a complicated set-up involving three to four columns coupled with column switching and backflushing¹⁴⁻¹⁸. In addition HCs such as 1,3-butadiene were not adequately resolved by any of these methods¹⁹.

We develop a simple method based on a single capillary column for separating the alkanes, olefins and aromatic HCs from the unburned methanol present in the exhaust. This paper describes the methodology, the validation, and the application of the method to measuring individual HCs in gasoline-, methanol- and variable-fueled vehicle exhaust. In addition, we also describe a modified method for performing methanol measurements so that the methanol and HC emissions can be determined in a single vehicle test.

EXPERIMENTAL

Apparatus

All analyses were performed by using a Varian Vista 6000 gas chromatograph (Varian, Sunnydale, CA, U.S.A.) equipped with a direct capillary injector, gas sampling valve and flame ionization detector. Data collection was performed with a Varian Vista 401 data system. The analytical column for individual HC analysis was a J & W (J & W Scientific, Folsom, CA, U.S.A.) DB-1 60 m × 0.32 mm I.D. (1.0- μ m film) fused-silica capillary column. The analytical column for unburned methanol analysis was a Quadrex (Quadrex, New Haven, CT, U.S.A.) 007 methyl silicone 50 m × 0.53 mm I.D. (5.0- μ m film) Thickote fused-silica capillary column.

Exhaust emissions for HC analyses were collected in 10-l Tedlar[®] bags (SKC, Eight-Four, PA, U.S.A.) that contained both a dual hose/valve fitting and a septum injection port. Exhaust gases for unburned methanol analysis were collected in 25-ml midget impingers (Ace Glass, Vineland, NJ, U.S.A.) containing HPLC-grade water (Fisher Scientific, Pittsburgh, PA, U.S.A.). The exhaust gases were pumped into the Tedlar bags for HC analysis and were drawn through the midget impingers for methanol analysis with a Gilian Model HFS113UT (Gilian, Wayne, NJ, U.S.A.) portable air sampling pump.

Test vehicles

The method was applied to measuring HCs and unburned methanol emissions from both production gasoline- and developmental methanol- end variable-fueled vehicles. As stated earlier, the variable-fueled vehicles were designed to operate on methanol, gasoline or any combination of the two fuels. All the vehicles tested were equipped with production three-way catalytic converters.

Total organics measurement

Previous experience with methanol vehicles indicated that the standard non-heated flame ionization detector used in the emission test cell for gasoline vehicle exhaust HC analysis could not be used for methanol vehicles¹². To minimize methanol losses, a heated flame ionization detector maintained at 125°C was used. Heated sample lines (125°C) from the constant-volume sampling (CVS) dilution system to the analyzer were also used. In addition, an insulated flex pipe was run from the vehicle tailpipe to the CVS dilution tunnel.

Exhaust sampling procedure

Exhaust samples were collected as the vehicles were being tested by using the 1975 Federal Test Procedure (FTP) driving cycle¹⁵. The procedure consists of driving the vehicle on a chassis dynamometer over prescribed driving cycles.

The FTP uses the Urban Dynamometer Driving Schedule (UDDS), which is 1372 s in duration and is composed of two segments; a 505-s "cold start transient" phase and a 867-s "stabilized phase". The 1975 FTP consists of the 505-s cold start "transient" phase and the 867-s "stabilized" phase followed by a 505-s hot start "transient phase". Diluted exhaust samples were collected for both individual HCs and methanol from the CVS system for each of the cold, stabilized and hot phases of the test. The samples were collected at a point just upstream of the CVS heat exchanger. The sampling rate for both the Tedlar bags and midjet impingers was 0.9 l/mjn.

A background air sample from the CVS tunnel dilution air was obtained in Tedlar bags before the test, and the results were subtracted from the results of each of the cold, stabilized, and hot bags.

The methanol samples were collected in single midjet impingers that were immersed in an ice bath. After collection, the samples were transferred to 25-ml volumetric flasks and were diluted to volume with HPLC-grade water. Aliquots (1 μ l) of this solution were then injected on the Quadrex 007 methyl silicone column for the methanol analysis. By using this procedure, only methanol and other water-soluble exhaust gas species were collected, thus eliminating HC interference. The collection efficiency for methanol was in excess of 97% with a single impinger for both standard methanol calibration gases and diluted exhaust samples^{11,12}.

Standard preparation

Certified gas phase standards for many of the alkanes, olefins, and aromatics were purchased from Scott Specialty Gases (Troy, MI, U.S.A.) in Scotty IV cylinders. Serial dilutions were prepared in Tedlar bags by measuring known quantities of these gases with a mass flow meter (Tylan, Carson, CA, U.S.A.) and diluting with HC-free air. Other HC standards were prepared by injecting known quantities of pure HC liquids in a Tedlar bag and diluting with a known quantity of HC-free air.

Aqueous methanol standards for the GC methanol analysis were prepared by injecting known quantities of methanol in HPLC-grade water. Certified gas phase methanol standards in aluminum cylinders were also purchased from Scott Specialty Gases and were used in many of the validation experiments.

Chromatographic conditions

The individual HCs were separated on the DB-1 fused-silica capillary column by using the experimental conditions listed in Table I. These conditions were empirically selected to separate methanol from the C₄-HC species and to provide resolution of as many other HCs as possible.

Unburned methanol was analyzed by a modification of the method of Smith and Urban^{16,17}. In our scheme, exhaust methanol is sampled in a midjet impinger at a lower sampling rate than in the previous procedure, with final analysis by direct injection onto a capillary column. The experimental conditions are listed in Table II. Other capillary columns that produced equivalent results to those of the Quadrex column were the J & W DB-WAX 30 m × 0.53 mm I.D. (1.0- μ m film) and the J & W DB-1 30 m × 0.53 mm I.D. (1.0- μ m film) fused-silica capillary columns.

Compound identification

Individual HCs were identified by comparing their retention times with those obtained with known HC standards. In addition, compounds for which we could not obtain standards were identified by comparing the relative retention times of those GC peaks to those obtained from an independent HC analysis of the fuel²⁰.

Fuels

The gasoline used in these tests was Howell EEE, purchased from Howell (Howell, MI, U.S.A.). Howell EEE is a high-aromatic-content gasoline, similar to the indolene fuel used in emission certification testing.

The methanol used in these tests was purchased from Borden Chemicals and was of greater than 99% purity.

TABLE I
CHROMATOGRAPHIC CONDITIONS OF INDIVIDUAL HYDROCARBON ANALYSIS

Column	DB-1 60 m × 0.32 mm I.D. fused-silica capillary (1.0- μ m film)
Carrier gas	He, 5.75 ml/min
Carrier gas make-up	He, 30 ml/min
Temperature program	-50°C, hold for 4 min, 6°C/min to 110°C, 10°C/min to 140°C, hold for 10 min
Detector	Flame ionization detector (heated to 275°C)
Sample injection	Valco gas sampling valve, heated to 175°C
Sample size	0.5 ml

TABLE II
CHROMATOGRAPHIC CONDITIONS OF UNBURNED METHANOL ANALYSIS

Column	Quadrex 007 methyl silicone, 50 m × 0.53 mm I.D. fused-silica (5.0- μ m film)
Carrier gas	He, 6.50 ml/min
Carrier gas make-up	He, 30 ml/min
Oven temperature	Isothermal, 75°C
Detector	Flame ionization detector
Sample injection	syringe
Sample size	1.0 μ l

RESULTS

Quantitative aspects of this work

One of the ultimate goals of this project was to compare our GC HC results to those obtained by the flame ionization detection (FID) analyzer in the Vehicle Emission Laboratory. To facilitate intercomparison of our GC results with the FID total-HC results obtained in the Vehicle Emission Laboratory, quantitation was performed by calibrating both detectors with propane calibration gas. Since the GC result is the sum of the individual HC results, the GC result and the FID result will agree if the responses of the two detectors are identical or if all HCs give identical responses. On the GC system, we measured the individual HC response factors by injecting known concentrations from the Scott calibration mixtures. The results in Table III show an

TABLE III
CALIBRATION FACTORS FOR SELECTED HC SPECIES

Calibration factor expressed as area counts/ppm C.

<i>Species</i>	<i>Calibration factor</i>	<i>Species</i>	<i>Calibration factor</i>
Methane	1629	Pentane	1409
Ethylene	1392	<i>trans</i> -2-Pentene	1275
Ethane	1389	<i>cis</i> -2-Pentene	1275
Acetylene	1254	2,2-Dimethylbutane	1370
Propylene	1361	Cyclopentane	1375
Propane	1456	Isohexane	1358
Isobutane	1314	Hexane	1383
Isobutylene	1290	Methylcyclopentane	1297
1-Butene	1393	Benzene	1322
1,3-Butadiene	1311	Cyclohexane	1273
<i>trans</i> -2-Butene	1450	3-Methylhexane	1361
<i>cis</i> -2-Butene	1450	Heptane	1389
1-Butyne	1256	Methylcyclohexane	1268
Isopentane	1439	Toluene	1325
1-Pentane	1301		

Average calibration factor 1357 \pm 80

average calibration factor of 1357 ± 80 area units per ppm of HC, expressed as ppm of carbon atoms. This corresponds to a relative standard deviation of 6.0%, which is well within the uncertainty (10%) of some of the Scott certified gas mixtures. Hence, the responses of all HCs are roughly equal, and the GC total-HC results should agree with the vehicle Emission Laboratory FID total-HC results.

Chromatographic aspects of this work

Fig. 1 shows a chromatogram of the Howell EEE fuel used in these studies, vaporized inside a Tedlar bag. The chromatogram shows the excellent resolution obtained for many of the gasoline constituents including butane, isopentane, pentane, isohexane, isooctane, benzene, toluene, *m/p*-xylene and *o*-xylene. Many of the species that we identified both in the fuel and in the exhaust are listed in Table IV.

For the analysis of individual HCs from methanol vehicles, the GC column must adequately resolve methanol from the gasoline HCs. Fig. 2 shows a chromatogram of the Howell EEE fuel, spiked with methanol to simulate exhaust from a methanol-gasoline-fueled vehicle. The non-polar DB-1 stationary phase allows methanol to be eluted early in the chromatogram in a region of relatively few gasoline HC peaks. In actuality, methanol would only interfere with *trans*-2-butene, *cis*-2-butene, 1-butyne and 2,2-dimethylpropane. Typically, the total amount of these four species is about 1% of the total HC emissions from a gasoline-fueled vehicle. In addition, as the percentage of methanol in the fuel was increased, the total concentration of these species decreased, thereby making their contribution to the total HC emission negligible. In short, the method allows excellent resolution of most of the HC species present in vehicle exhaust.

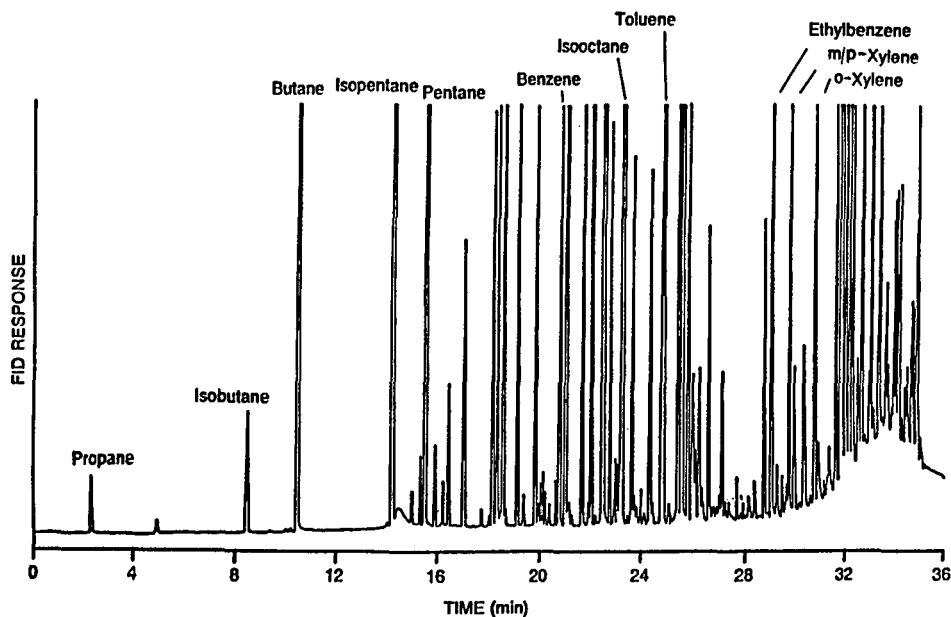


Fig. 1. Chromatogram of vaporized Howell-EEE fuel in a Tedlar bag.

TABLE IV
RETENTION TIMES OF SELECTED HC SPECIES

<i>Species</i>	<i>Retention time (min)</i>	<i>Species</i>	<i>Retention time (min)</i>
Methane	2.33	2-Methyl-2-hexene	23.70
Ethylene	2.53	<i>cis</i> -2-Heptene	23.81
Ethane	2.63	2,3-Dimethyl-2-pentane	24.10
Acetylene	2.73	Methylcyclohexane	24.32
Propylene	4.73	2,5-Dimethylhexane	24.79
Propane	4.97	3,4-Dimethylhexane	24.86
Propyne	6.95	<i>cis</i> -1, <i>trans</i> -2,4-Trimethylcyclopentane	25.07
Isobutane	8.47	2,3,4-Trimethylpentane	25.41
Isobutylene	9.96	Toluene	25.54
1-Butene	10.01	2-Methylheptane	25.78
1,3-Butadiene	10.19	4-Methylheptane	25.97
Butane	10.44	3,4-Dimethylhexane	26.08
<i>trans</i> -2-Butene	11.08	3-Methylheptane	26.23
<i>cis</i> -2-Butene	11.57	<i>cis</i> -1, <i>trans</i> -2,3-Trimethylcyclopentane	26.35
1-Butyne	11.83	2,2,5-Trimethylhexane	26.61
2,2-Dimethylpropane	12.06	C ₈ -Olefins	
3-Methyl-1-butene	13.67	1,1-Methylethylcyclopentane	26.69
Isopentane	14.25	C ₈ -Olefins	26.77
1-Pentene	14.99	<i>trans</i> -4-Octene	26.81
2-Methyl-1-butene	15.32	<i>cis</i> -3-Octene	26.92
Pentane	15.50	Octane	27.11
Isoprene	15.62	2,3,4-Trimethylhexane	27.30
<i>trans</i> -2-Pentene	15.89	<i>cis</i> -1,2-Dimethylcyclohexane	28.00
<i>cis</i> -2-Pentene	16.22	2,4-Dimethylheptane	28.12
2-Methyl-2-butene	16.42	Propylcyclopentane	28.32
2,2-Dimethylbutane	17.00	Ethylbenzene	28.73
Cyclopentene	17.68	<i>m/p</i> -Xylene	28.99
4-Methyl-1-pentene	17.97	4-Methyloctane	29.23
Cyclopentane	18.12	2-Methyloctane	29.45
2,3-Dimethylbutane	18.28	3-Methyloctane	29.62
Isohexane	18.48	<i>o</i> -Xylene	29.73
3-Methylpentane	19.08	C ₉ -Cycloalkanes	
1-Hexane	19.29	Nonane	30.30
2-Methyl-1-pentene	19.34	C ₉ -Cycloalkanes	30.74
Hexane	19.80	2,2-Dimethyloctane	30.86
<i>trans</i> -2-Hexene	19.99	2,4-Dimethyloctane	31.29
<i>cis</i> -2-Hexene	20.34	Propylbenzene	31.59
2,2-Dimethylpentane	20.60	1-Methyl-4-ethylbenzene	31.79
Methylcyclopentane	20.76	C ₁₀ -Cycloalkane	31.86
2-Methyl-2-pentene	20.91	C ₁₀ -Cycloalkane	32.00
2,4-Dimethylcyclopentane	20.96	1-Methyl-2-ethylbenzene	32.17
2,2,3-Trimethylbutane	21.13	3-Ethylcyclohexane	32.28
3-Methyl-1-hexene	21.24	C ₁₀ -Cycloalkane	32.33
Benzene	21.66	1,2,4-Trimethylbenzene	32.67
3,3-Dimethylpentane	21.91	Isobutylbenzene	32.97
Cyclohexane	22.01	Decane	33.03
2-Methylhexane	22.47	C ₁₀ -Aromatics	
2,3-Dimethylpentane	22.74	C ₁₁ -Aromatics	
3-Methylhexane	22.95	Undecane	35.46
Isooctane	23.19	C ₁₂ -Aromatics	
<i>trans</i> -3-Heptane	23.57	Dodecane	38.53
Heptane	23.64		

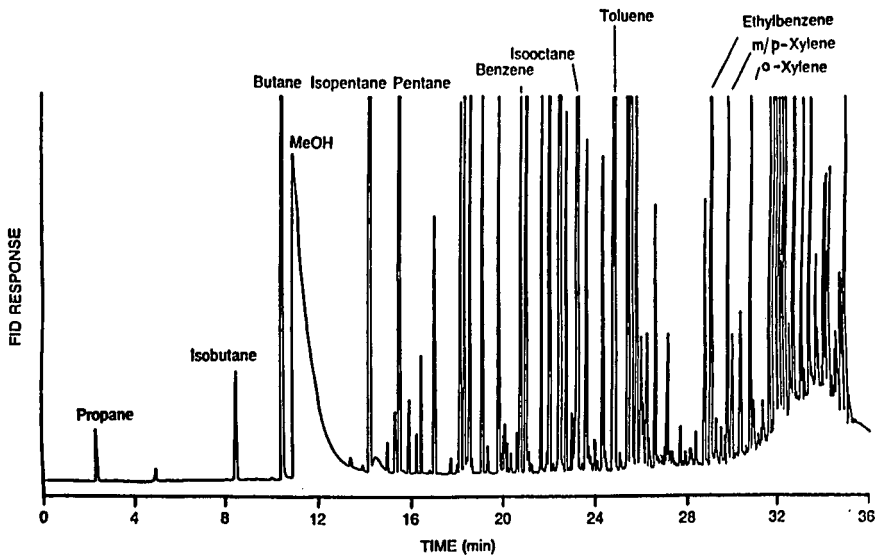


Fig. 2. Chromatogram of vaporized Howell-EEE fuel with methanol in a Tedlar bag. MeOH = Methanol.

Fig. 3 shows a typical chromatogram obtained by placing a HC standard mixture in a Tedlar bag. The elution order, as with all methyl silicone phases, is based on boiling point for members of a homologous series and therefore aids in determining

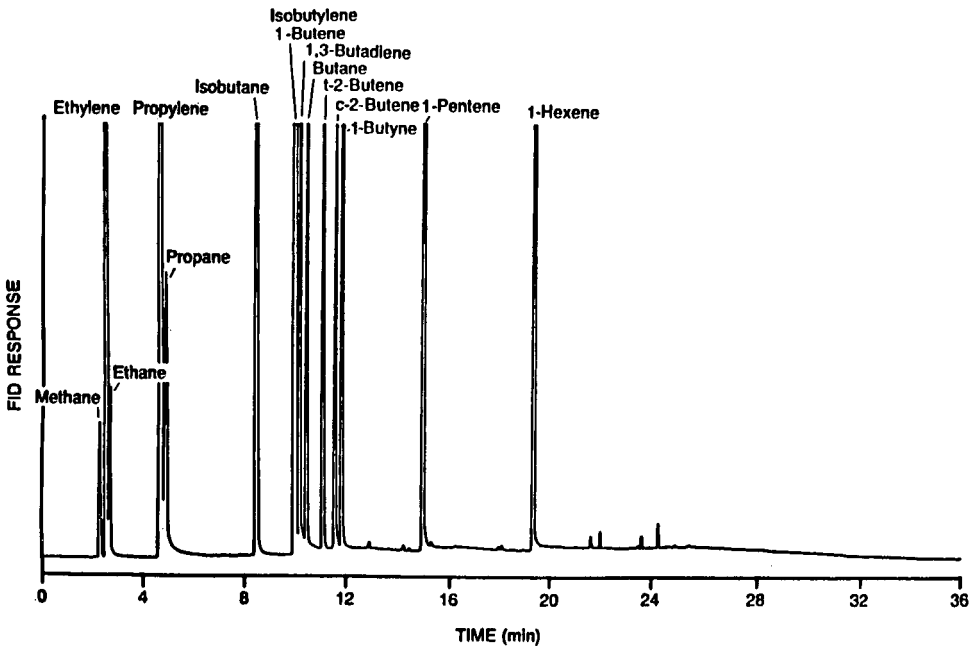


Fig. 3. Chromatogram of HC standards in a Tedlar bag. t = *trans*; c = *cis*.

the elution order for compounds in multicomponent mixtures. This effect is easily seen in the elution of 1-butene, 1-pentene, and 1-hexene in that mixture. The column does an excellent job of separating other olefins such as ethylene from ethane and methane, propylene from propane, and, even more importantly, 1,3-butadiene from butane and other C₄-HC species. This represents a marked improvement over previous attempts to separate 1,3-butadiene from other C₄-HC species.¹⁴

Unburned methanol, which was also collected in the Tedlar bags, was not quantitated by the above procedure because of adsorptive losses of methanol onto the walls of the Tedlar bags. We confirmed these adsorptive losses by placing a known quantity of methanol from a certified methanol calibration gas cylinder inside a bag and repeatedly analyzing gas samples from the bag over a 6-h period. From these experiments, we found that over 70% of the initial methanol disappeared over the 6-h period. In addition, the peak shape for methanol under the GC conditions for the HC analysis was quite poor and not ideal for quantitative integration. Therefore, it was decided that methanol should be collected and analyzed separately from the individual HCs.

Fig. 4 shows a chromatogram of the methanol analysis from one of the neat-methanol-fueled vehicles (M100). The methanol peak shape is very sharp and well resolved from any potential interferences. Acetonitrile, which is a potential interferent, may be present as a contaminant in the water impingers. This is because the aldehyde emission samples, which are collected concurrently with the methanol samples, are collected in impingers containing an acetonitrile solution of 2,4-dinitrophenylhydrazine.²¹ Therefore, cross contamination of acetonitrile from the aldehyde to the methanol impingers can occur and should be avoided. The thick-film Quadrex column provides excellent resolution between methanol and acetonitrile and will eliminate this interference.

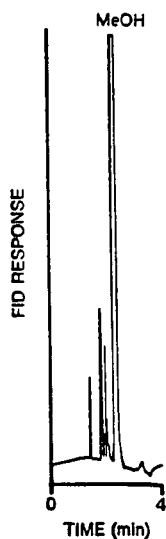


Fig. 4. Chromatogram of cold-start methanol emissions from a dedicated neat-methanol (M100) vehicle.

Fig. 5 is a typical chromatogram showing the cold-bag emissions from the variable-fueled vehicle running on M0 (*i.e.*, 100% Howell EEE). The major HC that was emitted was toluene, which accounted for over 17% of the HC emissions in the cold bag. This result was not unexpected because the toluene content of the Howell EEE fuel can range from 15 to 20%²¹. Ethylene, propylene, isobutylene, isopentane, pentane, benzene and isooctane are other major HCs species emitted, and they accounted for 7.6, 6.1, 4.7, 4.5, 3.1, 3.5 and 8.9% of the total, respectively. 1,3-Butadiene was well resolved from 1-butene and butane and it accounted for about 0.6% of the total HC emissions in the cold bag.

Fig. 6 shows a chromatograms of the cold-bag emissions from the variable-fueled vehicle running on M85 fuel (*i.e.*, 85% methanol and 15% Howel EEE). The methanol peak was completely resolved from the HC peaks. The HC peaks are mainly derived from the gasoline portion of the fuel as evidenced by the characteristic pattern of gasoline HC present in the exhaust. Toluene was the most abundant HC and accounted for over 13% of the total HC in the exhaust. Ethylene, propylene, isobutylene, isopentane, pentane, and benzene are also present, and these accounted for 11.7, 7.3, 5.0, 5.2, 3.7, and 3.8% of the total, respectively.

Fig. 7 shows a chromatogram of the cold-bag emissions from a developmental vehicle that was dedicated to run on neat methanol (M100). It was evident that the major organic species emitted in the cold bag from M100 combustion was methanol. Methane, ethylene, propylene, propane, propyne and isobutylene are other HCs that were present in the cold bag. These species comprise 35.8, 10.0, 3.2, 10.6, 31.1 and 3.1%, respectively, of the total HC emissions. The total HC emissions were about 6.5 ppm C which was about a factor of ten lower than the total HC emissions from a gasoline (M0) vehicle test.

GC column HC recovery experiments

Potential adsorption of HCs on the GC column was evaluated in a series of experiments in which we injected both known HC calibration standards and gasoline

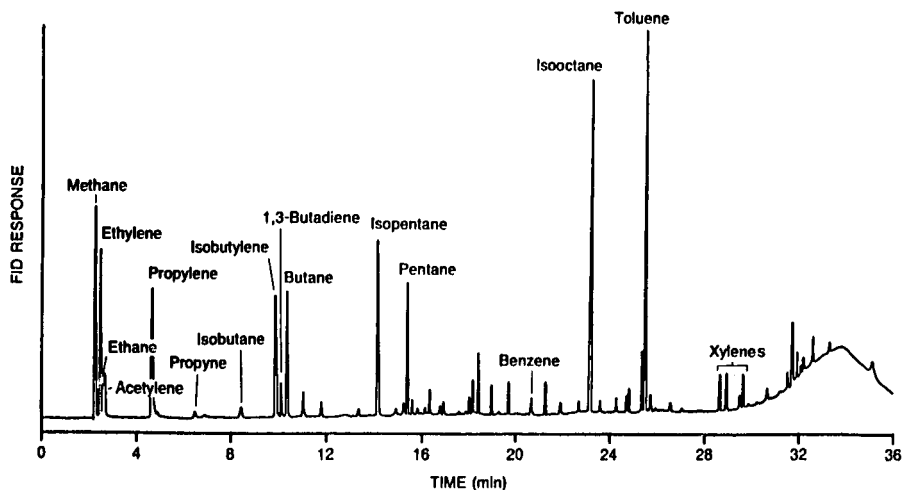


Fig. 5. Chromatogram of cold-bag emissions from a variable-fuel vehicle run on 100% Howell-EEE (M0).

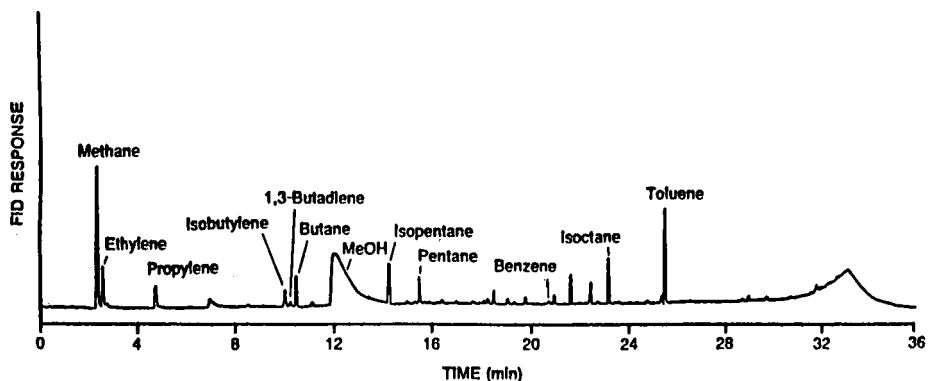


Fig. 6. Chromatogram of cold-bag emissions from a variable-fuel vehicle run on 85% methanol and 15% Howell-EEE (M85).

vehicle exhaust samples using the normal GC temperature program and an elevated isothermal temperature of 125°C. The high-temperature isothermal run was chosen so that all the exhaust HC components would be eluted into several large peaks in a short time period. The total area of the peaks was then compared without regard to resolution of the individual species, to the total area that was obtained by running the normal temperature program. These results, shown in Table V, indicated that the sum of the individual peak concentrations of the exhaust sample and standards agreed to within 97% of the total area obtained with the high-temperature isothermal run.

In another experiment, we replaced the analytical column with a 1 m × 0.53 mm I.D. piece of uncoated, deactivated fused-silica capillary tubing and reinjected the same gasoline exhaust and standard samples at the high-temperature conditions. In this case, the HCs were not separated, but eluted as one large sharp peak. As before, we found that the total area of both the exhaust and standard samples agreed to within 97% of the total area of the high-temperature runs.

These results suggested that no adverse adsorption effects of organics were

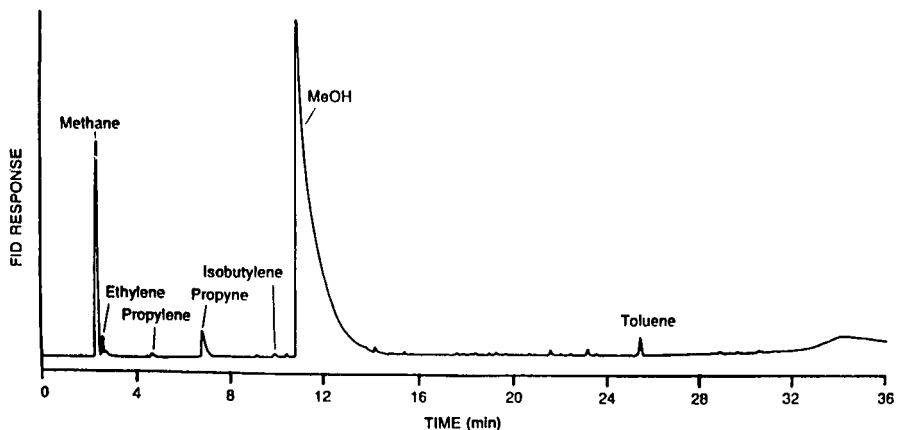


Fig. 7. Chromatogram of cold-bag emissions from a dedicated M100 vehicle.

TABLE V
INTERCOMPARISON OF HC RECOVERY STUDIES

Species	Total concentration (ppm C)		
	DB-1 column, normal GC program	DB-1 column, 125°C isothermal	Uncoated fused-silica, 125°C isothermal
C ₁ -C ₄ Alkanes ^a	51.2	52.1	50.6
Toluene ^a	22.7	22.4	21.1
Cold bag (M0) ^b			
Gasoline vehicle	31.4	31.8	30.8

^a Gas standards in a Tedlar bag.

^b Vehicle exhaust.

occurring and that the individual HCs, including the higher-molecular-weight constituents, were being quantitatively eluted from the column during the normal GC temperature program.

Sample and standard stability studies

Because of the large number of samples that can be collected in a day, the analyst usually does not have sufficient time to analyze all the samples in a typical working day. Therefore, it is important that the exhaust HC samples are stable in the Tedlar bags and do not degrade with time. We examined the stability of both exhaust and standard HC calibration samples in Tedlar bags by periodically analyzing samples from the bags over a 48-h time period. The data in Table VI show that most of the alkanes and olefins are stable in the bag and that the variation in average concentration in the bag was about 1-6% over a 48-h time period. The average concentration for 1,3-butadiene, ethylbenzene, *m/p*-xylene, and *o*-xylene varied by about 40.0, 13.3, 10.5, and 10.7%, respectively over a 48-h time period. In addition, the concentration of 1,3-butadiene continually decreased by over 25% within 24 h and by over 70% within 48 h of sample collection. Although not shown in Table VI, the total integrated area for the cold bag of a gasoline vehicle test did not vary by more than 5% over 24 h, thereby indicating that the exhaust HCs are stable in the bag. In addition, we spiked another cold-bag exhaust sample from a gasoline vehicle test with methanol and monitored the total peak area over a 24-h time period, and again found that the total HC peak area did not vary by more than $\pm 5\%$. These results show that methanol does not have any adverse effects on the exhaust HC stability in the bag.

Similarly, HC standards prepared in Tedlar bags were analyzed over a 48-h period (Table VII). In these experiments, C₁-C₆ normal alkanes, C₄ olefins, benzene, and toluene were prepared in separate bags and analyzed over a 48-h period. The data showed that the average concentration of these species varied from 0.6 to 2.5% over the 48-h period.

The exhaust sample bags were stored at room temperature under normal laboratory lighting. However, precautions were taken to avoid exposure to sunlight and possible photochemical effects during transport from the vehicle Emission Laboratory to the analytical laboratory. The most important sample, and therefore the first

TABLE VI

EXHAUST HC STABILITY STUDY OF THE COLD-BAG EMISSIONS FROM THE VARIABLE-FUELED VEHICLE RUN ON M0

R.S.D. = Relative standard deviation.

Species	Concentration (ppm C)				Average concentration (ppm C)	R.S.D. (%)
	Time (h)					
	0.2	4	24	48		
Methane	5.44	5.19	5.14	5.32	5.27	2.66
Ethylene	2.59	2.58	2.56	2.55	2.57	0.78
Propylene	2.03	1.93	1.94	1.88	1.94	3.10
Propane	0.26	0.25	0.26	0.26	2.04	3.85
Isobutylene	1.92	1.96	1.75	1.92	0.25	6.25
1,3-Butadiene	0.22	0.17	0.14	0.07	0.15	40.00
Butane	1.49	1.44	1.44	1.43	1.45	2.07
Isopentane	2.23	2.21	2.25	2.19	2.22	1.35
Pentane	1.66	1.63	1.61	1.60	1.62	1.85
Isohexane	0.56	0.54	0.56	0.53	0.55	3.64
Benzene	1.46	1.45	1.44	1.36	1.43	2.80
Isooctane	2.45	2.41	2.44	2.35	2.41	1.66
Toluene	5.37	5.27	5.21	4.75	5.15	5.24
Ethylbenzene	0.32	0.27	0.27	0.34	0.30	13.33
<i>m/p</i> -Xylene	0.41	0.38	0.41	0.33	0.38	10.53
<i>o</i> -Xylene	0.27	0.24	0.26	0.19	0.24	16.67
Propylbenzene	0.54	0.48	0.52	0.53	0.52	5.77
Others	7.34	7.09	7.32	7.09	7.21	1.94

TABLE VII

STABILITY STUDY OF HC STANDARDS PLACED IN TEDLAR BAGS

Species	Concentration (ppm C)				Average concentration (ppm C)	R.S.D. (%)
	Time (h)					
	0.2	4	24	48		
Methane	9.57	9.48	9.40	9.37	9.45	0.95
Ethane	9.62	9.42	9.49	9.50	9.51	0.84
Propane	10.33	10.42	10.20	10.22	10.29	0.97
Butane	10.68	10.42	10.66	10.50	10.56	1.23
Pentane	11.43	11.62	11.44	11.32	11.45	1.05
Isopentane	10.53	10.64	10.22	10.18	10.39	2.12
Propylene	8.40	8.50	8.10	8.15	8.29	2.20
1,3-Butadiene	6.39	6.28	6.31	6.16	6.28	1.59
Isobutylene	8.29	8.43	8.26	8.10	8.27	1.69
Benzene	18.82	18.93	18.65	17.89	18.57	2.53
Toluene	19.85	19.95	19.68	19.92	19.85	0.60

TABLE VIII
 INTERCOMPARISON OF VEHICLE EMISSION LABORATORY FID AND GC EXHAUST HYDROCARBON METHOD MEASUREMENTS
 Diff. means percentage difference of GC versus the FID value.

Vehicle	Fuel	Concentration (ppm C)		Cold bag		Stabilized bag		Hot bag	
		FID/GC	Diff. (%)	FID/GC	Diff. (%)	FID/GC	Diff. (%)	FID/GC	Diff. (%)
Gasoline A	Howell-EEEE ^a	36.19/ 34.20	5.6	1.27/0.53	50.8	9.13/ 7.52	17.8		
Gasoline B	Howell-EEEE	37.59/ 32.55	13.4	1.11/0.79	28.8	7.05/ 5.80	17.7		
Gasoline C	Howell-EEEE	35.40/ 31.88	9.9	1.35/0.85	37.0	18.60/16.74	10.0		
Gasoline D	Howell-EEEE	45.39/ 43.72	3.7	1.11/0.66	10.5	8.37/ 7.69	8.1		
Gasoline E	Howell-EEEE	51.78/ 47.83	7.6	3.12/3.23	+3.5	14.85/12.44	16.2		
Variable fuel	Howell-EEEE ^a	82.12/ 69.50	15.4	6.24/4.98	20.2	14.85/11.59	22.0		
Variable fuel	methanol ^{a,b}	143.91/163.76	+ 13.7	4.41/0.20	95.4	2.37/ 0.36	84.8		

^a Average of two tests.

^b Methanol means neat methanol.

bag analyzed, was the cold bag. Efforts were made to analyze the cold bag within 1 h after collection in the VEL.

The stability of the aqueous methanol samples and standards was also evaluated by repeated analysis over a two-week period. Similarly, we found that both the samples and standards stored in the laboratory at room temperature did not show any significant deterioration over two-week period, but refrigeration would assure good quality control. In actual practice, the samples, once received from the Vehicle Emission Laboratory, were transferred into graduated vials and stored at 4°C in a refrigerator.

Linearity and detection limits

The linearity of the GC method for HCs was evaluated by injecting known concentrations of propane, butane, isooctane, and toluene at concentrations ranging from 3 to 200 ppm C. At these concentrations, no deviation from linearity was observed.

The linearity of the methanol method was evaluated by injecting standard aqueous solutions ranging from 7.9 to 790 µg/ml methanol. Again no deviation from linearity was observed.

The detection limit of the GC method for individual HCs was about 50 parts per billion (10⁹) C based on a signal-to-noise ratio of three and a 0.5-ml sample size. This corresponds to a vehicular mass emission rate of about 0.1 mg/mile HC for the FTP test.

The detection limit of the aqueous methanol GC method was about 0.25 ppm methanol based on a 25-ml impinger sample and a 8-l exhaust gas volume. This corresponds to a vehicular mass emission rate of about 1.3 mg/mile methanol for the FTP test.

DISCUSSION

Method validation and application

The method was validated by measuring the individual HC emissions and methanol emissions from vehicles running on M0 and M100, and then comparing the results to the total HC emissions measured with the FID analyzer in the Vehicle Emission Laboratory. By using this approach, the two methods should give equivalent results by using these two fuels. By using M0, the sum of the individual HC concentrations determined by GC should be equivalent to the total HC concentration reported by the FID analyzer. By using M100, the methanol determined by the GC method should be equivalent to that reported by FID if the FID analyzer is properly calibrated. Because of the lower FID response of methanol on a ppm C basis relative to propane, we calibrated the FID analyzer with methanol calibration gas and determined the overall methanol response factor. We then used the methanol response factor to calculate the concentration of methanol in the exhaust. The results should agree, assuming that the HC emitted by using M100 was negligible. Looking at Fig. 7, we can see that this assumption was valid, thus making additional intercomparisons meaningful.

Table VIII summarizes the intercomparison results. There was very good agreement in the cold-bag emissions between the Vehicle Emission Laboratory FID results

and the total GC HC results for both the M0 and M100 vehicles. The differences between the two methods for the cold-bag emissions ranged from 3 to 13%. There was also rather good agreement for the hot-bag emissions between the two methods for the gasoline test and the differences in this case ranged from 8 to 18%.

The differences in the stabilized-bag emissions results for the two methods appear large, but in fact, have little effect on the composite FTP results. The main reason is that both the methanol and the HC emissions are extremely low during the stabilized portion of the FTP and approach background-air levels of 3–4 ppm C. The inherent uncertainty of subtracting two very small numbers (*i.e.*, the stabilized and background air bags) is present in both the GC and FID analysis techniques, and thus gives rise to the imprecision. In addition, small changes in the background-air HC levels during the test could affect the results, especially at these extremely low levels. The background-corrected Vehicle Emission Laboratory FID HC emissions during the stabilized portion of the test ranged from 1.1 to 3.7 ppm C, while the background-corrected emissions for the GC HC emissions ranged from 0.29 to 3.23 ppm C for the stabilized portion of the test. Considering that the overall levels are barely above background, large variations are not surprising.

Similarly, attention should be given to the large discrepancy between the FID and GC results for the hot-start portion of the FTP for the M100 vehicle. As with the stabilized bag, the catalyst dramatically reduces unburned methanol emissions in the hot-start phase to near detection limit levels. As before, the uncertainties involved in subtracting these small background and sample levels exaggerate the variability.

We also assessed the accuracy of the impinger GC methanol method by collecting known volumes of Scott certified methanol calibration gas in dual impingers connected in series and analyzing these samples by GC. The results of these experiments, shown in Table IX, indicated that the GC methanol method results agreed very well with the Scott certification value, with the differences between the two methods ranging from 2.4 to 9.2%. Although not shown in Table IX, we found that more than 97% of the methanol was collected in the first impinger for both these laboratory tests and for preliminary exhaust emissions tests on an M100 vehicle. This reconfirmed our previous findings and ensured that methanol was effectively collected for these tests.

TABLE IX
INTERCOMPARISON OF METHANOL MEASUREMENT METHODS

<i>Concentration (ppm methanol)</i>		
<i>Scott certified value^a</i>	<i>GC method</i>	<i>Difference (%)</i>
29.2	31.9	9.2
47.6	50.4	5.9
93.8	96.1	2.4
496.0	464.6	6.3
Average 6.0 ± 2.8		

^a Certification value ± 5%.

CONCLUSION

We have developed a method for determining individual exhaust HCs from gasoline-, methanol- and variable-fueled vehicles. This method, in conjunction with an impinger-GC method for methanol, allows one to determine the methanol and non-methanol exhaust HC from methanol- and variable-fueled vehicles. The data that can be generated, along with detailed aldehyde data which are also collected during vehicle tests, should provide the necessary input for atmospheric models that assess the photochemical impact of methanol- and variable-fueled vehicles as compared to gasoline-fueled vehicles.

ACKNOWLEDGEMENTS

I thank the following individuals: Fayette Colden (retired) and Robert Potter of Advanced Engineering Staff for their cooperation in supplying and preparing the vehicles used in these tests; Russell Adams of Advanced Engineering Staff for collecting the samples generated from the emission tests; and Dr. Ronald Williams of the Environmental Science Department for his helpful discussions and inputs during the course of this project.

REFERENCES

- 1 *Business Week*, June 29 (1987) 100.
- 2 *Chem. Eng. News*, August 10 (1987) 19.
- 3 *Air Quality Benefits of Alternative Fuels, EPA Draft Report*, prepared by Interagency Task Force on Alternate Fuels, Office of Mobile Sources, Ann Arbor, MI, June 1987.
- 4 D. Moses and C. Saricks, *SAE Paper No. 872053*, Society of Automotive Engineers, Toronto, November 1987.
- 5 R. J. Nichols and J. M. Norbeck, *APCA Paper No. 85-35.3*, Air Pollution Control Association, Detroit, MI, June 1985.
- 6 J. W. Shiller, *Paper Presented at Specialty Workshop on Post 1987 Ozone Issues, San Francisco, CA, November 18, 1987*. Air Pollution Control Association-Golden West Chapter, San Francisco, CA.
- 7 *Proceedings of the APRAC Methanol Workshop, Atlanta, GA, April 19-21, 1988, CRC Report No. 564*. Coordinating Research Council, Atlanta, GA 1988.
- 8 D. L. Hilden and F. B. Packs, *SAE Paper No. 760378*, Society of Automotive Engineers, Detroit, MI, February 1976.
- 9 R. R. Toepel, J. E. Bennethum and R. E. Heruth, *SAE Paper No. 831744*, Society of Automotive Engineers, San Francisco, CA, November 1983.
- 10 J. E. Bennethum and N. Srinivasan, *Proceedings VI International Symposium on Alcohol Fuels Technology*, 1 (1984) 38.
- 11 F. Lipari and D. Keski-Hynilla, *SAE Paper No. 860307*, Society of Automotive Engineers, Detroit, MI, February 1986.
- 12 F. Lipari and F. L. Colden, *SAE Paper No. 872051*, Society of Automotive Engineers, Toronto, November 1987.
- 13 R. A. Potter, *Presented at Fourth Washington Conference on Alcohol Fuels, Washington, DC, November 1984*.
- 14 F. B. Black, L. E. High and J. E. Sigsby, *J. Chromatogr. Sci.*, 14 (1976) 257.
- 15 H. E. Dietzman, *Final Report EPA 600-1-79-017*, U.S. Environmental Protection Agency, Research Triangle Park, NC, February 1979.
- 16 L. R. Smith and C. Urban, *Final Report EPA 460/3-82-004*, U.S. Environmental Protection Agency, Research Triangle Park, NC, March 1982.
- 17 L. R. Smith, *Final Report Project CAPE-30-81*, Coordinating Research Council, Atlanta, GA, May 1985.

- 18 C. J. Raible and F. W. Cox, *SAE Paper No. 790690*, Society of Automotive Engineers, Detroit, MI, June 1979.
- 19 P. M. Carey, *Technical Report EPA-AA-TSS-PA-86-J*, U.S. Environmental Protection Agency Office of Mobile Sources, Ann Arbor, MI, June 1985.
- 20 B. E. Nagel, General Motors Research Laboratories, Warren, MI, personal communication, 1989.
- 21 F. Lipari and S. J. Swarin, *J. Chromatogr.*, 247 (1982) 297.

CHROM 22 075

Confirmation and application of transmission near infrared absorption technique for absolute quantitation of functional groups on silica gel

S. G. BUSH*^a and J. W. JORGENSON

Department of Chemistry, University of North Carolina, Chapel Hill, NC 27599-3290 (U.S.A.)

(First received March 16th, 1989; revised manuscript received October 6th, 1989)

SUMMARY

A transmission near infrared (NIR) technique has been demonstrated to be useful for the qualitative and quantitative measurement of silica surface functionalities. Confirmation of this method's quantitative capabilities has been performed using a newly developed deuterium-exchange method and the more established methods of tritium radioisotopic exchange and carbon analysis.

This NIR technique has been utilized for the evaluation of surface modification reactions for reducing the silanol content of modified silicas. This effort led to the development of "direct butylation" as a promising method for deactivation of porous silica surfaces. Complementary surface characterization information was obtained using solid state NMR, BET adsorption, mercury intrusion porosimetry and gas chromatography.

INTRODUCTION

Silanol groups on silica gels and other siliceous materials are known to be major centers for solute-surface interaction in chromatography¹. Adsorption of solutes at these sites can be the desired mechanism of retention as in normal-phase liquid chromatography. However, the strong interaction between solutes and silanols is often an undesired secondary retention mechanism causing tailed peaks² and resulting in subsequent difficulties for qualitative and quantitative analysis. Because of their importance in chromatographic processes, much research has focused on (1) techniques for quantitating silanols and other surface functionalities on the silica surface^{3–5}, and (2) physical and chemical methods for modifying or removing silanol contributions to retention^{6–8}.

As described in a previous paper⁹, a transmission near infrared (NIR) absorption technique has been developed in our laboratory for the non-destructive

^a Present address: Rohm and Haas Company, Building 8B, 727 Norristown Road, Spring House, PA 19477, U.S.A.

evaluation of surface groups on silica gel. In the present paper, this system's utility in the quantitation of silanols and hydrocarbon functionalities on the silica surface will be shown. The NIR technique is compared to more established quantitative techniques such as carbon analysis and tritium radioisotopic exchange and a newly developed technique using deuterium isotopic exchange combined with NIR spectroscopy.

In addition, we will present surface modification reactions we have developed with the aid of the NIR technique. The direct silylation of silicon dioxide using alkyl lithiums has thus been optimized for use with porous silicas. The chromatographic possibilities of these surfaces is shown using gas-solid chromatography.

EXPERIMENTAL

Materials

An irregular silica gel, Davison 62 (Davison, U.S.A.) with a BET surface area of $267 \text{ m}^2/\text{g}$ was used. Reagent-grade carbon tetrachloride and pyridine from Fisher Scientific (Fair Lawn, NJ, U.S.A.) were dried over molecular sieve 4A. The diethyl ether was vacuum evaporated from the methyl lithium (1.5 *M* in diethyl ether) (Aldrich, Milwaukee, WI, U.S.A.) and dry tetrahydrofuran (THF) added back to form a 0.75 *M* solution. Butyl lithium (2.7 *M* in hexanes) (Aldrich) was diluted with THF to 1.4 *M*. Trimethylchlorosilane (TMCS) and phosphorus pentachloride (Aldrich); Scintiverse scintillation cocktail (Fisher); hydrogen chloride gas (Carolina Specialty Gases, Raleigh, NC, U.S.A.); deuterated water (99.5 atom% ^2H by NMR) (Sigma, St. Louis, MO, U.S.A.); and tritiated water (5 $\mu\text{Ci}/\text{ml}$) (Amersham, Arlington Heights, IL, U.S.A.) were all used as received.

Equipment

Transmission spectra in the NIR were obtained on a Varian (Palo Alto, CA, U.S.A.) Cary 17 UV-VIS-NIR scanning spectrometer in the absorbance mode. The NIR cell (for description see ref. 9), deuterium-exchange apparatus, tritium-exchange apparatus and flow-through reaction apparatus were all fabricated in-house and treated with TMCS to minimize surface silanols. Scintillation counting was done on an Isocap/300 6872 liquid scintillation system (Searle Analytic, Des Plaines, IL, U.S.A.). Gas chromatographic analyses were performed using a Varian Series 1400 gas chromatograph equipped with a flame ionization detector. Data were acquired using a UNC microcomputer (Chapel Hill, NC, U.S.A.) using an interface and statistical moment² software developed in-house. A Blue M (Blue Island, IL, U.S.A.) laboratory oven was used for heating silica samples. Integration of NIR spectral peaks was performed using a planimeter.

Procedures

(1) *NIR analysis.* The silica sample was placed in the NIR cell and dried by simultaneous heating (180°C) and helium purging of the sample. CCl_4 was added as a refractive index matching medium, the helium bubbles removed and the silica packed using flow, gravity and a glass wool plug. The spectrum was then scanned from 2400–1200 nm ($4167\text{--}8333 \text{ cm}^{-1}$) (for details, see ref. 9.)

(2) *Deuterium-exchange method.* The NIR cell was modified by adding vacuum stopcocks in place of standard PTFE stopcocks for better system sealing. About three

grams of silica gel were added to the cell and dried. A preliminary "blank" spectrum was taken of the silica gel and the CCl_4 was driven off. A 500- μl volume of deuterated water was then added and allowed to equilibrate for more than 5 h at 80°C . The equilibrated water was driven off at 180°C with helium flow for 5 h, CCl_4 added, and a spectrum taken. This process was repeated until the NIR spectrum showed no further change indicating the complete exchange of surface silanols to the deuterated form. After CCl_4 removal, the cell was weighed and the weight of dried silica obtained by difference.

Under dry nitrogen, 1200 μl of distilled water were added to the cell which was then sealed and allowed to equilibrate for 12 h at 80°C . The water was subsequently driven off using helium flow and heat and condensed in a liquid nitrogen cold trap. The trapped water was then pipetted into a 1-cm pathlength cuvette and placed in the sample beam of the Cary 17. The spectrum was scanned against distilled water ($^1\text{H}_2\text{O}$) in the reference beam from 1800–1500 nm at 0.1 nm/s and the absorbance measured at 1670 nm. A standard series of $^2\text{HO}^1\text{H}$ solutions were prepared, the absorbance measured and then plotted. The concentration of deuterium in the condensed water was obtained by interpolation of the least squares fit (correlation = 0.995).

(3) *Tritium-exchange method.* This experimental procedure for the radioisotopic exchange of silica was derived from work done by Unger¹⁰ with some changes for experimental convenience. The apparatus used is shown in Fig. 1. About 2 g of the silica sample were added to disconnected component 1 at joint 3. Samples rested on the

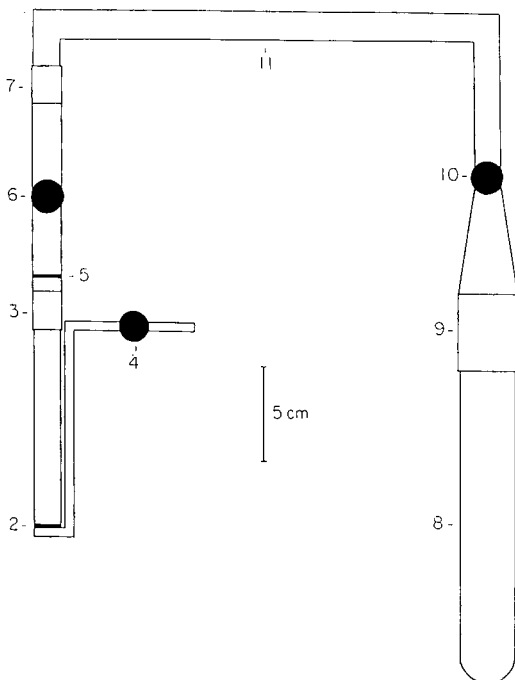


Fig. 1. Tritium (HTO) exchange apparatus. 1 = "Silica component": glass tubing; 2,5 = coarse glass frit; 3,7,9 = ground glass joint; 4,6,10 = PTFE vacuum stopcock; 8 = "ampule component": round-bottom glass tubing; 11 = connecting glass tubing.

sintered glass frit 2. The silica was dried as before with heat and helium flow, component 1 sealed and weighed and the weight of dry silica obtained by difference.

Under a dry nitrogen atmosphere component 1 was reconnected to the apparatus. Meanwhile, a sealed ampule containing a weighed amount (± 0.1 mg) of tritiated water (*ca.* 50 μ l; 10 μ Ci/ml) and a stir bar were placed in component 8 which was then connected to the rest of the apparatus at 14/40 joint 9. The entire system was made vacuum tight by sealing the ground glass joints 3, 7 and 9 with high vacuum grease and by using vacuum stopcocks 4, 6 and 10 for evacuation control. A vacuum was pulled on the entire system through stopcock 4. The stopcock was then closed while the other two stopcocks 6 and 10 remained open to permit free flow of water vapor in the system. After breaking the ampule with the stir bar, the entire apparatus was allowed to equilibrate at 80°C for 12 h. Condensation of the equilibrated vapor was then accomplished by heating component 1 at 180°C while cooling component 8 with liquid nitrogen for 5 h. Heating tape was wrapped around the exposed apparatus to minimize vapor condensation and prevent "freeze-up" of the vacuum grease in joint 9. Stopcock 10 was then closed and the entire system brought to room temperature.

The vacuum was released for component 1 and component 11 by opening stopcocks 4 and 6 successively and component 1 was removed from the apparatus. Sintered disc 5 prevented silica from being pulled into the rest of the system. Stopcock 10 was then opened releasing the vacuum to component 8. Scintiverse and dioxane (15 ml each) were added to the condensed water and stirred for 30 min. A 15-ml portion of the resulting solution was aliquoted into a scintillation vial and counted. System blanks were performed by carrying out this procedure without the silica gel sample. "Simple" blanks were carried out by counting a 15-ml aliquot of a solution of 15 ml dioxane, 15 ml Scintiverse and a weighed amount (*ca.* 50 μ l) of tritiated water. Comparison of the system blank to the simple blank (both in units of counts per minute per gram of tritiated water) revealed a tritium recovery of 99.4% (2% relative standard deviation) for the system blank.

(4) *Carbon analysis.* Carbon analysis of modified and unmodified silica gels was performed by Galbraith Labs. (Knoxville, TN, U.S.A.).

(5) *Surface modification.* All surface modification reactions were carried out in the double necked flow through reaction flask (Fig. 2). The silica rested on the coarse sintered glass frit 1. This arrangement allowed for the easy removal of reagents through the PTFE stopcock 2 and limited exposure of air or water sensitive surfaces to the atmosphere. Because of the air/water sensitivity of many of the reagents and silica surfaces, all reactions and transfers were carried out under nitrogen and all glassware was dried before use. *Safety note:* alkyl lithium reagents are extremely pyrophoric! Great care must be observed in their use.

(a) *Silylations.* A variety of silane coverages were provided by varying reagent amounts in the following general procedure for silylation of silica gel: About 10 g of dried silica gel were added to the flow-through vessel. A solution of 70 ml CCl_4 , up to 30 ml TMCS and up to 5 ml pyridine, was added to the silica gel. After refluxing overnight, the silica was finally washed with CCl_4 , CHCl_3 , CH_2Cl_2 , acetone, THF, water and THF.

(b) *Chlorination-methylation.* A 4-g amount of PCl_5 was dissolved in 100 ml of dry CS_2 . The $\text{PCl}_5\text{-CS}_2$ solution was added to 3 g dried silica in the reaction vessel.

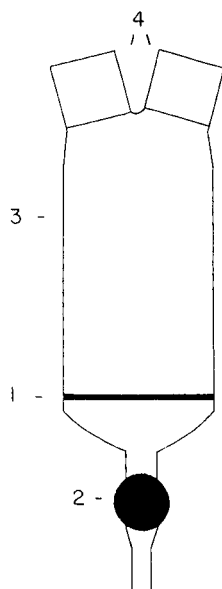


Fig. 2. Flow through reaction flask. 1 = Coarse glass frit; 2 = PTFE stopcock; 3 = large-bore glass tubing; 4 = 19/22 female ground glass joints.

After refluxing the mixture for 5 h, the silica was then washed with dry CS_2 and dried with helium flow and heat. Next 50 ml of methyl lithium (0.75 M in THF) were added and the mixture swirled occasionally for 15 min. The solution was slowly forced into (under the surface of) isopropanol with nitrogen pressure in order to destroy excess methyl lithium. After washing with fresh THF, the silica was dried with helium flow and heat. The silica was neutralized by alternatively pulsing hydrogen chloride gas and helium gas (to cool silica) through the flask. Finally the silica was washed with 4 M hydrochloric acid, water, and THF, the silica dried and the NIR spectrum taken.

(c) Methyl lithium only. Procedure is the same as above except no prior chlorination step was used.

(d) Butyl lithium. A 100-ml volume of butyl lithium (1.4 M in THF/hexanes) was added to 6 g of dried silica. After swirling occasionally over a 15-min period, the butyl lithium was slowly forced into isopropanol with nitrogen pressure (as with methyl lithium). The silica was washed with fresh THF and dried with helium flow and heat. Hydrogen chloride and helium were alternately pulsed through the cell followed by washing with 4 M hydrochloric acid, water, THF, water and THF. After drying, the NIR spectrum was obtained.

(6) *Solid state NMR*. All NMR spectra were obtained at the Colorado State University Regional NMR Center on a modified Nicolet NT-200 (^{29}Si) or NT-150 (^{13}C) spectrometer. (For further details, see refs. 11–13.)

(7) *Gas chromatography*. Weighed amounts of silica adsorbents were packed via tapping into 1 m \times 1/8 in. O.D. stainless-steel tubing. The columns were coiled and preconditioned at 225°C for 12 h. Sample introduction was performed by syringe injections of saturated acetone vapor at room temperature. Methane was used as a dead time marker.

RESULTS AND DISCUSSION

Since developing the NIR technique previously described⁹, we have focused our attention in two directions: (1) evaluation of the quantitative applicability of the technique and (2) application of the technique to the development of useful surface reactions for silica.

First a methodology for quantitation using the NIR method was adopted. Quantitative comparisons were then performed by a deuterium isotopic exchange method recently developed in our laboratory and by two literature methods, tritium radioisotopic exchange and carbon analysis. From the first procedure we obtained a measure of the surface concentration of silanols on the unmodified silica. The more established techniques were used to evaluate the unmodified silica and several TMCS-modified silicas of various surface coverages. Results were then compared to NIR data on the same samples.

Concurrent with these studies novel surface modification routes were explored with the NIR technique. Of particular interest is the direct alkylation of the surface with alkyl lithium which was further evaluated with solid state NMR and gas solid chromatography.

Confirmation of NIR technique

Calculation of percent silanol removal. As shown in Fig. 3, the removal of silanols on silica gel can be monitored in the NIR by comparing traces from unmodified (dotted line) and TMCS-modified (solid line) samples⁹. If the sample has been properly dried (as monitored by removal of the water combination band at 5277 cm^{-1}) the peak at 7220 cm^{-1} can be attributed solely to the overtone of the silanol stretch ($2\nu_s$)⁹ while the bands grouped near 5800 cm^{-1} can be attributed to various overtones of the methyl C-H stretches.

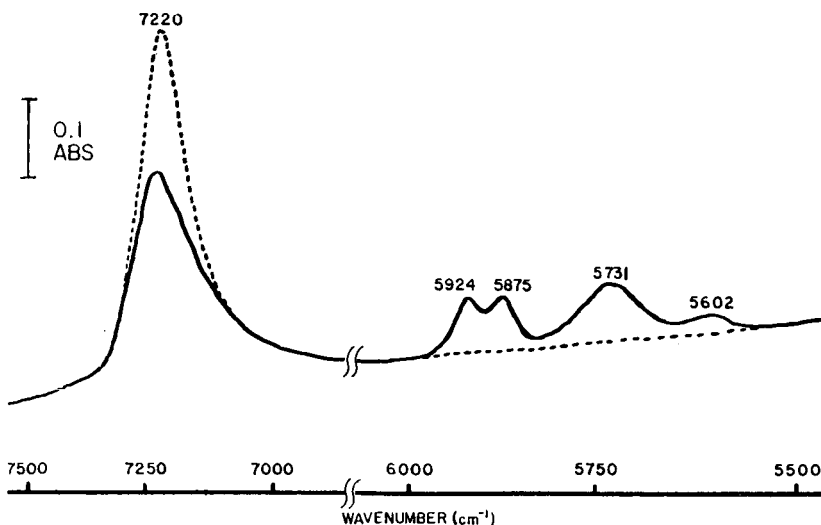


Fig. 3. NIR absorption as a function of trimethylchlorosilane reaction with the silica surface. Broken curve: unmodified silica gel (dry); solid curve: trimethylchlorosilane modified silica.

Silanol removal can be quantitated by drawing a baseline tangent under the OH overtones for both the modified and unmodified silicas. The areas are then measured and percent removal obtained from the ratio. In practice two corrections must be applied as shown in the following equation:

$$P = \frac{M_{7220} - (CM_{5800} + D_{7220}) \cdot 100}{U_{7220} - D_{7220}} \quad (1)$$

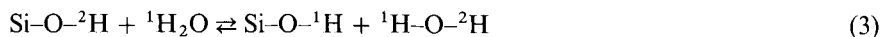
where P is the percent unreacted silanol, and M_{7220} and U_{7220} are the integrated absorbances for the peak at 7220 cm^{-1} for the modified and unmodified silica, respectively. D_{7220} is the area of the silanol overtone for a silica gel that has been exhaustively exchanged with deuterated water (approximately 5% of total silanol). This correction accounts for the contribution to the silanol peak of "buried" silanols¹⁴ which are inaccessible to $^2\text{H}_2\text{O}$ and therefore also inaccessible to reagents and chromatographic solutes.

The second correction factor, C , is needed to account for the overlap of the silanol overtone with weak C-H combination bands due to any alkyl functionalities bound to the silica surface. C was obtained for methyl groups by taking the NIR spectrum of an analogue, tetramethylsilane in CCl_4 , at several tetramethylsilane concentrations. A plot of integrated absorbance for the C-H peaks at 7220 cm^{-1} (y axis) versus the C-H peaks at 5800 cm^{-1} (x axis) yielded a straight line of equation:

$$y = Cx \quad (2)$$

where the slope, C , was found to be 0.304. For modified silicas the area of the C-H peaks overlapping with the silanol overtone at 7220 cm^{-1} (y value) can be obtained by multiplying C by M_{5800} which is the area under the C-H overtone peaks grouped at 5800 cm^{-1} (x value). The value of 0.304 for C has been found to be valid for other alkyl groups including butyl and octadecyl¹⁵ functionalities.

Deuterium-exchange technique. Silanol concentration in the unmodified silica was studied by the method described in procedure 2. This method exploits the equilibrium between ^2H and ^1H in the system:



After exhaustive deuteration and drying of the silica surface, the only sources of exchangeable hydrogen are the deuterated (^2H) silanols (we have found that any contribution from the apparatus is insignificant). Therefore, when a known volume of excess $^1\text{H}_2\text{O}$ (approximately 19-fold excess of exchangeable ^1H) is added to the system, allowed to equilibrate and then separated from the surface and condensed, the number of deuterium atoms displaced and consequently the concentration of deuterium atoms in that known volume of water can be related to the number of silanols on the surface. Even with the large excess used, this number must be corrected for the minority of deuterium atoms left behind on the surface by the partition equilibrium effect.

The number of mmoles of ^2H in the condensed water, $n_w(^2\text{H})$ is:

$$n_w(^2\text{H}) = \frac{2C_v V \rho(^2\text{H}_2\text{O})}{M(^2\text{H}_2\text{O})} \quad (4)$$

where C_v is the concentration of deuterium in the condensed water (volume fraction of ^2H in total hydrogen), V the volume of water after equilibration (ml), $\rho(^2\text{H}_2\text{O})$ the density of deuterated water (g/ml) and $M(^2\text{H}_2\text{O})$ the molecular weight of deuterated water (g/mole). The factor 2 converts moles of water to moles of hydrogen. Similarly, the number of mmoles of ^1H in the condensed water, $n_w(^1\text{H})$ can be calculated from the equation:

$$n_w(^1\text{H}) = \frac{2(1 - C_v)V\rho(^1\text{H}_2\text{O})}{M(^1\text{H}_2\text{O})} \quad (5)$$

where $\rho(^1\text{H}_2\text{O})$ and $M(^1\text{H}_2\text{O})$ are the density and molecular weight, respectively of water ($^1\text{H}_2\text{O}$).

The equilibrium constant for eqn. 3 can be expressed as

$$K = \frac{n_s(^1\text{H}) \cdot n_w(^2\text{H})}{n_s(^2\text{H}) \cdot n_w(^1\text{H})} \quad (6)$$

where K is the equilibrium constant and $n_s(^1\text{H})$ and $n_s(^2\text{H})$ are the mmoles of silanol in the ^1H and ^2H form, respectively. For our purposes we will assume K to be 1. (Even changing the K value to 1.5 would result in only a 4% difference in the surface concentration of silanols). The assumption that $K = 1$ will be justified later in the paper. Since $n_w(^2\text{H})$ and $n_w(^1\text{H})$ are already calculated and since the mmoles of ^1H silanol equals the mmoles of displaced ^2H in the water [*i.e.* $n_s(^1\text{H}) = n_w(^2\text{H})$], eqn. 6 can be used to calculate $n_s(^2\text{H})$. The total mmoles of silanol hydrogen, n_s :

$$n_s = n_s(^1\text{H}) + n_s(^2\text{H}) \quad (7)$$

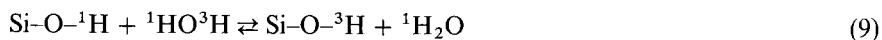
can then be used to calculate the surface concentration of silanols, α_{OH} ($\mu\text{mole}/\text{m}^2$), by the equation:

$$\alpha_{\text{OH}} = \frac{n_s \cdot 10^3}{Sm} \quad (8)$$

where S is the surface area (m^2/g) and m is the mass (g) of the silica gel. The factor 10^3 converts mmoles to μmoles . Table I gives values for duplicate runs of this experiment. The average α_{OH} value of $9.5 \mu\text{moles}/\text{m}^2$ corresponds well with literature values¹⁶.

Tritium-exchange method. TMCS-modified silicas of various coverages were obtained by procedure 5a, the NIR spectrum taken and the results listed in Table II. We then characterized these batches of silica by the tritium exchange (procedure 3) and carbon analysis (next section).

The tritium-exchange method employs the exchange of tritiated water with surface silanols:



Before the surface concentration of silanols can be calculated, two assumptions are made. First, we assume that hydrogen exchange at the surface of the apparatus is

TABLE I
DEUTERIUM-EXCHANGE METHOD

$\rho(^2\text{H}_2\text{O}) = 1.105$ g/ml; $M(^2\text{H}_2\text{O}) = 20.03 \cdot 10^{-3}$ g/mmol; $\rho(^1\text{H}_2\text{O}) = 0.998$ g/ml; $M(^1\text{H}_2\text{O}) = 18.02 \cdot 10^{-3}$ g/mmol; $K = 1$; $S = 267$ m²/g.

Run No.	C_v	V	$n_w(^2\text{H})$	$n_w(^1\text{H})$	$n_s(^2\text{H})$	n_s	m	α
1	0.055	1.20	7.28	125.6	0.42	7.70	3.01	9.58
2	0.057	1.20	7.55	125.3	0.45	8.00	3.19	9.39
Average								9.5

insignificant and that the only important sources of exchangeable hydrogen are silanols and water. Therefore, the total mmoles of hydrogen, n_t , can be expressed as:

$$n_t = n_s + n_w \quad (10)$$

where n_s and n_w are the mmoles of hydrogen due to silanol and water, respectively. This assumption is reasonable since the percent recovery for the system blank (see procedure 3) was found to be virtually 100% indicating essentially no loss of tritium to the apparatus.

Secondly, it is supposed that the isotopic equilibrium effect between ^1H and ^3H is negligible or non-existent. In other words, the probability that any given ^3H atom will end up on the surface is the same as the probability that any given ^1H atom will end up on the surface. The reasonableness of this condition will be examined below.

Given these two assumptions, if a weighed amount of tritiated water of a known specific activity, a_0 (counts per minute per gram of tritiated water), is allowed to equilibrate with the surface silanols in a dried silica sample and if the resulting equilibrated water is removed from the surface and condensed (procedure 3), the amount of tritium (and therefore the specific activity of the tritium) on the silica gel, a_s , is directly proportional to the number of silanols and the activity of tritium remaining in the water, a_w , is directly proportional to the number of hydrogen atoms in the water.

The initial specific activity, a_0 , is equal to the total activity of the system, a_t (counts min⁻¹ g⁻¹) and can be related to a_s and a_w :

$$a_0 = a_t = a_s + a_w \quad (11)$$

TABLE II
NIR ANALYSIS OF TMCS COVERAGES

$D_{7220} = 3.1$; $C = 0.304$; $P = \%$ unreacted silanol.

Batch No.	U_{7220}	M_{7220}	M_{5800}	P
0	79.4	—	—	100%
1	—	74.6	2.3	93%
2	—	70.0	7.1	85%
3	—	60.7	11.3	71%
4	—	53.1	19.0	58%

Finally we can calculate the number of moles of silanol using the equation:

$$\frac{a_w}{a_t} = \frac{n_w}{n_t} = \frac{n_w}{n_w + n_s} \quad (12)$$

The concentration of silanols assuming no isotope effect ($\alpha_{OH(T)}$, $\mu\text{mole}/\text{m}^2$), can then be calculated using eqn. 8.

Triplicate samples of the unmodified silica were analyzed by this method and $\alpha_{OH(T)}$ values of 9.32, 9.51 and 9.42 $\mu\text{moles}/\text{m}^2$ were obtained. The average of 9.42 ± 0.10 is essentially the same within the precision of the experiments as the value of $9.5 \pm 0.1 \mu\text{moles}/\text{m}^2$ obtained from the deuterium method. Since the isotope equilibrium effect was assumed to be absent in both cases and because the same answer is derived using that assumption, we conclude that contrary to previously published results¹⁰ the isotopic effect on equilibrium is very small or non-existent. This can be restated as:

$$K = \frac{n_s(^2\text{H}) \cdot n_w(^1\text{H})}{n_s(^1\text{H}) \cdot n_w(^2\text{H})} = \frac{n_s(^3\text{H}) \cdot n_w(^1\text{H})}{n_s(^1\text{H}) \cdot n_w(^3\text{H})} = 1 \quad (13)$$

and:

$$\alpha_{OH} = \alpha_{OH(T)} \quad (14)$$

Data from the radioisotopic (tritium) analysis of the modified and unmodified silica gels are given in Table III. A plot of surface coverage by tritium exchange (α in Table III) *versus* percent unreacted silanol by NIR (Table II) is presented in Fig. 4. Note the good linear relationship. The NIR technique is quantitative for silanols over a wide range of coverages. The y intercept for 0% silanol by NIR (totally reacted surface) is very close to the zero silanol surface coverage by ^3H exchange. This makes good physical sense since there would be no silanol coverage NIR signal if all the silanols were reacted.

TABLE III
SURFACE SILANOL COVERAGE BY TRITIUM EXCHANGE

$S = 267 \text{ m}^2/\text{g}$.

Sample	a_w/a_t	n_w	n_s	m^a	$\alpha_{OH(T)}$
Batch 0	0.535	5.44	4.73	1.90	9.32
	0.532	5.54	4.87	1.92	9.51
	0.522	5.44	4.98	1.98	9.42
Batch 1	0.538	5.33	4.58	1.91	8.98
	0.537	5.40	4.66	1.93	9.05
Batch 2	0.572	5.36	4.01	1.88	7.99
	0.573	5.28	3.93	1.83	8.04
Batch 3	0.612	5.37	3.40	1.83	6.97
	0.625	5.37	3.22	1.87	6.45
Batch 4	0.661	5.26	2.70	1.83	5.52

^a Mass corrected for weight of TMS groups added to the surface using carbon analysis data.

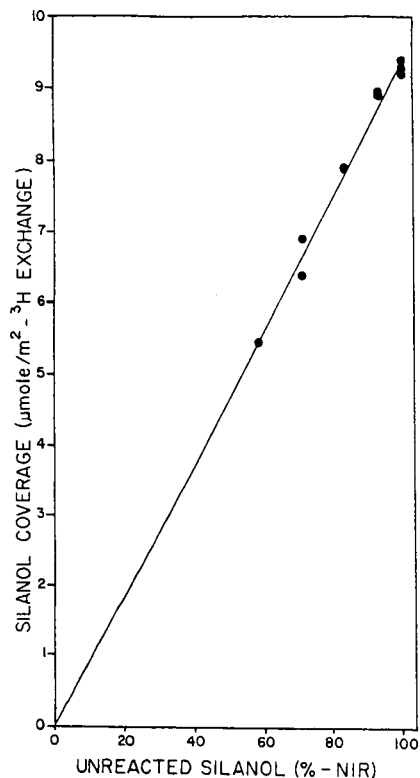


Fig. 4. Silanol coverage by tritium exchange *versus* percent unreacted silanol by NIR spectroscopy (See Tables II and III for data. Line represents least-squares fit of data (intercept = $1.7 \cdot 10^{-3}$; $r = 0.993$).

Carbon analysis

Samples from batches 0–4 were sent out for carbon analysis (procedure 4). The received %C data were converted to total carbon coverage $\alpha_{\text{TMS(u)}}$ ($\mu\text{mole}/\text{m}^2$), by the equation¹⁷

$$\text{TMS(u)} = \frac{\%C \cdot 10^6}{12 \cdot N \cdot 100 \left(1 - \frac{\%C \cdot M_s}{12 \cdot N \cdot 100} \right)} \cdot S \quad (15)$$

where N is the number of carbon atoms in the silane (three for TMCS), M_s the molecular weight of the silane reagent less the reactive group (73 for TMCS) and S is the surface area. The total carbon coverage, $\alpha_{\text{TMS(u)}}$ was then corrected to the “true” TMCS coverage, α_{TMS} ($\mu\text{mole}/\text{m}^2$), by subtraction of the carbon coverage value for the unmodified silica (batch 0), α_{uc} .

The contribution from the unmodified silica is apparently due to ubiquitous carbon physically adsorbed to the surface and to inaccuracies in the carbon analysis method for small amounts of carbon. The values resulting from eqn. 15 are given in

TABLE IV
CARBON ANALYSIS OF TMCS SURFACE COVERAGE

Batch No.	%C	α_{uc}	$\alpha_{TMS(u)}$	α_{TMS}
0	0.49	0.51	—	—
1	0.81	—	0.86	0.35
2	1.57	—	1.69	1.18
	1.87	—	2.02	1.51
3	2.54	—	2.79	2.28
4	3.67	—	4.13	3.62

Table IV and plotted *versus* NIR coverage as shown in Fig. 5. Once again a linear plot is obtained further confirming the quantitative abilities of the NIR technique. A y intercept of $8.69 \mu\text{moles}/\text{m}^2$ is lower than expected from the silanol coverage values observed with previous methods ($9.5 \mu\text{moles}/\text{m}^2$ —see above). The relative difference of 9% is probably due to the lower precision of the total carbon measurements (17% difference for the duplicate determinations for batch 2), the uncertainty introduced by a relatively large blank value (batch 0), and the inability to produce data for higher coverages ($>42\%$ —see *Surface modification* section below).

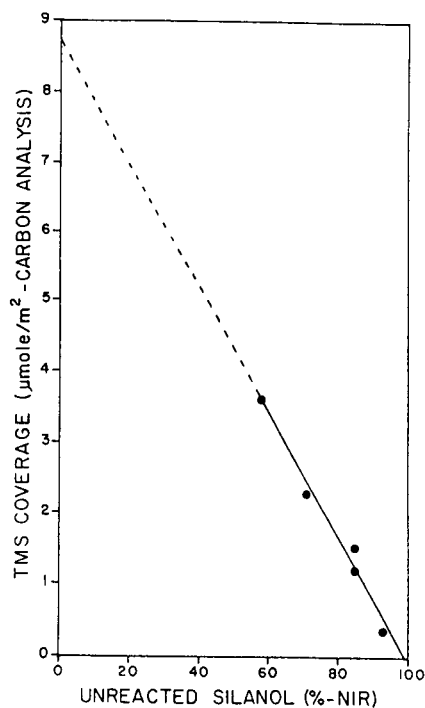


Fig. 5. Trimethylsilyl (TMS) coverage by carbon analysis *versus* percent unreacted silanol by NIR spectroscopy. See Tables II and IV for data. Line represents least-squares fit of data (intercept = $8.6 \mu\text{moles}/\text{m}^2$; $r = 0.991$).

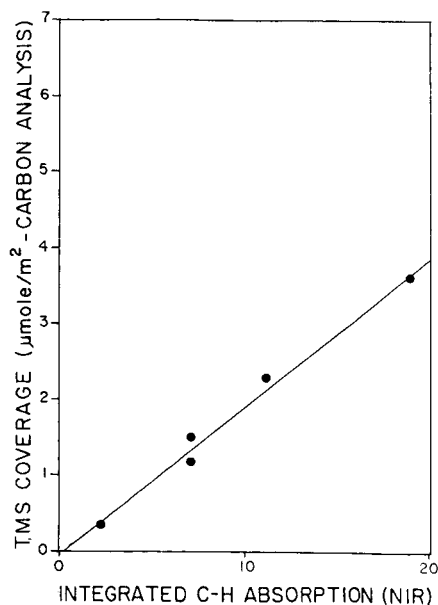
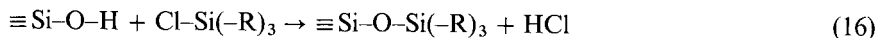


Fig. 6. Trimethylsilyl (TMS) coverage by carbon analysis versus integrated NIR C-H overtone absorption (near 5800). See Tables II and IV for data. Line represents least-squares fit of data (intercept = $9.4 \cdot 10^{-2}$ $\mu\text{moles}/\text{m}^2$; $r = 0.993$).

If the TMS coverage values (Table IV) are plotted against M_{5800} values for C-H absorption (Table II) the plot in Fig. 6 results. The linearity of this graph shows that the NIR technique can also be used to quantitate C-H groups on the surface.

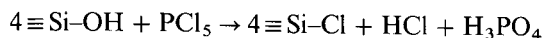
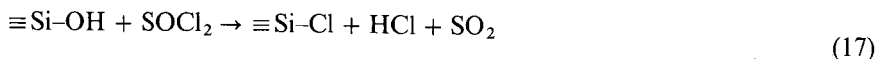
Surface modification

Silylation. The most popular means for the modification of siliceous chromatographic materials is to react surface silanols with various silanes, in particular chlorosilanes:

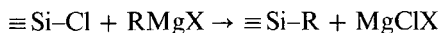


where R can correspond to a variety of functionalities. Even when using the smallest silanes ($\text{R} = \text{CH}_3$; TMCS), both literature studies and our own studies (see batch 4 above) have shown that a maximum of about 40–50% of the surface silanols are removed.

Chlorination/alkylation. We feel that one important reason for this incomplete silylation is simply steric, *i.e.*, the trimethylsilyl groups are too large to pack closely enough on the surface for greater than 50% removal of silanols. Therefore, we looked to a two-step reaction route found in the literature¹⁸ where the silanols are first chlorinated to $\equiv\text{Si-Cl}$ groups by chlorinating reagents such as SOCl_2 or PCl_5 :



The chlorinated surface is then reacted with an organolithium or Grignard reagent to form a Si-C bond:



If R was chosen to be a small enough functionality such as a methyl group, we felt that the reduced steric hindrance might allow for a more complete removal of silanol groups.

Effects of both chlorination and methylation steps in the modification procedure 5b are shown in Fig. 7. The top broken line corresponds to the unmodified silanol overtone (U_{7220}). The bottom broken line corresponds to the silanol overtone for the silica after the chlorination step and represents a 54% removal of silanols from the silica surface (and therefore 54% surface coverage of $\equiv\text{Si-Cl}$). Unfortunately, after the methylation step the silanol signal rebounded to 90% of the unmodified band's intensity indicating only a 10% reaction of silanols. However, we found that by repeatedly cycling the silica through the two steps we could reduce the apparent silanol content of the silica gel to the point that only 35% of the silanols were remaining by the NIR technique.

Several observations made about the adsorbents resulting from this repeated reaction of the silica surface did not fit with the previously stated reaction scheme (eqns. 21 and 22). First, polysilicic acid was observed in the methyl lithium-THF solution during its removal through the sintered glass disc and into the isopropanol. In addition the silica became more "flocculent" (*i.e.*, its packing density decreased) with

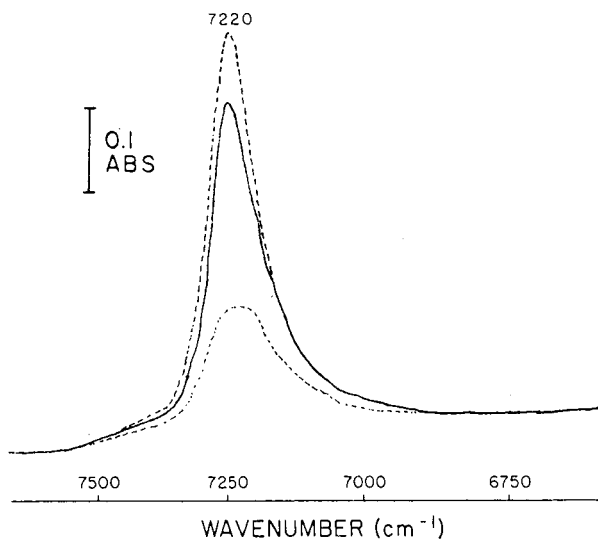


Fig. 7. NIR absorption as a function of surface reaction with phosphorous pentachloride and methyl lithium. Top broken curve: unmodified silica (dry); bottom broken curve: intermediate spectrum of PCl_5 chlorinated surface; solid curve: spectrum after addition of methyl lithium.

repeated reaction. These two observations indicated some sort of break-up of the silica network. Finally, it was noted from the NIR spectrum of the silica that the increase in C-H adsorption (5800 cm^{-1}) as compared to the reduction in silanol absorption (7220 cm^{-1}) was significantly more than would be expected from a one for one replacement of hydroxyl groups (or $\equiv\text{Si}-\text{Cl}$ groups) with methyl groups.

Direct alkylation. In an attempt to explain these unexpected observations we proceeded to monitor what happened if the silica surface was reacted with methyl lithium alone (procedure 5c). We found as above that polysilicic acid formed during methyl lithium addition, that flocculence increased, and that relatively large amounts of methyl were being added to the surface. Fig. 8 shows the NIR spectra of a silica that has been cycled seven times through procedure 5c.

Unmodified silica samples were also reacted with butyl lithium (procedure 5d) so that a broader view of alkyl lithium-silica reactions could be built. During the initial reaction cycle polysilicic acid was observed in the butyl lithium-hexanes-THF mixture indicating, as with the methyl lithium, some sort of silica network break-up. However, this effect lessened with later cycles, and unlike the methyl lithium reaction, packing density and mechanical stability seemed to stay constant. (Possible reasons for these observed differences will be given below.) A relatively large increase in butyl coverage was also observed (see Fig. 9).

Apparently two different reactions occur at the silica surface upon addition of alkyl lithium. Silanols can react directly with the alkyl lithium reagents:



(This reaction has been used to evaluate the silanol coverage of silica gels¹⁹.) On the other hand the break-up of the silica lattice can be attributed to a second reaction with siloxanes¹⁸:

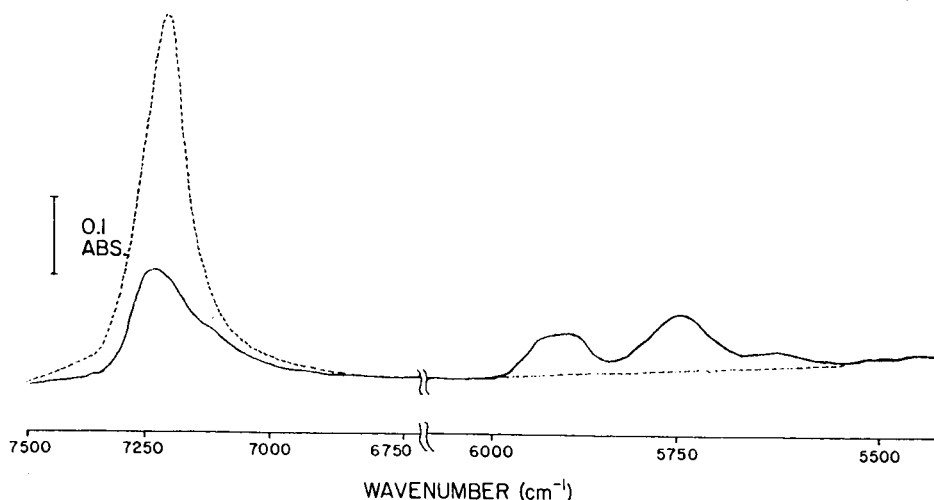
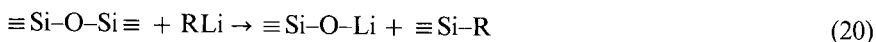


Fig. 8. NIR absorption for a repeatedly methylated (methyl lithium) silica. Broken curve: unmodified silica (dry); solid curve: silica subjected to seven cycles of direct methylation.

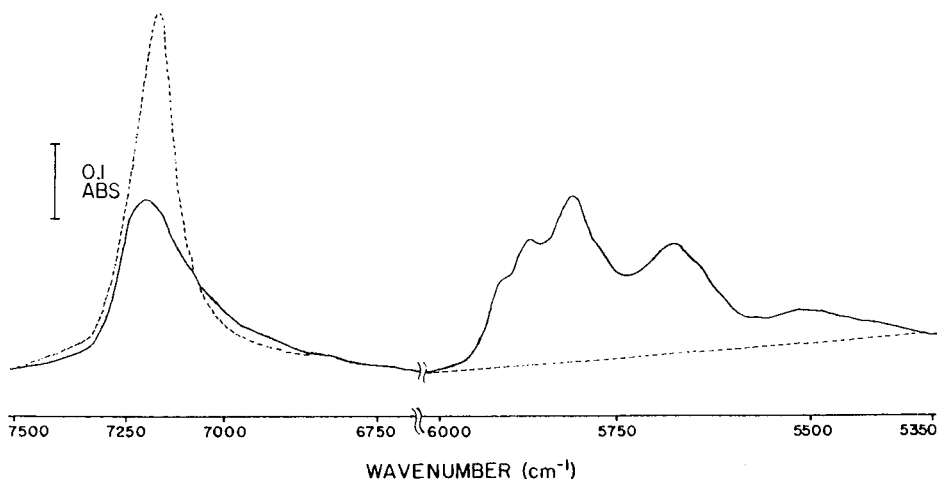


Fig. 9. NIR absorption for a repeatedly butylated (butyl lithium) silica. Broken curve: unmodified silica (dry); solid curve: silica subjected to eight cycles of direct butylation.

resulting in carbon directly bonded to the surface. In our alkylation procedures any remaining alkyl lithium is then removed, and the Si-O-Li groups formed in eqns. 19 and 20 are (exothermically) neutralized to the silanol:



If these silanol groups are close enough together they are known to condense with heat:



to reform stable siloxane bonds.

We propose that the net effect of these reactions (19-22) is an overall loss of silanol and a significant gain in alkyl coverage:



The overall reaction scheme 23 is meant only as a statement of net gains and losses of silica surface functionalities. No overall balanced equation is written due to the disruptive nature of the alkyl lithium reaction with the silica (*i.e.*, “chunks” of polysilicic acid are removed from the silica network). Depending on the conditions of the reaction cycle(s), the increase in alkyl coverage is usually 2-3 times greater than the loss of silanol.

The evidence for direct methylation and direct butylation of the silica surface is given separately below.

Direct methylation. As already noted the case for methyl lithium’s disruption of the silica surface is supported both by the formation of polysilicic acid and the increased flocculence of the silica. In addition the BET surface area of the silica was found to increase by up to 25% upon repeated reaction and the pore size distribution

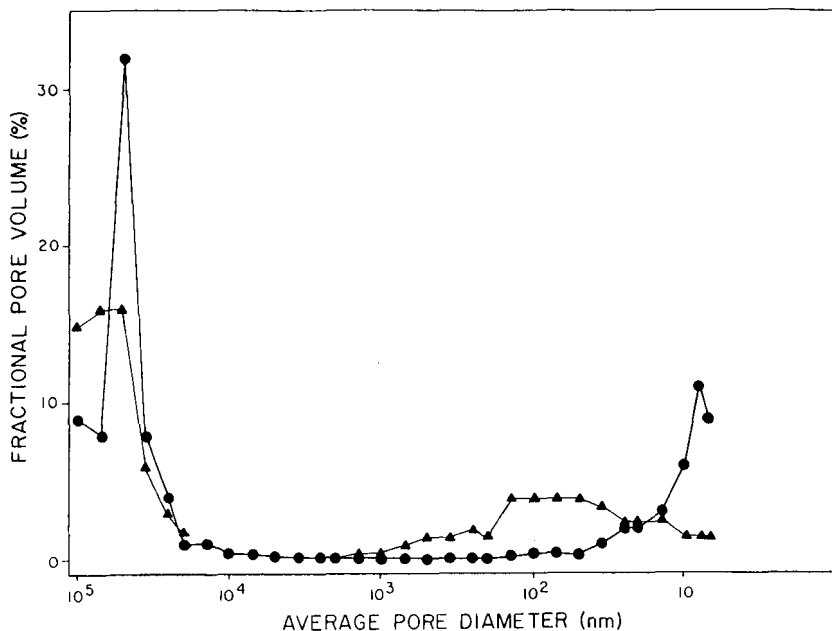


Fig. 10. Fractional pore volume versus average pore diameter for methylated silica. ● = Unmodified silica gel; ▲ = methylated silica.

dispersed greatly in the 10–100-nm region from the sharp maximum at 10 nm for the unmodified silica (see Fig. 10).

The NIR spectrum of the methylated silica (Fig. 8) has a four peak pattern (5924, 5875, 5731, 5602 cm^{-1}) in the C–H overtone region which is peculiar to methyl groups (see Fig. 3). This methyl coverage has been shown to be non-extractable by monitoring the C–H overtone bands before and after washing the adsorbent with THF, methylene chloride, acetone, 4 M hydrochloric acid (aq.), and water, and heating the silica up to 200°C. The identical spectra obtained confirm that the absorptions are due to chemically bonded methyl groups (as opposed to being only physically adsorbed). There is no evidence in the C–H overtone region for any other type of hydrocarbon groups.

Solid state NMR has also been used in order to obtain complementary surface information (see procedure 6). In the carbon-13 spectrum (see Fig. 11a) we have only one absorption at 0 ppm which corresponds to a methyl group bonded directly to Si^{13} [as with the solid reference tetra (trimethylsilyl) methane]. The ^{29}Si spectrum (Fig. 11b) gives a peak corresponding to silicon bound to methyl¹² (near –21 ppm) as well as a broad peak for silanol and siloxane silicons (–98 and –110 ppm, respectively). These spectra further confirm formation of Si–CH₃ bonds via direct methylation.

Direct butylation. Like the methyl lithium, butyl lithium causes disruption of the silica network as evidenced by the formation of polysilicic acid in the initial reaction cycles (procedure 5d). However, after a few cycles this effect diminishes. We believe that this diminution is due to the larger steric volume of the butyl lithium than methyl lithium in solution coupled with the bulky butyl groups bonded to the surface. That is,

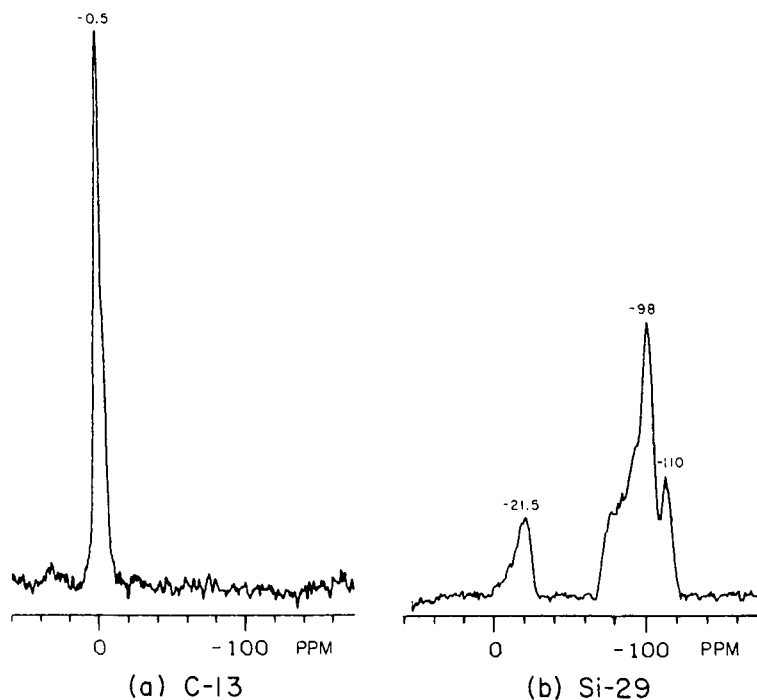


Fig. 11. Solid state cross-polarization magic angle spinning NMR spectra for methylated silica. All numbers in units of ppm. (a) Carbon-13 NMR of methylated silica. Peak at -0.5 ppm corresponds to methyl bound to silicon: $\equiv\text{Si}-\text{CH}_3$. (b) Silicon-29 NMR of methylated silica. Peak assignments: -21.5 ppm, silicon bound to methyl; -98 ppm, silicon bound to silanol; -110 ppm, silicon bound to siloxane only.

the butyl lithium causes less disruption than methyl lithium after initial cycles, because bound butyl sterically hinders butyl lithium from reaching more siloxanes. Due to this effect there is no great loss of mechanical stability and packing density. In fact we have found that the surface area actually decreases (from 267 to 213 m^2/g). This is apparently due to the analogous effect seen when silica is treated with silanes (for example batch 4 above has a surface of 211 m^2/g .) The pore size data (Fig. 12) show a slight dispersion from the unmodified silica. However, the effect is much smaller than for the methylated silica which is also indicative of the smaller amount of surface disruption caused by butyl lithium.

As with methyl groups on the methylated silica, the NIR technique reveals that a relatively large number of non-extractable butyl groups have been chemically bonded to the butylated silica gel. The carbon-13 NMR displays a three peak pattern (Fig. 13) corresponding to (1) methyl bound to carbon, (2) methylene bound to silica and (3) two methylenes bound to carbon. This is the expected pattern for a butyl group bonded directly to silicon. The silicon-29 spectrum was not obtained.

As with the methyl lithium, the evidence supports the breakage of siloxane bonds to form silicon-carbon bonds.

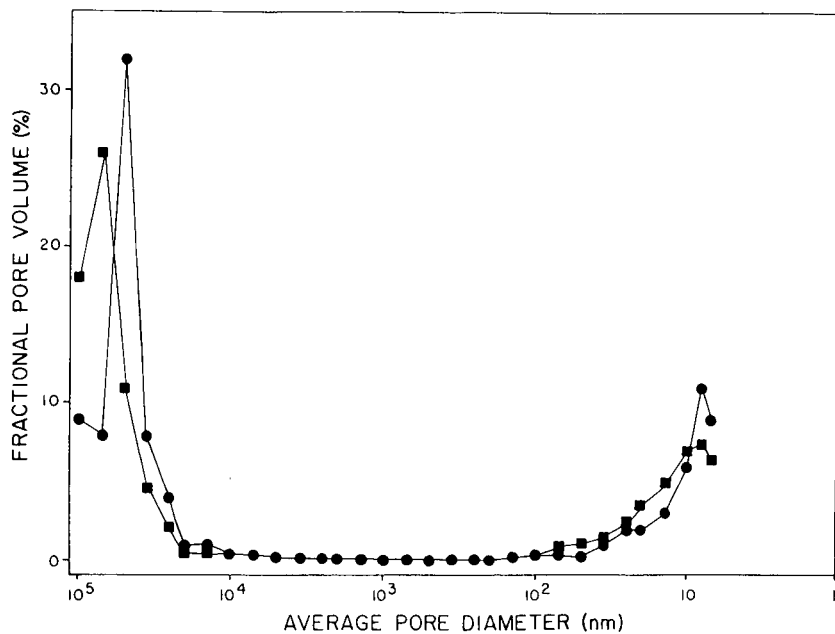


Fig. 12. Fractional pore volume versus average pore diameter for butylated silica. ● = Unmodified silica gel; ■ = butylated silica.

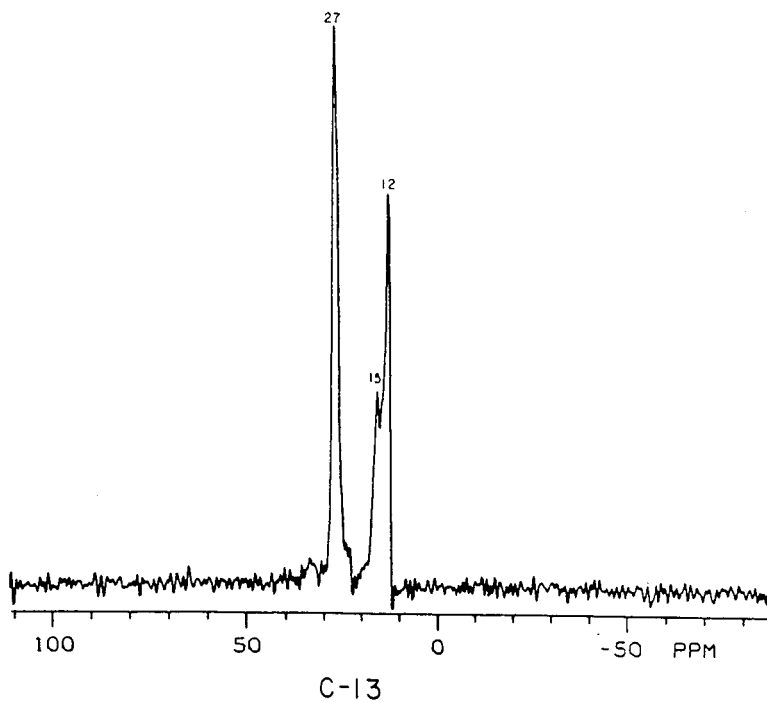


Fig. 13. Solid state cross-polarization magic angle spinning NMR spectra of butylated silica. All numbers in units of ppm. Peak assignment: $\equiv\text{Si}-\text{CH}_2-\text{CH}_2-\text{CH}_2-\text{CH}_3$, where peak 1 = 12 ppm; 2 = 15 ppm; 3 = 27 ppm.

(2) (3) (3) (1)

Gas chromatography

Since our final goal was to produce interesting and hopefully useful chromatographic surfaces, the ultimate test of the adsorbents produced was chromatography. Gas-solid chromatography (GSC) was chosen because of the relative simplicity of interactions between solute and adsorbent (*i.e.*, there are no additional interactions with a liquid mobile or supported phase as in liquid chromatography or gas-liquid chromatography). Acetone was chosen as polar probe of the silica surface, because of its strong physical interactions²⁰ with silanols on the silica surface. The butylated adsorbent was chosen as a representative alkylated silica because of its mechanical stability.

Initially comparisons were attempted between the unmodified silica and the butylated silica, but it was found that the acetone was too highly retained on the native silica even under extreme conditions of column temperature and flow-rate. We therefore used a fully reacted TMCS silica (batch 4 above) for a direct comparison with the butylated silica. The results of this comparison are summarized in Fig. 14 and Table V. The conditions are given in the figure legend. Note that for equivalent

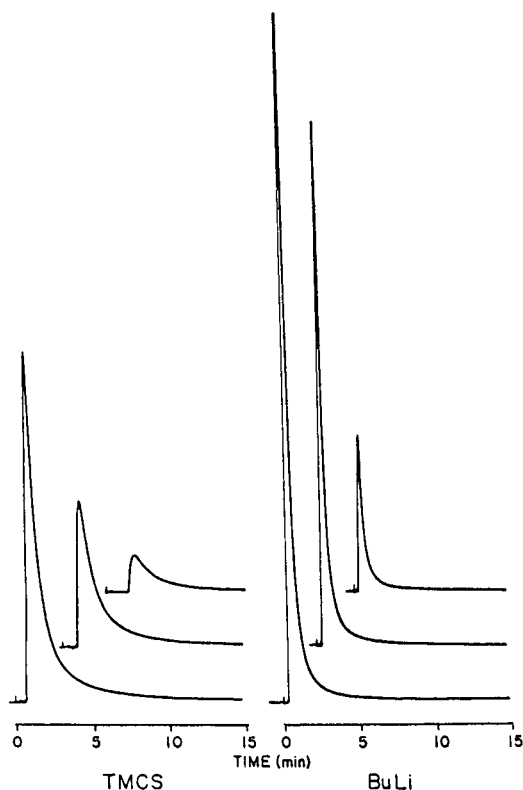


Fig. 14. Direct gas chromatographic comparison of acetone retention profiles for a TMCS (batch 4) and a butylated silica. All conditions are the same for each column. Column temperature: 200°C; flow-rate: 17 ml/min; weight of adsorbent: 1.6 g. The traces for each column correspond to 5 (bottom trace), 2 (middle trace), and 0.5 μ l (top trace) of saturated acetone vapor. "Tics" shown on traces correspond to injection times. BuLi = Butyl lithium.

TABLE V

GSC RETENTION DATA FOR ACETONE ON SILYLATED AND BUTYLATED COLUMNS

Retention time and capacity factor calculated using statistical moments.

Column (adsorbent)	Injection volume (μl)	Retention time (s)	Capacity factor (k')
TMCS	0.5	219	17
	2	170	13
	5	146	11
Butyl lithium	0.5	59	3.8
	2	61	4.0
	5	63	4.1

injection volumes (5, 2 and 0.5 μl of acetone vapor) the chromatographic peaks are sharper and less tailed for the butylated silica column as compared to the silylated silica column. In addition, both the average and range of the retention times and the capacity factors (both calculated using statistical moments) for these chromatograms (Table V) are significantly smaller for the butylated column.

Evidently the interaction with the polar acetone molecule is less intense for the butylated column. This is probably due to two reasons. First, the calculated surface concentration of silanols (eqn. 22) for the butylated and silylated silica were 5.0 and 5.5 $\mu\text{moles}/\text{m}^2$, respectively. Secondly, the calculated surface coverage of alkyl groups for the butylated and silylated silica were 9.5 and 3.7 $\mu\text{moles}/\text{m}^2$, respectively. Apparently the 10% lower silanol content for the butylated adsorbent means fewer high energy silanol sites are available while the dramatically higher alkyl coverage (2.6 times higher) does a better job of sterically restricting solute access to the remaining silanols. The combination gives a less active chromatographic surface.

CONCLUSION

The NIR technique has been shown to be a useful technique for studying silica gel modification. It is non-destructive, gives good qualitative and quantitative information for important surface functionalities, is relatively convenient and is inexpensive. One possible limitation of this technique in its application is the method for correcting silanol absorption for C-H combinations (eqn. 1). For silicas with very high carbon coverages, the correction becomes relatively large and the approximation of a baseline for integration (M_{7220}) is more difficult. This problem can be solved by using computer aided peak subtraction and integration.

The present work with alkyl lithium confirms and expands on the direct alkylation of silica done by Boehm *et al.*¹⁹, and sheds a new light on the chlorination/alkylation methods found in the chromatographic literature (*e.g.* ref. 7). The preliminary GSC data given in this paper indicate that direct alkylation (particularly butylation) may have a useful role to play in the deactivation and modification of siliceous materials for chromatography.

SYMBOLS

a_0	Initial specific activity of tritiated water
a_s	Specific activity of tritiated silanols (after equilibration)
a_t	Total specific activity
a_w	Specific activity of tritiated water (after equilibration)
C	Correction factor for C–H combination bands at 7220 cm^{-1}
C_v	Volume fraction of deuterium in total hydrogen
%C	Percent weight of carbon in modified silica gel
D_{7220}	Integrated absorbance at 7220 cm^{-1} for deuterated silica
K	Equilibrium constant
m	Mass of silica gel (g)
M_{5800}	Integrated absorbance at 5800 cm^{-1} for modified silica
M_{7220}	Integrated absorbance at 7220 cm^{-1} for modified silica
$M(^1\text{H}_2\text{O})$	Molecular weight of water
$M(^2\text{H}_2\text{O})$	Molecular weight of deuterated water
M_s	Molecular weight of silane minus reactive group
N	Number of carbon atoms in the silane
n_s	mmoles of hydrogen in silanol
$n_s(^1\text{H})$	mmoles of ^1H in silanol
$n_s(^2\text{H})$	mmoles of ^2H in silanol
$n_s(^3\text{H})$	mmoles of ^3H in silanol
n_t	Total mmoles of hydrogen
n_w	mmoles of hydrogen in condensed water
$n_w(^1\text{H})$	mmoles of ^1H in condensed water
$n_w(^2\text{H})$	mmoles of ^2H in condensed water
$n_w(^3\text{H})$	mmoles of ^3H in condensed water
P	Percent unreacted silanol
S	Specific surface area of silica (m^2/g)
U_{7220}	Integrated absorbance at 7220 cm^{-1} for unmodified silica
V	Volume of water after equilibration (ml)
α_{OH}	Surface concentration of silanols
$\alpha_{\text{OH(T)}}$	Surface concentration of silanols by tritiation method
α_{TMS}	Surface coverage of TMS groups
$\alpha_{\text{TMS(u)}}$	Uncorrected surface coverage of TMS groups
α_{uc}	Carbon coverage for unmodified silica
$\rho(^1\text{H}_2\text{O})$	Density of water
$\rho(^2\text{H}_2\text{O})$	Density of deuterated water

ACKNOWLEDGEMENTS

NMR spectra were obtained at the Colorado State University Regional NMR Center, funded by National Science Foundation Grant No. CHE-8208821. We acknowledge the help of Drs. Mark Miller and Richard Linton in obtaining the NMR spectra. We also acknowledge the help of Kevin Bruce in obtaining surface area and porosimetry data.

REFERENCES

- 1 K. K. Unger, *Porous Silica*, Elsevier, Amsterdam, 1979, pp. 76–83.
- 2 J. R. Conder and C. L. Young, *Physicochemical Measurement by Gas Chromatography*, Wiley, New York, 197, p. 37.
- 3 L. Nondek and V. Vyskocil, *J. Chromatogr.*, 206 (1981) 581.
- 4 G. E. Maciel and D. W. Sindorf, *J. Amer. Chem. Soc.*, 102 (1980) 7606.
- 5 R. S. McDonald, *J. Phys. Chem.*, 62 (1958) 1168.
- 6 R. Rowan and J. B. Sorrell, *Anal. Chem.*, 42 (1970) 1716.
- 7 B. Banner, D. C. Locke and J. T. Schmermund, *Anal. Chem.*, 44 (1972) 90.
- 8 J. J. Kirkland and L. R. Snyder, *Introduction to Modern Liquid Chromatography*, Wiley, New York, 1978, pp. 272–280.
- 9 S. G. Bush, J. W. Jorgenson, R. W. Linton and M. L. Miller, *J. Chromatogr.*, 260 (1983) 1.
- 10 K. K. Unger, *Porous Silica*, Elsevier, Amsterdam, 1979, pp. 73–74.
- 11 G. E. Maciel and D. W. Sindorf, *J. Am. Chem. Soc.*, 102 (1980) 7606.
- 12 G. E. Maciel and D. W. Sindorf, *J. Am. Chem. Soc.*, 103 (1983) 4263.
- 13 G. E. Maciel and D. W. Sindorf, *J. Am. Chem. Soc.*, 105 (1983) 1848.
- 14 V. Y. Davydov and A. V. Kiselev, *Russ. J. Phys. Chem. (Engl. Transl.)*, 27 (1963) 1404.
- 15 M. L. Miller, R. W. Linton, S. G. Bush and J. W. Jorgenson, *Anal. Chem.*, 56 (1984) 2204.
- 16 A. V. Kiselev and L. T. Zhuralev, *Russ. J. Phys. Chem. (Engl. Transl.)*, 39 (1965) 236.
- 17 G. Ahr and E. Engelhardt, *Chromatographia*, 14 (1981) 227.
- 18 J. J. Fripiat and J. Uytterhoeven, *J. Phys. Chem.*, 66 (1962) 800.
- 19 H. P. Boehm, M. Schneider and H. Wistuba, *Angew Chem., Int. Ed. Engl.*, 4 (1965) 600.
- 20 V. K. Chuikina, A. V. Kiselev and K. D. Sacherbakova, *Russ. J. Phys. Chem. (Engl. Transl.)*, 40 (1966) 830.

Preparative affinity chromatography of proteins

Influence of the physical properties of the base matrix

SUNANDA R. NARAYANAN*, SAMUEL KNOCHS, Jr. and LAURA J. CRANE

Research and Development Laboratories, J. T. Baker Inc., 222 Red School Lane, Phillipsburg, NJ 08865 (U.S.A.)

(First received August 7th, 1989; revised manuscript received October 31st, 1989)

SUMMARY

Several silica-based high-performance affinity media differing in pore size and surface area were synthesized for the immobilization of proteins containing primary amino groups. Surface characterization of these silica-based media was carried out by mercury intrusion porosimetry and the pore surface area and pore diameters were compared. The intrinsic binding capacities for proteins of different molecular weights were determined by static binding studies. Concanavalin A was covalently immobilized on these media and its dynamic binding capacity was determined in the affinity mode by frontal uptake studies. The studies show that binding capacity increases with increasing pore size, then decreases as the pore size becomes sufficiently large to significantly decrease the surface area. Thus, an ideal affinity chromatographic support would have sufficiently large pores accessible for proteins to penetrate, yet would preserve the maximum surface area for binding. These studies suggest that a final bonded phase pore diameter of at least 200 Å is desirable for the preparative affinity chromatography of proteins of molecular weight in excess of 150 000 daltons.

INTRODUCTION

As early as 1970, Cuatrecasas¹ pointed out that an affinity sorbent containing a very high concentration of the ligand, much of which is inaccessible to the protein, is not very efficient for chromatography. It was later observed that staphylococcal nuclease, a small protein of molecular weight of 17 000, had to be purified on a very porous support¹. It is now very well accepted that before a protein can efficiently bind to a porous support, it has to diffuse into the pores^{2–4}. Based on these observations, it follows that if the size of the pores is insufficient for the protein to rapidly diffuse, the efficiency of the column will be diminished even if the other characteristics of the medium are suitable for the binding of the protein to the affinity ligand. Physical characterization of the pore structure of the chromatographic supports is therefore necessary for establishing an efficient, cost-effective purification protocol⁵.

The pore structure parameters most commonly used to characterize chromatographic supports include the following: the mean or average pore diameter (\AA), the specific pore surface area (m^2/g) and the specific pore volume (ml/g). We have investigated the influence of these parameters with new affinity ligand using silica as a chromatographic support because of its desirable characteristics for high-resolution and high-performance chromatography.

The use of silica for high-performance liquid chromatography (HPLC) is well documented⁶⁻⁹. The speed and resolution combined with the ability to obtain high flow-rates and the rigid surface have attracted more and more scientists to use silica-based sorbents for preparative HPLC of proteins¹⁰⁻¹². Among the various attributes of silica, the most attractive in the context of affinity chromatography is the range of porosities, particle sizes and surface areas that are commercially available from the manufacturers of silica. This feature makes it possible to design a support optimized for a specific purification protocol which is based on the properties of the protein to be isolated as well as the properties of those contaminating the crude extract. Although the above-mentioned factors play a crucial role in any purification method, on a preparative scale the support must also possess good binding capacity in order to be efficient and cost effective.

Several reports have dealt with the effect of particle size, pore size and surface area in HPLC¹³⁻¹⁶. Walters¹⁷ studied the efficiency of diol-bonded silica of varying pore size and concluded that in affinity chromatography two factors were responsible for poor binding capacities at intermediate pore size: restricted diffusion and slow adsorption-desorption kinetics. Horstmann *et al.*¹⁸ observed the binding of proteins on Sepharose-based affinity sorbents of varying particle sizes and reported that the maximum capacities obtained increased with decreasing particle size in Sepharose-based affinity sorbents.

Rounds *et al.*² demonstrated that in anion-exchange chromatography, the binding of proteins is dependent on accessible surface area (that is the total pore surface area excluding the external particle surface) rather than the total surface area of the support indicating that wide pores in addition to high surface areas provide maximum capacity. In 1987, Kopaciewicz *et al.*¹⁹ reported that both pore and particle size influence the frontal uptake of proteins in anion-exchange chromatography. They also observed that frontal uptake of proteins was inversely related to flow-rate and particle size of the adsorbent. A ligand density study was conducted by Wu and Walters²⁰ on silica-based affinity supports of pore size ranging from 300 to 4000 \AA and they concluded that the optimum pore size of the silica for protein immobilization was 300-1000 \AA . Recently Forster and Anderson²¹ studied the effect of pore size on the capacity and efficiency of Protein A-derivatized silicas. Results presented indicated that binding capacity was related to surface area and the ability of the solute to diffuse in and out of the porous silica. The authors suggested improvement in the peak symmetry if the pore size either totally includes or excludes the solute. All these studies have contributed to our understanding of how the surface characteristics of a sorbent influence the binding of molecules, be it in the ion-exchange or affinity mode.

Although the intrinsic binding capacity (that is the amount of affinity ligand bound) of an adsorbent can provide information while choosing an affinity support, it does not always indicate the efficiency or the loading capacity (the amount of protein bound to the affinity ligand) of the adsorbent. The amount of ligand coupled or the

ligand concentration is the first step in affinity chromatography while the amount of protein that will bind to the ligand is the crucial factor that determines the success and efficiency of the purification protocol. Loading capacity in affinity chromatography thus depends on the ligand concentration, the pore size, the particle size and the surface area available for the binding of multiple molecules.

This work deals with systematic evaluation of a newly developed affinity sorbent, Glutaraldehyde-P, for HPLC. We report here the studies conducted on surface characterization of Glutaraldehyde-P preparations on silicas of varying pore sizes and surface areas and attempt to accurately interpret the effect of these physical properties on the binding of proteins of different molecular weights by static adsorption and by frontal uptake measurements in the affinity mode.

MATERIALS AND METHODS

Materials

Proteins used in these studies were purchased from Sigma (St. Louis, MO, U.S.A.). The protein assay reagent was from Biorad. Glutaraldehyde and sodium cyanoborohydride were from Aldrich. All other chemicals were products of J. T. Baker.

Instrumentation

HPLC was conducted on two high-performance pumps (Beckman Instruments), a variable-wavelength detector (Beckman Instruments) and a two-channel recorder (Kipp and Zonen). Pore structure analysis was performed by mercury intrusion porosimetry by using an Autoscan-33 from Quantachrome (Syosset, NY, U.S.A.).

Methods

Activation of the affinity sorbent. Silica was first treated with a hydrophilic polymer according to our patented chemistry, to which glutaraldehyde was covalently attached^{22,23}. The amount of aldehyde linked in each case was carefully controlled by optimizing the reaction conditions. The aldehyde content was determined by the procedure of Narayanan *et al.*²² and Parkinson and Wagner²⁴.

Sample preparation for mercury porosimetry studies. In order to obtain a representative sample for mercury porosimetry studies, a rotary microriffler (Quantachrome, Syosset, NY, U.S.A.) was used to reduce the sample size to approximately 0.35 g. The sample was dried at 80°C overnight in a vacuum oven, cooled in a desiccator and the weight was accurately determined.

Pore structure analysis. The pore structure analysis of the Glutaraldehyde-P affinity sorbent was carried out by mercury intrusion porosimetry. Assuming the pores to be cylindrically shaped, the basic principle of mercury porosimetry is expressed by the Washburn equation in the following manner

$$Pd = -4\gamma \cos \theta \quad (1)$$

which allows one to determine the diameter d of the pores into which mercury will intrude as a function of the applied pressure P . If the surface tension γ of mercury and its contact angle θ are taken as 480 dynes/cm and 140° (this was experimentally

determined for silica) respectively, eqn. 1 can be simplified to the following

$$Pd = 213.4 \text{ p.s.i. } \mu\text{m} \quad (2)$$

Scanning porosimetry provides a means of measuring the volume of mercury intruded into the pores in a sample as a function of the pressure, which is continuously increased from below ambient to 33 000 p.s.i. The volume of mercury is monitored by means of a capacitance bridge, as the quantity of mercury in the stem of the sample cell decreases as filling of the pores occurs. For example, one can calculate from the Washburn eqn. 1 that at initial pressures of 0.5 p.s.i., pores and interparticle voids having a diameter of $426 \mu\text{m}$ will fill with mercury. The lower pore size limit of the instrument is determined by the maximum pressure achievable in the porosimeter and is 64.6 \AA at 33 000 p.s.i.

A variety of physical properties of the silica can be determined from these pressure-volume measurements:

- (1) pore diameter distribution and the average (mean) or median pore diameter;
- (2) intruded volume of mercury;
- (3) $D_v(d)$ volume distribution function as a function of diameter d ;
- (4) $D_s(d)$ surface area distribution function as a function of diameter d ;
- (5) cumulative pore surface area.

Calculations were carried out as described by Lowell and Shields²⁵.

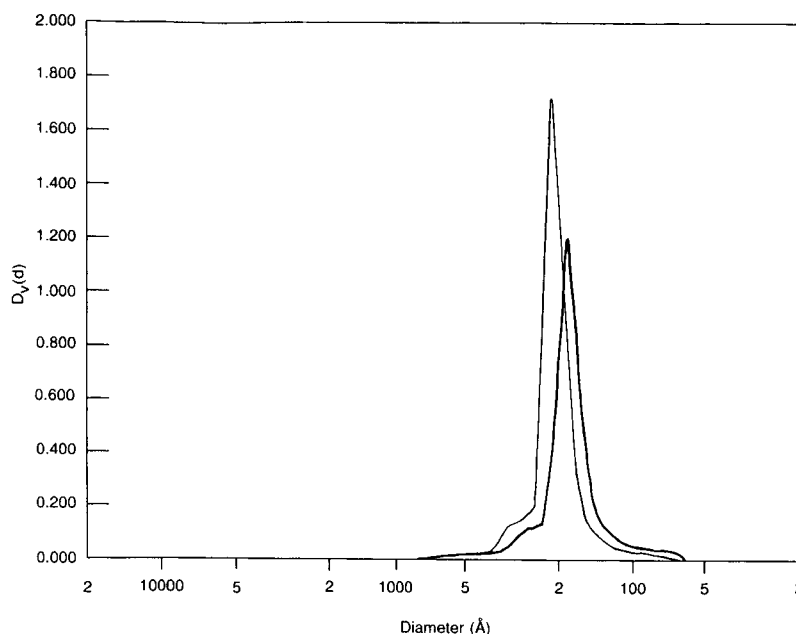
Static coupling of proteins. Glutaraldehyde-P preparations were washed with an excess of 2 *M* sodium chloride and then with 0.1 *M* potassium phosphate buffer, pH 7.4. An amount of 50 mg of each bonded phase sample was carefully weighed into a test tube and treated with 2.5 ml of 0.1 *M* potassium phosphate buffer, pH 7.4 containing 15 mg protein. Sodium cyanoborohydride was added (final concentration 0.1 *M*) in small amounts and the reaction was left undisturbed overnight at 4°C. The bonded phase was then washed extensively with 0.5 *M* sodium chloride and then with 0.1 *M* potassium phosphate, pH 7.4. The amount of protein adsorbed was determined by relating the loss of protein in the reaction mixture to the weight of bonded phase. Concanavalin A (Con A) was immobilized on Glutaraldehyde-P as outlined in an earlier report²².

Column packing. The silica preparations activated by glutaraldehyde and coupled with Con A were packed into $50 \times 4.6 \text{ mm}$ I.D. columns by slurry packing by using 0.1 *M* potassium phosphate buffer, pH 6.0 containing 0.5 *M* sodium chloride, 1 mM calcium chloride and 1 mM manganese chloride.

Frontal uptake studies. Con A immobilized on silica of varying pore size was packed into $50 \times 4.6 \text{ mm}$ I.D. columns and equilibrated with 0.025 *M* Tris-HCl, pH 6.8 containing 0.2 *M* sodium chloride, 1 mM calcium chloride and 1 mM manganese chloride. Horseradish peroxidase (5 mg/ml) was injected at 1 ml per minute until the break-through peak was visible. The buffer was changed to 0.02 *M* Tris-HCl, pH 6.8 containing 0.2 *M* sodium chloride, 1 mM calcium chloride, 1 mM manganese chloride and 0.025 *M* methyl- α -D-glucopyranoside and the amount of peroxidase released was monitored at 406 nm.

RESULTS AND DISCUSSION

Fig. 1 gives the pore volume distribution as a function of diameter of one



X axis scale units: Å

Y axis scale units: $\text{cm}^3 / (\text{Å}) (\text{g}) \times 10\text{E}-2$

Fig. 1. Volume distribution curve for Glutaraldehyde-P (preparation 2) before (line) and after (bold line) treatment with glutaraldehyde. $D_v(d)$ and diameter are calculated by mercury intrusion porosimetry as described in Materials and Methods. $D_v(d)$ in $\text{cm}^3/\text{Å} \cdot \text{g} \times 10^{-2}$.

particular Glutaraldehyde-P affinity matrix (preparation 2, see Table I) before and after it is activated by glutaraldehyde. The volume distribution $D_v(d)$ for intrusion per unit change in pore diameter d is plotted against diameter d . The figure illustrates a shift and a decrease in pore volume distribution of the bonded phase after it is treated with glutaraldehyde. Similar shifts are observed in the case of the pore surface area distribution of the support material when it is clad with the polymer (Fig. 2). In this case the surface area distribution $D_s(d)$ for intrusion per unit change in pore diameter d is shown. In an ideal support, the pore size distribution is unimodal and preparation 2 fulfills this requirement (Fig. 1). A heterogeneous or bimodal distribution of pores

TABLE I

PORE STRUCTURE ANALYSIS OF GLUTARALDEHYDE-P (PREPARATION 2)

The physical properties were determined by mercury intrusion porosimetry and corrected for interparticle void. See Materials and Methods for details.

Sample	Pore volume (ml/g)	Pore surface area (m^2/g)	Median pore diameter (Å)
Starting material	0.95	182	211
After polymer treatment	0.76	150	204
After glutaraldehyde treatment	0.66	143	190
After binding of Con A	0.55	122	183

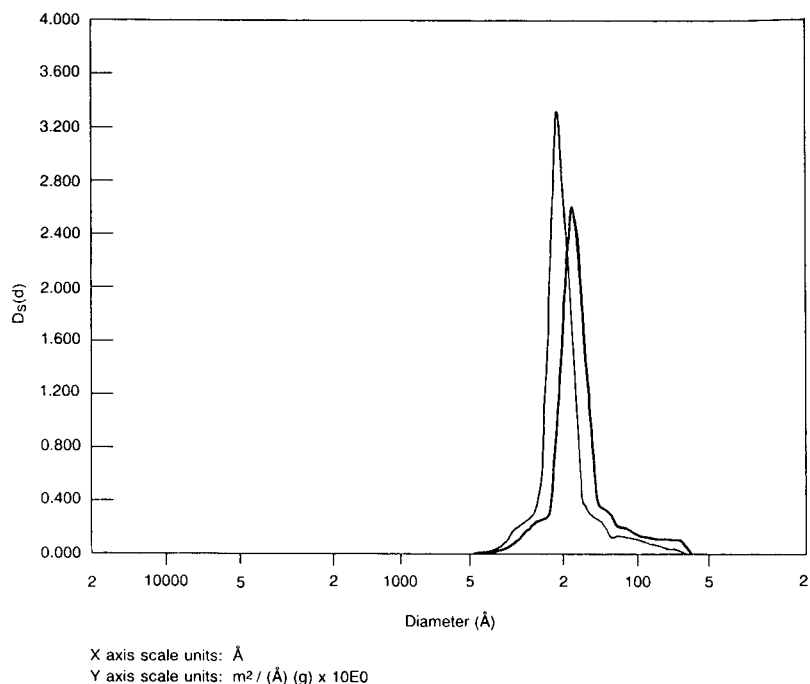


Fig. 2. Pore surface area distribution of Glutaraldehyde-P (preparation 2) before (line) and after (bold line) treatment with glutaraldehyde. $D_s(d)$ and diameter are calculated as described in Materials and Methods. $D_s(d)$ in $\text{m}^2/\text{Å} \cdot \text{g}$.

would affect the chromatographic resolution. The fact that the pore volume and the pore surface area distribution shifted towards smaller pore diameter when silica was treated with the polymer suggests that the pores were evenly coated in the interior and not blocked by the polymer.

Table I lists the physical properties of preparation 2 (Table II) before and after it is clad with glutaraldehyde. The data has been corrected for interparticle void volume

TABLE II

SURFACE CHARACTERIZATION AND PROPERTIES OF GLUTARALDEHYDE-P PREPARATIONS

Pore volume, pore surface area, and pore diameter were determined by mercury intrusion porosimetry and corrected for interparticle void.

Preparation	1	2	3	4
Property				
Pore volume (ml/g)	0.26	0.66	0.83	0.77
Pore surface area (m^2/g)	130	143	85	46
Pore diameter (median) (Å)	88	190	408	776
Carbon coverage (m^2/g)	385	424	460	280
Aldehyde ($\mu\text{mol}/\text{m}^2$)	1.3	1.8	1.53	1.3
Con A (mg/g)	80	140	104	86

in each case. After the bonded phase was treated with glutaraldehyde there is a 42% reduction in pore volume, 35% reduction in pore surface area and 13% reduction in the average pore diameter. Binding of Con A (a large protein of molecular weight 102 000) did not show any substantial change in the pore diameter.

Table II gives the pore diameter and surface area of Glutaraldehyde-P preparations used in our study. The carbon surface coverage determined by elemental analysis correlates fairly well with the experimentally determined amount of glutaraldehyde ($\mu\text{mol}/\text{m}^2$) which in turn correlates with the ligand binding capacity of the matrices for Con A (Fig. 3), indicating that the functional groups on the activated matrices are generally accessible to the protein.

Fig. 4 compares the binding capacities of glutaraldehyde-activated silica preparations of different pore diameters and surface areas for proteins of various molecular weights. In order to compare accessible surface areas of sorbents with different pore diameter and surface area, the protein binding capacity of the affinity sorbent was divided by the molecular weight of the protein and expressed as μmoles of protein per gram of the support. A large protein like thyroglobulin (molecular weight 670 000) is totally excluded from preparation 1 (average pore diameter 88 Å) while a medium sized protein like peroxidase (molecular weight 40 000) binds less to preparation 4 despite the large pore size (average pore diameter 776 Å).

Recently, Regnier²⁶ postulated that steric phenomena play a significant role in the interaction of large molecules in chromatography, be it in an ion-exchange, hydrophobic interaction or affinity chromatographic process. Though the binding mechanism of a protein to an affinity support is not based singularly on the molecular size of the protein, there seems to be a fairly good correlation between the binding capacity and the surface area and pore size of the support.

Consequently, silica packings of low surface area and large pore diameters are not necessarily the best candidates for chromatographic supports. Surface area and pore size should be optimized for protein size classes in order for the affinity support to be most efficient and cost effective. This is illustrated in Fig. 5. Although the ligand

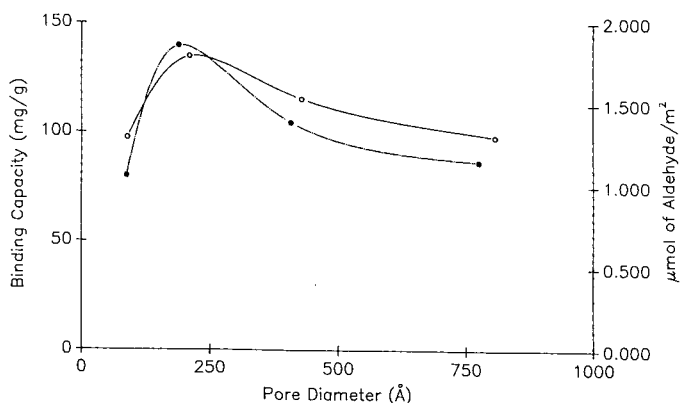


Fig. 3. The effect of pore diameter on the amount of glutaraldehyde (O) and Con A bound (●) to Glutaraldehyde-P affinity matrices. Con A concentration was determined by Bradford assay and glutaraldehyde content was estimated as described in Materials and Methods. An amount of 50 mg Glutaraldehyde-P was treated with 15 mg protein and immobilization was carried out as described in Materials and Methods.

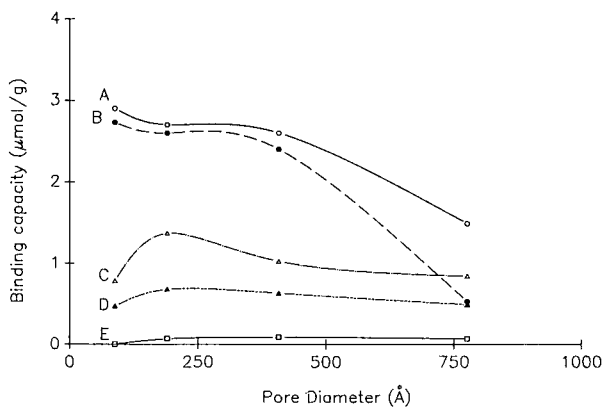


Fig. 4. The effect of pore diameter on the specific binding capacity of Glutaraldehyde-P affinity media for different proteins. (A) Lactoglobulin A; (B) horseradish peroxidase; (C) Con A; (D) glyceraldehyde-3-phosphate dehydrogenase; (E) thyroglobulin. The binding capacity of these supports for each protein was calculated by dividing the total binding capacity by the molecular weight of the respective protein. See Materials and Methods for more details.

concentration of preparation 3 (mean pore diameter 408 Å) is comparable to preparation 2, the surface area of the support is half of that of preparation 2; the loading capacity for horseradish peroxidase on Con A–Glutaraldehyde-P is higher in the case of preparation 2 (Table I and Fig. 5). Preparation 1 has a similar binding capacity for Con A as preparation 2 but due to its limited pore diameter, it does not bind the same amount of peroxidase onto the Con A bonded surface. Preparation 2 is an ideal matrix with both pore size and surface area optimal for maximum binding capacity for proteins of a wide molecular weight range (Table I and Fig. 5). In general, an average pore diameter of at least 200 Å may be desirable for chromatography of large proteins of molecular weight in excess of 150 000.

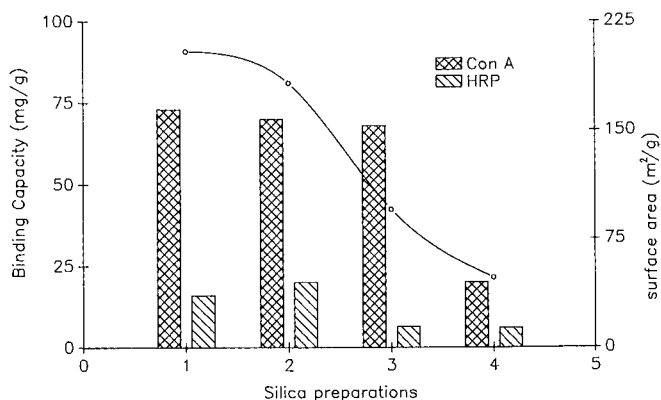


Fig. 5. The effect of pore diameter and surface area on the binding capacity of Glutaraldehyde-P affinity preparations for covalently bound Con A. Horseradish peroxidase (HRP) was bound to Con A in the dynamic mode as described in Materials and Methods. An amount of 2 g of Glutaraldehyde-P was allowed to react with 200 mg of protein and immobilization was carried out as described in Materials and Methods.

The above data exemplifies the importance of the physical properties of the support material for affinity chromatographic separations of proteins. It highlights the importance of choosing the right support to make the affinity medium. In this way, the binding and loading capacity can be greatly controlled, and lead to a more efficient, optimized purification.

Use of the same support for affinity separation of small molecules shows that the pore diameter is much less important for binding. The chromatographic separation of closely related *p*-nitrophenyl sugar derivatives on the same samples of Con A–Glutaraldehyde-P is given in Fig. 6. All three preparations showed similar resolution in the analytical range.

In conclusion, these experimental results illustrate the importance of understanding the surface and physical characteristics of the support material for optimum application of affinity chromatography. More and more preparative-scale purifications are being based on biological recognition, where maximum loading of the

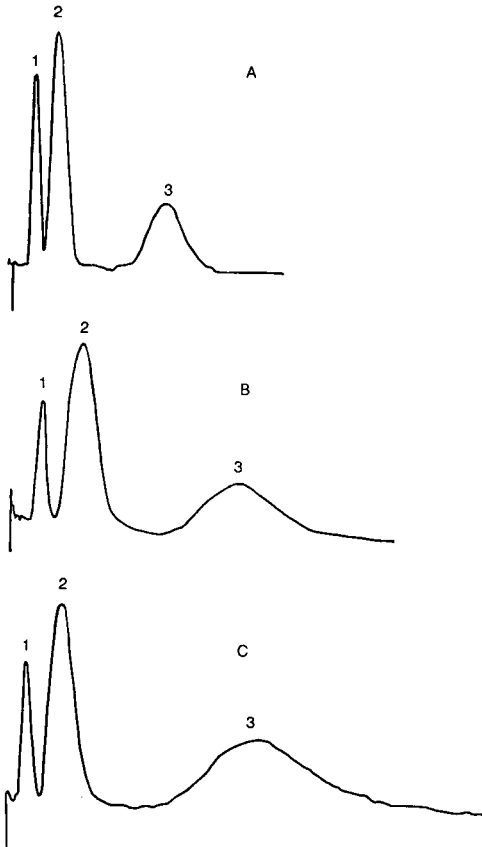


Fig. 6. Separation of *p*-nitrophenyl sugar derivatives on Glutaraldehyde-P affinity media. (A) Preparation 1; (B) preparation 2; (C) preparation 3. Peaks: 1 = *p*-nitrophenyl- β -D-glucoside; 2 = *p*-nitrophenyl- α -D-glucoside; 3 = *p*-nitrophenyl- α -D-mannoside. Con A–Glutaraldehyde-P was equilibrated with 0.025 *M* Tris–HCl, pH 6.8 containing 0.2 *M* NaCl, 1 *mM* MnCl₂ and 1 *mM* CaCl₂ at 2 ml/min. Absorbance was monitored at 305 nm.

column is well above the analytical range. A better understanding of how to increase loading without affecting the specificity and stability of the medium may well make affinity-based separation procedures less costly and should considerably expand the use of affinity chromatography on a process scale.

ACKNOWLEDGEMENTS

We are grateful to Dr. S. Kakodkar for synthesizing the bonded phases and to Drs. D. Nau, S. Berkowitz and M. Henry for their valuable suggestions in the preparation of this manuscript.

REFERENCES

- 1 P. Cuatrecasas, *J. Biol. Chem.*, 245 (1970) 3059–3065.
- 2 M. A. Rounds, W. Kopaciewicz and F. E. Regnier, *J. Chromatogr.*, 362 (1986) 187–196.
- 3 S. H. Chang, R. Noel and F. E. Regnier, *Anal. Biochem.*, 48 (1976) 1839.
- 4 G. Vanacek and F. E. Regnier, *Anal. Biochem.*, 121 (1982) 156.
- 5 K. K. Unger, *Porous Silica, its Properties and Use as Support in Column Liquid Chromatography (Journal of Chromatography Library, Vol. 16)*, Elsevier, Amsterdam, 1979.
- 6 H. Engelhardt and H. Elgass, in Cs. Horváth (Editor), *High Performance Liquid Chromatography—Advances and Perspectives*, Vol. 2, Academic Press, New York, 1980, pp. 57–108.
- 7 M. T. W. Hearn (Editor), *HPLC of Proteins, Peptides and Polynucleotides*, Verlag Chemie, Boca Raton, FL, 1990.
- 8 S. A. Berkowitz, *Adv. Chromatogr.*, 29 (1989) 176–269.
- 9 J. A. Thompson, *Biochromatogr.*, 2 (1987) 68.
- 10 Y. D. Clonis, K. Jones and C. R. Lowe, *J. Chromatogr.*, 363 (1986) 31–36.
- 11 J. X. Huang and G. Guiochon, *Biochromatogr.*, 3 (1988) 40.
- 12 D. R. Nau, *J. Chromatogr.*, (1990) submitted for publication.
- 13 G. Guiochon and M. Martin, *J. Chromatogr.*, 326 (1985) 3–32.
- 14 F. Katz, K. L. Ogan and R. P. W. Scott, *J. Chromatogr.*, 289 (1984) 65–83.
- 15 J. H. Knox and H. P. Scott, *J. Chromatogr.*, 316 (1984) 311–332.
- 16 K. K. Unger, J. N. Kinkel, B. Anspach and H. Giesche, *J. Chromatogr.*, 296 (1984) 3–11.
- 17 R. R. Walters, *J. Chromatogr.*, 249 (1982) 19–28.
- 18 B. J. Horstmann, C. N. Kenny and H. A. Chase, *J. Chromatogr.*, 361 (1986) 179–190.
- 19 W. Kopaciewicz, S. Fulton and S. Y. Lee, *J. Chromatogr.*, 409 (1987) 111–124.
- 20 D. Wu and R. R. Walters, *J. Chromatogr.*, 458 (1988) 169–174.
- 21 W. S. Foster and J. A. Anderson, presented at *Pittsburgh Conference on Analytical Chemistry and Applied Spectroscopy, New Orleans, LA, 1988*, Paper No. 395.
- 22 S. R. Narayanan, S. V. Kakodkar and L. J. Crane, *J. Chromatogr.*, (1990) submitted for publication.
- 23 H. E. Ramsden, *U.S. Pat.*, 4 540 486 (1985).
- 24 A. E. Parkinson and E. C. Wagner, *Ind. Eng. Chem.*, 6 (1934) 433–436.
- 25 S. Lowell and J. E. Shields, in B. Scarlett (Editor), *Powder Surface Area and Porosity (Powder Technology Series)*, Chapman and Hall, New York, 1987.
- 26 F. E. Regnier, *Science (Washington, D.C.)*, 238 (1987) 319.

CHROM 22 122

Large-scale purification of factor VIII by affinity chromatography: optimization of process parameters

MARCEL P. W. M. TE BOOY, ANITA FABER, EGGE DE JONGE and ERNST P. WOLTERINK
Central Laboratory of the Netherlands Red Cross Blood Transfusion Service, P.O. Box 9406, 1006 AK Amsterdam (The Netherlands)

WAANDER RIETHORST, TOM BEUGELING and ADRIAAN BANTJES
University of Twente, Department of Chemical Technology, 7500 AE Enschede (The Netherlands)
and

JAN OVER and BOUDEWIJN W. KÖNIG*
Central Laboratory of the Netherlands Red Cross Blood Transfusion Service, P.O. Box 9406, 1006 AK Amsterdam (The Netherlands)

(First received July 5th, 1989; revised manuscript received October 27th, 1989)

SUMMARY

The optimization of a new process for the extraction of human coagulation factor VIII (FVIII) from plasma with the tailor-made affinity matrix dimethylamino-propylcarbonylpentyl-Sepharose CL-4B (C3–C5 matrix) is described. First, plasma is applied to DEAE-Sephadex A-50 anion exchanger in order to separate a number of proteins, including coagulation factors II, IX and X (prothrombin complex), from FVIII. Subsequently, the unbound fraction of the ion exchanger, containing FVIII, is contacted with the C3–C5 affinity matrix. Optimization of the FVIII affinity chromatographic procedure is accomplished in terms of the ligand density of the matrix, adsorption mode (batch-wise *versus* column-wise adsorption and matrix to plasma ratio), and conditions of pH and conductivity to be applied on washing and desorption. In scale-up experiments, by processing 20 l of plasma, the recovery (340 U VIII:C/kg plasma) and the specific activity (s.a.) (1.2 U VIII:C/mg protein) are better than those obtained by cryoprecipitation (recovery 300 U VIII:C/kg plasma, s.a. 0.3 U VIII:C/mg protein). The newly developed process using the specially designed C3–C5 affinity matrix has potential application in the process-scale purification of FVIII.

INTRODUCTION

Preparations of coagulation factor VIII (FVIII) and Von Willebrand factor (vWf) are used in the treatment of patients suffering from haemophilia A or Von Willebrand's disease. Cryoprecipitation is the technique most commonly used to recover these components from human donor plasma^{1,2}. Unfortunately, the FVIII

yield and specific activity (s.a.) of cryoprecipitate are usually low: only 40% of FVIII in plasma can be recovered with an s.a. of 0.3 U factor VIII activity (VIII:C) per mg of protein. As impurities in the cryoprecipitate might cause side effects^{3,4}, successive purification methods have been developed⁵⁻¹¹ which yield FVIII preparations with s.a. varying from 1 to 3000 U VIII:C/mg protein. However, high degrees of purification inevitably imply a low recovery; final recoveries of VIII:C of less than 20% are common in plasma fractionation on a full process scale. These low recoveries are mainly due to the use of cryoprecipitate as the source material for FVIII preparations with a higher purity.

Higher recoveries may be obtained when cryoprecipitation is replaced by a more efficient method. Therefore, it was investigated whether direct application of (affinity) chromatography to plasma could result in an FVIII preparation which is better in terms of recovery and degree of purification. Considering the limited availability of human donor plasma, a high recovery was of greater importance in this investigation than a high degree of purification. Further, a reproducible and controllable process is necessary to meet the good manufacturing practices (GMP) requirements set for the production of pharmaceuticals (*e.g.*, protein) for use in humans¹².

The synthesis of several affinity matrices, specially developed for isolation of FVIII directly from plasma, was reported previously^{13,14}. One of these FVIII affinity matrices, dimethylaminopropylcarbonylpentyl-Sepharose Cl-4B, proved to be the most suitable for the purification of FVIII from plasma¹⁴. In this paper, results are presented concerning the optimization of a chromatographic FVIII purification procedure, with this tailor-made affinity matrix, characterized by a relatively high recovery and s.a. of FVIII.

EXPERIMENTAL

Materials

Normal plasma pools were prepared from 30-80 donations of citrate-phosphate-dextrose-adenine (CPDA-1)-anticoagulated plasma [Central Laboratory of the Netherlands Red Cross Blood Transfusion Service (CLB), Amsterdam, The

TABLE I
OVERVIEW OF BUFFERS AND THEIR COMPOSITIONS

Buffer type ^a	pH	[Sodium chloride] (M)	[Sodium acetate] (M)	[L-Lysine] (M)
A	7.0	0.18		
B	7.0	2.0		
C	7.4	—	0.1	0.1
D	7.4	1.0	0.1	0.1
E	7.4	X ^b		
F	Y ^b	0.17		
G	7.4	Z ^b	0.1	0.1
H	7.4	0.04		0.1

^a The buffers contained also 10 mM sodium citrate and 1 mM calcium chloride.

^b X = 0.10-0.25 M NaCl; Y = pH 6-8; Z = 0.25-1.50 M NaCl.

Netherlands]. Human serum albumin and specific antisera against human albumin, fibronectin, fibrinogen and factor II were from the CLB. DEAE-Sephadex A-50, Sepharose CL-4B and chromatographic columns (C10/20, C16/30, C26/30, K50/30 and BP 113/30) were obtained from Pharmacia (Uppsala, Sweden). Affinity matrices with various ligand densities were obtained as described below. All chemicals were purchased from Merck (Darmstadt, F.R.G.). In Table I, an overview of the composition of the buffers used is presented.

Synthesis of affinity matrix

For synthesis of the affinity matrix, the method described by Riethorst¹³ was used: a known amount (settled gel volume) of Sepharose CL-4B was solvent exchanged from water to dimethylformamide (DMF) by washing the support extensively with dry DMF on a sintered-glass filter (G3). Subsequently, the support was activated (1.5 h, 20°C) with 1,1'-carbonyldiimidazole (CDI). The degree of activation was varied by the amount of CDI, dissolved in DMF, added to the support (0.10–0.32 mmol/ml of settled gel in water). The CDI-activated support was washed with DMF and, subsequently, 6-aminohexanoic acid was coupled (20°C, 10 h) by mixing a solution of the amino acid in water (pH 12.6) with the gel suspension (0.9 mmol of the amino acid per ml of settled gel in water). After coupling, the gel was washed with DMF and water, the ligand density of the carboxylic acid end groups on the support was determined (see below) and the support was again solvent exchanged to DMF. Carboxylic acid end-groups were esterified (20°C, 16 h) with N-hydroxysuccinimide (4–6 times the amount of carboxylic acid groups) using an equal amount of 1-ethyl-3-(3-dimethylaminopropyl)carbodiimide as a coupling agent. After washing with DMF, dimethylaminopropylamine (20 times the amount of carboxylic acid groups) was coupled onto the matrix (20°C, 16 h). After solvent exchange to water, the density of the dimethylaminopropylcarbonylpentyl (C3–C5) ligands on the affinity support was determined (see below). Finally, C3–C5 affinity matrices were obtained with various ligand densities (40–100 μmol/ml of settled wet gel). The structure of the affinity matrix (C3–C5 matrix) is shown in Fig. 1.

Assays

Ligand densities of affinity matrices (μmoles of amine per ml of settled wet gel volume) were calculated from the hydrochloric acid titration curve of the sodium hydroxide equilibrated matrix¹⁵. FVIII activity (VIII:C) was determined in a chromogenic substrate assay (Coatest factor VIII, KabiVitrum, Stockholm, Sweden). FVIII and vWf protein concentrations [factor VIII antigen (VIII:Ag) and vWf antigen (vWf:Ag), respectively] were determined in sandwich enzyme-linked immunosorbent assays (ELISAs) using monoclonal antibodies directed against factor VIII (CLB-CAG-A and CLB-CAG-117) and vWf (CLB-RAG-20 and CLB-RAG-35), respectively. Coagulation factors II, VII, IX and X were determined with assays^{16–18}

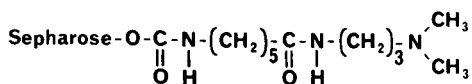


Fig. 1. Structure of the C3–C5 affinity ligand.

using artificial substrate plasmas for FII and FX, congenitally deficient substrate plasma for VFII and immunodepleted substrate plasma for FIX determination. The vWf multimeric structure was analysed using agarose gel electrophoresis¹⁹.

The vWf activity [vWf-associated ristocetin cofactor activity (vWf:RCo)] was determined by ristocetin-induced agglutination of washed platelets²⁰. A normal plasma pool, calibrated against 30 normal plasmas, was used as a standard in all assays for coagulation factors, vWf:RCo and vWf:Ag. Traces of thrombin, if present, were determined by adding a 0.3% (w/w) fibrinogen solution (KabiVitrum) to an equal volume of sample. One mixture was incubated for 20 h at 24°C and one for 6 h at 37°C. After incubation, the mixtures were checked for fibrin formation. Albumin, IgG, IgA and IgM were determined in a nephelometer analyser (Behring, Marburg, F.R.G.). Fibrinogen, fibronectin and factor II antigen concentrations were determined by single radial immunodiffusion²¹, using specific antisera (CLB). C₁-esterase inhibitor activity was determined in a chromogenic substrate assay (Behrichrom, Behring, R.R.G.). Total protein content was determined with the BCA-protein assay (Pierce, Rockford, IL, U.S.A.), using purified human serum albumin (CLB) as a protein standard.

Chromatographic procedures

Batch-wise adsorption of plasma proteins onto the DEAE-Sephadex A-50 ion exchanger was achieved by adding various amounts of plasma to the pre-swollen matrix [26.7 g of dry ion exchanger per litre of 0.9% (w/v) sodium chloride]. The adsorption was carried out for 15–90 min at 15°C. After separation of the anion exchanger from the plasma using 20- μ m netting (Type NY-20-hc, ZBF, Rueschlikon, Switzerland), the ion exchanger was suspended in buffer A (Table I) and poured into a chromatographic column. After settling of the gel, the anion exchanger was washed with buffer A at a flow-rate of 24 cm/h. Proteins, such as FII, FIX and FX, were desorbed from the DEAE-Sephadex by elution, at the same flow-rate, with four column volumes of buffer B (Table I).

Batch-wise adsorption of plasma proteins onto the C3–C5 matrices was achieved by “end-over-end” mixing of at least 2 ml (wet gel volume) of equilibrated matrix (buffer E, Table I, $x = 175$ mM) with various amounts of plasma. Adsorption times varied from 5 min to 6 h (adsorption temperature 20°C). The C3–C5 matrix, separated from the supernatant plasma by centrifugation (3 g, 5 min), was transferred to a column and after settling the gel was washed (3–6 bed volumes) and proteins (*e.g.*, FVIII) were eluted (6–10 bed volumes) at a flow-rate of 30–60 cm/h. For the buffers applied, see Results. For column-wise adsorption, the C3–C5 matrix was packed under pressure (0.15 bar) and equilibrated with buffer E (Table I, $x = 175$ mM). Fresh thawed plasma (volume 18–35 times the bed volume) was incubated batch-wise for 60 min at 15°C with preswollen DEAE-Sephadex A-50 (0.5 g of ion exchanger per kg of plasma). After filtration (0.5- μ m filter, Profile type R1f005; Pall, Portsmouth, U.K.), the filtrate was applied to the affinity matrix at a flow-rate of 30 cm/h. After protein adsorption, the matrix was washed with 3–6 column volumes of buffer E (Table I, $x = 175$ mM) and proteins were desorbed by elution with 5–10 column volumes of buffer D (Table I) at the same flow-rate. The desorption fraction of the C3–C5 matrix was concentrated and dialysed against buffer H (Table II) using a haemodialysis cartridge with a cut-off of 100 000 (type HF 40; Fresenius, Bad Homburg, F.R.G.).

TABLE II

BATCH-WISE *VERSUS* COLUMN-WISE ADSORPTION OF FVIII ONTO THE C3-C5 MATRIX

Pretreated plasma is adsorbed onto the C3-C5 matrix (ligand density 90 $\mu\text{mol/ml}$), column-wise washing with six bed volumes of buffer type C (see Table I), flow-rate 30-60 cm/h. Column-wise desorption with ten bed volumes of buffer type D, flow-rate 30 cm/h.

Adsorption type	Time (min)	G:P ratio ^a (v/v)	FVIII		Protein desorbed (%)
			Adsorbed (%)	Desorbed (%)	
Batch	60	1:20	>95	61	0.3
	60	1:25	85	55	0.3
	60	1:30	75	45	0.3
	360	1:20	>95	51	0.4
Column	70	1:20	>95	69	0.5
	220	1:20	>95	61	0.5
	360	1:20	>95	51	0.5
	450	1:25	>95	49	0.5
	540	1:30	>95	51	0.5
	630	1:35	>95	35	0.4

^a G:P ratio is the ratio (v/v) of C3-C5 matrix to plasma pretreated with 0.5 g of dry DEAE-Sephadex A-50 per kg of plasma.

RESULTS

Separation of coagulation factors II, IX and X from factor VIII

Under conditions such that FVIII is completely absorbed onto the C3-C5 matrix, other coagulation factors (II, IX and X) are simultaneously absorbed from plasma¹⁴. Therefore, in order to separate FII, FIX and FX from FVIII, an additional ion-exchange step with DEAE-Sephadex A-50 was introduced prior to adsorption of proteins onto the C3-C5 matrix. Fig. 2 shows the time-dependent kinetics of ad-

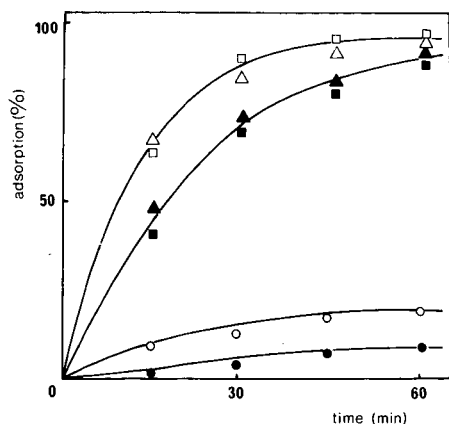


Fig. 2. Time-dependent adsorption of coagulation factors II (\square), VIII (\circ) and IX (\triangle) from normal plasma onto DEAE-Sephadex A-50 at ratios of 0.75 (open symbols) and 0.50 (solid symbols) of dry DEAE-Sephadex A-50 per kg of plasma. Batch-wise adsorption at 15°C.

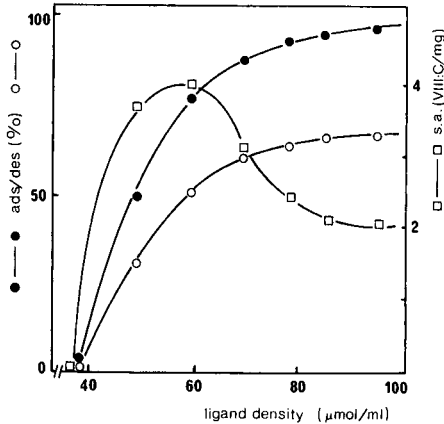


Fig. 3. Adsorption (●) and desorption (○) of VIII:C from the C3-C5 matrix and specific activity (s.a.) (□) of desorbed VIII:C as a function of the ligand density of the affinity matrix. Batch-wise incubation for 1 h of 30 ml of plasma, pretreated with 0.5 g of dry DEAE-Sephadex A-50 per kg of plasma and 2 ml of C3-C5 matrix. Column-wise washing with 12 ml of buffer type C (see Table 1) at a flow-rate of 60 cm/h. Column-wise desorption with 20 ml of buffer type D at a flow-rate of 30 cm/h at 20°C.

sorption of coagulation factors II, VIII and IX onto the DEAE-Sephadex A-50 anion exchanger at two different ratios of anion exchanger to plasma (0.5 and 0.75 g of dry DEAE-Sephadex A-50 per kg of plasma). As the adsorption kinetics of FIX and FX are essentially the same, only the ad-/desorption data for FIX are presented. Fig. 2 shows that an optimum separation of FVIII from FII and FIX can be obtained by using an incubation time of 60 min at a ratio of 0.5 g of anion exchanger per kg of plasma. Under these conditions, >90% of the coagulation factors II and IX are removed by adsorption onto the anion exchanger at the cost of a 10–15% loss of VIII:C in the unbound fraction. Plasma pretreated with DEAE-Sephadex A-50, as described above, is used as the starting material for the purification of FVIII by means of the C3-C5 affinity matrix.

Effect of ligand density of the C3-C5 matrix on purification of FVIII

Results of batch-wise adsorption experiments with DEAE-Sephadex A-50 pretreated plasma (Fig. 3) show that a minimum ligand density (>40 μmol/ml) is required for adsorption of FVIII onto the C3-C5 matrix. For complete adsorption of FVIII (in 60 min at a gel-to-plasma ratio of 1:20, v/v), a ligand density of >80 μmol/ml is necessary. The total protein ad-/desorption increases linearly with an increase in ligand density (results not shown). The optimum result with respect to recovery and s.a. of desorbed FVIII is obtained in the range 80–90 μmol/ml: 60% of FVIII is recovered, with an s.a. of 1.8 U VIII:C/mg protein (Fig. 3).

Effect of the composition of wash and desorption buffers on FVIII purity

Varying the pH of the wash buffer between pH 6 and 8 shows that an optimum with respect to FVIII and protein recovered in the desorption fraction is reached between pH 7.0 and 7.5 (Fig. 4A). Increasing the sodium chloride concentration in the wash buffer from 100 to 250 mM results in a linear decrease in the amount of

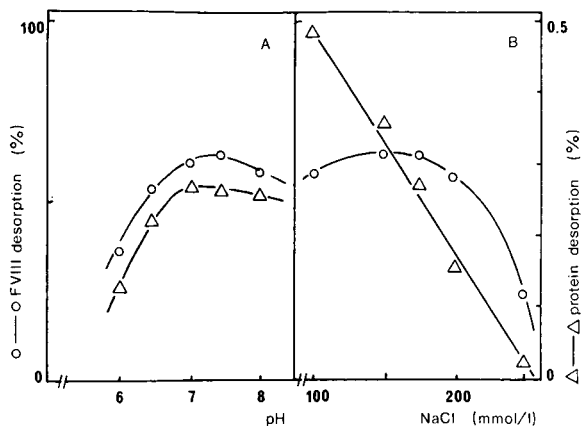


Fig. 4. Effect of (A) pH and (B) NaCl concentration of wash buffer on desorption of VIII:C (○) and protein (Δ) from the C3-C5 matrix. Batch-wise incubation for 1 h of 30 ml of plasma (pretreated with 0.5 g dry of DEAE-Sephadex A-50 per kg of plasma), 2 ml of C3-C5 matrix (ligand density 90 μmol/ml); column-wise washing with 12 ml of buffer type F (A) or type E (B) (see Table I) at a flow-rate of 60 cm. Column-wise desorption with 20 ml of buffer type D at a flow-rate of 30 cm/h at 20°C.

protein desorbed; an optimum in terms of recovery of desorbed FVIII and effective removal of contaminating proteins by salt washing is obtained at a sodium chloride concentration between 150 and 175 mM (Fig. 4B). Fig. 5 shows that the optimum concentration of sodium chloride to be used in the desorption buffer, in terms of the maximum amount of desorbed VIII:C in combination with a minimum of total desorbed protein, is in the range 0.75–1.25 M.

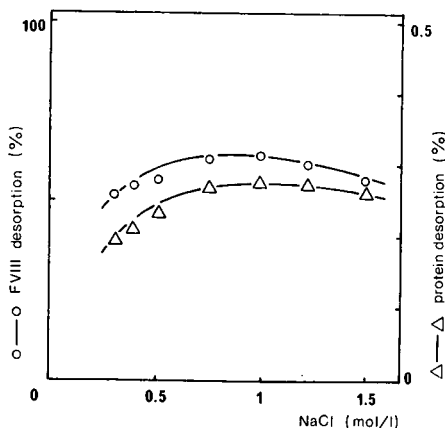


Fig. 5. Effect of NaCl concentration in the elution buffer on desorption of VIII:C (○) and protein (Δ) from the C3-C5 matrix. Batch-wise incubation for 1 h of 30 ml of plasma (pretreated with 0.5 g of DEAE-Sephadex A-50 per kg of plasma), 2 ml of C3-C5 matrix (ligand density 90 μmol/ml); column-wise washing with 12 ml of buffer type E, $X = 0.17$ (see Table I), at a flow-rate of 60 cm/h. Column-wise desorption with 20 ml of buffer type G at a flow-rate of 30 cm/h at 20°C.

Batch-wise versus column-wise adsorption of FVIII

The data in Table II indicate that a decrease in the matrix-to-plasma ratio at a constant batch-wise incubation time (1 h) results in a reduction in the amount of adsorbed and desorbed FVIII. The amount of desorbed total protein, however, is not affected by the matrix-to-plasma ratio. The ratio of 1:20 for the latter is the minimum applicable under these conditions. Prolongation of the incubation time from 60 to 360 min results in a decrease in the amount of FVIII desorbed, whereas the amount of protein desorbed is slightly increased. The results of the column-wise adsorption of FVIII reveal that an extension of the contact time, by increasing the bed height of the column, or an increase in the amount of plasma applied to the matrix has an adverse effect on the amount of desorbed FVIII, whereas the amount of total protein desorbed is not affected.

Scaling up of FVIII purification process

Batch-wise adsorption and column-wise desorption experiments were scaled up from an initial gel volume of 2 ml up to 200 ml. Column-wise adsorption and desorption experiments were scaled up from 10 ml to a gel volume of 1000 ml. In all experiments, plasma pretreated with DEAE-Sephadex A-50 was used as the FVIII source. The amount of plasma applied was usually 15–25 times the gel volume. Prior to column-wise adsorption, the starting material was filtered. Results of scale-up experiments (Table III) show that the FVIII recovery and the amount of total protein desorbed from the C3–C5 matrix are independent of scale size.

Characterization of FVIII concentrate

The FVIII concentrate, obtained from concentration and dialysis of the eluate of the C3–C5 matrix, contained 35 U VIII:C/ml with a specific activity of 1.2 U VIII:C/mg protein. Analysis of vWf:RCo, vWf:Ag and FVIII:Ag revealed (see Table IV) that the VIII:C/VIII:Ag, VIII:C/vWF:RCo and vWf:RCo/vWf:Ag ratios are

TABLE III

SCALING UP OF PROCESS PARAMETERS FOR FVIII PURIFICATION FROM PLASMA WITH THE C3–C5 AFFINITY MATRIX

Adsorption from plasma (pretreated with 0.5 g of dry DEAE-Sephadex A-50 per kg of plasma) onto C3–C5 matrix (ligand density 90 μ mol/ml), batch-wise adsorption in 1 h, column-wise adsorption at a flow-rate of 30 cm/h. Column-wise washing with six bed volumes of buffer type C (see Table I), flow-rate 30–60 cm/h. Column-wise desorption with ten bed volumes of buffer type D, flow-rate 30 cm/h.

C3–C5 matrix (ml)	Plasma (ml)	Factor VIII recovery (%) ^a	Protein recovery (%) ^a	Process time (h)
2	30	57	0.30	2
10	200	58 (55)	0.30 (0.53)	2 (9)
20	400	61 (51)	0.31 (0.49)	5 (9)
100	2000	52 (57)	0.33 (0.40)	5 (8)
200	4000	(56)	(0.50)	(11)
1000	20 000	(52)	(0.46)	(11)

^a Recovery compared with the amount in plasma. Data in parentheses are for column-wise adsorption and desorption.

TABLE IV

CHARACTERIZATION OF FVIII CONCENTRATE ISOLATED BY AFFINITY PURIFICATION WITH C3-C5 MATRIX

<i>Protein</i>	<i>Amount per ml</i>	<i>Recovery (%)^a</i>
VIII:C	35 U	46
VIII:Ag	42 U	55
vWf:RCo	40 U	50
vWf:Ag	44 U	55
Fibronectin	5.2 mg	
Fibrinogen	5.0 mg	
Prothrombin	0.6 mg	
IgG	1.2 mg	
IgA	0.3 mg	
IgM	3.2 mg	
Albumin	3.2 mg	
Total protein	29 mg	

^a Recovery relative to starting plasma.

close to unity. Further, the vWf multimeric pattern of the concentrate (data not shown) is the same as that of the starting plasma. In addition to FVIII and vWf, fibronectin, fibrinogen, IgM, albumin and trace amounts of IgG, IgA and FII were present in the FVIII concentrate (Table IV). These contaminants constitute about 70% of the total amount of protein present. Under the conditions used, neither FVII nor C₁-esterase inhibitor adsorbed onto the C3-C5 matrix.

DISCUSSION

Separation of coagulation factors II, IX and X from factor VIII

Similarly to the use of FVIII concentrates in the treatment of haemophilia A, FIX concentrates are applied for treatment of haemophilia B patients. Commonly FIX concentrates are prepared by ion-exchange chromatography of the supernatant plasma after cryoprecipitation²²⁻²⁴. Since FVIII and FIX, present in plasma, both adsorb onto the C3-C5 matrix and are difficult to separate by means of step-wise sodium chloride elution¹⁴, an additional separation step is needed when both FVIII and FIX concentrates are to be produced. For this purpose, ion-exchange chromatography with DEAE-Sephadex A-50 was implemented prior to application of the plasma onto the C3-C5 matrix. At DEAE-Sephadex-to-plasma ratios of 0.5-0.75 (g dry DEAE-Sephadex per kg plasma), both FII and FIX are removed from plasma relatively fast (Fig. 2). The similarity in the adsorption behaviour of these coagulation factors was also observed by Heystek *et al.*²³. Under these conditions, the adsorption of FVIII is much slower, and the loss of FVIII during the 60-min incubation is limited to 10-15%. Differences in adsorption rate of FII, FIX and FVIII, at low ratios of ion exchanger to plasma, are probably due to the large size difference between FIX and FII ($M_r < 1 \cdot 10^5$ kDa) on the one hand and FVIII, which is complexed to vWf ($M_r > 1 \cdot 10^6$ kDa), on the other. The size of the protein not only affects the diffusion rate but also excludes the larger proteins from penetration into the smaller pores of the ion

exchanger. At a ratio of 0.5 g of DEAE-Sephadex A-50/kg pf plasma, an effective separation between FIX and FVIII is obtained in 1 h. FIX is adsorbed to the extent of >90% whereas FVIII adsorption is less than 15%. Although FVIII adsorption in this step means a direct loss, the overall recovery after desorption from the C3–C5 matrix (57%, Table III) is only slightly lower than that with normal plasma when directly contacted with the C3–C5 matrix and eluted therefrom (62%¹⁴). An additional advantage of treatment of plasma with DEAE-Sephadex A-50, prior to adsorption onto the C3–C5 matrix, is that the binding capacity for FVIII on the C3–C5 matrix is increased from 10 U VIII:C/ml gel¹⁴ to 16 U VIII:C/ml gel (ligand density 90 $\mu\text{mol/ml}$). Further, the s.a. of desorbed FVIII is improved from 1.2 U VIII:C/mg protein¹⁴ to 2.1 U VIII:C/mg protein. The s.a. of the FIX preparation eluted from DEAE-Sephadex A-50 (recovery 55%) is 2.5 U FIX/mg protein. Owing to the low ratio of DEAE-Sephadex A-50 to plasma, this s.a. of FIX is better than that for preparations obtained by reported procedures (1.0–1.5 U FIX/mg protein^{22–24}).

Effect of ligand density

For the determination of the optimum ligand density of the C3–C5 matrix, a compromise is made between s.a., adsorption time, economics and recovery. Compared with high ligand densities, the lower ligand densities give a higher s.a. at lower yields (Fig. 3) and need longer adsorption times and/or higher matrix-to-plasma ratios (data not shown). As a matrix-to-plasma ratio of 1:20 (v/v) is considered to be the maximum for production purposes, a ligand density of 90 $\mu\text{mol/ml}$ is required to give fast and complete adsorption of FVIII. At this ligand density, the s.a. of desorbed FVIII still meets our goals. It is remarkable that, independent of the ligand density applied, the ratio of desorbed to adsorbed FVIII is a constant factor (0.65). This sets clear limits to the maximum recovery of FVIII in this type of chromatographic process step. Nevertheless, this result is better than that with chromatography of FVIII on aminohexyl-Sepharose, where a ratio of <0.50 is found^{25,26}.

Effect of composition of the wash and desorption buffer

Because the developed purification method for FVIII described is for process-scale chromatography, the compositions of the buffers are kept relatively simple. Variations in pH (6.0–8.0) and sodium chloride concentration (100–1500 mM) in the buffers are limited owing to the lability of FVIII. The optimum sodium chloride concentration in the wash buffer is 170 mM; higher sodium chloride concentrations result in desorption of FVIII and at lower concentrations removal of contaminating proteins is not as effective. The optimum pH of the wash buffer in combination with a sodium chloride concentration of 170 mM is 7.4. At higher pH the FVIII is less stable, resulting in denaturation of FVIII, and at lower pH more protein, including FVIII, is washed from the matrix. These results are in accordance with results obtained with aminohexyl-Sepharose^{25,26}. Variation of the sodium chloride concentration in the desorption buffer had a minor effect on the s.a. of FVIII. As the desorption of FVIII is tailing at low sodium chloride concentration, a sodium chloride concentration in the desorption buffer of 1 M is used as an optimum concentration with respect to FVIII recovery.

Batch-wise versus column-wise adsorption of FVIII and scaling up of process parameters for FVIII purification

The results in Table II show that batch-wise and column-wise adsorption (same adsorption time) differ mainly in the total amount of protein (adsorbed and) desorbed. There are also differences in the final FVIII recovery, but these seem to be caused by the longer process time and are independent of the adsorption principle. For the choice of the adsorption mode to be applied on a production scale, where plasma volumes of 750–1000 l are processed, not only aspects such as recovery and purity are important parameters, but also whether the process meets GMP requirements¹². From the latter point of view, it may be clear that a batch-wise adsorption process, despite its higher recovery and purity, is not to be preferred. Therefore, column-wise adsorption is chosen as the adsorption mode for further scaling up. This choice has an impact on the process time. As the maximum flow-rate is not limited by the adsorption kinetics of FVIII, it is determined by the maximum flow-rate at which the C3–C5 matrix, *i.e.*, Sepharose CL-4B, can be operated. A bed height of 10 cm, which can still be used on a process scale, and a sample volume of 20 column volumes results in an adsorption time of 6–7 h. Scaling up experiments with the C3–C5 matrix (Table III) show that despite the long process time for column-wise adsorption and desorption, the FVIII recovery is > 50% and the purity of the eluate is > 1 U VIII:C/mg protein. These parameters are independent of the process scale, which offers good prospects for further scaling up.

Characterization of FVIII concentrate

The overall recovery after concentration and dialysis of the eluate of the C3–C5 matrix is 46%, which is an improvement over the FVIII preparations obtained by cryoprecipitation, where recoveries of 40% are common³. The s.a. of the concentrate is > 1.0 U VIII:C/mg protein, which is higher than that obtained with cryoprecipitation (0.3 U VIII:C/mg protein) and comparable to the s.a. of common intermediate-pure FVIII concentrates, prepared from cryoprecipitate at a much lower (> 20%) FVIII recovery³. The quality of the concentrated FVIII preparation is good as the VIII:C-to-VIII:Ag ratio is close to unity, indicating that the amount of inactive FVIII is low. The same holds true for the vWf:RCo-to-vWf:Ag ratio, indicating that all vWf present in the concentrate is active. The FVIII-to-vWf ratio is also 1.0, which is favourable for preservation of VIII:C as FVIII is stabilized by vWf. In comparison with common intermediate-pure FVIII concentrates, these data are better, as in most of these concentrates the VIII:C-to-VIII:Ag and vWf:Rco-to-vWf:Ag ratios are < 1.0 and the FVIII-to-vWf ratio is > 1.0²⁷. The presence of high-molecular-weight multimers of vWf in the FVIII concentrate implies that this preparation, in contrast to other FVIII concentrates, can also be of use in the treatment of von Willebrand's disease.

CONCLUSION

With the purification method described, an FVIII concentrate can be obtained with a high yield and a relatively high yield and a relatively high s.a. as compared with cryoprecipitation. The process can meet GMP requirements, is reproducible and has the potential for automation. The implementation of the FVIII purification method

into the fractionation of plasma has no negative effects on the purification of FIX (prepared from the DEAE-Sephadex A-50 desorption fraction), FVII and C₁-esterase inhibitor, albumin and immunoglobulins which are present in the unbound fraction of the C3-C5 affinity matrix. Therefore, this affinity chromatographic method for FVIII purification from plasma has great potential for replacing cryoprecipitation. Further optimization of the method will be carried out with respect to reduction of the process time of elimination of blood-borne viruses, such as human immunodeficiency virus (HIV), hepatitis B virus and hepatitis non-A, non-B virus³.

ACKNOWLEDGEMENTS

We thank Miss J. Brummel and Miss B. V. Driessen for technical assistance and Dr. H. Hiemstra for critically reading the manuscript.

REFERENCES

- 1 J. G. Pool, E. J. Hershgold and A. R. Pappenhagen, *Nature (London)*, 203 (1964) 312.
- 2 J. G. Pool and A. E. Shannon, *New Engl. J. Med.*, 273 (1965) 1443.
- 3 H. R. Roberts and B. G. Macik, in M. Verstraete, J. Vermeylen, R. Lijnen and J. Arnout (Editors), *Thrombosis and Haemostasis 1987*, Leuven University Press, Leuven, 1987, p. 563.
- 4 M. N. Lederman, C. Saunders, Z. Toosi, N. Lemon, B. Everson and O. D. Ratnof, *J. Lab. Clin. Med.*, 107 (1986) 471.
- 5 J. Margolis, C. M. Galloich and P. Rhoades, *Vox Sang.*, 46 (1984) 341.
- 6 K. M. Brinkhous, E. Shanbrom, H. R. Roberts, W. P. Webster, L. Fekete and R. H. Wagner, *J. Am. Med. Assoc.*, 205 (1968) 613.
- 7 J. Newman, A. J. Johnson, S. Karpatkin and S. Puszkin, *Br. J. Haematol.*, 2 (1971) 1.
- 8 C. A. Fulcher and T. S. Zimmerman, *Proc. Natl. Acad. Sci. U.S.A.*, 79 (1982) 1648.
- 9 V. S. Hornsey, B. D. Griffin, D. S. Pepper, L. R. Micklem and C. V. Prowse, *Thromb. Haemostas.*, 57 (1987) 102.
- 10 M. Griffith, S. Liu, G. Neslund, I. Tsang, D. Lettelier and R. Berkebile, *Thromb. Haemostas.*, 58 (1987) 307.
- 11 P. A. Miescher and E. R. Jaffe (Editors), *Semin. Hematol.*, 25 Suppl. 1 (1988) 1-45.
- 12 G. Auerhoff, *Pharm. Ind.*, 50 (1988) 209.
- 13 W. Riethorst, *Ph. D. Thesis*, Technical University, Twente, 1988.
- 14 M. P. W. M. te Booy, W. Riethorst, A. Faber, J. Over and B. W. König, *Thromb. Haemostas.*, 61 (1989) 234.
- 15 E. A. Peterson and H. A. Sober, *J. Am. Chem. Soc.*, 78 (1956) 751.
- 16 J. J. Veltkamp, E. F. Drion and E. A. Loeliger, *Thromb. Diath. Haemorrh.*, 19 (1968) 279.
- 17 K. W. E. Denson, *Acta Haematol.*, 15 (1961) 105.
- 18 R. Biggs, *Human Blood Coagulation, Haemostasis and Thrombosis*, Blackwell, Oxford, 2nd edn., 1976.
- 19 Z. Ruggeri and T. S. Zimmerman, *J. Clin. Invest.*, 65 (1980) 1318.
- 20 H. J. Weiss, J. Rogers and H. Brand, *J. Clin. Invest.*, 52 (1973) 2697.
- 21 G. Mancini, A. O. Carbonara and J. F. Heremans, *Immunochemistry*, 2 (1965) 235.
- 22 S. M. Middleton, I. H. Bennett and J. K. Smith, *Vox Sang.*, 24 (1973) 441.
- 23 J. Heystek, H. G. J. Brummelhuis and H. W. Krijnen, *Vox Sang.*, 25 (1973) 113.
- 24 L. Pejaudier, V. Kichenin-Martin, M. C. Boffa and M. Steinbuch, *Vox Sang.*, 52 (1987) 1.
- 25 D. E. G. Austen, *Br. J. Haematol.*, 43 (1979) 669.
- 26 A. Faure, M. Caron and D. Tepenier, *J. Chromatogr.*, 257 (1983) 387.
- 27 A. Yoshioka, M. Shima, M. Nishino, N. Yoshikawa and H. Fukui, *Drug Res.*, 37 (1987) 753.

Reversed-phase high-performance liquid chromatographic separation of the enantiomers of N-[4,4-di(3-methylthien-2-yl)-but-3-enyl] nipecotic acid on a Pirkle-type phenylglycine stationary phase

ABU M. RUSTUM* and LORENZO GUTIERREZ

Analytical Research Department, Pharmaceutical Products Division, Abbott Laboratories, North-Chicago, IL 60064 (U.S.A.)

(First received June 15th, 1989; revised manuscript received November 22nd, 1989)

SUMMARY

The enantiomers of N-[4,4-di(3-methylthien-2-yl)-but-3-enyl] nipecotic acid hydrochloride are separated by reversed-phase high-performance liquid chromatography on a commercially available chiral stationary phase. Prior to chromatography, the chiral compound was derivatized into an amide by reacting it with an achiral amine. The amide derivative of the *S*- and *R*-enantiomers were baseline resolved on a commercially available Pirkle-type L- or D-phenylglycine chiral stationary phase with a selectivity factor (α) of 1.2. The limit of detection of the *S*-enantiomer is less than 0.03% in the *R*-enantiomer. The derivatized enantiomers were monitored by UV at 260 nm and 0.20–0.01 a.u.f.s. Several other commercially available chiral stationary phases were also investigated to achieve optimum sensitivity and separation of the enantiomers of the chiral compound.

INTRODUCTION

The enantiomers of different drugs which have one or multiple asymmetric center(s), may differ widely in their pharmacodynamic and toxicological properties. To establish the enantiomeric purity of chiral drugs and to determine the chiral selectivity of the synthesis, simple, sensitive, and reproducible analytical methods are required.

Gas chromatography (GC) and high-performance liquid chromatography (HPLC) have been used to separate and quantify the enantiomers in a mixture^{1–9}. Numerous theoretical studies on the chiral stationary phases of HPLC and chiral derivatizing reagents have been conducted to understand the separation mechanisms of the enantiomers^{10–15}. The results of these studies aided scientists for better understanding and optimization of the separation parameters. Wainer^{16,17} has classified chiral stationary phases according to their mode of separation mechanism of chiral compounds which have different functional groups. Gal¹⁸ has conducted some useful

studies on the formation of diastereoisomers with optically pure reagents and subsequent chromatographic separations. Because of the availability of the technology, the United States Food and Drug Administration (U.S. FDA) has more stringent regulations for the marketing of drugs which have (an) optically active center(s)¹⁹. Therefore, an analytical method is required to study the pharmacokinetic behavior and other pharmacological activities of each of the pure enantiomers of a racemic drug to satisfy the requirements of the U.S. FDA.

In this work, D- and L-phenylglycine chiral stationary phases (CSPs) were used to separate and quantify the enantiomers of N-[4,4-di(3-methylthien-2-yl)-but-3-enyl] nipecotic acid hydrochloride. The chemical structure of the chiral compound is shown in Fig. 1. This compound has potential therapeutic use as an antiepileptic agent. The *R*-enantiomer has been found to be therapeutically more active than the *S*-enantiomer. An analytical method is required to determine the purity of the pharmacologically active enantiomer in order to obtain pharmacological, toxicological, and metabolic fate data of this potential drug candidate.

In this study, several chiral stationary phases were investigated in normal-phase and reversed-phase modes to obtain maximum resolution and sensitivity of the enantiomers.

EXPERIMENTAL

Equipment

An HPLC solvent delivery system (SP8800) equipped with an injector/autosampler (SP8780), an integrator (SP4270), and a variable-wavelength UV-visible detector (SP8450) was used in the experiment (Spectra-Physics, San Jose, CA, U.S.A.). A 25 cm × 4.6 mm, Pirkle Covalent L- or D-phenylglycine Hi-Chrom 5- μ m HPLC column was used in the method finally developed (Regis, Morton Grove, IL, U.S.A.). The other CSP columns investigated in this experiment were 5- μ m, 25 cm × 4.6 mm D-phenylalanine and 25 cm × 4.6 mm D-phenylglycine (Jones, Littleton, CO, U.S.A.), and a 25 cm × 4.6 mm, 5- μ m Cyclobond-I (Rainin, Woburn, MA, U.S.A.). Deionized water was collected from a Milli-Q System (Millipore, Bedford, MA, U.S.A.). All quantitative (volume transfer) work was performed with an Eppendorf digital pipette (VWR, Chicago, IL, U.S.A.). A filter apparatus, 4.7 cm (Millipore, Milford, MA, U.S.A.) with nylon-66 membrane filter, 4.7 cm × 0.45 μ m was used to filter the mobile phase (Alltech, Deerfield, IL, U.S.A.). Liquid chromatography-mass spectrometry (LC-MS) was performed on a Nermag Model R30-10 with Vestec thermospray interface (Nermag, France).

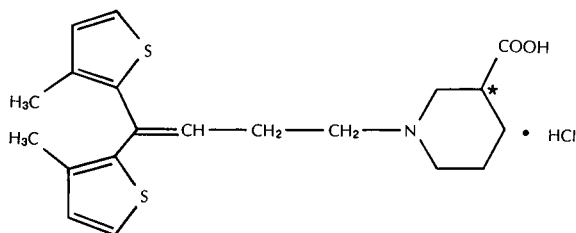


Fig. 1. Chemical structure of N-[4,4-di(3-methylthien-2-yl)-but-3-enyl] nipecotic acid hydrochloride; ★ indicates the chiral center.

Materials

HPLC-grade methanol, acetonitrile, glacial acetic acid (reagent grade), mono-basic potassium phosphate and phosphoric acid were purchased from Fisher Scientific (Fairlawn, NJ, U.S.A.). Ammonium acetate, ACS grade, was purchased from J.T. Baker (Phillipsburg, NJ, U.S.A.). The reagents 1-naphthalenemethylamine (NMA), 1-(3-dimethylaminopropyl)-3-ethylcarbodiimide·HCl (EDC) and 1-hydroxybenzotriazole hydrate (HOBT) were purchased from Aldrich (Milwaukee, WI, U.S.A.). The trifluoroacetic acid was purchased from Mallinckrodt (Paris, KY, U.S.A.). The glass scintillation vials were purchased from American Scientific Products (McGraw Park, IL, U.S.A.). The chiral compound (drug candidate) in its *S*- and *R*-enantiomeric forms was synthesized at Abbott Labs. (North Chicago, IL, U.S.A.).

Derivatization of the chiral compound

Ca. 25 mg of *S*- or *R*-enantiomer or racemic mixture of the chiral compound were transferred into a 20-ml scintillation vial. *Ca.* 10 mg of HOBT, 20 mg of EDC and 8 ml of methylene chloride were taken in a scintillation vial containing the chiral compound. The mixture was sonicated until all the solid materials dissolved in the methylene chloride solution. *Ca.* 15 μ l of NMA were added to the solution and sonicated again for another 10 min. The amide derivative of the parent compound is formed in this step which has the structural formula as shown in Fig. 2. At the completion of the reaction, some precipitate appeared and was removed by filtration through a filter paper. The precipitate was discarded and the filtrate was dried by evaporation with nitrogen. The dry residue was reconstituted into solution with 10 ml of the mobile phase. An aliquot (20–100 μ l) of this solution was injected into the HPLC system.

Preparation of blank

A blank for the derivatization of the chiral compound was prepared by using the same procedure as described, except that no chiral compound was added in the reaction.

Chromatographic conditions of the method finally developed

The mobile phase consisted of 0.10 *M* ammonium acetate (pH 3.70 \pm 0.05)–acetonitrile (61:39, v/v). The pH of the ammonium acetate solution was adjusted with glacial acetic acid. The rate of mobile phase delivery through the HPLC system was 1.5 ml/min. The derivatized chiral compound was monitored by a UV–visible detec-

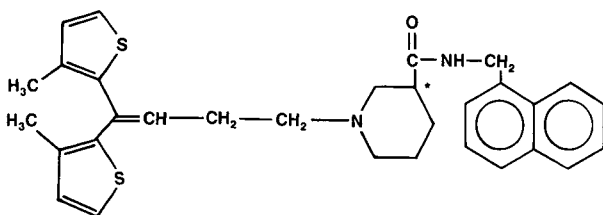


Fig. 2. Chemical structure of the amide derivative of N-[4,4-di(3-methylthien-2-yl)-but-3-enyl] nipecotic acid; ★ indicates the chiral center.

tor at 260 nm at a sensitivity of 0.20–0.01 a.u.f.s. The analytical column and the mobile phase were maintained at ambient temperature during analysis.

Calculation

Quantification of the *S*-enantiomer was done using the following equation:

$$\text{percent of } S\text{-enantiomer} = \frac{\text{peak area of derivatized } S\text{-enantiomer}}{\left(\begin{array}{c} \text{sum of the peak areas of derivatized} \\ R\text{- and } S\text{-enantiomers} \end{array} \right)} \times 100$$

Limit of quantification

The limit of quantification was determined by injecting the derivatized *R*-enantiomer with added amounts of the *S*-enantiomer. The peak of the derivatized *S*-enantiomer was clearly distinguished from the baseline noise when peak area percent of the *S*-enantiomer was 0.03% compared to the peak area of the *R*-enantiomer.

Test for interconversion of the enantiomers during derivatization reaction

The test for the interconversion of the enantiomers during the derivatization reaction was determined by taking the ratio of the weight of the *R*- and *S*-enantiomers, dividing it by the ratio of the peak areas of the *R*- and *S*-enantiomers and multiplying by 100.

RESULTS AND DISCUSSION

Fig. 3 is a typical chromatogram of the blank for the derivatization reaction of the chiral compound which shows that no chromatographic peak from the reagents elutes with the same retention time as those of the derivatized enantiomers. Fig. 4 is a typical chromatogram of the derivatized racemate of the chiral compound which shows that the peaks of derivatized *S*- and *R*-enantiomers are baseline resolved from each other.

The above chromatograms were obtained by using an L-phenylglycine column (Regis). The capacity factors (k') of derivatized *S*- and *R*-enantiomers were *ca.* 7.1 and 8.8 under the chromatographic conditions used in this experiment. The selectivity factor (α) for the derivatized enantiomers was 1.24. A D-phenylglycine column was also tested under identical conditions to those used for the L-phenylglycine column. The α values of the derivatized enantiomers (on D-phenylglycine) remained unchanged, except that the elution profiles of the enantiomers were reversed. This information can be used in trace analysis when the small peak of the trace enantiomer is overlapped by the huge peak of the bulk enantiomer which elutes before the trace enantiomer.

The quantification of the derivatized enantiomers was conducted by peak area percent. The response of the UV detector was linear to at least 30 μg of the derivatized *S*- or *R*-enantiomers. The retention times of the *S*- and *R*-enantiomers were determined by the individual injection of each pure enantiomer (derivatized) into the HPLC system. Complete evaporation of the methylene chloride after the derivatization reaction is very critical. If trace amounts of methylene chloride are present in the injected samples, the retention times of the enantiomers change abruptly. The abrupt

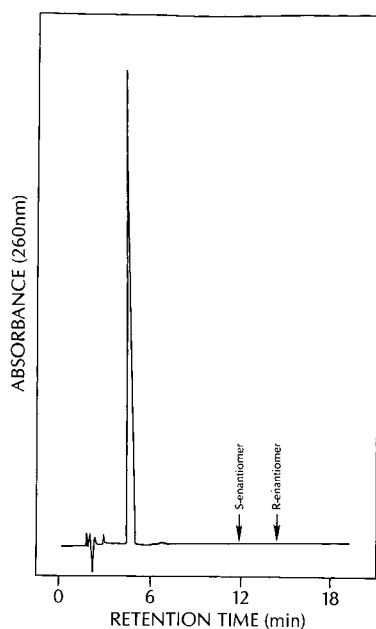


Fig. 3. Chromatogram of a blank for the derivatization reaction of the chiral compound. Column, 25 cm x 4.6 mm, 5 μ m, L-phenylglycine. Detector, 260 nm, 0.10 a.u.f.s.

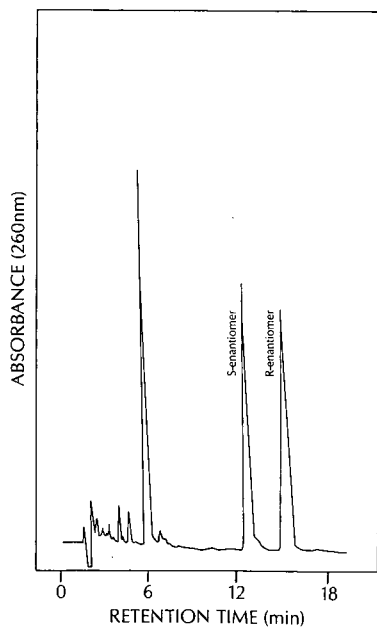


Fig. 4. Chromatogram of derivatized racemate of the chiral compound. Column, 25 cm x 4.6 mm, 5 μ m L-phenylglycine. Detector, 260 nm, 0.10 a.u.f.s.

change in the retention times of the enantiomers due to the presence of methylene chloride, was confirmed by adding one or two drops of methylene chloride in the sample solution prior to injection into the HPLC.

An experiment was conducted to determine if the derivatization reaction of the enantiomers (to form an amide) is dependent on the percent of the *S*- or *R*-enantiomer present in the reaction mixture. Different ratios of the *S*- and *R*-enantiomers were taken into a container and derivatized with NMA. This experiment showed that the peak area ratio of the derivatized product is equal to the weight ratios of the starting (underivatized) *S*- and *R*-enantiomers. The results of this experiment have been summarized in Table I. The data indicate that the interconversion of the enantiomers during the derivatization reaction is practically nil. The results of this experiment also indicate that the extent of derivatization of the *S*- and *R*-enantiomers with NMA is independent of the amount of each enantiomer present in the reaction mixture.

The completion of the derivatization reaction was studied by injecting the derivatized *S*- or *R*-enantiomer into the HPLC system and monitoring the underivatized peak of the enantiomers in the chromatogram under the chromatographic conditions used in this experiment. The retention time of the underivatized peak of the *S*- and *R*-enantiomers were identical and *ca.* 8 min. No peak eluted with the same retention time as the underivatized enantiomers when the derivatized samples of the *S*- and *R*-enantiomers were injected into the HPLC system. This indicates that all the material (*S*- and *R*-enantiomers) used for derivatization formed the amide derivative by reacting with NMA. Therefore, it can be concluded that the derivatization reaction went into completion even when the ratios of the enantiomers in the reaction mixtures were different.

Identification of the derivatized *S*- and *R*-enantiomers (Fig. 4) of the chiral compound was conducted by LC-MS detection. Fig. 5 shows a total ion chromatogram of *m/z* 515. The peaks with retention times of *ca.* 14.3 and 17.5 min have $(M + 1)^+$ of 515. This corresponds to the molecular weight of the derivatized chiral compound which is 514, indicating that the two peaks are enantiomers having different retention times due to the different extents of chiral interaction with the CSP of the column.

To obtain further evidence for identification of the derivatized peaks in Fig. 4,

TABLE I

DATA ON THE INTERCONVERSION OF THE ENANTIOMERS DURING THE DERIVATIZATION REACTION

Weight ratio of <i>S</i> - and <i>R</i> -enantiomer (A)	Peak area ratio of <i>S</i> - and <i>R</i> -enantiomer (B)	Ratio (A/B × 100)
1.200	1.226	102.2
0.333	0.335	100.6
0.786	0.785	99.8
0.754	0.748	99.2
0.491	0.512	104.2
0.952	0.924	94.1

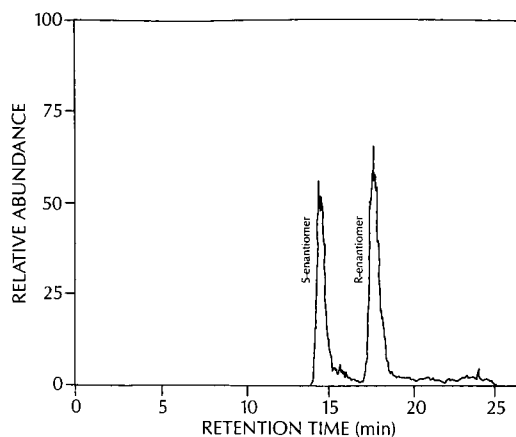


Fig. 5. Total ion chromatogram of m/z 515 of the derivatized chiral compound.

LC-MS analysis of the pure *S*-enantiomer and the *R*-enantiomer was conducted. Fig. 6A and B show the mass spectra (chemical ionization scan) of the derivatized *S*- and *R*-enantiomers. In both spectra, the main peak appeared with an m/z of 515 indicating that they have the same molecular weight, but are resolved on a CSP because of different spatial configurations (Figs. 4 and 5).

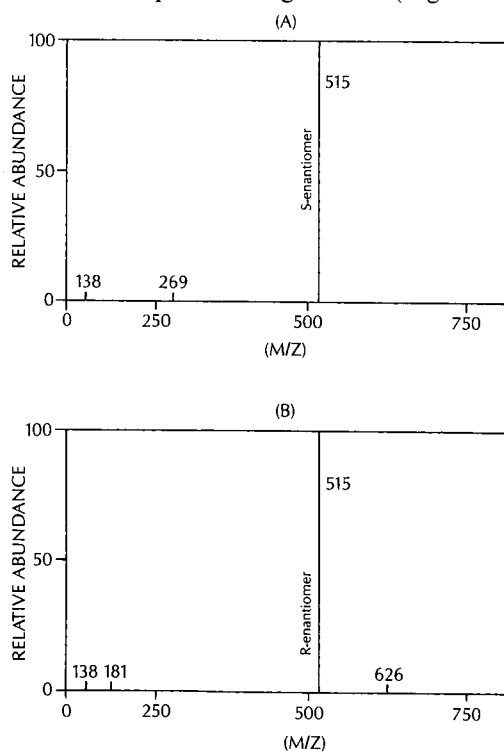


Fig. 6. Mass spectrum of the derivatized chiral compound, (A) m/z of *S*-enantiomer; (B) m/z of *R*-enantiomer.

Standard addition–recovery studies were conducted by two analysts to determine the accuracy of the method for the quantification of 0.05% (w/w) quantities of the *S*-enantiomer in the *R*-enantiomer. The recoveries of the derivatized *S*-enantiomer averaged 94.8% with 7.2% relative standard deviation (R.S.D.) over a range of addition levels from *ca.* 0.5% to 2.0%. The data from these experiments are summarized in Table II.

The precision of the method was also determined by two analysts using a 2–5 mg/ml sample of the derivatized *R*-enantiomer containing trace amounts of the *S*-enantiomer. The precision of the method is 9.0% R.S.D. The results are presented in Table III.

Derivatization of the acid functional group of the chiral compound into an amide (with NMA), was necessary to obtain the resolution of the enantiomers in both the reversed- and normal-phase modes for phenylglycine (D and L) columns. The underivatized chiral compound gave identical retention times (in the reversed- and normal-phase modes) for both the *S*- and *R*-enantiomers on all CSPs [except for bovine serum albumin (BSA)] investigated in this experiment. The identical retention times of the underivatized enantiomers indicate that no significant chiral interaction occurs during equilibration of the chiral compound with the CSP.

The separation of the enantiomers after derivatization may occur due to the deactivation of the strong acid group and also by the attachment of a naphthyl group in the chiral carbon of the molecule, which is rich in π -electrons. According to Pirkle and Hamper²⁰, as the ability of π -electron donation of a chiral molecule increases, the interaction of the molecule with the Pirkle type CSP also increases. The separation of the two enantiomers can only take place if one enantiomer on a time-average basis, has more interaction with the CSP than the other. The spatial configuration of the stationary phase determines which enantiomer should have more chiral interaction than the other, on a certain CSP.

The interesting part of this method is that the separation was achieved in reversed-phase mobile phase conditions. Most of the published literature shows that the separation of chiral compounds on phenylglycine-type of stationary phase takes place with solvents (mobile phase) having little or no hydrogen-bonding ability, because the

TABLE II
STANDARD ADDITION–RECOVERY DATA FOR *S*-ENANTIOMER

<i>Analyst</i>	<i>Baseline signal (A) (%)</i>	<i>Addition level (B) (%)</i>	<i>Theory (A + B) (%)</i>	<i>Found (C) (%)</i>	<i>Recovery [C/(A + B)] (%)</i>
1	0.046	0.500	0.546	0.513	94.0
1	0.046	1.000	1.046	1.100	105.2
1	0.046	2.000	2.046	1.988	97.2
2	0.046	0.570	0.616	0.542	88.0
2	0.046	2.240	2.286	2.050	89.7
				Mean recovery	94.8%
				S.D.	± 6.8
				R.S.D.	7.2%

TABLE III
PRECISION DATA FOR ANALYSIS OF *S*-ENANTIOMER PRESENT IN *R*-ENANTIOMER

<i>Analyst</i>	<i>Peak area % of S-enantiomer</i>
1	0.052
1	0.042
1	0.049
2	0.044
2	0.044
Mean recovery	0.046%
S.D.	±0.004
R.S.D.	9.0%

solvent molecules compete with the chiral molecule for the hydrogen-bonding sites of the stationary phase. Since the mobile phase used in this experiment is highly polar, the separation of the derivatized enantiomers cannot be explained satisfactory by the so-called "three point interaction theory of chiral separation"²⁰ when hydrogen bonding is considered to be an important factor in controlling the separation of the enantiomers. The separation of the enantiomers under the chromatographic conditions used in this experiment may have taken place predominantly due to steric interaction rather than hydrogen bonding with the stationary phase.

The separation of the derivatized enantiomers was also achieved on phenylglycine stationary phases in normal-phase conditions. The resolution mechanism of the enantiomers under normal-phase experimental conditions can be explained quite well by the "three point chiral interaction theory". The mobile phase used was hexane-acetonitrile-isopropanol-trifluoroacetic acid (69:8:19:4, v/v). All other chromatographic conditions were maintained identical to those of reversed-phase mode. The selectivity factor (α) under normal-phase conditions was greater than 1.40, which is higher than the reversed-phase mode. Baseline resolution of two peaks is obtained when α is 1.1. Therefore, in the normal-phase mode, one can obtain baseline separation of the derivatized *S*- and *R*-enantiomers by using a short column.

The moisture content in the solvents of normal-phase chromatography (mobile phase) is sensitive on α and on resolution. Therefore, irreproducible chromatographic parameters may be obtained due to the slight variation of the moisture content in the mobile-phase solvents. Reversed-phase chromatography is more resistant to this effect, and hence, is more reproducible. Also, the solvents in the normal-phase mode are not compatible with LC-MS for conducting the identification work. Therefore, the reversed-phase mode was chosen for separation and identification of the derivatized enantiomers.

An HPLC method to separate the underivatized enantiomers was developed by NOVO, Denmark²¹. A CSP of BSA attached to 7- μ m silica particles was used for the separation. The advantage of this method over the method developed in this report, is that the enantiomers can be separated without derivatization. This advantage was overshadowed by several disadvantages. It is quite difficult to reproduce the separation of the enantiomers (under the same mobile phase conditions) when columns from different batches from the same manufacturer were used. The BSA stationary

phase can be easily damaged if propanol is used in excess of 5% (with water) in the mobile phase. Chromatographic efficiency of the BSA column was lower than the phenylglycine column, probably due to the sluggish mass transfer of the enantiomers on the stationary phase, the mobile phase, or both. The elution order of the enantiomers cannot be reversed (for trace analysis) by using a BSA column, and the limit of detection is only 1% of the *S*-enantiomer in a mixture with the *R*-enantiomer.

A *D*-phenylalanine CSP (Apex Chiral AP) also separated the derivatized enantiomers in the normal-phase mode when a mobile phase of hexane–acetonitrile–isopropanol–trifluoroacetic acid (73:5:19:3, v/v) was used. The α value for this column was also greater than 1.40. This stationary phase did not give any separation of the derivatized enantiomers when used in the reversed-phase mode. The trifluoroacetic acid (TFA) in the mobile phase (under normal-phase conditions) was necessary in order to elute the derivatized enantiomers from the column. When TFA was not used, the derivatized and underivatized enantiomers did not elute from the column.

A *D*-phenylglycine stationary phase column from Jones (Apex Chiral PK) was also tested in the reversed-phase and normal-phase modes. The derivatized *S*- and *R*-enantiomers eluted with the same retention time in both modes. A β -cyclodextrin stationary phase (Cyclobond-I) was also investigated both in the reversed-phase and normal-phase modes. Separation of the derivatized or underivatized enantiomers was not obtained on this stationary phase.

The phenylglycine stationary phase (Regis) used in this method to separate the derivatized enantiomers was found to be extremely stable. The efficiency, selectivity and other chromatographic properties of the phenylglycine column remained unchanged after 200 injections of the derivatized enantiomers. On several occasions, the back pressure of the column increased after 20–40 injections. This problem was eliminated by replacing the inlet frit of the column with a new one or by sonicating the old frit in acetone – 6 *M* nitric acid (50:50) for a few minutes. Two phenylglycine columns from Regis (with different lot numbers) were tested for separation and selectivity of the enantiomers. The resolution and selectivity factors of the two columns were almost identical. The results of this experiment indicate that the separation of the enantiomers is reproducible from column to column when purchased from the same manufacturer.

CONCLUSION

The reversed-phase HPLC method (to separate the derivatized enantiomers) presented here is relatively simple, sensitive and highly reproducible. The pre-chromatographic derivatization of the acid functional group of the chiral compound with an achiral amine into an amide is reproducible, simple and does not convert one enantiomer to another during derivatization. The derivatized sample of the chiral compound needs no extra clean-up steps. This minimized the manipulative error and resulted in good reproducibility. The attachment of a naphthyl group with the chiral compound aided the separation of the enantiomers and also enhanced the UV signal and hence increased the sensitivity. The α value of *D*-phenylglycine and *L*-phenylglycine stationary phases (Regis) were almost identical (1.24) for the derivatized *S*- and *R*-enantiomers. These results indicate that the separation of the derivatized enantiomers is reproducible from column to column having different spatial config-

uration of the stationary phase. This method may be useful to separate (with minor manipulation of the chromatographic conditions) the enantiomers of other derivatives of nipecotic acid or many other compounds which have functional groups and spatial configuration similar to the chiral compound analyzed in this experiment.

REFERENCES

- 1 A. Sioufi, G. Kaiser, F. Leroux and J. P. Dubois, *J. Chromatogr.*, 450 (1988) 221.
- 2 M. Gazdag, G. Szepesi and K. Milhalyfi, *J. Chromatogr.*, 450 (1988) 145.
- 3 B. Blessington and N. Crabb, *J. Chromatogr.*, 454 (1988) 450.
- 4 T. Arai, H. Koike, K. Hirata and H. Oizumi, *J. Chromatogr.*, 448 (1988) 439.
- 5 L. R. Gelber and J. L. Neumeyer, *J. Chromatogr.*, 257 (1983) 317.
- 6 H. Furukawa, *Chem. Pharm. Bull.*, 23 (1975) 1625.
- 7 J. N. LePage, W. Lindner, G. Davies, D. Seitz and B. L. Karger, *Anal. Chem.*, 51 (1979) 433.
- 8 N. Nimura, Y. Kasahara and T. Kinoshita, *J. Chromatogr.*, 213 (1981) 327.
- 9 E. Gil-Av, A. Tishbee and P. E. Hare, *J. Am. Chem. Soc.*, 102 (1980) 5115.
- 10 W. H. Pirkle and R. Däppen, *J. Chromatogr.*, 404 (1987) 107.
- 11 D. W. Armstrong, X. Yang, S. M. Han and R. A. Menges, *Anal. Chem.*, 59 (1987) 2594.
- 12 D. W. Armstrong, *Anal. Chem.*, 59 (1987) 84A.
- 13 R. W. Souter, *Chromatographic Separations of Stereoisomers*, CRC Press, Boca Raton, FL, U.S.A., 1985.
- 14 J. D. Morrison (Editor), *A Symmetric Synthesis*, Vol. I, Academic Press, New York, 1983.
- 15 M. Zeif and L. J. Crane (Editors), *Chromatographic Chiral Separations*, Marcel Dekker, New York, 1988.
- 16 I. W. Wainer, *Trends Anal. Chem.*, 6 (1987) 125.
- 17 I. W. Wainer, *A Practical Guide to the Selection and Use of HPLC Chiral Stationary Phases*, in press.
- 18 J. Gal, *LC-GC, Mag. Liq. Gas Chromatogr.*, 5 (1987) 106.
- 19 W. H. DeCanp, *Chirality*, 1 (1989) 2.
- 20 W. H. Pirkle and B. C. Hamper, *J. Chromatogr.*, 450 (1988) 199.
- 21 L. Nygard, *Report No. A2690-S*, Ed. 1 (unpublished), NOVO Industri, Copenhagen, 1988.

CHROM 22 170

Evaluation of refractive index artifacts in liquid chromatographic absorbance detection

Extension to non-ideal injection and gradient elution

CHRISTINE E. EVANS and VICTORIA L. McGUFFIN*

Department of Chemistry, Michigan State University, East Lansing, MI 48824 (U.S.A.)

(First received June 21st, 1989; revised manuscript received November 23rd, 1989)

SUMMARY

An anomalous response is often observed in high-sensitivity absorbance detection upon a rapid change in solvent composition. This detector artifact appears to be related to refractive index gradients arising when the injection solvent differs from the mobile phase or during solvent programming. Because this anomalous response is often of the same magnitude as the true solute absorbance, misinterpretation of the acquired chromatogram may result. Characterization of this refractive index artifact has been accomplished by modelling the Z-pattern flow cell as a dynamic lens, with constantly changing refractive index profiles both radial and axial to the direction of flow. A ray-tracing algorithm is utilized to predict the final image diameter and the apparent absorbance caused by the changing refractive index conditions. Initial predictions for an ideal, delta function injection show excellent correlation with the experimentally observed response for a commercially available absorbance detector. Simulations are extended to include the more complex axial profiles commonly encountered in liquid chromatography, including those arising from non-ideal injection conditions as well as solvent programming. Predictions based on this model show good agreement with the shape, direction and magnitude of the observed detector response. In addition to aiding in the characterization of solute peaks, this ray-tracing model has direct implications for the accurate interpretation of system peaks in liquid chromatography. Although investigations described here are limited to the Z-pattern cell, this dynamic lens model may be adapted to the evaluation or improved design of any flow cell of interest.

INTRODUCTION

Absorbance detectors utilized in liquid chromatography often exhibit an anomalous response upon a rapid change in solvent composition. These artifacts appear to be related to gradients in refractive index created when the concentration is varied abruptly, as might occur upon injection or solvent programming¹. Although the

exact origin of this anomaly is not clear, rapid changes in solvent composition, and thus refractive index, apparently create a "dynamic lens" inside the flow cell. As qualitatively described by Betteridge *et al.*², the continually changing refractive index conditions cause incident light to be refracted toward and away from the photodiode transducer, resulting in a detector response even though no absorbing species are present. More recently, Hancock and Synovec³ cite an interferometric mechanism as the origin of this anomalous response. Unfortunately, only a few published studies have attempted to address the origin and nature of this anomaly.

Previous investigations of the refractive index artifact have focussed on the elimination of this deleterious effect in absorbance detection. To minimize the refractive index dependence, modifications in both external optics and cell design have been proposed for the most common flow cell configuration, the Z-pattern cell. The role of external optics has been investigated by Stewart for static⁴ as well as dynamic⁵ refractive index conditions. In both cases, optical calculations indicate the necessity of focussing incident radiation near the flow cell exit to allow all light to pass through the cell under all refractive index conditions. When incident light is focussed in this manner, the throughput is no longer limited by the flow cell exit aperture, and thus, the dependence of detector response on refractive index is minimized. Implementation of this external optical arrangement has proven difficult due to chromatographic requirements for small detector cell volumes. For example, this optical design would require that incident radiation from an extended source be focussed at the exit of a cell less than 0.5 mm diameter and 1 cm long. Although focussing the incident light in this manner is feasible⁶, such external optics become difficult if a rugged detection system with interchangeable cell options is desired. Alternatively, the flow cell body can be redesigned as proposed by Little and Fallick⁷. In their design, the cell exit aperture is larger than the entrance aperture, thus allowing all incident light to pass through the cell regardless of solvent refraction. Unfortunately, the change in radius within the flow cell often results in an increase in cell volume and may complicate flow dynamics, leading to additional band broadening. For these reasons, the above modifications have not been implemented in many commercially available absorbance detectors.

Although the refractive index artifact is often detrimental in absorbance detection, it can be utilized to advantage in the design of refractive index detectors for both flow injection analysis and liquid chromatography. Betteridge *et al.*² couple a light-emitting diode source ($\lambda = 565$ nm) and photodiode detector together with a 95- μ l U-pattern flow cell for the detection of various salt solutions injected into a flowing stream of water. The detector response, similar in shape to the first derivative of a Gaussian function, is observed with detection limits of approximately $1 \cdot 10^{-3}$ M (0.1%) sodium chloride. Bornhop *et al.*⁸ also utilize this refractive index response in a simple capillary flow cell design by focussing a helium-neon laser ($\lambda = 633$ nm) slightly off-center and perpendicular to the cell. In this case, refraction of the incident light produces an interference pattern. A small-area photodiode is then utilized to monitor the movement of the interference fringes induced by the changing refractive index conditions within the cell. Detection limits of $3 \cdot 10^{-6}$ M (0.9 ppm) are shown for sucrose in a separation of simple sugars. Pawliszyn⁹ describes a fiber optic detector design as being sensitive to refractive index, and hence, to concentration gradients within the flow cell. The detected signal is evaluated based on Schlieren optics and is measured as a change in the deflection angle utilizing a position-sensitive

photodiode. A sheath flow cell is used to enhance the detector response resulting in a detection limit of approximately $5 \cdot 10^{-6} M$ (2 ppm) sucrose¹⁰. Recently, Hancock and Synovec³ have utilized a Z-pattern cell design for the refractive index detection of polymers in size-exclusion chromatography, with detection limits of $2 \cdot 10^{-9} M$ (0.9 ppm) polystyrene. Although many of these detector designs provide a simple and rugged means for solute detection, the exact nature of the detected signal has not yet been fully described in the literature. Ultimately, optimization of these designs requires a more detailed understanding of the refractive index artifacts responsible for the detector response.

In this study, theoretical predictions and experimental observations are combined in an effort to understand more clearly the nature of the refractive index artifact. Theoretical evaluation of the detector response is accomplished by modelling the flow cell as a dynamic lens. By incorporating refractive index gradients both radial and axial to the direction of flow, this ray-tracing model allows a more systematic evaluation of the possible origin(s) of the detector response. Preliminary simulations employing this model predict the detector response for a Z-pattern flow cell utilizing a parabolic radial refractive index gradient, characteristic of laminar flow¹¹. These initial predictions for an ideal Gaussian axial gradient confirm the derivative-shaped response commonly observed upon injection. Simulation results indicate that both the radial and axial components of the refractive index gradient are necessary to predict the detector response accurately. Although these preliminary simulations describe only ideal gradients, the model shows excellent agreement with the experimental measurement of both the final image size and intensity¹¹. Unfortunately, many gradients commonly encountered in liquid chromatography may not be ideal. In the present work, characterization of the refractive index artifact for non-ideal axial gradients is accomplished by correlating predicted detector response with experimental observations. By extending these studies to include complex axial gradients occurring upon injection or solvent programming, the validity of the "dynamic lens" model can be more rigorously tested under practical experimental conditions.

THEORY

The transmittance of electromagnetic radiation in any optical system can be described as the ratio of the light intensity transmitted (I) to that incident (I_0) on the flow cell. This concept forms the basis for absorbance detection in liquid chromatography, where the transmittance ($T = I/I_0$) is altered by any species which absorbs radiation at a given wavelength. It is assumed that the detector response is directly proportional to the concentration of absorbing species in the flow cell as a function of time. However, as with any optical system, the refractive index of the material present in the flow cell can also affect the system transmittance, and thus the apparent absorbance. Unlike deviations in Beer's law resulting from anomalous dispersion or changes in viewed volume¹², this refractive index artifact occurs even when no absorbing species are present.

With no absorbers within the flow cell, the system transmittance is a function of both the field stop and the aperture stop. Because the field stop restricts the field of view of the optical system and the aperture stop limits the amount of light reaching the detector, both must be considered when calculating the system transmittance. This

determination can be accomplished from the product of the field stop area and the solid angle subtended by the aperture stop¹³. Direct determination of the solid angle is possible by tracing the outermost incident ray which is transmitted through the optical system. By evaluating the angle of light deflection at each interface with the familiar Snell's law expression, the maximum incident angle limited by the aperture stop, and thus the system transmittance, can be determined. Since both optical stops are located at or within the flow cell for many absorbance detector designs, such calculations require information about light incident on the flow cell as well as refractive index conditions within the cell.

Although a variety of incident light conditions are possible, many optical designs for the common Z-pattern flow cell utilize the entrance aperture of the cell as the exit slit of the monochromator. In this case, the flow cell entrance aperture is overfilled and forms the field stop in the optical system, thereby restricting the field of view. The cell exit aperture can then act as the system aperture stop, limiting the amount of light reaching the detector. Thus, the flow cell transmittance can be calculated directly from the area of the cell entrance aperture and solid angle restricted by the cell exit aperture.

Calculation of the cell entrance area is trivial, but calculation of the solid angle requires knowledge of the refractive index conditions. For a static system, the refractive index of the solvent within the flow cell is known and thus, the transmittance may be calculated directly⁴. This is, however, not true in a dynamic chromatographic system, where the solution refractive index in the cell may be continually changing with time. Moreover, refractive index gradients arising within the flow cell itself due to flow pattern and mixing further complicate the transmittance calculation. Thus, to evaluate the transmittance under flow conditions, characterization of the refractive index profiles in the cell volume is necessary.

In a dynamic system, refractive index profiles exist within the flow cell both radial [$n(r)$] and axial [$n(z)$] to the direction of flow. Evaluation of these refractive index profiles requires expressions for the radial and axial concentration profiles [$C(r)$ and $C(z)$, respectively] as well as the refractive index dependence on concentration [$n(C)$].

Evaluation of $n(C)$

For ideal solvent systems, refractive index is a simple, linear function of concentration. However, the polar solvents utilized in reversed-phase liquid chromatography are highly interacting and the refractive index commonly exhibits a non-linear concentration dependence^{14,15}. For these non-ideal solvent systems, $n(C)$ may play a major role in determining the magnitude as well as the direction of the refractive index gradients present in the flow cell. Since these solutions do not behave ideally and solution theory cannot presently predict the refractive index dependence, experimental measurements of refractive index are necessary. These refractive index measurements can then be described by a polynomial expression for the concentration range of interest.

Evaluation of $C(r)$

The radial concentration profile arises from the flow profile within the flow cell, and may be complex for the Z-pattern cell design¹⁶. Because these flow patterns are not presently well understood or well characterized, some simplifying assumptions are necessary to model the radial profile. If the flow cell is considered as a simple

cylindrical tube, then the concentration (C) as a function of the radial distance (r) can be expressed as derived by Taylor¹⁷:

$$C(r) = C_{r=0} + \frac{R^2 u}{4D_M} \left[\frac{r^2}{R^2} - \frac{r^4}{2R^4} \right] \frac{dC_{r=0}}{dz} \quad (1)$$

Thus, the radial concentration profile for a cell of radius (R) depends on the linear velocity in the cell (u) and the diffusion coefficient (D_M), as well as the axial gradient at the center of the cell ($dC_{r=0}/dz$). If the residence time in the cell is short, the concentration profile may be modelled as a parabola by neglecting the $r^4/2R^4$ term.

Evaluation of $C(z)$

The axial concentration profile arises due to the convolution of the initial concentration profile with the Gaussian dispersion introduced by the chromatographic column or connecting tubing. Dispersion may be determined from the Van Deemter¹⁸ or Knox¹⁹ equations for packed chromatographic columns or the Golay²⁰ or Taylor–Aris^{17,21} equations for open-tubular columns. Finally, evaluation of the concentration profile reaching the detector may be solved mathematically either by Laplace transforms²² or by convolution of integrals²³.

In the convolution of integrals method, the input concentration profile is convolved directly with the Gaussian function. The input concentration as a function of time [$C(t_a)$] may be described by the initial concentration (C_0) and characteristic time constant (τ). In addition, this input profile is offset by the difference in time (t_R) between the profile introduction and evaluation. The convolution of the input function with a normalized Gaussian operator results in a final concentration function of the following form²³:

$$C(t) = \frac{1}{(2\pi)^{1/2} \sigma_t} \int_{\text{all } t_a \text{ values}} C(t_a) \exp \left[-\frac{(t - t_a)^2}{2\sigma_t^2} \right] dt_a \quad (2)$$

where σ_t^2 is the time variance contributed by the chromatographic system. This final concentration profile with respect to time [$C(t)$] is then evaluated by integrating over all possible values of input time (t_a). Subsequent conversion from the time to the distance domain is performed, yielding the final concentration profile with respect to distance [$C(z)$].

A number of input concentration profiles of importance for liquid chromatographic applications are created upon injection as well as by solvent programming. Under ideal injection conditions, the solute enters the chromatographic column as an instantaneous concentration pulse. Alternately, the solute may be swept onto the column in a rectangular plug determined by the length of the injection loop and the linear velocity of the mobile phase. Under less ideal circumstances, the injector may act as a mixing or dilution chamber, and an exponential concentration profile is introduced onto the column. Finally, the separation of complex mixtures often requires programming the mobile phase in a stepwise or linear manner, from the weak to the strong solvent. Each of these profiles will be investigated in turn, with the mathematical derivations and final concentration profiles given in the Appendix.

Evaluation of $n(r)$ and $n(z)$

Expressions for the concentration profiles in both the radial [$C(r)$] and the axial [$C(z)$] direction as well as the refractive index dependence on concentration have been derived. Thus, determination of refractive index profiles in both radial and axial directions is now possible for the input profiles of interest in liquid chromatography. Unfortunately, the explicit determination of the transmittance expressions as a function of time is not trivial and often they cannot be solved in closed form²⁴. In addition, transmittance expressions must be solved individually for each input function and each concentration dependence on refractive index. For these reasons, a modelling approach has been utilized for the prediction of detector response for these gradient conditions. By directly comparing the predicted response with experimental observations, a better understanding of the origin of this refractive index artifact is possible.

EXPERIMENTAL

Reagents

All organic solvents utilized in this study are high-purity, distilled-in-glass grade (Burdick and Jackson, Muskegon, MI, U.S.A.). Water is deionized and doubly distilled (Model MP-3A, Corning Glass Works, Corning, NY, U.S.A.).

Refractive index measurements

Refractive index measurements for binary mixtures of tetrahydrofuran–water and methanol–water are performed at 25°C with an Abbe refractometer (Model Abbe-3L, Bausch and Lomb, Rochester, NY, U.S.A.). Replicate measurements of a single sample, as well as replicate samples, yield a relative standard deviation better than ± 0.0001 . Polynomial expressions from non-linear least squares fitting of refractive index as a function of concentration are given in eqns. 3 and 4, and are shown graphically in Fig. 1. The coefficients of determination for the tetrahydrofuran–water and methanol–water systems are 0.980 and 1.42, respectively.

Chromatographic system

Solvent delivery and gradient introduction are accomplished utilizing a dual-syringe micropump (MPLC Model MG, Applied Biosystems, Santa Clara, CA, U.S.A.). Both internal and external loop injection valves (Model CI4W1 and EC6W, Valco, Houston, TX, U.S.A.) are utilized for sample introduction. External loops are fabricated from stainless steel tubing 0.25 mm I.D. with lengths of 11.8 cm (5.98 μ l), 19.7 cm (9.98 μ l), 39.5 cm (20.0 μ l) and 98.6 cm (50.0 μ l). A stainless steel tube (46.0 cm \times 0.25 mm I.D.) is used to connect the injector directly to the absorbance detector (Model Uvidec 100-V, Jasco, Tokyo, Japan). The detector, equipped with a 1- μ l Z-pattern flow cell (5 mm \times 0.50 mm I.D.), is operated at a monochromator wavelength of 589 nm with a 500 nm cutoff filter. A chart recorder (Model 585, Linear Instruments, Reno, NV, U.S.A.) is utilized to display the apparent absorbance caused by the refractive index artifact.

Simulations

The flow cell, modelled as a dynamic lens, is simulated utilizing a three-dimensional ray-tracing algorithm (Beam3, Stellar Software, Berkeley, CA, U.S.A.). This software package allows refracting and reflecting optical elements to be

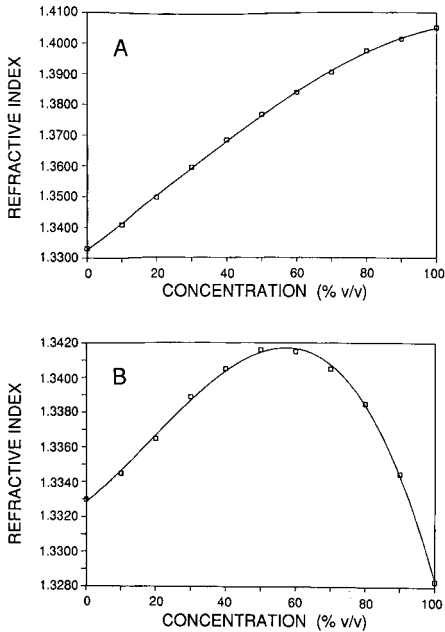


Fig. 1. Refractive index measurements as a function of the concentration of tetrahydrofuran in water (A) and the concentration of methanol in water (B).

arbitrarily positioned and their shape specified. In simulating the Z-pattern cell (Fig. 2), a point source is positioned 0.5 mm in front of the cell entrance and a detection screen is positioned 25.4 mm after the cell exit. Flat refracting elements ($n_D = 1.457$) representing the quartz cell windows are placed 1.0 mm apart at flow cell entrance and

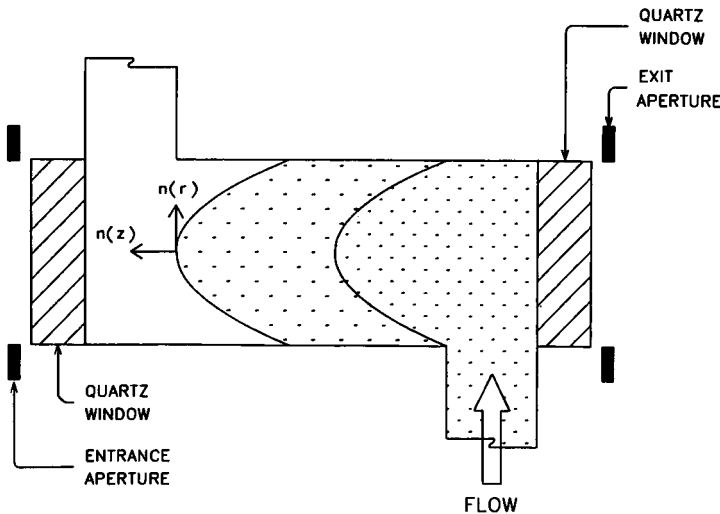


Fig. 2. Schematic diagram of Z-pattern flow cell with refractive index profiles radial $[n(r)]$ and axial $[n(z)]$ to the direction of flow.

exit, together with apertures of 0.5 mm diameter. The window interfaces inside the cell are positioned 5.0 mm apart, with parabolic refractive index interfaces placed 2.0 and 4.0 mm from the exit window. This parabolic radial profile remains constant while the axial gradient in the cell varies, dependent upon the input profile of interest (eqns. 12, 16, 20 and 24). The axial refractive index profile is incremented through the cell in a stepwise manner, with only a small fraction of the total profile contained in the cell at any given time. The detector response is then predicted by analyzing the image size and intensity at each step. Image size is determined by evaluating the final position of a single peripheral ray at the detector screen. Image intensity is predicted by evaluating the number of rays (I) successfully traversing the cell from 1000 incident rays (I_0). The predicted intensity is then normalized to the mobile phase solvent and the apparent absorbance is subsequently calculated as $[-\log(I/I_0)]$. The relative error in the predicted apparent absorbance is approximately 6% for simulations utilizing at least 500 incident rays. At present, the precision of the simulation model is limited by the reproducibility of the random number generator and is not improved by increasing the number of incident rays.

Implementation of this model requires knowledge of $n(C)$, as well as both $C(r)$ and $C(z)$ expressions. In these studies, reversed-phase solvent systems are chosen which exhibit nearly ideal, linear dependence of refractive index on concentration (tetrahydrofuran–water) as well as distinctly non-ideal behavior (methanol–water). Refractive indices for aqueous, binary mixtures of tetrahydrofuran and methanol are measured and the best fit polynomial expressions are calculated. For binary solutions of tetrahydrofuran and water, the refractive index relationship is given by

$$n(C) = 1.3326 + 0.08561C + 0.02146C^2 - 0.03475C^3 \quad (3)$$

where the concentration (C) is the volume fraction of tetrahydrofuran in the total volume. As can be seen in Fig. 1, aqueous mixtures of tetrahydrofuran exhibit a relatively linear refractive index response with concentration, showing only slight deviation at high concentrations. In contrast, mixtures of methanol and water, as given by

$$n(C) = 1.3329 + 0.01599C + 0.02521C^2 - 0.04568C^3 \quad (4)$$

show a maximum in refractive index with concentration (Fig. 1). These two extremes in refractive index behavior test the versatility of the model for solvents of interest in practical applications.

Secondly, the $C(r)$ expression is necessary to determine the curvature of the “solvent lens”. Since the flow pattern within the Z-pattern cell is hydrodynamically complex, calculations of the radial profile are not amenable to an analytical solution. Therefore, assumptions about the shape resulting from a more simplified flow profile are required. The radial profile is modelled as a parabolic profile utilizing the Taylor expression (eqn. 1), neglecting the $r^4/2R^4$ term. The shape and curvature of surfaces of constant concentration and hence refractive index, are given by $[(C - C_{r=0})/(dC_{r=0}/dz)]$. Thus, the curvature of the parabolic solvent lens, given by $(R^2u/4D_M)$, remains constant for specified flow conditions. All simulations assume a volumetric flow-rate of 50 $\mu\text{l}/\text{min}$, yielding a mobile phase linear velocity (u) of 0.424 cm/s for the flow cell

radius (R) of 0.25 mm. A diffusion coefficient (D_M) of approximately $1 \cdot 10^{-5} \text{ cm}^2/\text{s}$ is determined from the Wilke–Chang equation²⁵ for both tetrahydrofuran–water and methanol–water mixtures at 25°C. Because the flow-rate and solvents utilized for these simulations are constant, the parabolic lens shape and curvature remain the same for all simulations.

Finally, the $C(z)$ expression must be evaluated for the experimental conditions of interest if direct comparison of simulated results with experimental observations is desired. Therefore, simulation input parameters are obtained directly from the experimental conditions whenever possible. The actual concentration expressions are derived in the Appendix using the convolution of integrals method and are given in eqns. 12, 16, 20 and 24. This technique requires information about the Gaussian operator as well as the input function of interest.

In these studies, the initial concentration profile is generated experimentally by either an injection valve or a gradient dual-syringe pump. The Gaussian operator is experimentally formed utilizing a non-retentive open tube. Direct connection between the detector flow cell and the injection valve or gradient pump is accomplished with stainless steel tubing. Since the solvents are unretained, the time to traverse the tube (t_R) is the ratio of the distance travelled ($L = 46.0 \text{ cm}$) to the linear velocity ($u = 1.64 \text{ cm/s}$) and is equal to 27.1 s. The length variance (σ_L^2) contributed by this tube is calculated from the Taylor–Aris expression^{17,21}.

$$\sigma_L^2 = R^2 u / 24 D_M \quad (5)$$

For the experimental conditions described, the connecting tube contributes a length variance of 50.8 cm^2 and a corresponding time variance of 18.9 s^2 . If no additional broadening occurs between the connecting tube ($R = 0.127 \text{ mm}$) and the flow cell ($R = 0.250 \text{ mm}$), the time variance is assumed constant and the length variance in the cell is 3.40 cm^2 at a corresponding linear velocity of 0.424 cm/s in the cell.

A number of axial concentration profiles commonly encountered in liquid chromatography have been investigated to test the validity of the simulation model. Mathematical expressions for these input functions as well as the axial concentration profiles determined by convolution of integrals are given in the Appendix. For simulations of the exponential input function (eqn. 12), the ratio of the exponential time constant (τ) and the Gaussian standard deviation (σ_t) are varied from an ideal Gaussian function ($\tau/\sigma_t = 0.00$) to the exponentially modified Gaussian ($\tau/\sigma_t = 0.25$ – 2.00). The axial concentration expression resulting from a more ideal, rectangular plug injection (eqn. 16) is also of interest. For these simulations, injection volumes of 1, 6, 10, 20 and $50 \mu\text{l}$ are investigated. The time of the rectangular injection (τ) is calculated from the ratio of the injection loop length (L_{inj}) and linear velocity (u). The injection loop diameter was chosen to be equal to the connecting tube diameter, to minimize any dispersion due to transfer between the tubes and thus the linear velocity remains constant. The length of injection loops results in τ/σ_t ratios of 0.297, 1.78, 2.97, 5.94 and 14.9, corresponding to the various injection volumes. This produces a wide range of axial concentration profiles at the detector from a nearly Gaussian profile for the $1\text{-}\mu\text{l}$ injection to an almost rectangular profile for the $50\text{-}\mu\text{l}$ injection. The concentration profile formed for step gradient input is given in eqn. 20. For these simulations, a solvent program from 0 to 100% (v/v) is evaluated which employs 10 steps (m) of 10% (v/v) increment at a step time interval (τ) of 5 min. A comparable

linear gradient (eqn. 24) from 0 to 100% (v/v) in 45 min (τ) is also calculated. Finally, these axial concentration gradients are combined with the expressions for $n(C)$ to determine the axial refractive index profile utilized as input to the simulation model.

RESULTS AND DISCUSSION

In an effort to understand the origin of the refractive index artifact in absorbance detection, the response of a commercially available detector is measured under both injection and solvent programming conditions. These measurements are then compared with predictions of the apparent absorbance based on the "dynamic lens" model. Because the refractive index artifact is simulated for the flow conditions used experimentally, direct comparison of theoretical prediction with experimental observation is possible. In addition, one solvent system with a nearly ideal, linear refractive index dependence on concentration (tetrahydrofuran–water) is contrasted with a distinctly non-ideal system (methanol–water). This direct comparison of complex input profiles and solvent systems tests the versatility and applicability of this "dynamic lens" model for the elucidation of this important artifact of absorbance detection.

δ input function

While the δ input function was addressed in a previous publication¹¹, the conclusions are summarized here for completeness. A δ function input, when convolved with a Gaussian operator, results in a purely Gaussian concentration profile. For the linear change in refractive index exhibited for small changes in concentration, the axial refractive index profile is also Gaussian in shape. Both the predicted and experimentally observed response show the characteristic derivative-shaped signal for image diameter as well as image intensity. At the beginning of the Gaussian profile, both the axial and radial refractive index gradients are positive, thereby focussing the incident radiation. In the second half of the profile, the axial gradient is negative while the radial gradient remains positive, effectively defocussing the final image. Since the exit to the flow cell acts as the aperture stop under simulation as well as experimental conditions, the amount of light blocked by the flow cell exit changes continuously with the axial gradient within the cell. Thus, the "solvent lens" in the cell and the limiting aperture after the cell combine to yield the apparent derivative shape of the detector response, whether expressed as image intensity or apparent absorbance.

Exponential input function

The time-dependent concentration profiles calculated for the exponential input function convolved with the Gaussian function operator (eqn. 8), are shown graphically in Fig. 3. As expected, an increasing exponential modification (increased τ/σ_t) reduces the maximum concentration present at the detector. This reduction in the concentration maximum results in a concomitant decrease in the magnitude of the concentration gradient (dC/dz) in the flow cell.

Predicted detector response for these concentration profiles, measured at the first and second deflection of the derivative-shaped curve, is summarized in Table I for the injection of 1 μ l tetrahydrofuran into water. The predicted deflection maximum

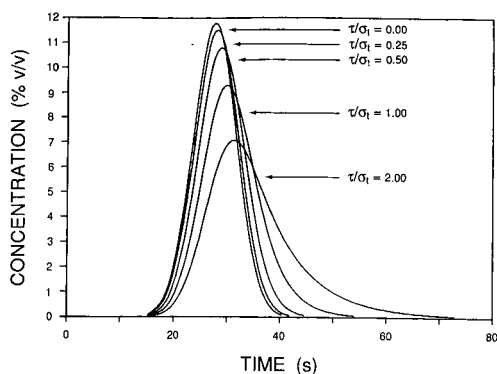


Fig. 3. Calculated concentration dependence, based on eqn. 11, for a Gaussian profile with variance σ_t^2 modified by a varying exponential time constant (τ).

occurs when the refractive index gradient in the cell (dn/dz) reaches a maximum value. For this reason, the refraction index gradient is tabulated together with the corresponding image diameter and apparent absorbance at each deflection maximum. For the ideal Gaussian function ($\tau/\sigma_t = 0$), the predicted image diameter exhibits an approximately symmetric response (-0.16 then $+0.17$) relative to that for pure water (1.00). In contrast, the magnitude of the apparent absorbance is greater for the first deflection (-0.15) than the second ($+0.10$). For the first deflection, the axial and radial refractive index gradients are positive and the incident light is refracted toward the cell axis, thereby increasing light transmitted and decreasing the apparent absorbance. Because light is refracted toward the cell axis under these conditions, light rays can traverse the cell at a radial position further from the cell axis than for a negative axial gradient. At these radial positions, the parabolic profile forms a much steeper refractive index gradient and more light can be transmitted. However, when the axial gradient is negative, light is refracted away from the axis and must traverse the cell at a radial position nearer the cell axis to pass through the exit aperture. In this case, the portion of the radial profile encountered by light rays is less steep and the light

TABLE I

PREDICTED RESPONSE FOR EXPONENTIALLY MODIFIED GAUSSIAN PROFILE UTILIZING THE TETRAHYDROFURAN-WATER SYSTEM

τ/σ_t	$dn/dz \text{ (mm}^{-1}\text{)} \times 10^3$		Relative image diameter		Apparent absorbance	
	1st ^a	2nd ^b	1st ^a	2nd ^b	1st ^a	2nd ^b
0.00	0.29	-0.29	0.841	1.168	-0.15	0.10
0.25	0.28	-0.27	0.846	1.158	-0.14	0.09
0.50	0.25	-0.23	0.860	1.135	-0.13	0.08
1.00	0.21	-0.16	0.885	1.094	-0.09	0.05
2.00	0.15	-0.08	0.919	1.049	-0.05	0.01

^a Maximum value at first deflection relative to pure water.

^b Maximum value at second deflection relative to pure water.

is refracted to a lesser extent. This asymmetry in refractive index conditions encountered within the cell results in an asymmetry in the magnitude of the detector response, even for a symmetric axial profile. Thus, in contradiction to previous assumptions¹⁰, the existence of asymmetry in the refractive index artifact may not necessarily be indicative of an asymmetric axial profile.

As the τ/σ_t ratio increases, the magnitude of the concentration gradient (dC/dz) decreases for both the positive and negative axial gradient. However, the magnitude of the negative gradient decreases more rapidly than the positive gradient, as can be discerned from the slope of the profiles in Fig. 3. This difference in the concentration gradient at the front and back of the profile is a direct result of the asymmetry of the exponential function. This asymmetry in the concentration profiles is directly reflected in the refractive index profiles for the tetrahydrofuran–water system. As can be seen in Table I, the relative image diameter predicted at the first and second deflection of the derivative-shaped response likewise increases in asymmetry with increasing τ/σ_t ratio. This results in a concomitant increase in the asymmetry of the predicted apparent absorbance with increasing τ/σ_t ratio. If the exponential modification is sufficiently great, as shown for a τ/σ_t ratio of 2.00, the second deflection is no longer detected and the resulting apparent absorbance response appears as a unidirectional peak. Simulations of the exponential input function have been discussed only for the tetrahydrofuran–water system to isolate the change in positive and negative gradient occurring for varying τ/σ_t ratios. Experimental verification of the detector response was not attempted due to the difficulty in matching τ/σ_t values.

In summary, an inherent asymmetry in the apparent absorbance is predicted for a symmetrical Gaussian axial gradient. This asymmetry in detector response increases as τ/σ_t ratio increases, due to the growing asymmetry in the positive and negative gradient portions of the axial profile. If the exponential contribution to the axial profile becomes too great, the second deflection may not be detected. Thus, the shape as well as the magnitude of the detector response are directly affected by the exponential input function.

Rectangular input function

Detector response has also been predicted for the rectangular input function which might occur upon plug injection. Rectangular injections of 1, 6, 10, 20 and 50 μl

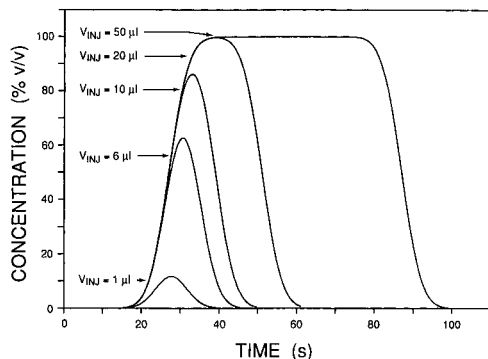


Fig. 4. Calculated concentration dependence, based on eqn. 15, for a Gaussian profile with variance σ_t^2 modified by a varying rectangular injection volume.

have been simulated utilizing the concentration profiles calculated from eqn. 16. The time-dependent concentration profiles (eqn. 15) resulting from the convolution of a rectangular input function with a Gaussian operator are shown in Fig. 4. Both tetrahydrofuran–water and methanol–water systems are employed to evaluate the effect of ideal as well as non-ideal solvent mixtures on the detector response.

Predicted response for injections of tetrahydrofuran into water are shown in Fig. 5. For a 1- μl injection of tetrahydrofuran into water, Fig. 5-1A illustrates the axial refractive index profile utilized as input to the simulation model. The axial profile shows a nearly Gaussian shape, where the refractive index gradient (Fig. 5-1B) is first positive and then becomes negative. The positive portion of the refractive index gradient coupled with the positive parabolic radial gradient causes light to be refracted toward the center of the flow cell. This focussing of the incident light results in the initial decrease in the image diameter (Fig. 5-1C) relative to that for pure water. A concomitant decrease in the apparent absorbance (Fig. 5-1D) is seen because more light is allowed through the flow cell exit which is acting as the system aperture stop. The opposite effect results when the axial gradient becomes negative; that is, the light is now refracted away from the flow cell center and thus the image diameter increases. Because more light is now blocked by the exit aperture, the apparent absorbance increases. These continually changing refraction conditions give rise to the characteristic derivative-shaped response.

As the volume is increased to 6 μl of tetrahydrofuran injected into water, the axial refractive index profile (Fig. 5-6A) increases in magnitude but remains approximately Gaussian in shape. The shape and direction of the resulting refractive index gradient (Fig. 5-6B) are the same as shown for a 1- μl injection, but the magnitude of the gradient has increased. The predicted image diameter (Fig. 5-6C) resulting from the gradient has also increased in magnitude but remained the same in all other respects. In contrast, the overall magnitude of the predicted apparent absorbance (Fig. 5-6D) has increased, but the predicted response reaches a plateau as the apparent absorbance decreases. This appears to be the direct result of the increased focussing power of the “solvent lens”; that is, dn/dz increases to such an extent that the exit of the flow cell no longer limits the light transmitted through the cell. At these high gradients, the light is focussed enough so the aperture stop gradually moves toward the entrance of the cell, until the cell entrance acts as both the aperture and field stop. When the limiting apertures are preceding the solvent lens, the apparent absorbance is no longer a function of the axial refractive index gradient and therefore, remains constant within this time region.

As the injection volume is increased to 10 μl of tetrahydrofuran into water, the refractive index profile (Fig. 5-10A) increases only slightly in magnitude and becomes less Gaussian in shape. Although the refractive index gradient (Fig. 5-10B) is only slightly greater than for the 6- μl injection, the plateau effect in the predicted apparent absorbance (Fig. 5-10D) is even more pronounced because more time is spent under these high gradient conditions. For a 20- μl injection of tetrahydrofuran into water, the concentration, and thus the refractive index (Fig. 5-20A), has reached a maximum value equal to that for pure tetrahydrofuran. This results in a time interval between steep gradient regions when dn/dz (Fig. 5-20B) equals zero. The steep gradient regions are approximately equal in magnitude to that for a 10- μl injection (Fig. 5-10B), but are now distinctly separated in time. This separation is reflected in both the predicted

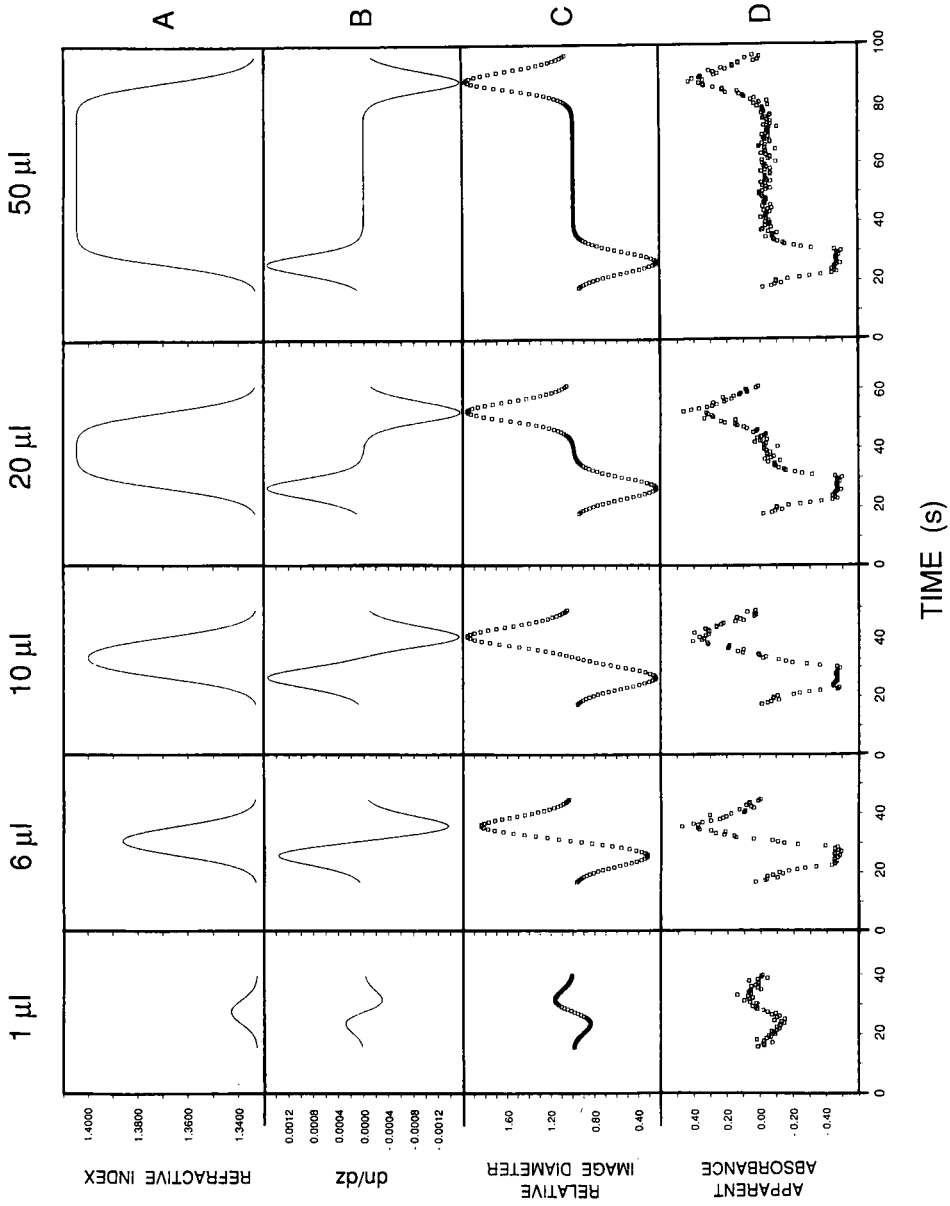


Fig. 5. Calculated absolute refractive index (A) and refractive index gradient (B) in the cell (mm^{-1}), and resultant relative image diameter (C) and apparent absorbance (D) predicted for varying volumes of tetrahydrofuran injected into water.

image diameter (Fig. 5-20C) and the apparent absorbance (Fig. 5-20D). In an actual chromatogram, it would be difficult to determine whether the detector response arose from the refractive index artifact or was the true absorbance response from two independent solutes. This distinction would become nearly impossible for the 50- μ l injection of tetrahydrofuran into water, where the predicted response is well separated in time (Fig. 5-50D). Thus, although a single component is injected, the predicted response is difficult to distinguish from two independent chromatographic peaks for large injections of these ideal solvents.

Experimental observations for the tetrahydrofuran–water system are shown in Fig. 6. The experimental concentration profile (Fig. 6A), measured with an absorbing solute, is nearly Gaussian in shape for 1- and 6- μ l injections, and reaches the maximum possible concentration for 20- and 50- μ l injections. The corresponding refractive index artifacts are shown for a 20% (v/v) mixture of tetrahydrofuran–water injected into pure water (Fig. 6B), due to complications in hydrodynamic mixing for injections of a pure organic solvent into pure water. Excellent agreement with predicted response (Fig. 5) is seen for the shape of the observed apparent absorbance for the tetrahydrofuran–water system. Although an increase in magnitude of the apparent absorbance is predicted with increasing injection volume, a slight decrease is observed experimentally in some cases for reasons which are not clear. In general, however, the trend in the shape, direction, and relative magnitude corresponds directly with that predicted by the “dynamic lens” model.

Further investigation of this absorbance anomaly employed the less ideal methanol–water solvent system. As described previously, mixtures of methanol and water interact in such a way to give a maximum in the refractive index dependence on concentration (Fig. 1B). However, predicted response behavior for injections of 1 μ l of methanol into water, shown in Fig. 7, are similar to those for the tetrahydrofuran–water system (Fig. 5). Although the magnitude of the image diameter response (Fig.

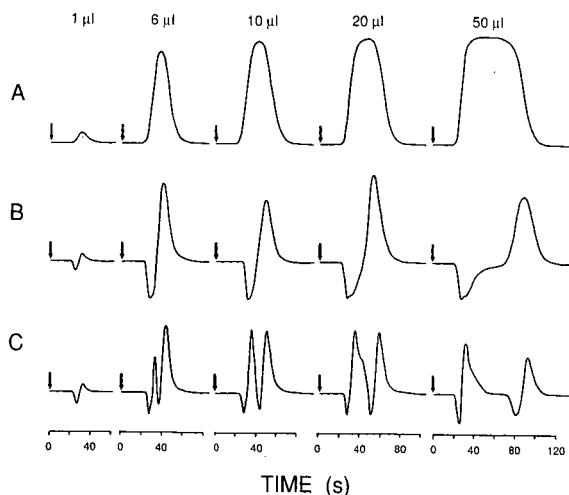


Fig. 6. Observed detector response ($\lambda = 250$ nm) for injection of varying volumes of 1% (v/v) acetone–methanol into methanol (A); 1.500 a.u.f.s. Apparent absorbance observed ($\lambda = 589$ nm) for injection of 20% (v/v) tetrahydrofuran–water into water (B) and 90% (v/v) methanol–water into water (C); 0.200 a.u.f.s.

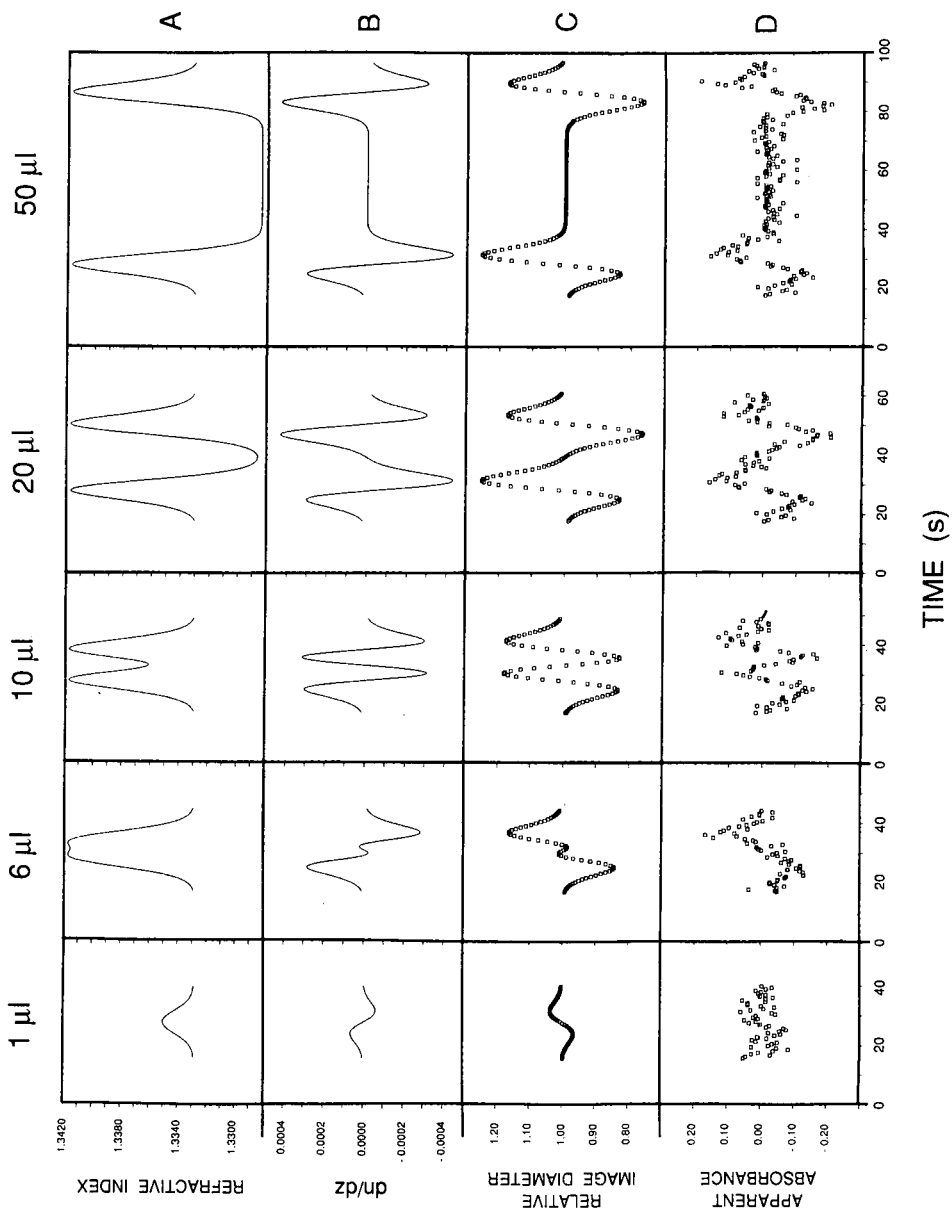


Fig. 7. Calculated absolute refractive index (A) and refractive index gradient (B) in the cell (mm^{-1}), and resultant relative image diameter (C) and apparent absorbance (D) predicted for varying volumes of methanol injected into water.

7-1C) is smaller than for tetrahydrofuran injected into water, the shape and direction of the response are identical. The apparent absorbance (Fig. 7-1D) predicted by the model is difficult to discern due to variability in the random number generator utilized in the simulation.

The non-linearity of refractive index with concentration becomes more important as the injection volume increases. This can be seen for the 6- μl injection of methanol into water, where the magnitude of the refractive index profile (Fig. 7-6A) has increased but the shape is distinctly non-Gaussian. This unusual refractive index profile results because the maximum in the concentration profile is greater than 50% (v/v) (Fig. 4), and thus, is slightly greater than the maximum in the refractive index *versus* concentration relationship (Fig. 1B). This results in a small decrease in the refractive index profile at the concentration maximum. The refractive index gradient (Fig. 7-6B), in this case, is beginning to exhibit multiple changes in sign, giving rise to an unusual shape in the predicted image diameter (Fig. 7-6C). The predicted apparent absorbance (Fig. 7-6D), however, appears to exhibit only two deflections, presumably due to the variability in the random number generator used for the simulation.

The non-linearity of refractive index with concentration continues to influence the refractive index profile for injections of 10 μl of methanol into water. Since the maximum in the concentration profile is greater than 80% (v/v), substantially past the maximum in the refractive index *versus* concentration relationship, a bimodal refractive index profile results (Fig. 7-10A). The axial refractive index gradient (Fig. 7-10B), although comparable in magnitude to the 6- μl injection, clearly shows multiple changes in sign. Predicted image diameter (Fig. 7-10C) and apparent absorbance (Fig. 7-10D) for this injection, likewise change in direction several times as the refractive index profile traverses the cell.

The concentration profile for injection of 20 μl of methanol into water reaches the maximum for pure methanol, resulting in a complex refractive index profile (Fig. 7-20A). The shape of the axial refractive index gradient (Fig. 7-20B) now appears as the derivative of two separate Gaussian refractive index profiles. Thus, the image diameter (Fig. 7-20C) and apparent absorbance response (Fig. 7-20D) predicted by the simulation model show two partially resolved derivative-shaped peaks. Although this response is predicted for a single injection, it is difficult to distinguish from the response arising from the injection of two, more ideal solvents that have been separated by a column.

This difficulty becomes most pronounced for a 50- μl injection of methanol into water. In this case, since the refractive index gradients (Fig. 7-50B) are well separated in time, both the image diameter (Fig. 7-50C) and apparent absorbance (Fig. 7-50D) also exhibit two, apparently separate responses. Thus, the non-linear nature of $n(C)$ can play a major role in determining the shape, direction and magnitude of the apparent absorbance response.

Experimental observations for the injection of 90% (v/v) methanol-water into pure water are shown in Fig. 6C. Excellent agreement is seen in the shape, direction, and relative magnitude of the observed apparent absorbance with that predicted (Fig. 7) for this non-ideal solvent system. The observed response exhibits some asymmetry, not predicted utilizing the ray-tracing model. This observed asymmetry may be caused by small misalignment in the commercial detection system. In addition, deviations from a symmetric, parabolic flow profile may also contribute to the observed

asymmetry. The correlation between the predicted and observed apparent absorbance, however, appears very good for this non-ideal solvent system.

In summary, the refractive index dependence on concentration has a substantial effect on the form of the refractive index profile for large rectangular injections. For a nearly ideal solvent system, large injections can result in an apparent absorbance response which appears as two, separate solute peaks, one negative and one positive. In other cases, it is difficult to distinguish the refractive index artifact caused by the injection of a single, non-ideal component from that caused by a mixture of two ideal components separated by a chromatographic column. This result has important implications for the evaluation of system peaks in liquid chromatography utilizing absorbance detection^{26,27}. In fact, the analysis of system peaks may be more complex than has been previously thought.

Stepwise input function

Detector response has also been predicted for the more complex gradients utilized for solvent programming in liquid chromatography. The concentration profile resulting from the convolution of a discontinuous step function with the Gaussian operator is given by eqns. 19 and 20. Refractive index profiles have been calculated and

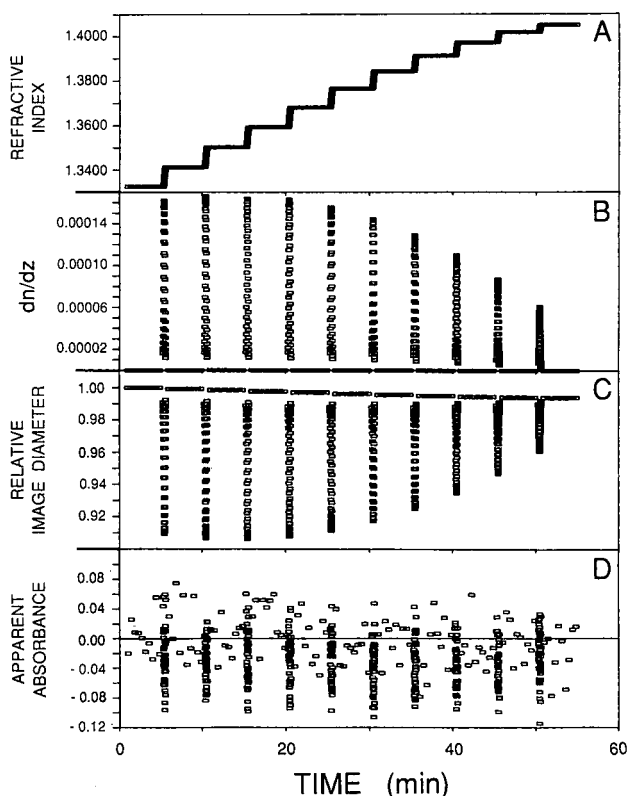


Fig. 8. Calculated absolute refractive index (A) and refractive index gradient (B) in the cell (mm^{-1}), and resultant relative image diameter (C) and apparent absorbance (D) predicted for a stepwise increase of tetrahydrofuran into water from 0 to 100% (v/v) in 10% (v/v) increments.

simulations accomplished for the tetrahydrofuran–water system as well as the methanol–water system.

Predicted detector response for an input function of ten steps of 10% (v/v) tetrahydrofuran in water, from 0 to 100% (v/v), is shown in Fig. 8. Although the concentration increment of the steps is equal, the refractive index profile (Fig. 8A) shows a decrease in step height with increasing concentration of tetrahydrofuran. This decrease in the magnitude of the refractive index steps reflects the slight non-linearity in the refractive index *versus* concentration relationship for high concentrations of tetrahydrofuran in water. This non-linearity results in a marked decrease in the axial refractive index gradient (Fig. 8B) for steps above 50% (v/v). Predicted values for the relative image diameter (Fig. 8C) at each step show the decrease expected for a positive axial refractive index gradient. A direct correspondence can be seen between the magnitude in the axial gradient and the predicted image diameter. In addition, a small decrease in the image diameter at each plateau between steps is predicted due to the change in absolute refractive index. The apparent absorbance (Fig. 8D) predicted for these steps is difficult to see due to scatter in the data caused by the reproducibility of the random number generator. However, changes in apparent absorbance at each step appear to be negative, as is expected from the predicted image diameter (Fig. 8C).

Experimental observations for the tetrahydrofuran–water step gradient, illustrated in Fig. 9B, show excellent agreement with response predicted by the ray-tracing model. As predicted, a negative peak can be seen in the observed apparent absorbance

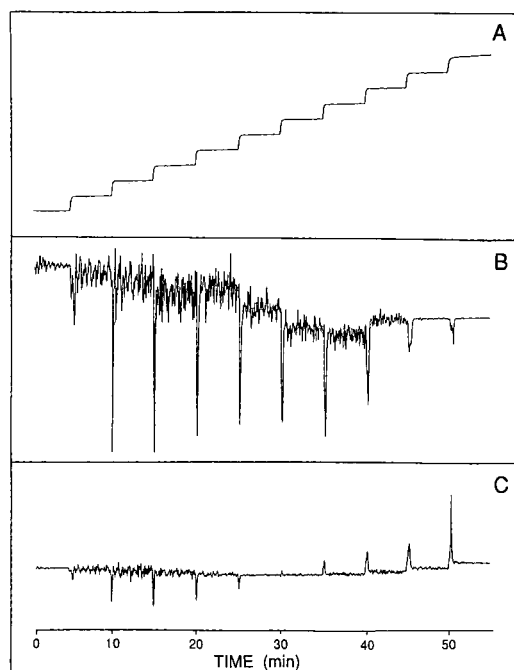


Fig. 9. Observed detector response ($\lambda = 250$ nm) for stepwise increase in 1% (v/v) acetone–methanol into methanol from 0 to 100% (v/v) in 10% (v/v) increments (A); 0.160 a.u.f.s. Apparent absorbance observed ($\lambda = 589$ nm) for the same stepwise solvent program for 20% (v/v) tetrahydrofuran–water into water (B) and 90% (v/v) methanol–water into water (C); 0.040 a.u.f.s.

at each 10% (v/v) increase in the tetrahydrofuran concentration. In addition, the magnitude of the peaks decreases as the concentration of tetrahydrofuran increases, as predicted by the model (Fig. 8). The apparent noise between steps, which arises from poor mixing, becomes less pronounced at high concentrations of tetrahydrofuran due to the improvement in solvent mixing and the reduction in the refractive index dependence on concentration.

Further simulations of the step function input are shown in Fig. 10 for the non-ideal methanol–water system. A maximum in the refractive index profile (Fig. 10A) is seen for equal steps of 10% (v/v) methanol into water, as expected from the refractive index dependence on concentration (Fig. 1B). This alters not only the magnitude of the axial gradient (Fig. 10B) at each step, but the direction as well. Each step from 0% (v/v) to approximately 50% (v/v) methanol in water shows a positive axial gradient, while steps in the concentration range greater than 50% (v/v) are negative. The change in the direction and magnitude of the axial refractive index gradient are mirrored in the predicted image diameter (Fig. 10C). Predicted apparent absorbance (Fig. 10D) is, again, difficult to discern due to simulation constraints, but it is expected to be similar in direction and shape to the predicted image diameter. Thus, the same stepwise concentration profile exhibits a completely different detector

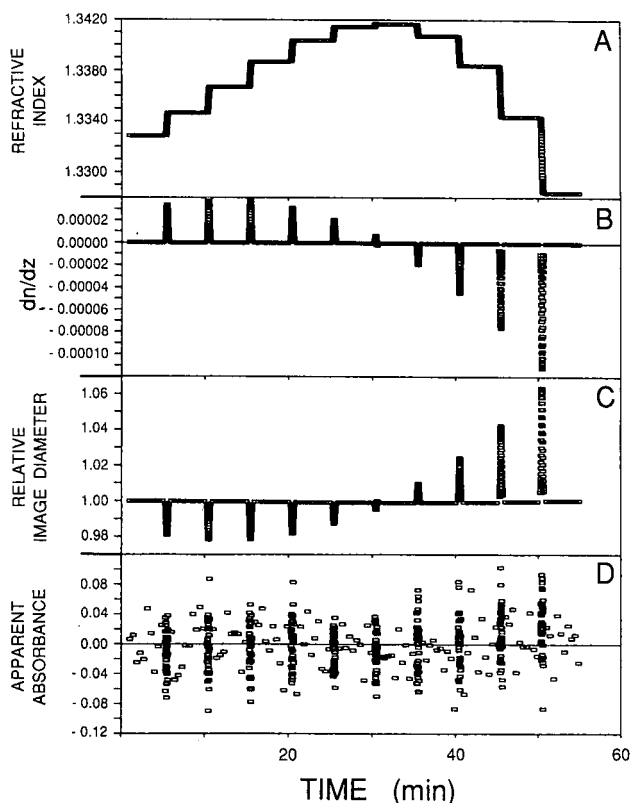


Fig. 10. Calculated absolute refractive index (A) and refractive index gradient (B) in the cell (mm^{-1}), and resultant relative image diameter (C) and apparent absorbance (D) predicted for a stepwise increase of methanol into water from 0 to 100% (v/v) in 10% (v/v) increments.

response for the methanol–water and the tetrahydrofuran–water systems, and the magnitude and direction depend directly on the refractive index *versus* concentration [$n(C)$] relationship.

Experimental observation of the refractive index artifact for the methanol–water system is illustrated in Fig. 9C. The shape and direction of the observed apparent absorbance corresponds directly with that predicted by the “dynamic lens” model. In addition, the relative magnitude of the observed and predicted response are in excellent agreement.

In summary, a complex refractive index artifact often results from a stepwise solvent program. Under these conditions, a steep rise in concentration over a short time results in high axial gradients in concentration and thus refractive index. The refractive index dependence on concentration appears to determine both the magnitude and the direction of the apparent absorbance response. Good agreement is seen between theoretical predictions utilizing this ray-tracing model and experimental observations with a commercially available absorbance detector. As illustrated in Fig. 9, the step gradient input can give rise to apparent absorbance peaks which are often not discernable from analyte absorbance. Moreover, these artifacts frequently occur during a chromatographic analysis where analyte peaks might be expected, as upon a rapid increase in solvent strength.

Linear input function

The input function most often utilized in gradient elution has also been investigated. The concentration profile of the linear input function convolved with the Gaussian operator is given by eqn. 24. For direct comparison with the stepwise function, the linear profile has been simulated for 0 to 100% (v/v) in 45 min (τ).

Simulation predictions are given in Figs. 11 and 12 for the tetrahydrofuran–water system and the methanol–water system, respectively. All axes are the same as for Figs. 8 and 10 to facilitate the direct comparison with step gradient predictions. For both the tetrahydrofuran–water and the methanol–water systems, the overall change in refractive index is identical for the step and linear gradient studies. However, the step profile incorporates several discontinuous changes while the linear profile is continuously changing. This gradual change in concentration for the linear profile results in an axial refractive index gradient (Figs. 11B and 12B) in the flow cell which is approximately two orders of magnitude less than that for the step profile. These small gradients are directly reflected in the magnitude of the predicted detector response for both relative image diameter and apparent absorbance. Thus, only a small baseline offset is predicted for the linear concentration gradient. This result is experimentally observed and shown in Fig. 13 for both tetrahydrofuran–water and methanol–water systems.

In summary, the linear solvent programs commonly utilized in liquid chromatography create only a small axial refractive index gradient in the flow cell. This results in a substantial reduction in the magnitude of the refractive index artifact in comparison to that for the stepwise solvent program. In fact, the linear profiles utilized for gradient elution appear to create a refractive index artifact which is related more to the absolute refractive index than to the refractive index gradient in the flow cell.

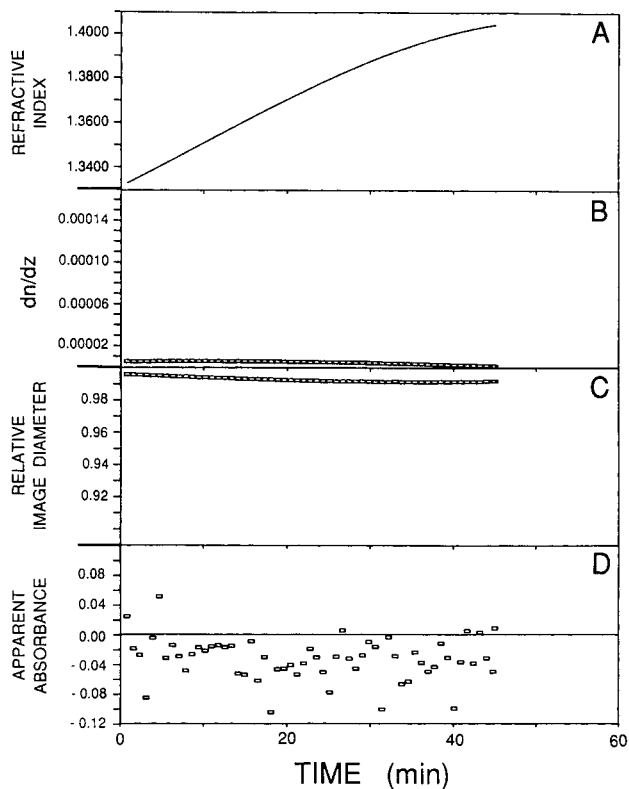


Fig. 11. Calculated absolute refractive index (A) and refractive index gradient (B) in the cell (mm^{-1}), and resultant relative image diameter (C) and apparent absorbance (D) predicted for a linear increase of tetrahydrofuran into water from 0 to 100% (v/v).

CONCLUSIONS

The “dynamic lens” model provides an accurate description of the direction, shape and magnitude of the refractive index artifact under a wide variety of solvent conditions. Excellent agreement between predicted and experimental detector response is observed when refractive index gradients are incorporated with components both radial and axial to the direction of flow. Although the studies described herein utilize equipment and experimental conditions typical of microbore columns, identical detector response is expected for conventional chromatographic systems under comparable hydrodynamic and optical conditions.

For the solvent systems of interest in reversed-phase liquid chromatography, the direction and magnitude of the refractive index gradients are directly dependent on the refractive index *versus* concentration relationship. In the case where both the axial and radial refractive index gradients are positive, the incident light is focussed by the “dynamic lens” and the final image size decreases. If the limiting aperture resides at the flow cell exit, this decrease in the image size allows more energy to be transmitted through the cell, resulting in a decrease in the apparent absorbance. However, if the

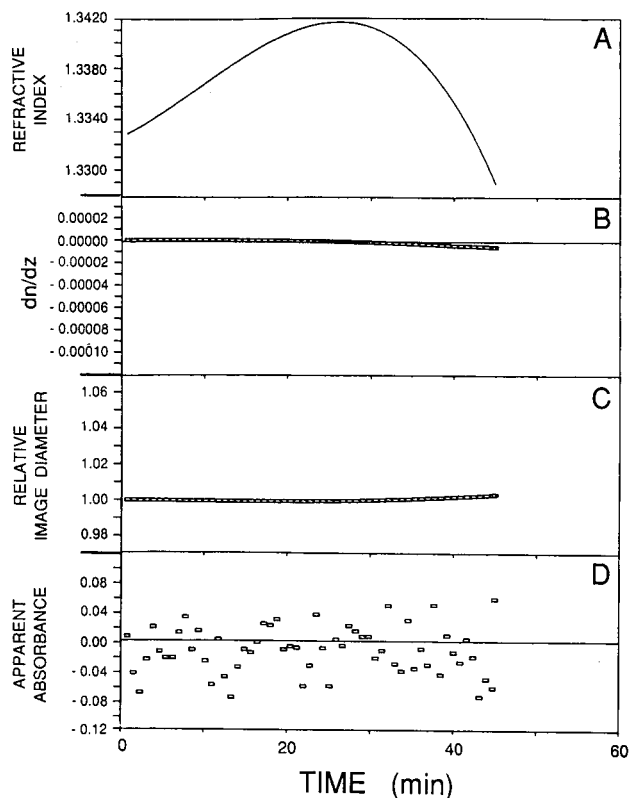


Fig. 12. Calculated absolute refractive index (A) and refractive index gradient (B) in the cell (mm^{-1}), and resultant relative image diameter (C) and apparent absorbance (D) predicted for a linear increase of methanol into water from 0 to 100% (v/v).

axial gradient is negative while the radial gradient remains positive, the incident light is defocussed and the final image size increases. This causes less energy to strike the photodiode and thus an increase in the apparent absorbance is observed. The position of the limiting aperture in the optical system ultimately determines whether the change in image size caused by the refractive index gradients will result in a change in the apparent absorbance. In addition, both axial and radial refractive index gradients must be present within the cell volume for this focussing effect to be observed.

These optical conditions must all be considered when evaluating the observed refractive index artifact. Because no single factor determines the apparent absorbance response at the photodiode, characterization of this artifact requires detailed knowledge of the optical configuration as well as the refractive index conditions present within the flow cell. With this understanding, it becomes possible to eliminate this refractive index artifact in absorbance detection or, alternatively, to optimize refractive index detectors which are based on this response. This understanding is also necessary for the accurate evaluation of system peaks, which are often measured directly from the apparent absorbance response observed upon the injection of a mixture of solvents. Thus, optical simulation of refractive index effects can aid in the

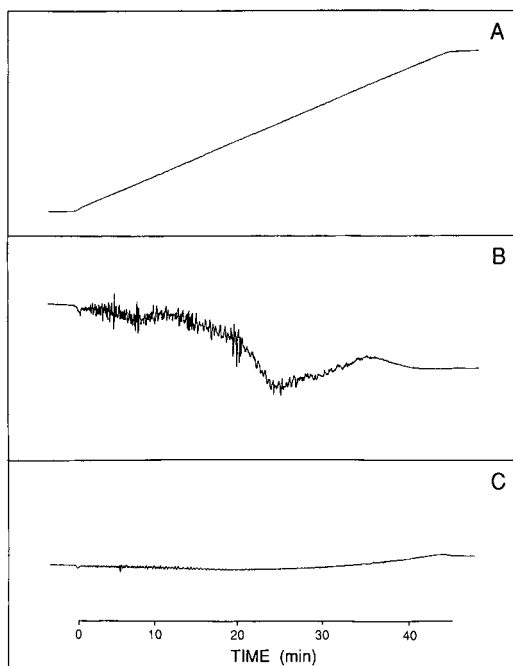


Fig. 13. Observed detector response ($\lambda = 250$ nm) for a linear increase in 1% (v/v) acetone-methanol into methanol from 0 to 100% (v/v) (A); 0.160 a.u.f.s. Apparent absorbance observed ($\lambda = 589$ nm) for the same linear solvent program for 20% (v/v) tetrahydrofuran-water into water (B) and 90% (v/v) methanol-water into water (C); 0.040 a.u.f.s.

design of improved detectors for liquid chromatography, as well as the more accurate evaluation of fundamental parameters of chromatographic separations. Although the “dynamic lens” model is illustrated here for the evaluation of refractive index artifacts in the Z-pattern flow cell, these ray-tracing simulations may be applied to the evaluation of any optical flow cell design where refractive index is an important factor in the detector response.

APPENDIX

Evaluation of the refractive index profiles present in the flow cell requires the calculation of the final axial concentration as a function of time and distance, $C(t)$ and $C(z)$, respectively. The axial concentration profiles necessary for the simulations are derived below for injection and gradient elution conditions common in liquid chromatographic separations.

Exponential input function

Under non-ideal injection conditions, the input concentration function which results from the injection of an initial concentration (C_0) has the form,

$$C(t_a) = C_0 \exp\left[-\frac{(t_a - t_R)}{\tau}\right] \quad \text{for } t_R \leq t_a \leq \infty \quad (6)$$

where the time constant (τ) is characteristic of the size and flow conditions present in the chamber and t_R is the time delay between the injector and detector. The concentration profile at the column exit [$C(t)$] may be evaluated for the exponential input by substituting eqn. 6 into eqn. 2.

$$C(t) = \frac{1}{(2\pi)^{1/2}\sigma_t} \int_{t_R}^{\infty} C_0 \exp\left[-\frac{(t_a - t_R)}{\tau}\right] \exp\left[-\frac{(t - t_a)^2}{2\sigma_t^2}\right] dt_a \quad (7)$$

Expansion and rearrangement of eqn. 7 yields

$$C(t) = \frac{C_0}{(2\pi)^{1/2}\sigma_t} \exp\left[-\frac{(t - t_R)}{\tau}\right] \exp\left(\frac{\sigma_t^2}{2\tau^2}\right) \int_{t_R}^{\infty} \exp\left[-\frac{\left(t - \frac{\sigma_t^2}{\tau} - t_a\right)^2}{2\sigma_t^2}\right] dt_a \quad (8)$$

Substitution of $x = (t - \sigma_t^2/\tau - t_a)/(2)^{1/2} \sigma_t$ and $dx = -[1/(2)^{1/2} \sigma_t] dt_a$ into eqn. 8 results in

$$C(t) = -\frac{C_0}{(\pi)^{1/2}} \exp\left[-\frac{(t - t_R)}{\tau}\right] \exp\left(\frac{\sigma_t^2}{2\tau^2}\right) \int_{(t - \sigma_t^2/\tau - t_a)/(2)^{1/2}\sigma_t}^{-\infty} \exp(-x^2) dx \quad (9)$$

This integral cannot be solved precisely and the error function [$\text{erf}(y)$] must be utilized in the final result. The indefinite integral of the form

$$\text{erf}(y) = \frac{2}{(\pi)^{1/2}} \int_0^y \exp(-x^2) dx \quad (10)$$

when substituted into eqn. 9, yields the final concentration expression for the convolution of an exponential input function with a Gaussian operator.

$$C(t) = \frac{C_0}{2} \exp\left[-\frac{(t - t_R)}{\tau}\right] \exp\left(\frac{\sigma_t^2}{2\tau^2}\right) \left[1 + \text{erf}\left(\frac{t - \frac{\sigma_t^2}{\tau} - t_R}{(2)^{1/2}\sigma_t}\right) \right] \quad (11)$$

However, the concentration profile as a function of distance [$C(z)$], rather than time, is necessary for the calculation of the axial concentration gradient and thus the refractive index gradient in the flow cell. This conversion from time (t) to distance (z) is easily accomplished by noting for constant linear velocity (u) conditions, the time is given by $t = z/u$ and the time variance for a non-retained solute is given by $\sigma_t^2 = \sigma_L^2/u^2$. This results in a final concentration profile as a function of distance of

$$C(z) = \frac{C_0}{2} \exp\left[-\frac{(z - z_R)}{u\tau}\right] \exp\left(\frac{\sigma_L^2}{2u^2\tau^2}\right) \left[1 + \text{erf}\left(\frac{z - \frac{\sigma_L^2}{u\tau} - z_R}{(2)^{1/2}\sigma_L}\right) \right] \quad (12)$$

where σ_L^2 is the length variance contributed by the column or connecting tubing and z_R is the retention distance, analogous to the retention time. Since the functions within the original convolution integral in eqn. 2 are commutative, the final concentration profile (eqns. 11 and 12) is the same regardless of where the exponential broadening occurs. Thus, the same final concentration expression results whether the exponential input arises from a non-ideal injection, a mixing volume, or a detector time constant.

Rectangular input function

A rectangular injection of duration time τ may be described by the following input concentration profile.

$$C(t_a) = C_0 \quad \text{for} \quad t_R \leq t_a \leq t_R + \tau \quad (13)$$

Convolution of this rectangular injection function with a Gaussian operator is accomplished by substitution into eqn. 2 with the following result:

$$C(t) = \frac{C_0}{(2\pi)^{1/2}\sigma_t} \int_{t_R}^{t_R + \tau} \exp\left[-\frac{(t-t_a)^2}{2\sigma_t^2}\right] dt_a \quad (14)$$

Evaluation of this integral utilizing the error function (eqn. 10) yields the final expression for the concentration profile arriving at the detector:

$$C(t) = \frac{C_0}{2} \left\{ \operatorname{erf}\left[\frac{t-t_R}{(2)^{1/2}\sigma_t}\right] - \operatorname{erf}\left[\frac{t-t_R-\tau}{(2)^{1/2}\sigma_t}\right] \right\} \quad (15)$$

Again this expression can be converted to distance units, resulting in a concentration profile as a function of distance:

$$C(z) = \frac{C_0}{2} \left\{ \operatorname{erf}\left[\frac{z-z_R}{(2)^{1/2}\sigma_L}\right] - \operatorname{erf}\left[\frac{z-z_R-u\tau}{(2)^{1/2}\sigma_L}\right] \right\} \quad (16)$$

In the limit of small injection time τ , the rectangular injection yields a δ function input and thus a final concentration profile that is purely Gaussian in form.

Stepwise input function

For a gradient program employing a sequence of m steps, of equal duration τ , the input concentration profile can be described by

$$C(t_a) = \sum_{n=1}^m \frac{C_0}{m} \quad \text{for} \quad t_R + (n-1)\tau \leq t_a \leq t_R + n\tau \quad (17)$$

where n is the step number and C_0 is the final concentration of the strong solvent. The stepwise input function is then convolved with a Gaussian operator utilizing eqn. 2, resulting in

$$C(t) = \frac{1}{(2\pi)^{1/2}\sigma_t} \sum_{n=1}^m \frac{C_0}{m} \int_{t_R+(n-1)\tau}^{t_R+m\tau} \exp\left[-\frac{(t-t_a)^2}{2\sigma_t^2}\right] dt_a \quad (18)$$

This function is evaluated utilizing eqn. 10 to yield the final concentration profile as a function of time.

$$C(t) = \frac{C_0}{2m} \sum_{n=1}^m \left\{ \operatorname{erf}\left[\frac{t-t_R-(n-1)\tau}{(2)^{1/2}\sigma_t}\right] - \operatorname{erf}\left[\frac{t-t_R-m\tau}{(2)^{1/2}\sigma_t}\right] \right\} \quad (19)$$

Conversion to distance units results in the final concentration profile for the stepwise input function.

$$C(z) = \frac{C_0}{2m} \sum_{n=1}^m \left\{ \operatorname{erf}\left[\frac{z-z_R-(n-1)u\tau}{(2)^{1/2}\sigma_L}\right] - \operatorname{erf}\left[\frac{z-z_R-mu\tau}{(2)^{1/2}\sigma_L}\right] \right\} \quad (20)$$

Although this expression for the final axial profile contains equal concentration increments (C_0/m) and a constant step length ($u\tau$), by judicious choice of input functions a variable step height or length may be incorporated.

Linear input function

The input concentration profile for a linear solvent program of duration τ , may be described as follows:

$$C(t_a) = \frac{C_0(t_a - t_R)}{\tau} \quad \text{for} \quad t_R \leq t_a \leq t_R + \tau \quad (21)$$

Convolution of the linear input function is accomplished by substituting eqn. 21 into eqn. 2, resulting in the following form:

$$C(t) = \frac{C_0}{(2\pi)^{1/2}\sigma_t\tau} \int_{t_R}^{t_R+\tau} (t_a - t_R) \exp\left[-\frac{(t-t_a)^2}{2\sigma_t^2}\right] dt_a \quad (22)$$

Integration of eqn. 22 is facilitated by noting that $x \exp(-x^2)$ is a function of the derivative of $\exp(-x^2)$. Thus, the final concentration profile from the convolution of a linear ramp with a Gaussian function is

$$C(t) = \frac{C_0\sigma_t}{(2\pi)^{1/2}\tau} \left\{ \exp\left[-\frac{(t-t_R)^2}{2\sigma_t^2}\right] - \exp\left[-\frac{(t-t_R-\tau)^2}{2\sigma_t^2}\right] \right\} - \frac{C_0(t_R-t)}{2\tau} \left\{ \operatorname{erf}\left[\frac{(t-t_R)}{(2)^{1/2}\sigma_t}\right] - \operatorname{erf}\left[\frac{(t-t_R-\tau)}{(2)^{1/2}\sigma_t}\right] \right\} \quad (23)$$

Again, converting to distance units yields the axial concentration profile

$$C(z) = \frac{C_0\sigma_L}{(2\pi)^{1/2}u\tau} \left\{ \exp \left[-\frac{(z-z_R)^2}{2\sigma_L^2} \right] - \exp \left[-\frac{(z-z_R-u\tau)^2}{2\sigma_L^2} \right] \right\} - \frac{C_0(z-z_R)}{2u\tau} \left\{ \operatorname{erf} \left[\frac{z-z_R}{(2)^{1/2}\sigma_L} \right] - \operatorname{erf} \left[\frac{z-z_R-u\tau}{(2)^{1/2}\sigma_L} \right] \right\} \quad (24)$$

as a function of the length standard deviation (σ_L) and the linear velocity (u).

ACKNOWLEDGEMENTS

We gratefully acknowledge the kind gift of high-purity solvents from the Burdick and Jackson Division of Baxter Healthcare Corp. We also wish to thank Dr. M. D. Morris (University of Michigan) and Dr. T. A. Nevius (The Anspec Co.) for helpful discussions, and Dr. S. R. Crouch (Michigan State University) for his thoughtful and critical evaluation of this work.

REFERENCES

- 1 L. R. Snyder and J. J. Kirkland, *Introduction to Liquid Chromatography*, Wiley, New York, 1979, p. 133.
- 2 D. Betteridge, E. L. Dagless, B. Fields and N. F. Graves, *Analyst (London)*, 103 (1978) 897.
- 3 D. O. Hancock and R. E. Synovec, *Anal. Chem.*, 60 (1988) 1915.
- 4 J. E. Stewart, *Appl. Opt.*, 20 (1981) 654.
- 5 J. E. Stewart, *Anal. Chem.*, 53 (1981) 1125.
- 6 C. F. deMay and C. C. Helms, *U.S. Pat.*, 4 192 614 (1980).
- 7 J. N. Little and G. J. Fallick, *J. Chromatogr.*, 112 (1975) 389.
- 8 D. J. Bornhop, T. G. Nolan and N. J. Dovichi, *J. Chromatogr.*, 384 (1987) 181.
- 9 J. Pawliszyn, *Anal. Chem.*, 58 (1986) 243.
- 10 J. Pawliszyn, *Anal. Chem.*, 58 (1986) 3207.
- 11 C. E. Evans and V. L. McGuffin, *J. Chromatogr.*, 459 (1988) 119.
- 12 J. D. Ingle and S. R. Crouch, *Spectrochemical Analysis*, Prentice-Hall, Englewood Cliffs, NJ, 1988, p. 373.
- 13 F. A. Jenkins and H. E. White, *Fundamentals of Optics*, McGraw-Hill, New York, 1976, pp. 115-126.
- 14 S. M. McCown, D. Southern, B. E. Morrison and D. Gartiez, *J. Chromatogr.*, 352 (1986) 465.
- 15 E. D. Katz, C. H. Lochmuller and R. P. W. Scott, *Anal. Chem.*, 61 (1989) 349.
- 16 K. Peck and M. D. Morris, *J. Chromatogr.*, 448 (1988) 193.
- 17 G. Taylor, *Proc. R. Soc. London, Ser. A*, 219 (1953) 186.
- 18 J. J. van Deemter, F. J. Zuiderweg and A. Klinkenberg, *Chem. Eng. Sci.*, 5 (1956) 271.
- 19 J. H. Knox, *J. Chromatogr. Sci.*, 15 (1977) 352.
- 20 M. J. E. Golay, in D. H. Desty (Editor), *Gas Chromatography 1958*, Academic Press, New York, 1958, pp. 36-55.
- 21 R. Aris, *Proc. R. Soc. London, Ser. A*, 235 (1956) 67.
- 22 C. N. Reilley, G. P. Hildebrand and J. W. Ashley, Jr., *Anal. Chem.*, 34 (1962) 1198.
- 23 J. C. Sternberg, *Adv. Chromatogr.*, 2 (1966) 205.
- 24 E. W. Marchand, *Gradient Index Optics*, Academic Press, New York, 1978, pp. 3-6.
- 25 C. R. Wilke and P. Chang, *AIChE J.*, 1 (1955) 264.
- 26 R. M. McCormick and B. L. Karger, *Anal. Chem.*, 52 (1980) 2249.
- 27 S. Levin and E. Grushka, *Anal. Chem.*, 59 (1987) 1157.

Post-column adjustment of conditions for peroxyoxalate chemiluminescence detection for high-performance liquid chromatography

NOBUAKI HANAOKA

Shimadzu-Kansas Research Laboratory, 2095 Constant Avenue, Lawrence, KS 66046 (U.S.A.)

(First received April 14th, 1989; revised manuscript received October 17th, 1989)

SUMMARY

Post-column adjustment of the conditions for high-performance liquid chromatography (HPLC) with a peroxyoxalate chemiluminescence (PO-CL) detector was examined using fatty acids, derivatized with 9-anthryldiazomethane, as analytes. Out of fourteen parameters that affect the response of a PO-CL detector, solvent, catalyst, oxalate, mixing and transport volumes for the PO-CL reagents and the reservoir materials were decided on the basis of previously published studies. For the determination of the other parameter values, data for myristic acid, dansylalanine and diphenylanthracene by flow-injection analysis, the results of HPLC measurements on myristic acid and data from published work were compared. From the results, a working knowledge for determining the optimum conditions for PO-CL detection was obtained.

INTRODUCTION

One of the most important tasks in maximizing the capability of high-performance liquid chromatography (HPLC) is optimizing the conditions for the detection of separated analytes. This is especially true for a peroxyoxalate chemiluminescence (PO-CL) detector as there are many parameters that can affect the detector response. To obtain the highest sensitivity and stability with a PO-CL detector, many researchers have investigated the influence of the variables of PO-CL detection¹⁻⁷.

In this paper, we report an examination of the post-column adjustment of conditions for HPLC with a PO-CL detector. Fatty acids (FAs) derivatized with 9-anthryldiazomethane (ADAM) were chosen as analytes. These materials have a long excitation wavelength (365 nm)⁸ and were considered suitable for PO-CL detection⁹⁻¹¹. The premise for this study was to modify the eluate for PO-CL detection but not to change the separation conditions, as good separations have already been achieved. ADAM-derivatized FAs were separated with the same column and the same mobile phase as in previous work¹². The eluate was modified with a condition-

ing solution to regulate pH, concentration of catalyst and water content for PO-CL detection. A bis(2,4,6-trichlorophenyl)oxalate (TCPO)-H₂O₂ solution was delivered to the mixture of mobile phase and conditioning solution to excite ADAM-FA molecules to exhibit chemiluminescence. Recently, it was found that a TCPO-H₂O₂ mixture was stable when prepared in acetonitrile and stored in a borosilicate glass bottle¹³. This allowed the premixing of TCPO and H₂O₂ and the construction of a three-pump system for the delivery of the mobile phase, the conditioning solution and the TCPO-H₂O₂ mixture.

Initially, five parameters (type of oxalate, solvent, catalyst, and mixing and transport volumes for the PO-CL reagents, and reservoir material) were adopted from published data^{1-5,7,13,14}. For the determination of the other variables (pH, temperature, water content, cell volume of the detector, concentrations of imidazole, TCPO and H₂O₂ and flow-rates of the conditioning solution and TCPO-H₂O₂ mixture), the results of flow-injection analysis (FIA) of dansylalanine (Dns-Ala), diphenylanthracene (DPA) and myristic acid (C₁₄) and HPLC measurements of C₁₄ are discussed with reference to the results from published work^{1-7,15-22}. As a result, useful information concerning the conditioning of the eluate was obtained.

EXPERIMENTAL

Chemicals

ADAM was purchased from Research Organic and used without further purification. FAs [lauric (C₁₂), myristic (C₁₄), palmitic (C₁₆) and stearic (C₁₈) acids] and DPA were purchased from Sigma. All other reagents were the same as those in the previous study⁷.

Apparatus

The HPLC system is shown in Fig. 1. The column (C) was a 25 cm × 4.6 mm I.D. Zorbax ODS (Du Pont) and the column oven (V) was a Shimadzu CTO-6A. The waterbath (W) was a Brinkman RH-3 with both heating and cooling functions. A₁ and A₂ were stainless-steel pipes (1.1 mm × 0.5 mm I.D.). B₁ and B₂ were stainless-steel pipes, 1.1 m in length and of 0.5 mm I.D. B₁ and B₂ were stainless-steel pipes of

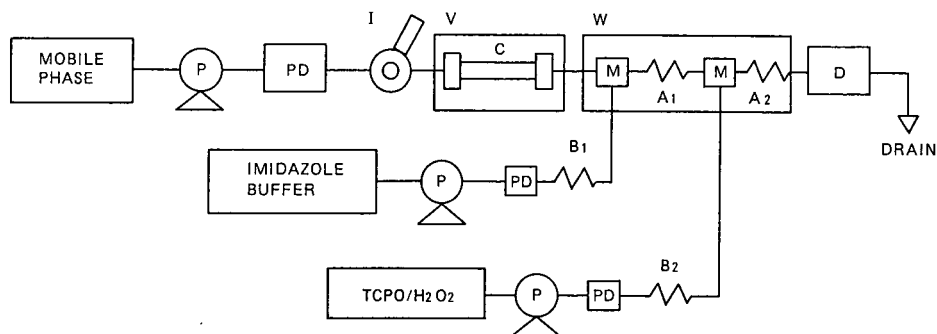


Fig. 1. Schematic diagram of HPLC system: P, pump; PD, pulse damper; I, injector; C, column; D, detector; V, column oven; W, waterbath; B₁, B₂, 0.1 mm I.D. stainless-steel tubes, each of length adjusted according to the flow-rates to apply pressures between 70 and 100 kg/cm²; A₁, A₂, 1.1 m × 0.5 mm I.D. stainless-steel tubes.

0.1 mm I.D. and their lengths were adjusted according to the flow-rate to apply a pressure of between 70 and 100 kg/cm² to the solutions. For example, the length was *ca.* 5 m for an aqueous imidazole buffer at a flow-rate of 0.2 ml/min for an applied pressure of 75 kg/cm². PD was a Shimadzu high-performance damper unit to decrease the pulsation from the pumps. The reservoir for the TCPO–H₂O₂ mixture was a Pyrex borosilicate glass bottle purchased from American Scientific Products. For FIA measurements, the column was replaced by a stainless-steel pipe (2 m × 0.5 mm I.D.). All other units including the detector were the same as those in the previous work⁷.

Procedure

HPLC measurements. The mobile phase [acetonitrile–water (96:4, v/v)] and the flow-rate (1.2 ml/min) were the same as in ref. 12. The sample was C₁₄ derivatized with ADAM according to the procedure of Nimura and Kinoshita⁸; 100 pmol in 20 μl of methanol was injected. A standard set of measuring conditions as outlined below was applied to all the measurements.

The conditioning solution was 100 mM aqueous imidazole buffer (pH 7.55; with this buffer, the pH of the final solution was 6.8) and the flow-rate was 0.5 ml/min. The oxalate–H₂O₂ solution was a mixture of equal volumes of 0.3 mM TCPO and 1.5 mM H₂O₂ in acetonitrile and delivered at 1.0 ml/min. The temperatures of the column oven and the waterbath were set at 40°C and room temperature (*ca.* 22°C), respectively. The cell volume of the detector was 30 μl. When one parameter was under examination, the others were kept unchanged.

FIA measurements. The standard set of conditions including the mobile phase were adopted except for the column temperature (see below). A 4-pmol amount of either Dns-Ala or DPA in 20 μl of mobile phase was measured. The C₁₄ analytical sample was prepared by evaporating the methanol after derivatization and dissolving of the residue in mobile phase. This sample concentration was also 4 pmol in 20 μl.

Measurements of pH effects. The pH of the conditioning solution was varied from 5.5 to 8.5 with nitric acid. The pH of the final solutions was also measured.

Water content. The water content of the imidazole solution varied from 20 to 100% for the tests. The pH of each solution was adjusted to 7.7 with nitric acid. The other measuring conditions were the same as above.

Temperature. In the HPLC measurements, the waterbath was kept at room temperature (*ca.* 22°C) and the temperature of the column oven was varied from 22 to 50°C. Next, the temperatures of both the waterbath and the column oven were changed simultaneously from room temperature to 50°C. In FIA measurements, the column oven was not used and the temperature of the waterbath was varied from room temperature to 50°C.

Concentration of reagents. The measured range of imidazole concentration in the conditioning solution was 20–200 mM. The change in the pH of final solution caused by varying the concentration of imidazole was countered by regulating the pH of the buffer solution. The pH of the buffer was 7.7 at 20 mM, 7.65 at 50 mM and 7.55 at 100 mM imidazole to achieve pH 6.8 for the final solution. The concentration ranges of TCPO and H₂O₂ in the TCPO–H₂O₂ mixture were 0.1–1.0 and 0.5–5.0 mM, respectively.

Cell volume. The cell volume of the detector was varied from 30 to 280 μl by

changing the I.D. of the flow cell. The cells used here were straight glass tubes 40 mm in length.

Flow-rate. The flow-rates of the imidazole buffer and the TCPO–H₂O₂ solution were varied independently from 0.2 to 0.6 ml/min in 0.2 ml/min steps and from 0.6 to 1.8 ml/min in 0.6 ml/min steps, respectively.

Measurements of FAs. A 125-nmol amount of each C₁₂, C₁₄, C₁₆ and C₁₈ were dissolved together in 100 ml of methanol and derivatized with ADAM according to the method described above. A 20- μ l volume of this solution was subjected to HPLC under the decided conditions (see below).

RESULTS AND DISCUSSION

Adoption of parameter values from published work

The fourteen factors that affect the response of a PO-CL detector are temperature, pH, water content, solvent, catalyst, oxalate, concentration of oxalate, concentration of H₂O₂, concentration of catalyst, volume of mixing tube A₂, cell volume of detector, flow-rate of imidazole buffer, flow-rate of oxalate–H₂O₂ mixture and reservoir material^{1–7,13,14}. If we obtain three data points for each variable, the total number would be 3¹⁴ = 4 783 969, making it highly impractical to acquire all the data; hence the number of data points must be reduced by determining some parameter values and/or defining their ranges in advance. Results from the literature were then used to fix certain parameters.

The following parameters were decided upon prior to the measurements: the oxalate was TCPO, which has been shown to be stable in a mixture with H₂O₂^{13,14}; acetonitrile was used as a solvent because in it the PO-CL intensities are the highest¹ and the TCPO–H₂O₂ mixture is stable^{13,14} (ethyl acetate is widely used as a solvent for TCPO^{1–4,15,17–22}, but a TCPO–H₂O₂ mixture is unstable in this solvent^{13,14}); imidazole was the best catalyst⁷; the reservoirs were Pyrex borosilicate glass bottles in which TCPO–H₂O₂ solution is stable for more than 6 h^{13,14}; and the mixing tube A₂ was 1.1 m \times 0.5 mm I.D. and the total volume of this tube and the mixer (M, 26 μ l) was 242 μ l. The time required for the fluorescent species to reach the detector after the start of the PO-CL reactions (*t*₁) was *ca.* 5 s when the total flow-rate was 3 ml/min. The PO-CL reaction reaches maximum intensity in *ca.* 5 s under normal conditions⁷.

The examining ranges for the other parameters could also be established with the help of the published results. The values decided on were as follows: the temperature should be from room temperature to 50°C⁷; the optimum pH is between 6.0 and 8.0^{2–5,7,15–22} and the measured pH range is 5.5–8.5; a rather hydrophobic final solution is preferable for stable measurements¹, and the flow-rate of the aqueous conditioning solution should be less than 0.6 ml/min; the concentration of TCPO must be more than 0.1 mM to avoid decomposition; the concentration ratio of TCPO–H₂O₂ was 1:5 to obtain simultaneously a stable solution and the highest signal intensity¹³; the cell volume was varied from 30 to 300 μ l and the “chemical band narrowing effect”³ was examined; in addition, the flow-rate of the TCPO–H₂O₂ mixture was fixed at less than 2 ml/min to avoid too rapid consumption of reagents.

Optimum pH

Many optimum pH values for PO-CL measurements using TCPO have been

reported^{2-5,7,15-22}. Among these values, those for the aqueous buffer or mobile phase are between 7.0 and 8.0^{3-5,15-22}. The optimum pH of the final mixture of aqueous buffer and the acetonitrile solution of TCPO-H₂O₂ was determined to be 6.7 by Hanaoka *et al.*⁷. In this work, the optimum pH values for imidazole buffer and the final solution were obtained by HPLC measurements of C₁₄ and were 7.7 and 6.8, respectively. At the same time, the three fluorescent species described under Experimental were measured by FIA, and the optimum values obtained were the same as those for C₁₄ by HPLC. From these results and the published values, it may be concluded that the optimum pH for PO-CL reactions with TCPO is independent of the nature of the fluorescent species and is between 7.0 and 8.0 in buffer or mobile phase and *ca.* 6.8 in the final solution.

It was also found that the background and noise levels changed according to the change in signal intensity and, consequently, the signal-to-noise ratio of the measurements was almost constant in the pH range 6.3-7.3 in the final solution. This finding shows that very strict attention to the optimum pH value that gives the highest signal intensity is not necessary for actual HPLC measurements as the signal-to-noise ratio is fairly constant over the pH range adopted.

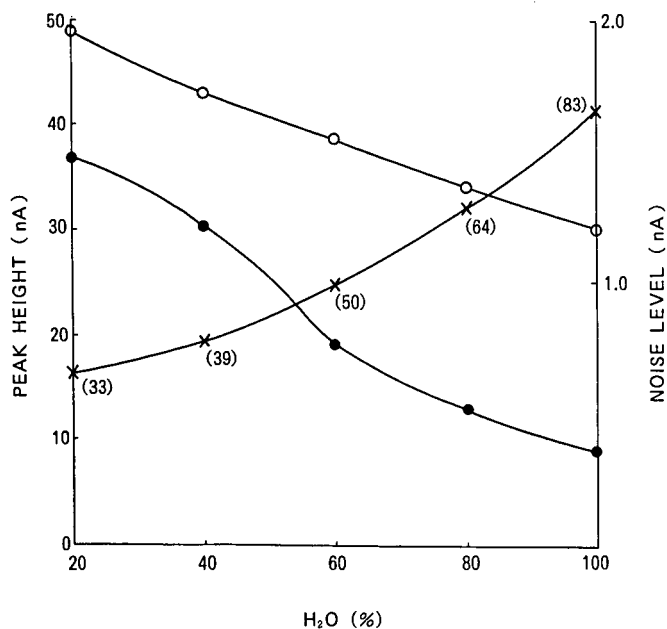


Fig. 2. Effect of water content on the peak height of myristic acid (C₁₄). Values in parentheses are signal-to-noise ratios for 100 mM C₁₄. LC column, 25 cm × 4.6 mm I.D. Zorbax ODS; mobile phase, mixture of 960 ml of acetonitrile and 40 ml of water; flow-rate, 1.2 ml/min; column temperature, 40°C; 100 pmol of C₁₄ derivatized with ADAM were injected. The eluate conditions were adjusted with 100 mM aqueous imidazole buffer (pH 7.55) and C₁₄ was excited with an admixture of 0.3 mM TCPO and 1.5 mM H₂O₂. The flow-rate of the buffer and TCPO-H₂O₂ solution were 0.5 and 1.0 ml/min, respectively. The water content of the imidazole buffer was varied from 20 to 100%. ○, Peak height; ●, noise level; ×, signal-to-noise ratio.

Effect of water content

The effect of water content as measured by HPLC of C₁₄ is shown in Fig. 2. Peak height was inversely proportional to the water content with a rate of decrease of height of *ca.* 1.2% per 1% increase in water content. In spite of the fact that the ADAM-derivatized C₁₄ sample contained considerable impurities, the response curve for the sample obtained by FIA over a range of water content agreed very well with the results from HPLC. Nevertheless, the responses to Dns-Ala and DPA were slightly different from that for the C₁₄ sample, and the rates of decrease of height were -0.7% and -1.8%, respectively, for each 1% increase in water content. These results indicate that the effect of water content on peak height depends on the analyte itself. The background and the noise levels are also dependent on the water content and, as shown in Fig. 2, the best signal-to-noise ratio was observed at 100%. Hence it was decided to make the buffer solution 100% aqueous.

Temperature effects

First, the temperature effects on HPLC measurements of C₁₄ were examined. When the waterbath was kept at room temperature (*ca.* 22°C), the noise level was independent of the change in temperature of the column oven. Therefore, the temperature of the oven was set at 40°C, the same as in the published separation conditions¹². However, when the temperature of the waterbath was elevated from 22 to 40°C, the noise level increased by *ca.* 50%. The increase in peak height caused by this change was only 20%, and it was decided to maintain the waterbath at room temperature. Increased responses for the other analytes were measured in the same waterbath temperature range by FIA and were also *ca.* 20%, indicating that the temperature of the PO-CL reaction is relatively independent of the species of the analyte.

Cell volume of the detector

De Jong *et al.*³ examined the influence of cell volume on the heights and widths of HPLC peaks. They found that the influence of the cell volume of a PO-CL detector on peak broadening was much smaller than that of the other detectors, and named this phenomenon the "chemical band narrowing effect". In our study, the cell volume was varied from 30 to 280 μ l, and the increase in peak width of C₁₄ was measured by HPLC. The results are shown in Table I. De Jong *et al.*³ observed no band broadening with a 70- μ l cell, but we observed a *ca.* 6% increase in the peak width at

TABLE I
INFLUENCE OF FLOW CELL VOLUME ON PEAK HEIGHT AND PEAK WIDTH
C₁₄ was measured by HPLC. Experimental conditions as in Fig. 2.

<i>Cell volume</i> (μ l)	<i>Half peak width</i> (μ l)	<i>Peak height</i> (nA)
30	1485	12.6
70	1570	24.1
125	1710	32.8
200	1850	37.4
280	1950	39.5

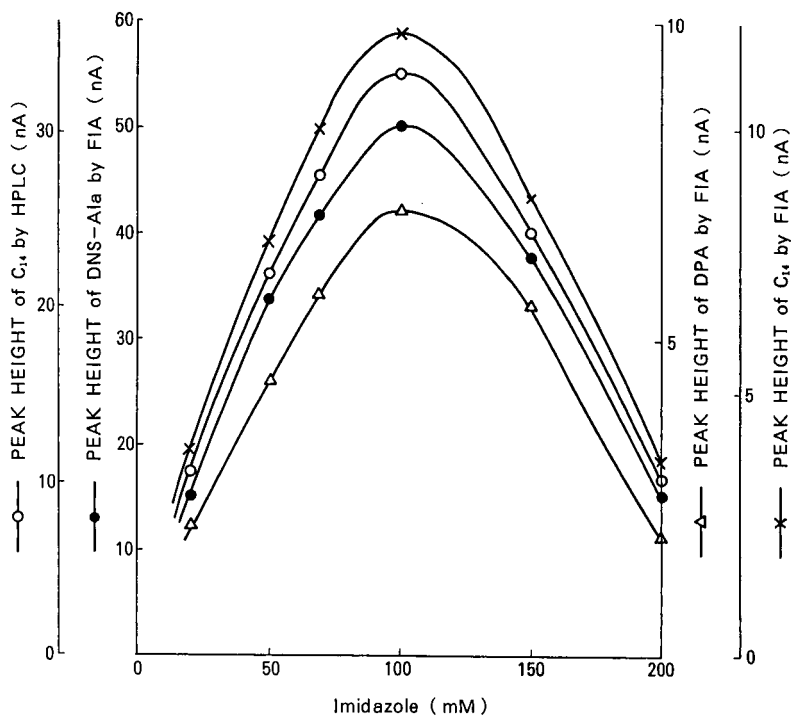


Fig. 3. Effect of imidazole concentration on peak height. Measurement conditions as in Fig. 2. The imidazole concentration in the conditioning solution was varied from 20 to 200 mM.

half-height here with a 70- μ l flow cell. The different observations might be due to the differences in the total flow-rate or in the composition of the final solution, or both. The cell volume decided on for this study was 30 μ l.

Effects of concentrations of imidazole, TCPO and hydrogen peroxide

The concentration ranges of TCPO and H₂O₂ and the concentration ratio were optimized according to the published results (see above). At the same time, it was assumed that the signal intensity would be proportional to the concentration of each reagent⁷. Both HPLC measurements of C₁₄ and FIA measurements of the other substances confirmed this supposition. Moreover, the background and noise levels changed according to the change in TCPO-H₂O₂ concentration; the signal-to-noise ratio was constant when the concentrations of TCPO and H₂O₂ were in the range 0.3–1.0 and 1.5–5.0 mM, respectively, while maintaining the 1:5 concentration ratio as previously established.

The influence of imidazole concentration on peak height is shown in Fig. 3. As is clearly seen, the influence was the same for all the analytes, and the largest signal was obtained at 100 mM (18.5 mM in the final solution). Also, the signal-to-noise ratio remained constant over the imidazole concentration range 20–100 mM, but the noise level increased and the signal-to-noise ratio deteriorated when the imidazole concentration exceeded 150 mM.

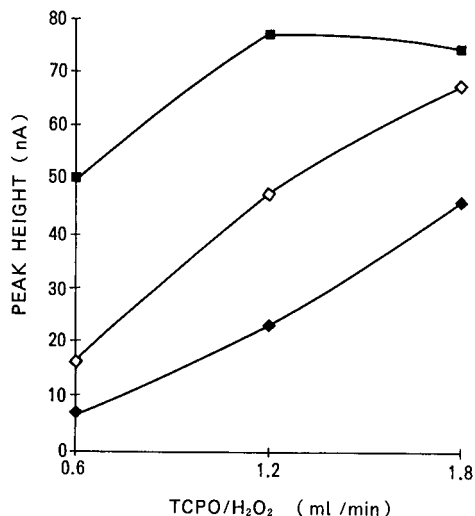


Fig. 4. Effect of flow-rate on the peak height of C_{14} measured by HPLC. Measurement conditions as above. The flow-rates of the imidazole solution and TCPO- H_2O_2 mixture were changed from 0.2 to 0.6 and 0.6 to 1.8 ml/min, respectively. Flow-rates of imidazole solution: \blacklozenge , 0.6; \diamond , 0.4; and \blacksquare , 0.2 ml/min.

Flow-rates of buffer solution and TCPO- H_2O_2 mixture

The parameters evaluated so far could be varied independently, and changes in their individual values did not affect the other parameters. However, changes in the flow-rates of the solutions can vary many of the controlling parameters of the final solution: pH, water content, concentration of TCPO, concentration of H_2O_2 , concentration of imidazole, t_1 and t_2 . In addition to these parameters, the ratios of sample

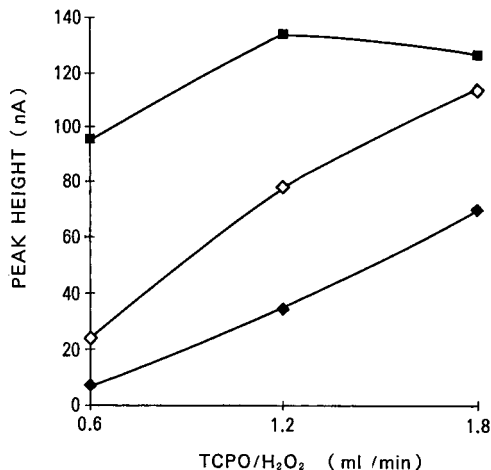


Fig. 5. Peak heights of Dns-Ala measured by FIA. A 2 m \times 0.5 mm I.D. stainless-steel pipe was used instead of an LC column. 4 pmol of Dns-Ala dissolved in 20 μ l mobile phase were injected. Measurements were made at room temperature. Other conditions and symbols as in Fig. 4.

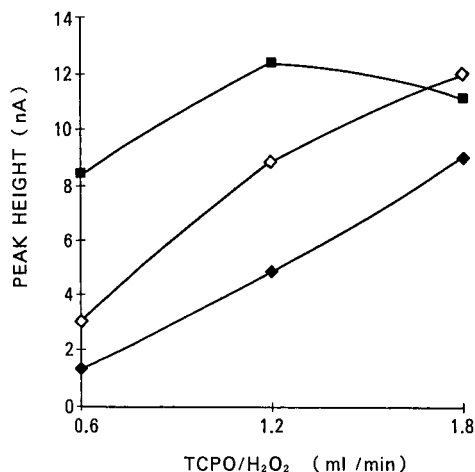


Fig. 6. Peak heights of DPA measured by FIA. Measurement conditions and symbols as in Fig. 5.

dilution by buffer and TCPO-H₂O₂ solutions are also dependent on each flow-rate, and affect the peak heights. Owing to these many factors, it is almost impossible to predict the effects of change in flow-rates from the previously published results, so the optimum values have to be determined empirically. The results of the HPLC assay of

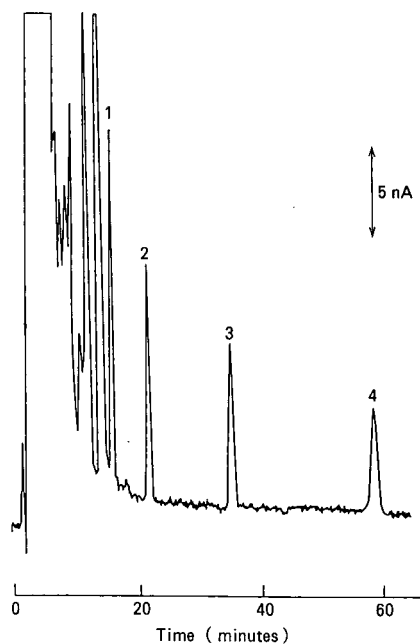


Fig. 7. Chromatogram of 25 pmol each of fatty acids: (1) C₁₂; (2) C₁₄; (3) C₁₆; (4) C₁₈. Separation conditions as in Fig. 2. The imidazole solution was 100 mM in 1000 ml of water (pH 7.55) and the flow-rate was 0.2 ml/min. The TCPO-H₂O₂ solution was a mixture of 0.3 mM TCPO and 1.5 mM H₂O₂ and the flow-rate was 0.6 ml/min. The waterbath was maintained at room temperature.

C₁₄ and FIA of Dns-Ala and DPA are shown in Figs. 4, 5 and 6, respectively. The influence of flow-rate on the peak height of C₁₄ is similar to that for Dns-Ala, but slightly different from that for DPA. These results suggest that the influence of flow-rate is slightly different for each analyte. Within the measured flow-rate range, no large differences in signal-to-noise ratio were observed for the analytes examined.

Determination of conditions for measurement of FAs

From examination of the results above, the measuring conditions for ADAM-derivatized FAs were established as follows. The conditioning solution was a 100-mM aqueous solution of imidazole (with which the best signal-to-noise ratio was obtained). The pH was adjusted to 7.55 with nitric acid to make the pH of final solution 6.8. The flow-rate was 0.2 ml/min. TCPO and H₂O₂ were dissolved in pure acetonitrile at concentrations of 0.3 and 1.5 mM, respectively, and the flow-rate was 0.6 ml/min. The adopted concentrations of TCPO and H₂O₂ are the lowest values with which a good signal-to-noise ratio was acquired. The flow-rate of each solution was decided for the same reason. The temperatures of the column oven and the waterbath were set at 40°C and ambient, respectively. A chromatogram of FAs under these conditions is shown in Fig. 7. The reproducibility of peak heights was within $\pm 2\%$ and the detection limit for C₁₄ was less than 1 pmol, which is slightly better than reported previously^{8,23}.

CONCLUSION

Of fourteen affecting factors, five were decided from previously published results: the oxalate was TCPO; the solvent was acetonitrile; the catalyst was imidazole; the material of the reservoir for the TCPO-H₂O₂ mixture was Pyrex borosilicate glass; and the length of the stainless-steel tube was adjusted so that t_1 was 5 s. The other important information also derived from those papers was that the concentration of TCPO must be more than 0.1 mM, the flow-rate of the conditioning solution should be less than 0.6 ml/min and the concentration ratio of TCPO to H₂O₂ should be 1:5. The remaining factors were examined in this study, and the following results were obtained.

The optimum pH of PO-CL with TCPO is independent of the nature of the analytes, and should be *ca.* 6.8 in the final solution. The signal-to-noise ratio is fairly constant in the pH range *ca.* 6.3–7.3, and very strict attention to some optimum value is not necessary for actual HPLC assay.

The effects of water content on peak heights are different for each analyte.

The temperature of the eluent affects the noise level considerably. The eluent should be kept at room temperature.

“Chemical band narrowing effects” as observed by de Jong *et al.*³ are not very large with TCPO and a total flow-rate of 2.7 ml/min. The cell volume should be 30 μ l or less to avoid the opposite effect, *i.e.*, band broadening.

The signal-to-noise ratio remained constant in concentration ranges of TCPO, H₂O₂ and imidazole of 0.3–1.0, 1.5–5.0 and 10–100 mM, respectively.

The signal-to-noise ratio was also unchanged for flow-rates of the conditioning solution and TCPO-H₂O₂ mixture of 0.2–0.6 and 0.6–1.8 ml/min, respectively.

ACKNOWLEDGEMENT

The author gratefully thanks Arjav Shah for assistance with data acquisition.

REFERENCES

- 1 S. Kobayashi and K. Imai, *Anal. Chem.*, 52 (1980) 424.
- 2 K. Honda, J. Sekino and K. Imai, *Anal. Chem.*, 55 (1983) 940.
- 3 G. J. de Jong, N. Lammers, F. J. Spruit, U. A. Th. Brinkman and R. W. Frei, *Chromatographia*, 18 (1984) 129.
- 4 R. Weinberger, *J. Chromatogr.*, 314 (1984) 155.
- 5 K. Honda, K. Miyaguchi and K. Imai, *Anal. Chim. Acta*, 177 (1985) 103.
- 6 G. J. de Jong, N. Lammers, F. J. Spruit, R. W. Frei and U. A. Th. Brinkman, *J. Chromatogr.*, 353 (1986) 249.
- 7 N. Hanaoka, R. S. Givens, R. L. Schowen and T. Kuwana, *Anal. Chem.*, 60 (1988) 2193.
- 8 N. Nimura and T. Kinoshita, *Anal. Lett.*, 13 (1980) 191.
- 9 M. M. Rauhut, B. G. Roberts, D. R. Maulding, W. Bergmark and R. Coleman, *J. Org. Chem.*, 40 (1975) 330.
- 10 P. A. Scherman, J. Holzbecher and D. E. Ryan, *Anal. Chim. Acta*, 497 (1978) 21.
- 11 P. Lechtken and N. J. Turro, *Mol. Photochem.*, 6 (1974) 95.
- 12 *Application Data Book of Shimadzu High Performance Liquid Chromatograph*, Shimadzu, Kyoto, 1984.
- 13 N. Hanaoka, *Anal. Chem.*, 61 (1989) 1298.
- 14 N. Imaizumi, K. Hayakawa, M. Miyazaki and K. Imai, *Analyst (London)*, 114 (1989) 161.
- 15 S. Kobayashi, J. Sekino, K. Honda and K. Imai, *Anal. Biochem.*, 112 (1981) 99.
- 16 K. W. Sigvardson and J. W. Birks, *Anal. Chem.*, 55 (1983) 432.
- 17 G. Mellbin, *J. Liq. Chromatogr.*, 6 (1983) 1603.
- 18 K. W. Sigvardson, J. M. Kennish and J. W. Birks, *Anal. Chem.*, 56 (1984) 1096.
- 19 G. Mellbin and B. E. F. Smith, *J. Chromatogr.*, 312 (1984) 203.
- 20 R. Weinberger, C. A. Mannan, M. Cerchio and M. L. Grayeski, *J. Chromatogr.*, 288 (1984) 445.
- 21 K. Miyaguchi, K. Honda and K. Imai, *J. Chromatogr.*, 316 (1984) 501.
- 22 M. L. Grayeski and A. J. Weber, *Anal. Lett.*, 17 (1984) 1539.
- 23 S. A. Barker, J. A. Monti, S. T. Christian, F. Benington and R. D. Morin, *Anal. Biochem.*, 107 (1980) 116.

CHROM 22 142

Development of an automated high-performance liquid chromatographic method for the on-line pre-concentration and determination of trace concentrations of pesticides in drinking water

CHRIS H. MARVIN and IAN D. BRINDLE

Department of Chemistry, Brock University, St. Catharines, Ontario L2S 3A1 (Canada)

C. DAVID HALL

Ontario Ministry of the Environment, Rexdale, Ontario M9W 5L1 (Canada)

and

MIKIO CHIBA*

Research Station, Agriculture Canada, Vineland Station, Ontario L0R 2E0 (Canada)

(First received July 4th, 1989; revised manuscript received November 8th, 1989)

SUMMARY

An automated reversed-phase high-performance liquid chromatographic (HPLC) method has been developed for the determination of trace concentrations of propoxur, carbofuran, carbaryl, propham, captan, chloroprotham, barban and butylate in drinking water. A 100-ml of sample water is passed through a 3-cm precolumn, packed with 5- μm ODS sorbent, at a flow-rate of 5 ml/min. The HPLC system is then switched to an acetonitrile-water gradient elution program. The analytes, which are concentrated on the precolumn, are eluted and separated on a 25-cm C_8 analytical column and determined by measuring the UV absorption at 220 nm. The resolution of analytes is excellent regardless of whether the elution from the precolumn is done unidirectionally or with backflushing. The precolumn can be used repeatedly for at least 30 samples without a significant decrease in efficiency. The total analytical time is 60 min. Tap, distilled, deionized, commercial spring and HPLC-grade waters were analyzed. The lowest detectable concentrations are in the range of $10 \cdot 10^{-12}$ – $460 \cdot 10^{-12}$ g/ml for the eight pesticides with 100 ml of sample.

INTRODUCTION

In recent years, for the determination of trace amounts of organic pollutants in water, much attention has been focused on sample preconcentration techniques involving the use of a solid sorbent phase, as opposed to conventional liquid-liquid extraction techniques^{1,2}. The use of a solid sorbent should, in theory, result in a more efficient recovery of analyte and better reproducibility between replicate sample ex-

tractions. Both the amount of organic solvent and the period of time needed for the procedure are greatly reduced. The evaporation procedure required in liquid-liquid extractions is also eliminated. Several workers have described solid phase extraction (SPE) methods for determination of selected carbamate pesticides using Waters Assoc. Sep-Pak cartridges in conjunction with reserved-phase high-performance liquid chromatography^{3,4}. EPA method 531²² uses HPLC for the determination of carbamates. None of the above methods, however, is completely automated using SPE and HPLC methodologies for the determination of multiple residues of carbamate pesticides in water.

Unlike organochlorine pesticides, carbamates are difficult to determine by gas chromatography (GC) mainly owing to their thermal lability⁵. Methods involving GC have been described^{6,7}. Spectrophotometric^{8,9}, enzymic^{10,11}, spectrofluorometric^{12,13} and mass spectral techniques^{14,15} for the determination of carbamates and their metabolic derivatives in various sample matrices have also been described. However, each of these methods has limitations making it inappropriate for the analysis of large volumes of aqueous solution containing pesticide residues at the 10^{-9} or 10^{-12} g/ml level. As a result, HPLC is generally regarded as the best technique for carbamate residue determination.

In an on-line pre-concentration method¹⁶⁻¹⁹, the entire sample can be analysed quantitatively. An on-line technique also offers the possibility of constructing a totally automated HPLC system for the determination of trace amounts of organic pollutants in aqueous samples. In this paper, we report the development of an automated on-line preconcentration and determination method for eight pesticides in drinking water. The parameters investigated included (1) size of packing material used in the precolumn, (2) the rate of sample loading onto the precolumn, (3) properties of the solid sorbent phase, (4) precolumn longevity, (5) cost of operation, (6) whether back-flushing of the precolumn is required, (7) type of analytical column and (8) minimum detectable concentrations. Seven of the eight pesticides were carbamate insecticides, herbicides or fungicides, chosen because they are of concern in Ontario environmental samples; the other pesticide was captan.

EXPERIMENTAL

Solvents

Acetonitrile was of HPLC grade from Fisher Scientific (Fairlawn, NJ, U.S.A.) and Caledon Labs. (Georgetown, Canada). Water used for the preparation of standards was distilled in glass in the laboratory.

Pesticides

Solid pesticide standards were obtained from the U.S. Environmental Protection Agency (EPA) (Research Triangle Park, NC, U.S.A.). Purities of the individual standards ranged from 97.5 to 100%. The pesticides, listed in the order in which they appear in the chromatograms, are (1), propoxur, (2) carbofuran, (3) carbaryl, (4) propham, (5) captan, (6) chlorpropham, (7) barban and (8) butylate.

Preparation of stock standard solutions

Solid standards were dissolved in acetonitrile and diluted in acetonitrile. These individual stock standard solutions were combined at different concentrations be-

cause of varying sensitivities to UV detection. The combined standard solution thus prepared was diluted with water to give standard water samples as below.

Water samples

Standard water samples were prepared by diluting 1 ml of the combined standard solution (prepared as above) to 1000 ml with distilled water from the laboratory unless indicated otherwise. The following types of water samples were investigated: two municipal tap waters, two distilled waters, three commercial HPLC-grade waters, two commercial spring drinking waters, one reverse osmosis water and one ion-exchange water.

Apparatus

The HPLC system consisted of a Model 510 pump, a Model 501 pump, a WISP Model 710B sample processor and a Model 484 tunable absorbance UV detector (all from Waters Assoc., Milford, MA, U.S.A.), a Fisher Recordall Series 5000 strip-chart recorder and a Digital Professional 350 computer system (Digital Equipment, Maynard, MA, U.S.A.) incorporating Waters Assoc. 840 chromatography software. A Waters Assoc. Model 600 Powerline solvent-delivery system was used in additional sample loading rate experiments.

Precolumns were 5- μm Spherisorb C₁₈ and C₈ 3 cm \times 4.6 mm I.D. cartridges from Brownlee Labs. (Santa Clara, CA, U.S.A.) and 3 cm \times 4.6 mm I.D. laboratory-packed with 10- μm Vydac Reverse Phase TP-201 (Separations Group, Hesperia, CA, U.S.A.), 10- μm Ultrasil ODS (Altex Scientific, Berkeley, CA, U.S.A.) and 40- μm Co-Pell ODS (Whatman, Clifton, NJ, U.S.A.). The analytical columns were a 5- μm Supelcosil LC-8 (25 cm \times 4.6 mm I.D.) (Supelco, Bellefonte, PA, U.S.A.) and a 5- μm Spherisorb C₁₈ (15 cm \times 4.6 mm I.D.) (Phenomenex, Torrance, CA, U.S.A.).

The on-line preconcentration apparatus (Fig. 1) incorporated two high-pressure in-line filters with 0.5- μm frits from Mandel Scientific (Guelph, Canada) and three Rheodyne (Cotati, CA, U.S.A.) Model 7000 two-position six-port switching valves, one of which was equipped with a Model 5701 air actuator controlled by a Model 7163 solenoid valve kit.

Operating conditions

The following conditions were used: wavelength, 220 nm; flow-rate, 1.5 ml/min; chart speed, 0.5 cm/min; detector sensitivity, 0.075 a.u.f.s. (1 mV = $1 \cdot 10^{-3}$ absorbance); recorder range, 10 mV full-scale and column temperature, ambient.

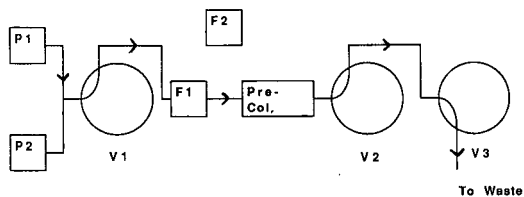
On-line preconcentration

A 100-ml volume of water sample was passed through the precolumn while the apparatus was in the 'load' position.

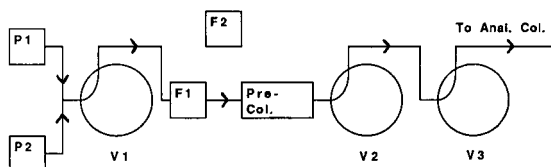
Elution

The following gradient program was run after switching the valves to the 'elute' position from the 'load' position, with elapsed time and composition of the acetonitrile-water mobile phase: initial, 30:70; 5 min, 30:70; 15 min, 60:40; 25 min, 60:40; 30 min, 30:70 and 35 min, 30:70. Changes in the percentage of acetonitrile throughout the gradient program occurred linearly. The final 10 min of the gradient program serve to return the system to the initial conditions to permit another analysis run.

SAMPLE LOAD



UNIDIRECTIONAL ELUTION



BACKFLUSH ELUTION

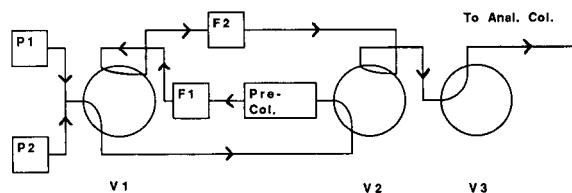


Fig. 1. Schematic diagram of the valve-switching system and the directions of liquid flow. V, P and F denote valves, pumps and filters, respectively; Anal. Col. = analytical column; Pre-Col. = precolumn. During the sample loading step, P1 dispenses sample. During the elution steps, P1 dispenses water and P2 dispenses acetonitrile as part of the mobile phase.

RESULTS AND DISCUSSION

The valving system employed in the on-line pre-concentration apparatus (Fig. 1) allows the application of the mobile phase to the precolumn in the same direction in which the sample was loaded (unidirectional elution), or in a direction opposite to that in which the sample was loaded (backflush elution). This makes the system more versatile than those employing only one high-pressure valve. Our studies revealed close similarities between unidirectional and backflush elutions. This is in sharp contrast to results obtained by straight injection of a concentrated stock solution (1000 times the concentration of the standard water samples used for this study) into the HPLC system (Fig. 2). The peak heights and shapes of the earlier eluting analytes are

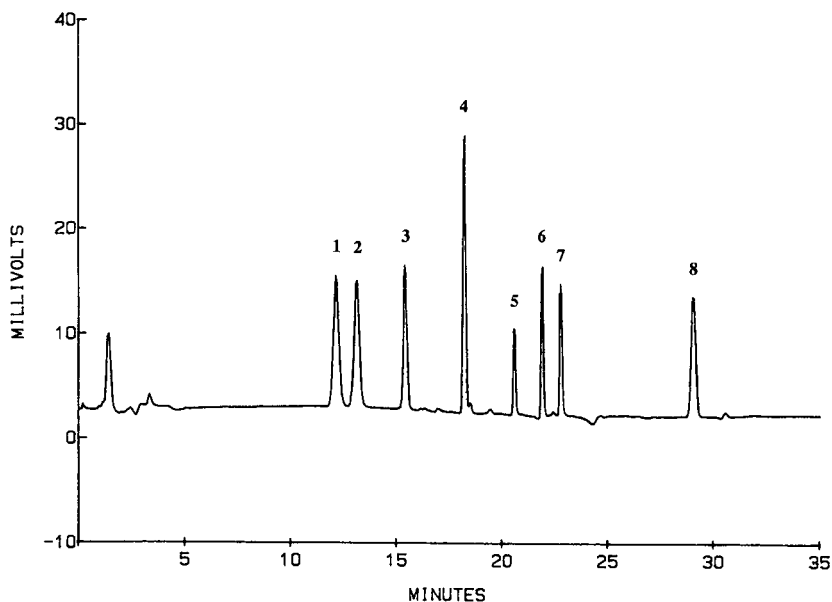


Fig. 2. Chromatogram resulting from a direct 150- μ l injection without the preconcentration procedure of a concentrated stock solution prepared in acetonitrile-water (30:70). Peak numbers as in Table I.

very different to those from the preconcentration sample runs. However, no difference was found in the average peak area counts by the two methods. Adsorption on and elution from the precolumn increases the peak sharpness for propoxur and carbofuran although the relative retention times for the two compounds are shifted closer together. A C_8 sorbent packing in the precolumn was also investigated as an alternative to the C_{18} packing. In contrast to the results obtained with the C_{18} packing, backflush elution improved the resolution between propoxur and carbofuran (Fig. 3). No difference was found in the average peak area counts when using the C_{18} or C_8 sorbent. In the developed method, a C_{18} sorbent was used and unidirectional elution was employed, as backflush elution offered no advantage when using a C_{18} sorbent. A C_{18} analytical column was also investigated but no improvement was found in the separation of the eight pesticides.

Table I gives the retention times of the eight pesticides, peak-area counts with their relative standard deviations (R.S.D.) from five replicate measurements at the concentrations listed and the minimum detectable concentrations. The minimum detectable concentrations were calculated based on a 100-ml sample using a 3:1 ratio of signal to baseline noise. The detection limit can be influenced by the number and concentration of co-eluting impurities in the sample matrix. The minimum detectable amounts can vary depending on the sample volume and concentration.

Fig. 4A shows a chromatogram for a distilled water sample with low concentration (one tenth of the concentrations listed in the sample concentration column in Table I) of the eight pesticides. At these concentrations, the peaks from the impurities in the sample matrix are roughly equal in height and area to those of the sample peaks. The reproducibility of the method is excellent, as evidenced by an average R.S.D. of *ca.* 2% for all of the compounds of interest. Background subtraction (as

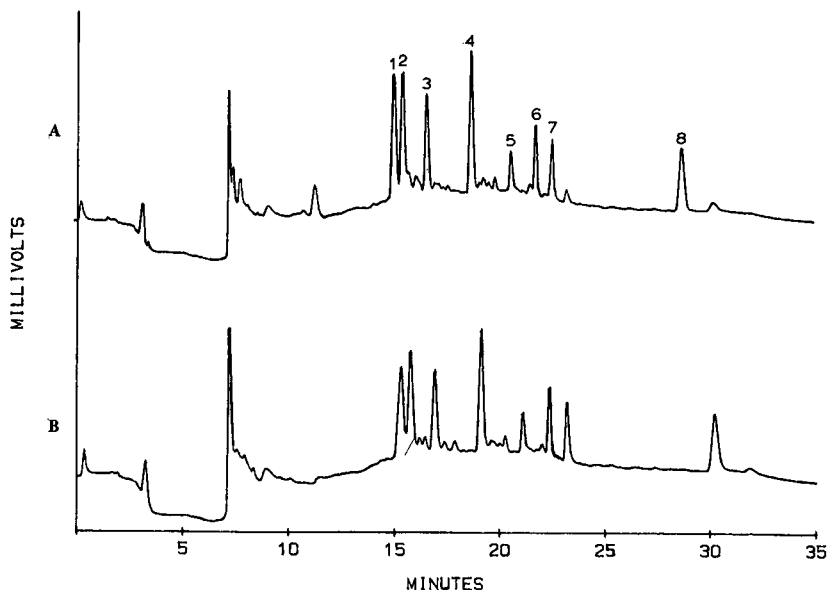


Fig. 3. Chromatograms showing the effect of (A) backflush elution and (B) unidirectional elution for a 5- μm C_8 precolumn. Each chromatogram is plotted at 90 mV. Peak numbers as in Table I.

shown in Fig. 4) would prove to be a valuable asset in the determination of analytes, but the absence of a blank for field samples makes this impossible. Baseline correction (gradient subtraction) could be used to improve the chromatogram profile but a solvent blank does not accurately duplicate the conditions to which the precolumn has been subjected.

Separation of the analytes when using a 40- μm sorbent is good but the peak areas for the first three eluting compounds (propoxur, carbofuran and carbaryl) are

TABLE I

SELECTED PESTICIDES, THEIR RETENTION TIMES, AVERAGE PEAK-AREA COUNTS \pm R.S.D. FROM FIVE REPLICATE MEASUREMENTS USING A 5- μm PRECOLUMN, SAMPLE CONCENTRATIONS AND MINIMUM DETECTABLE CONCENTRATIONS FOR A 100-ml SAMPLE

No. ^a	Compound	Retention time (min)	Peak area ($\times 10^3$)	Sample (10^{-9} g/ml)	Minimum detectable (10^{-12} g/ml)
1	Propoxur	16.00	598 \pm 3	3.84	65
2	Carbofuran	16.40	597 \pm 24	4.35	70
3	Carbaryl	17.35	377 \pm 7	0.42	10
4	Propham	19.25	580 \pm 12	3.17	50
5	Captan	21.10	164 \pm 6	9.70	460
6	Chloroprotham	22.25	242 \pm 6	0.98	30
7	Barban	23.00	252 \pm 5	1.08	40
8	Butylate	29.40	428 \pm 10	4.07	150

^a The pesticides are numbered to coincide with those in the figures.

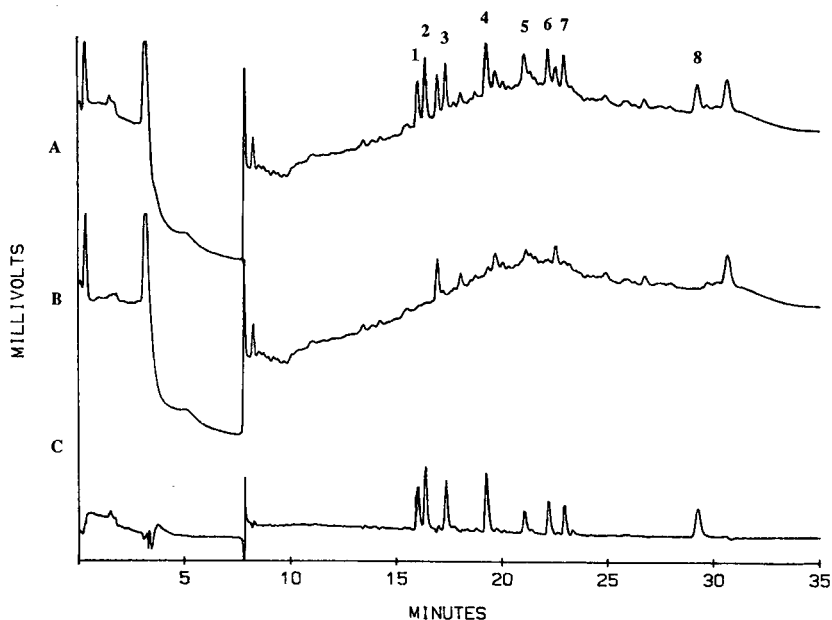


Fig. 4. Chromatograms corresponding to (A) a standard sample, (B) a distilled water blank and (C) chromatogram of A after subtracting B as a background. The samples were preconcentrated on a 10- μm Ultrasil ODS precolumn. The concentrations of the pesticides are one tenth those listed in Table I. Each chromatogram is plotted at 15 mV. Peak numbers as in Table I.

not as large as those of the 5- μm material. The peak areas with the 10- μm Ultrasil ODS sorbent were as large as those with the 5- μm sorbent except for propoxur and propham, whose peak areas were 65% and 75%, respectively, of those obtained with the 5- μm sorbent. The 5- μm material shows excellent retention of all eight analytes. From these results, it was concluded that the use of the 5- μm sorbent was most appropriate as no breakthrough of the early eluting pesticides was observed.

The results of the investigation of sample loading rate indicated no variation of retention of analytes under practical conditions. The flow-rates through the precolumns were increased in 1 ml/min increments from 3 to 6 ml/min for the 5- μm packing and from 3 to 7 ml/min for the 10- μm packing. In both instances the flow-rate did not significantly affect the retention of analytes by the precolumn. Investigation of higher flow-rates using the Model 501 single-head pump to determine the point of sample breakthrough was not possible owing to restrictions imposed by the high column back-pressures at flow-rates exceeding 6 ml/min for the 5- μm packing and 7 ml/min for the 10- μm packing. However, experiments with a dual-head pump (Model 600 Powerline) and a 5- μm precolumn showed that sample loading rates of 10 ml/min can be attained without breakthrough of any of the analytes. This result is in good agreement with those obtained by Goewie *et al.*²⁰ With the Model 501 pump, we judged that a sample loading rate of 5 ml/min with the 5- μm packing was most appropriate. Under these conditions, the total sample loading time for 100 ml is 20 min, which is adequate considering the subsequent 35-min chromatographic step. A completely automated procedure (including sample loading and analysis) takes approximately 60

min with the developed method. If the concentrations of carbamate residues are at least ten times those investigated in our study, or the detection limits achieved by conventional liquid-liquid extraction techniques are acceptable, then a sample size of only 5–10 ml is needed and the analysis time becomes much shorter. It is important to note that the sensitivity of the developed method when using 100 ml of sample is at least ten times greater than that of the method currently in use²¹.

The lifetime of the precolumn is an important economic consideration when making a choice between an SPE or an on-line preconcentration technique. Commercially available SPE cartridges are substantially cheaper (Canadian \$1.50–2.50) than 5- μm precolumns (Canadian \$60). However, in our study, one 5- μm precolumn stood up well to the analysis of at least thirty 100-ml water samples without showing any noticeable deterioration. The extent of deterioration was assessed by monitoring the resolution between propoxur and carbofuran and by monitoring the tailing of all analyte peaks. We judged that on a cost per analysis basis, the technique can compete with a method employing commercial SPE cartridges. The precolumn could be used substantially longer if only 10 ml or less of sample is used. The cost of operation of the method then becomes much lower.

The method was applied to the analysis of several kinds of water samples. Chromatograms of these water samples are shown in Fig. 5. Each water sample showed several peaks but they are all essentially unique for individual samples. The tap water samples are prone to huge peaks early in the chromatogram from early eluting impurities but the baseline is sufficiently stable after 15 min to allow for accurate determination of analytes.

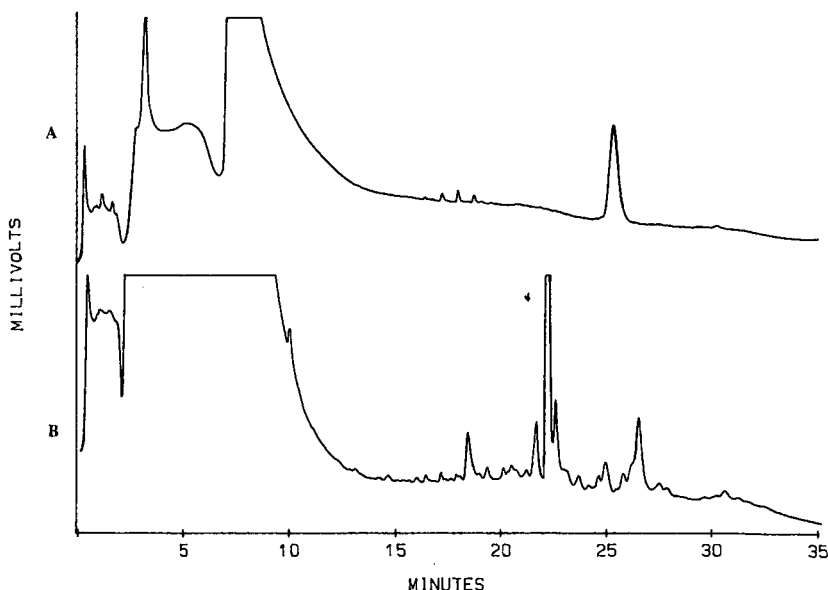


Fig. 5. Chromatograms of two commercial bottled spring waters, (A) a Canadian product and (B) a European product. Chromatograms are plotted at 40 mV. None of the above peaks corresponds to pesticides of interest in this study.

TABLE II
AVERAGE PEAK-AREA COUNTS OVER THREE ORDERS OF CONCENTRATION

<i>Pesticide</i>	<i>0.1 ppb^a</i> ($\times 10^2$)	<i>1 ppb</i> ($\times 10^3$)	<i>10 ppb</i> ($\times 10^4$)
Propuxur	600	598	618
Carbofuran	620	597	580
Carbaryl	400	377	397
Propham	520	580	553
Captan	175	164	162
Chloroprotham	300	242	263
Barban	270	252	230
Butylate	400	428	459

^a The American billion (10^9) is meant.

The method of determination of analytes that was originally followed was to calibrate the instrument by four injections of increasing volume of a concentrated stock solution without employing the preconcentration procedure, and subsequently comparing the peak areas. This approach, however, was found to be unacceptable. As demonstrated in Figs. 2 and 3, the peak shapes are substantially different although by area integration all compounds showed quantitative relationships. Because of this difference, three concentrations of standard solutions were prepared (for most of the analytes at 0.1, 1.0 and 10 ppb) and the resulting peak areas were calculated by using the developed method. Because the response of the compounds was linear (Table II), it was concluded that the peak-area counts from the preconcentration of the 1 ppb standard were adequate for daily calibration.

If a solvent delivery system with a three-solvent capability (*e.g.*, the Waters 600E Multisolvent Delivery System) is incorporated in the system that we used, the method lends itself easily to complete automation for a single analysis. This is achieved by computer software control which permits switching of the valving system from the sample load position to the elute position without manual manipulation. By the addition of a simple rotary switching device, the method could be automated for the analysis of many samples.

The lowest detectable concentrations given in the text could be improved by increasing the sample size, but this would also increase the time of analysis. Analysis time, sample loading rate and detection limit are all dependent on each other and must be selected according to the purpose of the analysis. The technique developed in this study is applicable to all sample matrices investigated.

CONCLUSION

The proposed method is simple, rapid, accurate, economical and reproducible. All of the sample can be injected into the HPLC system for analysis. The method also offers the possibility of complete automation for the analysis of many samples.

ACKNOWLEDGEMENTS

The authors thank the Research and Technology Branch of the Ontario Ministry of the Environment for financial support.

REFERENCES

- 1 G. A. Junk and J. J. Richard, *Anal. Chem.*, 60 (1988) 451.
- 2 E. Chladek and R. S. Maranaro, *J. Chromatogr. Sci.*, 22 (1984) 313.
- 3 A. W. Wolkoff and C. Creed, *J. Liq. Chromatogr.*, 4(8) (1981) 1459.
- 4 R. J. Bushway, *J. Chromatogr.*, 211 (1981) 135.
- 5 R. J. Kuhr and H. W. Dorough, *Carbamate Insecticides: Chemistry, Biochemistry and Toxicology*, CRC Press, Cleveland, OH, 1976.
- 6 J. N. Seiber, *J. Agric. Food Chem.*, 20 (1972) 443.
- 7 S. Lau and R. L. Marxmiller, *J. Agric. Food Chem.*, 18 (1970) 413.
- 8 J. E. Fahey, M. C. Wilson and E. J. Armbrust, *J. Econ. Entomol.*, 63 (1970) 589.
- 9 M. Chiba, *J. Agric. Food Chem.*, 29 (1981) 118-131.
- 10 W. Thornburg, *Anal. Chem.*, 43 (1971) 145R.
- 11 J. H. Ruzicka, *Pestic. Sci.*, 4 (1973) 417.
- 12 R. J. Argauer, H. Shimanuki and C. C. Aivarez, *J. Agric. Food Chem.*, 18 (1970) 688.
- 13 R. J. Argauer and W. Bontoyan, *J. Assoc. Off. Anal. Chem.*, 53 (1970) 1166.
- 14 R. O. Mümma and S. Khalifa, *J. Agric. Food Chem.*, 20 (1972) 1090.
- 15 J. A. Durden and W. J. Bartley, *J. Agric. Food Chem.*, 19 (1971) 441.
- 16 M. C. Harvey and S. D. Stearns, in J. F. Lawrence (Editor), *Liquid Chromatography in Environmental Analysis*, Humana Press, Clifton, NJ, 1984, Ch. 7 pp. 332-338.
- 17 J. J. Kirkland, *Analyst (London)*, 99 (1974) 1859.
- 18 J. N. Little and G. J. Fallick, *J. Chromatogr.*, 112 (1975) 389.
- 19 C. F. Poole and S. A. Schuette, *Contemporary Practice of Chromatography*, Elsevier, New York, 1984, pp. 461-462.
- 20 C. E. Goewie, W. F. Nielen, R. W. Frei and U. A. Th. Brinkman, *J. Chromatogr.*, 301 (1984) 325.
- 21 *Method PWACAR-W04A10, Determination of Carbamates in Water by HPLC*, Ontario Ministry of the Environment, Rexdale, 1988.
- 22 *EPA/600/4-85/054*, USEPA, EMSL, Cincinnati, OH.

High-performance liquid chromatographic determination of selected amino acids in rat brain by precolumn derivatization with phenylisothiocyanate

SONNY GUNAWAN, NANCY Y. WALTON and DAVID M. TREIMAN*

*Neurology and Research Services, Veterans Administration Medical Center, Los Angeles, CA 90073 (U.S.A.) and *Department of Neurology, Reed Neurological Research Center, UCLA School of Medicine, Los Angeles, CA 90024 (U.S.A.)*

(First received July 6th, 1989; revised manuscript received October 4th, 1989)

SUMMARY

We describe here a simple, sensitive, selective and reproducible assay method for quantitative determination of aspartate, glutamate, serine, glutamine, glycine and γ -aminobutyric acid in rat brain using reversed-phase high-performance liquid chromatography. The method is based upon formation of phenylthiocarbonyl derivatives of the amino acids. Good resolution of the six amino acids and the internal standard norvaline is achieved within 40 min. Other amino acids which have been reported to be present in rat brain do not interfere with the analysis. Standard curves for each of the amino acids exhibited good linearity ($r > 0.9993$) over the range 0.5–20 nmol. The coefficient of variation for the intra-day and inter-day determinations ranged from 0.4% at the highest to 11% at the lowest concentration limit. Storage of whole brains at -0°C for up to 8 weeks did not affect mean concentrations of the six amino acids.

INTRODUCTION

The role of amino acids in mammalian central nervous system synaptic transmission is an area of increasing scientific interest. γ -Aminobutyric acid (GABA) has been shown to be the primary inhibitory neurotransmitter in the mammalian brain, while glutamate and aspartate have excitatory actions at many sites^{1–3}. Glycine acts as an inhibitory transmitter in the spinal cord, but in brain it facilitates excitation arising from N-methyl-D-aspartate receptor activity⁴. Glutamine, while not thought to play any direct role in synaptic transmission, is a precursor of both glutamate and GABA. As investigations into these amino acids have increased, so too has interest in means of assaying their concentrations in physiological samples.

Automated amino acid analysis based on separation with sulfonated cation-exchange resins, postcolumn derivatization with ninhydrin and colorimetric detec-

tion⁵ has been widely used for over 20 years. A need for expensive dedicated equipment, long assay times and large sample volumes have led investigators to search for other amino acid assay methods.

Heinrikson and Meredith⁶ introduced a liquid chromatographic method for the separation and quantification of several amino acids after precolumn derivatization with phenylisothiocyanate (PITC). This method has been used for the analysis of primary and secondary amino acids in protein hydrolysates^{7,8} and for the determination of asparagine and glutamine in physiological fluids and cells⁹. However, aspartate, glutamate, serine, glutamine, glycine and GABA in rat brain extracts cannot be separated adequately when using methods described for protein hydrolysates^{7,8}. In another method based on PITC derivatization, the running time necessary to achieve separation was 80 min⁹.

This paper describes an analytical assay method for the quantitative determination of aspartate, glutamate, serine, glutamine, glycine and GABA in rat brain using precolumn derivatization with PITC and separation by reversed-phase high-performance liquid chromatography (HPLC). We developed this assay method to study changes in amino acid neurotransmitter concentrations in rat brain during experimental status epilepticus¹⁰.

EXPERIMENTAL

Materials

Amino acid and PITC were purchased from Pierce (Rockford, IL, U.S.A.). Triethylamine was obtained from Aldrich (Milwaukee, WI, U.S.A.). Glacial acetic acid was purchased from Fisher (Fairlawn, NJ, U.S.A.), sodium acetate trihydrate from Sigma (St. Louis, MO, U.S.A.) and ethanol from EM Science (Cherry Hill, NJ, U.S.A.). Acetonitrile (HPLC grade) was purchased from Mallinckrodt (Paris, KY, U.S.A.) and HPLC-grade water was obtained using a Nanopure reagent-grade water system from Barnstead (Boston, MA, U.S.A.).

Preparation of standard solutions

Aspartate, glutamate, serine, glutamine, glycine, taurine and GABA (0.5 mM each) were dissolved in 0.1 M hydrochloric acid and stored at 4°C for no longer than 1 week. The internal standard, norvaline (1 mM), was dissolved in 0.1 M hydrochloric acid and stored at 4°C for no more than 3 months. Norvaline was chosen as the internal standard because it is less hydrophilic than most other amino acids and, therefore, elutes late enough not to interfere with the endogenous amino acids in the brain.

Solvent A was 0.1 M sodium acetate buffer (pH 5.7) prepared by adding 13.61 g of sodium acetate trihydrate to 1 l of water, followed by 0.5 ml of triethylamine, 0.7 ml of glacial acetic acid and 5.0 ml of acetonitrile. Solvent B was acetonitrile–water (60:40).

Animal procedure and sample preparation

Male Sprague–Dawley rats (130–170 g) were decapitated. The brains were rapidly removed and frozen in acetone and dry ice (interval from decapitation to freezing averaged 60.7 s with a standard deviation of 17.1 s). Brains were weighed and homogenized in cold 80% ethanol (18 ml/g brain weight). Homogenization was

carried out in glass tissue grinders (Corning Pyrex No. 7725, New York, NY, U.S.A.), using a power drive for 5 min. The homogenate was centrifuged at 15 000 g for 15 min at 4°C. The supernatant was transferred to a glass culture tube and stored on ice. The pellet was rehomogenized and centrifuged as before. The combined supernatants from both extractions were vortexed thoroughly and stored at 4°C overnight. Supernatant samples of 50 µl were derivatized and assayed after extraction as described in the next section.

To study the stability of brain amino acids, whole brains, extraction supernatants and phenylthiocarbonyl (PTC) derivatives were stored at -70°C for 0, 1, 2, 4 and 8 weeks before assay. Six brains were stored for each of the stated times, then extracted, derivatized and assayed. Six brains were immediately extracted and the extraction supernatant was divided into five aliquots for storage for the stated times. Six brains were immediately extracted and six 50-µl aliquots of each were derivatized, with assay following storage for the stated times.

Derivatization of brain extract and standard curves

The internal standard, norvaline (5 nmol), was added to 50 µl of brain extract in a 75 × 10 mm borosilicate test tube and dried under vacuum. The residue was dissolved in 20 µl of ethanol-water-triethylamine (2:2:1) and evaporated to dryness under vacuum. A 30-µl volume of ethanol-water-triethylamine-PITC (7:1:1:1) was added to the residue and allowed to react for 20 min at room temperature to form the PTC derivatives of the amino acids⁷. Excess reagent was then removed under vacuum. For injection into the chromatograph, the PTC amino acid derivatives were dissolved in 300 µl of solvent A.

Standard curves for aspartate, glutamate, serine, glutamine, glycine and GABA were determined in a similar manner using mixtures of amino acids in six different amounts (0.5, 1, 2, 5, 10 and 20 nmol). The concentration of individual amino acids in brain samples was determined from the standard curve by calculating the ratio of the peak area of each amino acid to that of the internal standard.

Apparatus and chromatographic conditions

An Altex (Berkeley, CA, U.S.A.) HPLC system which consisted of two Model 110A pumps, a Model 421 controller and a Shimadzu (Columbia, MD, U.S.A.) Model C-R6A integrator was used. Absorbance was monitored with a Gilson (Middleton, WI, U.S.A.) Model 116 variable-wavelength detector at 254 nm, with sensitivity set at 0.1 a.u.f.s. A Rheodyne (Cotati, CA, U.S.A.) 7125 valve with a 20-µl loop was used for injection. The separation was carried out in a reversed-phase system with a Rainin (Emeryville, CA, U.S.A.) Dynamax C₁₈ Microsorb column as the stationary phase (250 × 4.6 mm I.D., particle size 5 µm) and a mobile phase gradient system modified from Cohen *et al.*⁸ and described in Table I. The flow-rate of the mobile phase was 0.6 ml/min. A total running time of 60 min is needed between sample injections to allow the system to equilibrate adequately.

RESULTS

Separation of selected amino acids

Fig. 1 shows a typical chromatogram of a standard mixture containing 5 nmol each of aspartate, glutamate, serine, glutamine, glycine, taurine and GABA after

TABLE I
GRADIENT PROGRAM FOR PTC AMINO ACID ANALYSIS

Time (min)	Solvent A (%)	Solvent B (%)
0.0	100	0
2.0	85	15
8.0	85	15
12.0	75	25
20.0	75	25
24.0	55	45
32.0	55	45
37.0	0	100
42.0	0	100
43.0	100	0
60.0	100	0

derivatization with PITC. Fig. 2 shows a chromatogram of a PTC-derivatized sample formed from 50 μ l of rat brain extract. In both cases 5 nmol norvaline were added to the samples prior to derivatization with PITC. As can be seen from the chromatograms, good resolution of the six amino acids and the internal standard was achieved in less than 40 min. The standard curves for each of the six amino acids exhibited good linearity over the range 0.5–20 nmol. The resulting correlation coefficients ranged from 0.9993 (glycine) to 0.9999 (GABA). Each standard concentration mixture was assayed five times on the same day. Precision between days was determined from standards that were derivatized and assayed on five separate days. The coefficient of variation ranged from 0.4 to 11.1% for within-day and from 1.5 to 11.0% for between-day peak-area ratio determinations. Table II shows the precision for within-day and between-day determinations of peak-area ratios in samples containing 0.5 or 20 nmol of amino acid standards. When peak area was used, the coefficient of variation (C.V.) for the within-day and between-day determinations ranged from 13.7 to 27.8% and 10.8 to 19.4%, respectively.

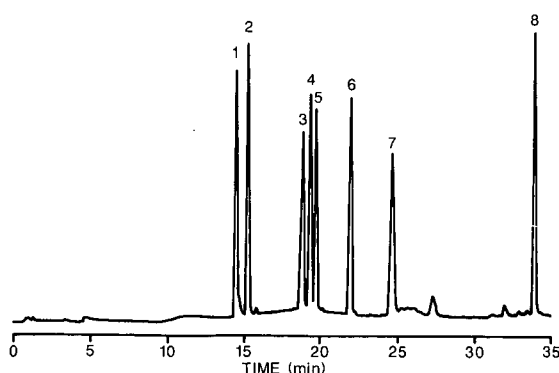


Fig. 1. Chromatographic separation of an amino acid standard mixture after derivatization with PITC. Peaks: 1 = aspartate; 2 = glutamate; 3 = serine; 4 = glutamine; 5 = glycine; 6 = taurine; 7 = GABA; 8 = norvaline. Each peak represents 5 nmol of compound.

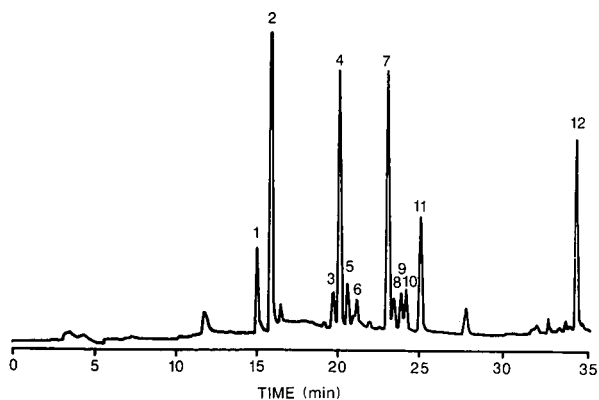


Fig. 2. Chromatographic separation of amino acids obtained from rat brain after extraction with 80% ethanol and derivatization with PITC. Norvaline (5 nmol) was added as internal standard. Peaks: 1 = aspartate; 2 = glutamate; 3 = serine; 4 = glutamine; 5 = glycine; 6 = glycerophosphoethanolamine; 7 = histidine and taurine; 8 = glutathione; 9 = threonine and proline; 10 = alanine and arginine; 11 = GABA; 12 = norvaline.

Interference

Interference studies were performed using other amino acids found in rat brain¹¹ plus cysteine, urea and ammonia.

Fig. 3 shows a chromatogram of 31 compounds after derivatization with PITC. A complete separation of all compounds was not attempted, but none of the compounds exhibited interference with aspartate, glutamate, serine, glutamine and glycine. Ammonia did not form a detectable PTC derivative. Histidine coeluted with taurine. Phosphoethanolamine formed a broad peak which eluted together with taurine, histidine, glutathione, threonine and proline. Methionine and cystathionine were not baseline-resolved from the internal standard and homocarnosine eluted closely to GABA. However, the concentrations of methionine, cystathionine and homocarnosine in rat brain are sufficiently low¹¹ so that interference which might be caused by these amino acids would be negligible. We confirmed this assumption by a separate experiment, in which two 50- μ l aliquots from the same rat brain extract sample were prepared and derivatized with PITC, one without (Fig. 4A) and one with (Fig. 4B) the addition of 5 nmol norvaline as the internal standard. Methionine and cystathionine were present in negligible amounts in the sample without norvaline. Fig. 5 shows two chromatograms obtained from rat brain extract, one without (Fig. 5A) and one with (Fig. 5B) the addition of 5 nmol homocarnosine. It can be seen that homocarnosine did not interfere with GABA and formed a negligible peak in the sample to which additional homocarnosine was not added.

Stability studies

Stability of amino acid concentrations when brain, extraction supernatant or PTC derivatives were stored at -70°C for up to 8 weeks was analyzed by least-squares analysis of variance (using a repeated measures design for extraction supernatant and PTC derivatives). When whole brains were stored, no statistically significant concentration differences were found secondary to storage time for the six selected

TABLE II
WITHIN-DAY AND BETWEEN-DAY PRECISION OF THE AMINO ACID ASSAY

Amino acid	Within-day precision			Between-day precision		
	Amount (nmol)	Mean peak-area ratio ^a	C.V. (%)	Amount (nmol)	Mean peak-area ratio ^a	C.V. (%)
Aspartate	0.5	0.07	11.1	0.5	0.06	11.0
	20.0	3.43	0.8	20.0	3.46	4.2
Glutamate	0.5	0.06	7.4	0.5	0.07	3.2
	20.0	3.47	0.5	20.0	3.54	5.4
Serine	0.5	0.07	2.1	0.5	0.06	4.3
	20.0	3.48	0.4	20.0	3.49	4.1
Glutamine	0.5	0.07	2.9	0.5	0.07	6.4
	20.0	3.61	0.5	20.0	3.62	1.5
Glycine	0.5	0.07	3.0	0.5	0.07	10.1
	20.0	3.71	0.6	20.0	3.77	5.2
GABA	0.5	0.07	5.1	0.5	0.07	9.5
	20.0	3.58	1.5	20.0	3.50	4.2

^a Defined as the ratio of amino acid peak area to that of the internal standard, norvaline. Each value is the mean of five assays.

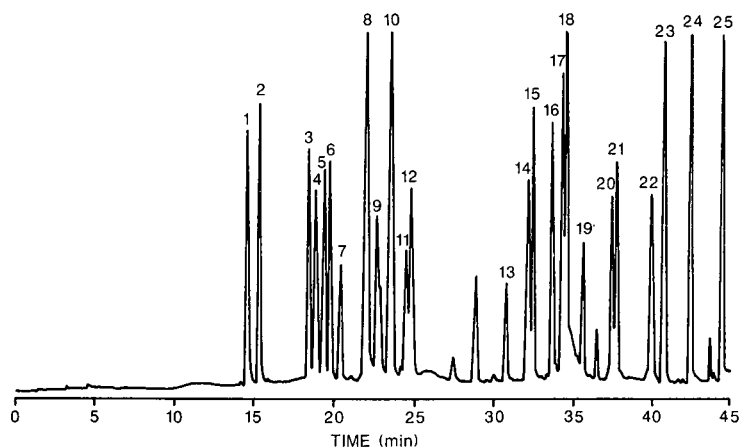


Fig. 3. Chromatogram of 31 amino acids and organic compounds found in rat brain after derivatization with PITC (5 nmol of each compound was used). Peaks: 1 = aspartate; 2 = glutamate; 3 = asparagine; 4 = serine; 5 = glutamine; 6 = glycine; 7 = glycerophosphoethanolamine; 8 = histidine and taurine; 9 = glutathione, threonine and proline; 10 = arginine and alanine; 11 = homocarnosine; 12 = GABA; 13 = hypotaurine; 14 = ethanolamine; 15 = tyrosine; 16 = valine; 17 = norvaline (internal standard); 18 = methionine and cystathionine; 19 = cysteine; 20 = isoleucine; 21 = leucine; 22 = phenylalanine; 23 = ornithine; 24 = lysine; 25 = urea. Phosphoethanolamine formed a broad peak and coeluted with taurine, histidine, glutathione, threonine and proline. Identities of unnumbered peaks is unknown.

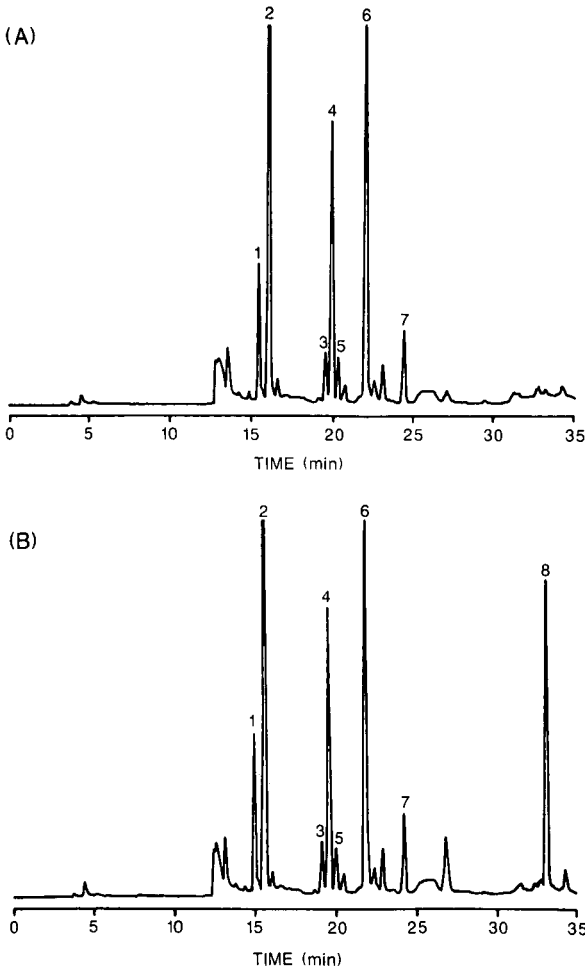


Fig. 4. Chromatograms obtained from rat brain extract after derivatization with PITC, one without (A) and one with (B) the addition of 5 nmol norvaline as internal standard. Peaks: 1 = aspartate; 2 = glutamate; 3 = serine; 4 = glutamine; 5 = glycine; 6 = histidine and taurine; 7 = GABA; 8 = norvaline.

amino acids ($p > 0.05$ in all cases). These results are shown graphically in Fig. 6. Stability was poorer when PTC derivatives or extraction supernatants were stored. Serine increased significantly when PTC derivatives were stored while glutamine decreased ($p < 0.05$). Aspartate and GABA rose significantly during storage of extraction supernatant ($p < 0.001$ and 0.05 , respectively), while glycine decreased ($p < 0.05$).

The mean amino acid concentrations found in the brains of the combined control (no storage) groups are presented in Table III.

DISCUSSION

Concentrations of amino acids in rat brain determined by the method described

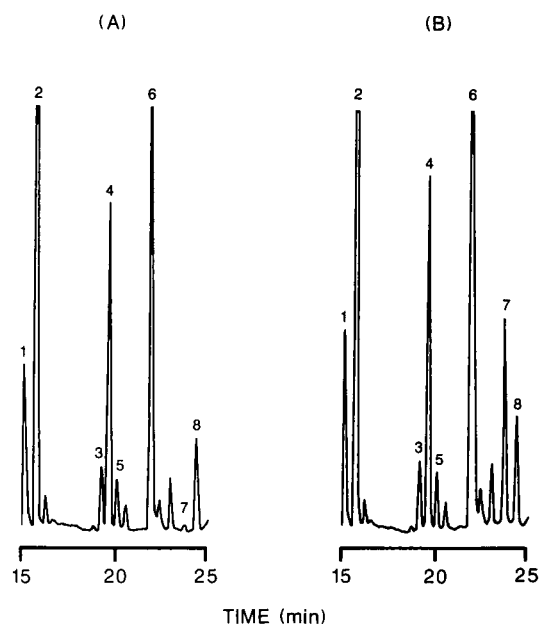


Fig. 5. Chromatograms obtained from rat brain extract after derivatization with PITC, one without (A) and one with (B) the addition of 5 nmol homocarnosine. Peaks: 1 = aspartate; 2 = glutamate; 3 = serine; 4 = glutamine; 5 = glycine; 6 = histidine and taurine; 7 = homocarnosine; 8 = GABA.

here were similar to values which have been reported by other method, including automated ion-exchange analysis and HPLC using other precolumn derivatization techniques. Table III shows how similar mean amino acid concentrations in rat brain determined by our method are compared to the classical technique using postcolumn derivatization with ninhydrin in an amino acid analyzer^{11,12}. In Table IV amino acid concentrations in rat hippocampus are compared with reports from the literature using other derivatization methods. Results using our method of PITC derivatization¹⁰ are similar and comparable to those obtained by HPLC methods using other precolumn derivatization techniques^{13,14}. It is difficult to compare results across experiments because, in addition to differences in analytical technique, variation in anatomic sample definition, sample preparation and species used can also change brain amino acid concentrations.

We believe our methodology has several advantages. The equipment required is relatively inexpensive and can be used for numerous other analytical procedures besides amino acid analysis. The derivatization is rapid and simple. Since the coupling reagent and solvent are volatile and readily removed by evaporation under reduced pressure, interference from reagent peaks is minimized. By employing a UV-absorbing rather than a fluorescence-active coupling reagent the instability as well as quantification difficulties which are associated with these derivatives is avoided.

Histidine and phosphoethanolamine elute closely enough to taurine that separation is not possible using this method. However, by changing the triethylamine concentration¹⁵ or altering the pH of the buffer used, it may be possible to optimize the system with regard to quantification of taurine or other amino acids which may be of

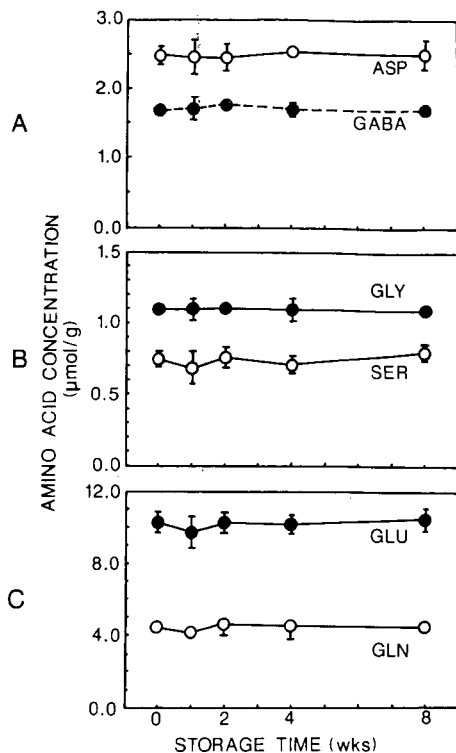


Fig. 6. Amino acid concentrations following storage of rat brains at -70°C prior to extraction, derivatization and assay. Each point is the mean of six brains \pm standard deviation.

interest. Although methionine and cystathionine may interfere with norvaline (see Fig. 3), their concentrations in rat brain, as reported by Perry *et al.*¹¹, are too low to interfere significantly. This is supported by the two chromatograms shown in Fig. 4. By using a relatively high concentration of the internal standard, norvaline (5 nmol), interference from methionine and cystathionine became negligible. None of the other amino acids reported to be present in rat brain, or urea or ammonia, interferes with the amino acid analysis described here.

Although Henrikson and Meredith⁶ and Bidlingmeyer *et al.*⁷ reported that PTC derivatives of protein hydrolysates are stable when stored dry and frozen, we found only intact rat brain (but not brain extracts or PTC derivatives) to be stable during storage at -70°C . Biological samples may include compounds which reduce stability when stored.

The methodology described here provides a relatively simple, rapid and inexpensive method for study of changes in brain amino acid levels associated with experimental variables of interest to the investigator. As is true with any analytical method applied to physiological problems, care in design of experiments is required to tease effects of interest out of the normal variability found in physiological samples.

TABLE III

CONCENTRATIONS OF SELECTED AMINO ACIDS IN RAT BRAIN AFTER DERIVATIZATION WITH PITC COMPARED TO METHODS USING NINHYDRIN WITH AMINO ACID ANALYZER

Amino acid	Concentration (mean \pm standard error of the mean) ($\mu\text{mol/g}$ brain)		
	PITC (n=18)	Ninhydrin ¹¹ (n=7)	Ninhydrin ¹² (n=4)
Aspartate	2.42 \pm 0.04	2.60 \pm 0.13	3.73 \pm 0.13
Glutamate	10.42 \pm 0.14	11.29 \pm 0.37	9.77 \pm 0.22
Serine	0.73 \pm 0.02	0.84 \pm 0.03	1.12 \pm 0.05
Glutamine	4.51 \pm 0.07	4.51 \pm 0.15	3.91 \pm 0.26
Glycine	1.10 \pm 0.02	1.06 \pm 0.04	1.04 \pm 0.05
GABA	1.75 \pm 0.03	1.79 \pm 0.07	1.26 \pm 0.05

TABLE IV

CONCENTRATIONS OF SELECTED AMINO ACIDS IN RAT HIPPOCAMPUS AFTER VARIOUS PRECOLUMN DERIVATIZATION METHODS

Amino acid	Concentration (mean \pm standard error of the mean) ($\mu\text{mol/g}$ brain)		
	PITC ¹⁰ (n=6)	<i>o</i> -Phthalaldehyde ¹³ (n=8)	Dansyl chloride ¹⁴ (n=5)
Aspartate	1.98 \pm 0.10	1.28 \pm 0.06	3.89 \pm 0.40
Glutamate	9.23 \pm 0.35	7.36 \pm 0.21	11.33 \pm 0.63
Serine	0.96 \pm 0.07	—	—
Glutamine	3.85 \pm 0.12	3.92 \pm 0.17	4.64 \pm 0.60
Glycine	0.81 \pm 0.02	0.37 \pm 0.12	—
GABA	1.83 \pm 0.07	2.45 \pm 0.21	2.03 \pm 0.08

ACKNOWLEDGEMENTS

This study was supported by grants from the Veterans Administration and the Epilepsy Foundation of America. We thank Barry Cole and Emilia Dauway for excellent technical support in carrying out this study.

REFERENCES

- 1 E. Roberts, T. N. Chase and D. B. Tower, *GABA in Nervous System Function*, Raven Press, New York, 1976.
- 2 J. C. Watkins and R. H. Evans, *Ann. Rev. Pharmacol.*, 21 (1981) 165.
- 3 F. Fonnum, *J. Neurochem.*, 42 (1984) 1.
- 4 D. R. Curtis and J. C. Watkins, *J. Neurochem.*, 6 (1960) 117.
- 5 S. Moore, D. H. Spackman and W. H. Stein, *Anal. Chem.*, 30 (1958) 1185.
- 6 R. L. Henrikson and S. C. Meredith, *Anal. Biochem.*, 136 (1984) 65.
- 7 B. A. Bidlingmeyer, S. A. Cohen and T. L. Tarvin, *J. Chromatogr.*, 336 (1984) 93.
- 8 S. A. Cohen, T. L. Tarvin and B. A. Bidlingmeyer, *Am. Lab.*, August (1984) 48.

- 9 L. E. Lavi, J. S. Holcenberg, D. E. Cole and T. Jolivet, *J. Chromatogr.*, 377 (1986) 155.
- 10 N. Y. Walton, S. Gunawan and D. M. Treiman. *Exp. Neurol.*, in press.
- 11 T. L. Perry, S. Hansen and S. S. Gandham, *J. Neurochem.*, 36 (1981) 406.
- 12 A. Lajtha and J. Toth, *Brain Res.*, 76 (1974) 546.
- 13 A. H. Hikal, G. W. Lipe, W. Slikker Jr., A. C. Scallet, S. F. Ali and G. D. Newport, *Life Sci.*, 42 (1988) 2029.
- 14 E. Westerberg, A. G. Chapman and B. S. Meldrum, *J. Neurochem.*, 41 (1983) 1755.
- 15 R. F. Ebert, *Anal. Biochem.*, 154 (1986) 431.

Studies on the uptake of N-methylisoquinolinium ion into rat striatal slices using high-performance liquid chromatography with fluorimetric detection

Y. HIRATA* and M. MINAMI

Department of Hygiene and Public Health, Nippon Medical School, 1-1-5 Sendagi, Bunkyo-ku, Tokyo 113 (Japan)

and

M. NAOI and T. NAGATSU

Department of Biochemistry, Nagoya University School of Medicine, Nagoya 466 (Japan)

(First received February 20th, 1989; revised manuscript received August 22nd, 1989)

SUMMARY

A simple and sensitive procedure for the measurement of N-methylisoquinolinium ion (NMIQ⁺), a putative neurotoxin, was devised using high-performance liquid chromatography (HPLC) with fluorescence detection. Separation of NMIQ⁺ was carried out by gel filtration and reversed-phase HPLC on a column of hydrophilic polymer gels (Asahipak GS-302H). The method was sensitive enough to measure 50 fmol of NMIQ⁺. Uptake of NMIQ⁺ into rat striatal slices was confirmed by this method.

INTRODUCTION

N-Methyl-1,2,3,6-tetrahydropyridine (MPTP) induces the degeneration of dopaminergic neurons, especially in nigro-striatal pathways in humans^{1,2} and monkeys³, resulting in a syndrome similar to Parkinson's disease. MPTP is first oxidized to 1-methyl-4-phenylpyridinium ion (MPP⁺) by monoamine oxidase (MAO)⁴ and then taken up into dopaminergic neurons through the dopamine reuptake system⁵. Although the molecular basis of this toxicity to destroy the nigro-striatal system has not been well elucidated, the discovery of MPTP has led to extensive studies in attempts to find similar neurotoxic substances that produce parkinsonism.

We have already reported that MPTP and MPP⁺ inhibited tyrosine hydroxylation, the rate-limiting step of the biosynthesis of catecholamines, in rat striatal slices^{6,7}. In addition to MPP⁺, several pyridinium ions structurally related to MPP⁺ were found to inhibit tyrosine hydroxylation⁸. Among them, N-methylisoquinolinium ion (NMIQ⁺) was suggested to be a possible naturally produced neurotoxin that might

induce parkinsonism. Both NMIQ⁺ and MPP⁺ were found to inhibit monoamine oxidase⁹. Thus, NMIQ⁺ inhibits MAO-B non-competitively with respect to the amine substrate, whereas it inhibits MAO-A in competition with the substrate. On the other hand, the presence of tetrahydroisoquinoline as a novel endogenous amine in the rat brain and also in the brain of both normal and parkinsonian human subjects has recently been documented^{10,11}. In addition, the administration of tetrahydroisoquinoline to mice and marmosets resulted in decreases in dopamine, biopterin, tyrosine hydroxylase activity and/or 3,4-dihydroxyphenylacetic acid, a dopamine metabolite^{12,13}. These results led us to study the mechanism of toxicity of isoquinoline compounds.

Tetrahydroisoquinoline and its derivatives were identified by gas chromatography–mass spectrometry (GC–MS)^{10,11}. N-Methylated isoquinoline derivatives, however, could not be measured by these methods. In this paper, we describe a procedure for the determination of NMIQ⁺ in crude samples by use of high-performance liquid chromatography (HPLC) with fluorescence detection. Uptake to NMIQ⁺ into rat striatal slices was confirmed using this method.

EXPERIMENTAL

Material

N-Methylisoquinolinium iodide was prepared from isoquinoline and methyl iodide⁸.

Measurement of amount of NMIQ⁺ taken up into striatal slices

Rat striatal slices were prepared as described previously⁶. Briefly, male Wistar rats (200–300 g) were decapitated, and striata were immediately dissected and cut into slices (0.22 mm thick) on a McIlwain tissue chopper. The slices were washed extensively before use in Krebs–Ringer hydrogencarbonate medium composed of 118 mM NaCl, 4.7 mM KCl, 2.5 mM CaCl₂, 25 mM NaHCO₃, 0.1 mM MgSO₄, 1.4 mM KH₂PO₄ and 8 mM glucose. The medium was saturated with an atmosphere of O₂–CO₂ (95:5). Incubation was carried out at 37°C in 1 ml of Krebs–Ringer hydrogencarbonate medium. The uptake was terminated by the addition of 3 ml of ice-cold Krebs–Ringer hydrogencarbonate medium. After three consecutive washes with the same medium, the slices were homogenized with the medium by sonication and the protein was removed by adding perchloric acid (0.16 M final concentration). The mixture was centrifuged at 5000 g for 20 min at 4°C. The supernatant was filtered through a Chromatodisc 13A (0.45 μm) and an aliquot was injected into an HPLC apparatus (Hitachi L-6200) with a fluorimetric detector (Hitachi F-1100). The fluorescence intensity at 375 nm was measured by excitation at 225 nm. The column used for multi-mode determination (gel filtration and reversed-phase chromatography) was an Asahipak GS-320H (250 mm × 7.6 mm I.D.) (Asahi Chemical, Kanagawa, Japan). The sample was eluted with 0.1 M sodium phosphate buffer (pH 2.6) at a flow-rate of 1.0 ml/min at room temperature. The determination of the amount of NMIQ⁺ taken up was performed by comparison of the fluorescence intensity (peak height) with that of an external standard (NMIQ⁺), using a Shimadzu CR-1A Chromatopack integrator. The protein concentration was measured by the method of Bradford¹⁴ using bovine serum albumin as a standard.

RESULTS AND DISCUSSION

Fig. 1 shows excitation and emission spectra of NMIQ⁺. NMIQ⁺ had an excitation maximum at 225 nm and an emission maximum at 375 nm. Fig. 2 shows curves reflecting the relative fluorescence intensity at various pH with overlapping values. The fluorescence intensity was relatively constant over a wide pH range. With increasing pH of the phosphate buffer used for elution in HPLC on the GS-320H column, the elution volume of NMIQ⁺ was increased and the fluorescence intensity of NMIQ⁺ was decreased. Therefore, we used phosphate buffer of pH 2.6 for the determination of NMIQ⁺ by HPLC with fluorescence detection. Linearity of the concentration of NMIQ⁺ using HPLC was observed from 50 fmol to 1 pmol, as shown in Fig. 3. The limit of the sensitivity by this assay was 50 fmol taking a signal-to-noise ratio of 5.

As an application of this method, NMIQ⁺ was incubated with rat striatal slices and the amount of NMIQ⁺ taken up into striatal slices was determined. Fig. 4 shows typical HPLC patterns. Rat striatal slices were found to take up and accumulate NMIQ⁺ by a temperature-dependent mechanism. Further, the described procedure allows, after simple deproteinisation, the immediate determination of NMIQ⁺ in brain homogenates by HPLC. As shown in Fig. 4, no interference by other compounds was observed. Compared with most other HPLC systems for the determination of substances in the brain such as biogenic amines and amino acids, in which laborious

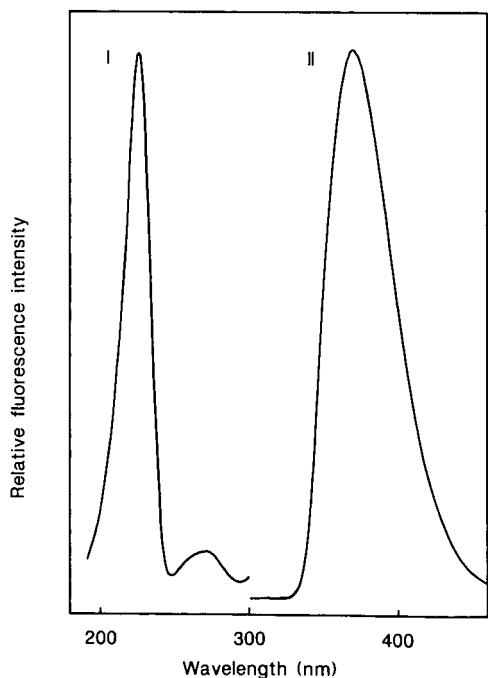


Fig. 1. Excitation and emission spectra of NMIQ⁺. The fluorescence spectra of NMIQ⁺ (10 μ M) were measured at room temperature. (I) Excitation spectrum of NMIQ⁺, measured at 375 nm emission wavelength; (II) emission spectrum of NMIQ⁺, measured by excitation at 225 nm.

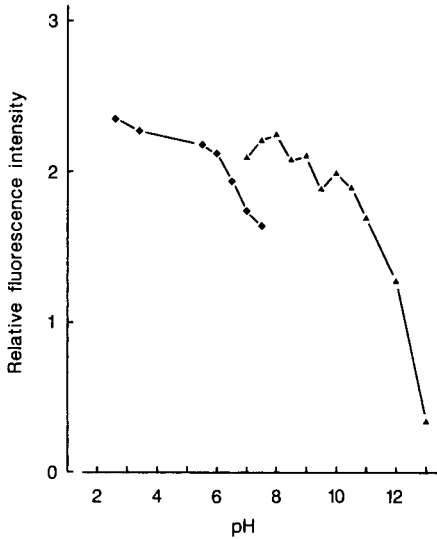


Fig. 2. Relationship between fluorescence intensity of NMIQ^+ and pH. The fluorescence intensity at 375 nm with excitation at 225 nm was measured in 0.1 M buffer. Sodium phosphate buffer was used from pH 2.6 to 7.7 and boric acid–sodium borate buffer from pH 7 to 13.

extraction and/or purification steps are essential before HPLC, the present study clearly shows that such pretreatment can be omitted with these chromatographic condition for NMIQ^+ . The recovery of NMIQ^+ added to rat brain homogenate was nearly 100%. The uptake was dependent on the amount of striatal slices (Fig. 5) and the reaction time. The uptake was linear up to 20 min at 37°C. The effect of reaction temperature was also examined. As shown in Fig. 6, the uptake increased in a temperature-dependent manner and reached the maximum at 27–37°C.

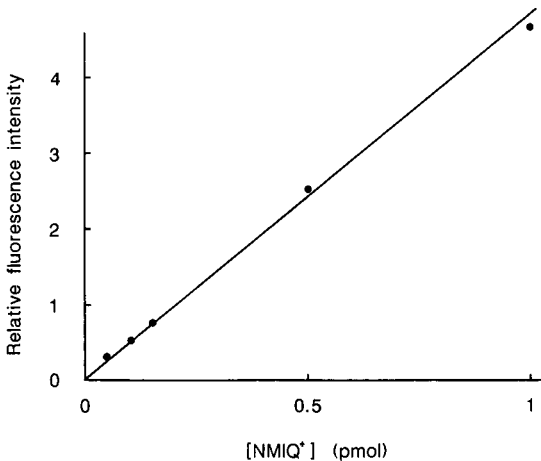


Fig. 3. Relationship between amount of NMIQ^+ and fluorescence intensity. The amounts of NMIQ^+ subjected to HPLC were plotted against the relative fluorescence intensity at 375 nm with excitation at 225 nm.

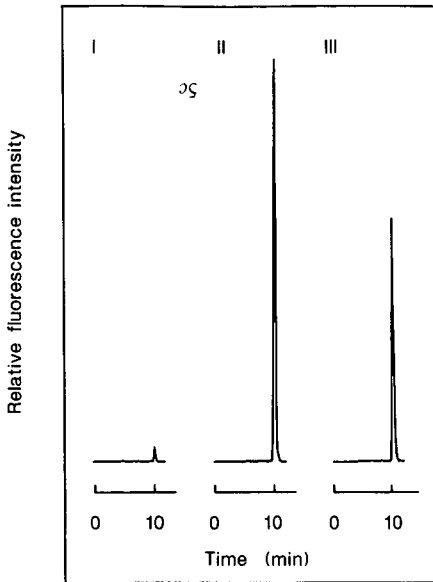


Fig. 4. High-performance liquid chromatograms of NMIQ⁺. (I) Rat striatal slices (0.9 mg protein) were incubated with NMIQ⁺ (5 nmol) for 1 h at 0°C; (II) rat striatal slices (1.0 mg protein) were incubated with NMIQ⁺ (5 nmol) for 1 h at 37°C, then analysed as described under Experimental; (III) NMIQ⁺ (5.3 pmol).

As reported previously, NMIQ⁺ inhibited tyrosine hydroxylation, the rate-limiting step of dopamine biosynthesis, in rat striatal slices at 10^{-6} – 10^{-3} M⁸. We determined the concentration of NMIQ⁺ that was taken up into striatal slices during the incubation under the same conditions. When striatal slices were incubated in the Krebs–Ringer hydrogencarbonate medium containing 10^{-6} – 10^{-3} M NMIQ⁺ for

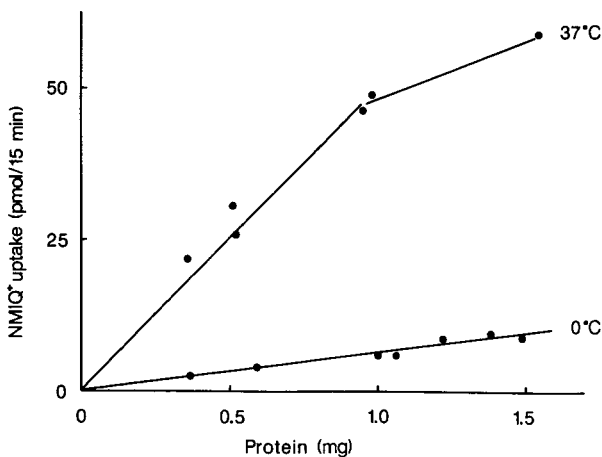


Fig. 5. Uptake of NMIQ⁺ in rat striatal slices. Slices were incubated for 15 min at 0 or 37°C in a Krebs–Ringer hydrogencarbonate medium containing $1 \mu\text{M}$ NMIQ⁺. The protein concentration in the slices is shown on the abscissa.

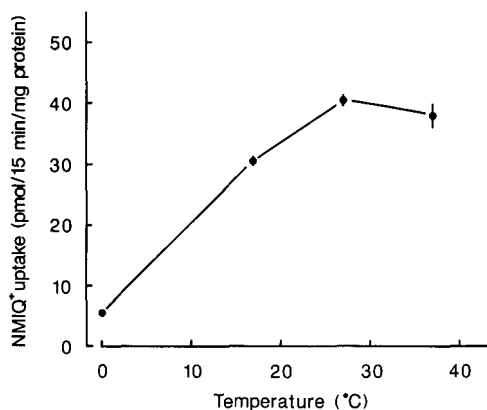


Fig. 6. Effect of temperature on NMIQ⁺ uptake in rat striatal slices. Slices were incubated for 15 min at 0, 17, 27 or 37°C in a Krebs-Ringer hydrogencarbonate medium containing 1 μ M NMIQ⁺. Each value is the mean \pm standard error of four experiments.

1 h at 37°C, NMIQ⁺ was taken up into striatal tissues as shown in Table I. The molarity in the tissue slices was also determined (Table I). The results suggest that NMIQ⁺ was concentrated in striatal slices to an extent 3–18 times higher than the concentration in the medium.

The effect of nomifensine, a selective inhibitor of dopamine uptake, was examined. The uptake of NMIQ⁺ from a 5 μ M solution was reduced in the presence of nomifensine (5 μ M). The NMIQ⁺ uptake (pmol/h \cdot mg protein) was 240.0 ± 4.7 , which was much lower than the control value of 502.1 ± 9.5 in the absence of nomifensine. The MPP⁺ uptake had been found to be mediated by the dopamine uptake system using mouse brain synaptosomes⁵. The present result also suggests that

TABLE I

EFFECT OF NMIQ⁺ CONCENTRATION IN THE INCUBATION MEDIUM ON DOPA FORMATION AND ON ITS UPTAKE INTO RAT STRIATAL SLICES

The slices were incubated for 1 h at 37°C.

NMIQ ⁺ (M)	DOPA formation ^a (% of control)	NMIQ ⁺ taken up	
		nmol/mg protein	μ M
0	100 \pm 2	0	
10 ⁻⁶	99 \pm 7	0.16 \pm 0.01	18
10 ⁻⁵	62 \pm 3 ^c	0.19 \pm 0.07	135
10 ⁻⁴	24 \pm 1 ^c	4.70 \pm 0.19	533
10 ⁻³	21 \pm 5 ^c	25.57 \pm 0.34	2905

^a Each value is the mean \pm standard error of four experiments; the control (100%) value was 778.4 \pm 18.9 pmol DOPA formed/h \cdot mg protein.

^b The molarity in the tissue slices was determined based on the assumption that 1 mg wet tissue weight was equivalent to 0.114 mg protein measured by the Bradford method using bovine serum albumin as a standard.

^c $P < 0.01$ for the difference from the control.

NMIQ⁺ is taken up into striatal slices by the dopamine uptake system. Furthermore, nomifensine at 5 μ M also prevented the inhibition of tyrosine hydroxylation caused by 5 μ M NMIQ⁺. These results suggest that NMIQ⁺ in addition to MPP⁺ is taken up into striatal dopamine neurons and then inhibits dopamine synthesis.

MPP⁺ inhibited tyrosine hydroxylation in rat striatal slices, as reported previously⁷. The concentration of MPP⁺ producing significant inhibition was lower than that of NMIQ⁺, and the maximum inhibition produced by MPP⁺ was greater than that caused by NMIQ⁺. This could be explained by the accumulation of NMIQ⁺ being less pronounced than that of MPP⁺. Thus, the previously related data on uptake systems were generated from the MPP⁺ neurotoxin using striatal synaptosomal preparations at nanomolar to micromolar concentrations^{5,15} whereas the concentrations used in this work were from micromolar to millimolar. MPTP is now the most potent neurotoxin to induce Parkinson's disease but the only known source of MPTP is artificial. The fact that NMIQ⁺ is taken up into dopaminergic neurons and inhibits dopamine synthesis supports the view that they may be naturally occurring neurotoxins involving the pathogenesis of parkinsonism and other neurodegenerative diseases of the central nervous system. Although NMIQ⁺ is a relative weak neurotoxin compared with MPP⁺, damage of dopaminergic neurons could be produced by a cumulative effect of exposure to minute quantities over many years.

The method reported here can be used for the determination of NMIQ⁺ in a small amount of crude sample. This procedure should have broad applications in biochemical and pharmacological studies on NMIQ⁺ toxicity.

REFERENCES

- 1 G. C. Davis, A. C. Williams, S. P. Markey, M. H. Ebert, E. D. Caine, E. D. Reicher and I. J. Kopin, *Psychiatr. Res.*, 1 (1979) 249–254.
- 2 J. W. Langston, P. Ballard, J. W. Tetrud and I. Irwin, *Science (Washington, D.C.)*, 219 (1983) 979–980.
- 3 R. S. Burns, C. C. Chiueh, S. P. Markey, M. H. Ebert, D. M. Jacobowitz and I. J. Kopin, *Proc. Natl. Acad. Sci. U.S.A.*, 80 (1983) 4546–4550.
- 4 K. Chiba, A. J. Trevor and N. Castagnoli, Jr., *Biochem. Biophys. Res. Commun.*, 120 (1984) 574–578.
- 5 K. Chiba, A. J. Trevor and N. Castagnoli, Jr., *Biochem. Biophys. Res. Commun.*, 128 (1985) 1228–1232.
- 6 Y. Hirata and T. Nagatsu, *Brain Res.*, 337 (1985) 193–196.
- 7 Y. Hirata and T. Nagatsu, *Neurosci. Lett.*, 57 (1985) 301–305.
- 8 Y. Hirata, H. Sugimura, H. Takei and T. Nagatsu, *Brain Res.*, 397 (1986) 341–344.
- 9 M. Naoi, Y. Hirata and T. Nagatsu, *J. Neurochem.*, 48 (1987) 709–712.
- 10 M. Kohno, S. Ohta and M. Hirobe, *Biochem. Biophys. Res. Commun.*, 140 (1986) 448–454.
- 11 T. Niwa, N. Takeda, N. Kaneda, Y. Hashizume and T. Nagatsu, *Biochem. Biophys. Res. Commun.*, 144 (1987) 1084–1089.
- 12 T. Nagatsu and Y. Hirata, *Eur. Neurol.*, 26, Suppl. 1 (1987) 11–15.
- 13 T. Nagatsu and M. Yoshida, *Neurosci. Lett.*, 87 (1988) 178–182.
- 14 M. M. Bradford, *Anal. Biochem.*, 72 (1976) 248–254.
- 15 J. A. Javitch, R. J. D'Amato, S. M. Strittmatter and S. H. Snyder, *Proc. Natl. Acad. Sci. U.S.A.*, 82 (1985) 2173–2177.

Chromatographic purification of glucose-6-phosphate dehydrogenase and lactate dehydrogenase from *Leuconostoc mesenteroides*^a

Z. GLATZ*, J. TOMANDL and O. JANICZEK

Department of Biochemistry, Purkynje University, Kotlářská 2, 611 37 Brno (Czechoslovakia)
and

A. MAREK

Research Institute of Pure Chemicals, Lachema, Karásek 28, 621 33 Brno (Czechoslovakia)

(First received February 9th, 1989; revised manuscript received November 2nd, 1989)

SUMMARY

A simple procedure for the simultaneous purification of glucose-6-phosphate dehydrogenase and lactate dehydrogenase from *Leuconostoc mesenteroides* is described. It involves ammonium sulphate precipitation, hydrophobic interaction chromatography and ion-exchange chromatography. The purity of the final fractions is checked by size-exclusion chromatography and by polyacrylamide gel electrophoresis in the presence of sodium dodecyl sulphate. The purified enzymes are suitable for enzymological studies and analytical biochemistry.

INTRODUCTION

Glucose-6-phosphate dehydrogenase (G6P-DH, E.C. 1.1.1.49) catalyses the first step in the pentose phosphate pathway, oxidizing glucose-6-phosphate with simultaneous reduction of NADP or NAD¹. Most glucose-6-phosphate dehydrogenases utilize only NADP as the sole coenzyme, but some *e.g.*, the enzyme from *Leuconostoc mesenteroides*, have the ability to use NAD in addition to NADP^{2,3}. The complete absence of cysteine in G6P-DH from *Leuconostoc mesenteroides*, which is unusual in dehydrogenases, is probably responsible for the excellent stability of this enzyme⁴. The resistance to inactivation under a variety of conditions and the dual nucleotide specificity have led to the widespread use of this enzyme in various clinical test kits as an indicator enzyme for the determination of several enzyme activities and for determining the concentrations of numerous metabolites⁵.

Several purification procedures for G6P-DH from *Leuconostoc mesenteroides* have been reported. Olive and Levy³ purified this enzyme by a procedure involving

^a Dedicated to the memory of Dr. J. Kovář (†1987).

precipitation with ammonium sulphate, treatment with protamine, ammonium sulphate fractionation, chromatography on hydroxyapatite followed by two crystallizations. Choi *et al.*⁶ reported a procedure for the purification of this enzyme by Cibacron Blue F3G-A-Sepharose and hydroxyapatite chromatography. More recently, a purification procedure involving tandem dye-ligand chromatography has been described⁷. Sixty-five immobilized triazine dyes were screened for their ability to purify G6P-DH. However, the best, Matrex Gel Purple A and Matrex Gel Orange B, used in this procedure as "negative" and "positive" adsorbents, respectively, are not commercially available.

In this paper, a rapid semi-preparative procedure for the isolation of G6P-DH from *Leuconostoc mesenteroides* using ammonium sulphate precipitation and two high-performance liquid chromatographic steps is described. In addition, the possibility of the simultaneous purification of NAD-dependent D-lactate dehydrogenase^{8,9}, which is present in considerable amounts in the sediment after ammonium sulphate precipitation, is discussed. This enzyme has already been purified by Garland¹⁰. In our procedure, the LDH is a sort of by-product, and a better yield of it could be obtained by easily modifying the procedure. This enzyme can also be used in analytical biochemistry for the determination of several enzyme activities and numerous metabolites⁵.

EXPERIMENTAL

Materials

Leuconostoc mesenteroides CCM 2083 (ATCC 12291) was obtained from the Czechoslovak Collection of Microorganisms (Brno, Czechoslovakia) and cultivated as described previously¹¹. Glucose-6-phosphate, glucose-1-phosphate, gluconate-6-phosphate, fructose-6-phosphate, sodium pyruvate, NAD and NADH were obtained from Boehringer (Mannheim, F.R.G.). The materials used for electrophoretic separation were mostly from Serva (Heidelberg, F.R.G.). The other chemicals (mostly from Lachema, Brno, Czechoslovakia) were of analytical-reagent grade.

Enzyme preparation

The cells (40 g wet weight) were suspended in 0.1 M sodium hydrogencarbonate solution (dilution 1:10) and then sonicated for 15 × 1 min in an ice-bath using a Dynatech (Fremingdale, NY, U.S.A.) sonic dismembrator. Cellular debris was separated by centrifugation at 20 000 g for 30 min. The crude cytosol was fractionated by ammonium sulphate precipitation. After removal of the first precipitate (60% saturation), most of G6P-DH and part of the LDH activities were salted out at 90% saturation. These initial procedures were carried out at 4°C and the subsequent chromatographic steps proceeded at room temperature, the eluted fractions being kept in an ice-bath.

The sediment was dissolved in 0.05 M sodium phosphate buffer (pH 7.4) containing 1.7 M ammonium sulphate and 1 mM EDTA and the enzymes were separated on a Phenyl-Superose HR 5/5 column (50 mm × 5 mm I.D.) from Pharmacia-LKB (Uppsala, Sweden) or on an HR 10/10 column (100 mm × 10 mm I.D.) packed with Spheron Micro 300 (12 μm) (Lachema). The columns were attached to a Pharmacia LKB fast protein liquid chromatography (FPLC) system consisting of

two P-500 pumps, an LCC-500 gradient programmer, a UV-1 monitor with an HR-10 cell, a FRAC-100 fraction collector and an REC-482 recorder. As starting and terminating buffers, 0.05 *M* sodium phosphate (pH 7.4) containing 1.7 *M* ammonium sulphate, 1 *mM* EDTA and 0.05 *M* sodium phosphate (pH 7.4) were used at flow-rates of 0.5 ml/min for the Phenyl-Superose column and 2 ml/min for the Spherul Micro 300 column. The samples were injected using a V-7 valve equipped with a 10-ml superloop (Pharmacia-LKB) or sample loops of various volumes. The fractions containing enzyme activities were pooled and concentrated with an Amicon (Danvers, MA, U.S.A.) ultrafiltration cell with a YM-10 membrane. The samples were desalted on an HR 10/10 fast desalting column (Pharmacia-LKB) and applied to a Mono Q HR 5/5 column from Pharmacia-LKB. The columns were attached to the above-mentioned chromatographic system. As starting and terminating buffers, 0.05 *M* sodium phosphate (pH 7.4) and the same buffer with 1 *M* sodium chloride, respectively, were used (flow-rate 1.0 ml/min).

Enzyme analysis

The activity of G6P-DH was determined spectrophotometrically in the presence of NAD and glucose-6-phosphate³, the activity of LDH in the presence of NADH and pyruvate⁸ and the activity of phosphogluconate dehydrogenase in the presence of NADP and gluconate-6-phosphate¹². The activities of NADH oxidase and NADPH oxidase were determined in the presence of NADH and NADPH, respectively¹³. The activities of phosphoglucomutase¹⁴ and phosphoglucose isomerase¹⁵ were determined by a coupling assay using G6P-DH as the indicator enzyme in the presence of glucose-1-phosphate and fructose-6-phosphate, respectively. The activities of alanine aminotransferase and creatine phosphokinase were detected by means of a Monotest (Boehringer). The temperature for all assays was 25°C. The protein concentration was calculated from the absorbance at 260 and 280 nm¹⁶. The spectrophotometric measurements were performed using a Cary 118 apparatus (Varian, Palo Alto, CA, U.S.A.).

The purity of the enzymes was checked both by size-exclusion chromatography (SEC) and by polyacrylamide gel electrophoresis in the presence of sodium dodecyl sulphate (SDS-PAGE). SEC was carried out on a Superose 12 column (Pharmacia-LKB) attached to the above-mentioned chromatography system, using 0.05 *M* sodium phosphate (pH 7.4) with 0.15 *M* sodium chloride as the mobile phase (flow-rate 0.7 ml/min). SDS-PAGE was performed as described previously¹⁷ in a Protean Double Slab Cell apparatus (Bio-Rad Labs., Richmond, CA, U.S.A.). The electropherograms were analysed in a VD 620 video densitometer (Bio-Rad Labs.).

RESULTS AND DISCUSSION

Conventional ammonium sulphate fractionation was carried out as the first purification step of the described isolation procedure. It brought about a five-fold purification of G6P-DH and a reduction of the sample volume (Table I). The sediment, after ammonium sulphate fractionation, also contained LDH with a high specific activity (*ca.* 417 nkat/mg). Moreover, this step was compatible with the subsequent hydrophobic interaction chromatography: salted-out homogenate could be used directly without removal of salts.

TABLE I

RAPID CHROMATOGRAPHIC PURIFICATION OF G6P-DH FROM *LEUCONOSTOC MES-ENTEROIDES*

Details of the procedure as described in the text. All data on LDH are given in parentheses.

Fraction	G6P-DH (LDH)				
	Protein (mg)	Total activity (μkat)	Specific activity (nkat/mg)	Purification (fold)	Recovery (%)
Crude supernatant	1100	90.9 (235.9)	83 (214)	1	100
Ammonium sulphate fractionation (60–90%)	189	80.9 (78.8)	428 (417)	5.2 (2)	90 (34)
Hydrophobic chromatography	9.6 (31)	56.3 (72.4)	5869 (2336)	71 (11)	63 (31)
Anion-exchange chromatography	1.7 (5.6)	51.8 (65.7)	30 470 (11 770)	367 (55)	58 (28)

Hydrophobic interaction chromatography proved to be a convenient method for further purification of G6P-DH and LDH. The chromatographic conditions were optimized on a Phenyl-Superose HR 5/5 column (loading capacity about 10 mg of protein). A Spheron Micro 300 HR 10/10 column (loading capacity *ca.* 200 mg of protein) was used for preparative chromatography with similar results. Elution with a decreasing salt concentration resulted in a relatively good separation of G6P-DH and

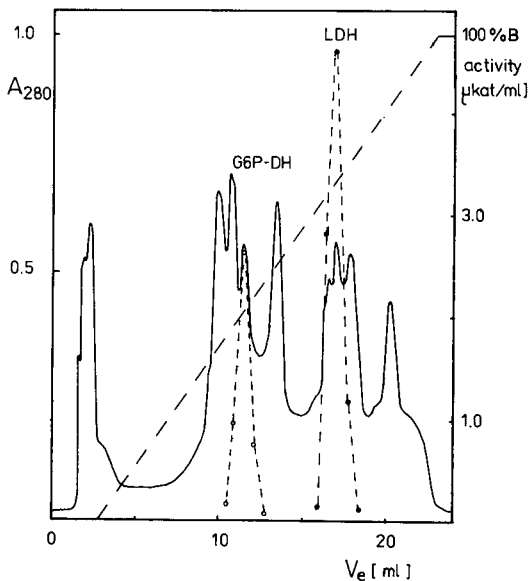


Fig. 1. Chromatography of crude enzyme preparation on a Phenyl-Superose column. Buffers: (A) 0.05 M sodium phosphate (pH 7.4) with 1.7 M sodium sulphate and 1 mM EDTA; (B) 0.05 M sodium phosphate (pH 7.4); flow-rate, 0.5 ml/min. V_e , elution volume; solid line, absorbance at 280 nm (A_{280}); dashed lines, gradient; (○) G6P-DH activity; (●) LDH activity. Approximately 10 mg of protein were applied to the column.

LDH from each other and most of the contaminants (Fig. 1). The purification of G6P-DH was *ca.* 14-fold and that of LDH was slightly worse (Table I). The activities of contaminant enzymes (which could interfere in appropriate clinical tests) were measured in the active fractions of G6P-DH and LDH after ammonium sulphate fractionation and hydrophobic interaction chromatography (Table II). It was shown that the enzyme preparations purified only by ammonium sulphate fractionation and hydrophobic interaction chromatography were applicable for use in clinical test kits. They contained only negligible activities of contaminating enzymes.

Chromatography on the strong anion exchanger Mono Q (after desalting) was chosen for the final step in the purification of both G6P-DH and LDH. Highly pure enzymes were eluted with a sodium chloride concentration gradient in both instances (Figs. 2 and 3). The purification of G6P-DH and LDH was *ca.* five-fold and the increase in specific activity achieved by the combination of hydrophobic and ion-exchange chromatographies was nearly 70-fold for G6P-DH and 30-fold for LDH (Table I). SEC and SDS-PAGE showed the homogeneity of G6P-DH (Figs. 4A and 5A). With LDH, if a completely pure enzyme is required subsequent SEC is applied as the final purification step (Figs. 4B and 5B).

The described purification procedure has several advantages over common methods for the purification of G6P-DH from *Leuconostoc mesenteroides*. In the three purification steps we obtained homogeneous G6P-DH with a five-fold higher specific activity than that reported by Hey and Dean⁷, who used tandem dye-ligand chromatography in a two-step procedure. Our yield was only slightly worse. The chromatographic materials used here are generally commercially available, in contrast with the dye-ligand matrices used by Hey and Dean⁷. The possibility of the simultaneous purification of G6P-DH and LDH is also an advantage. It is also interesting that even partially purified G6P-DH and LDH (after hydrophobic interaction chromatography) can be used in the appropriate clinical test kits (see Table II).

TABLE II

ACTIVITIES OF THE CONTAMINANT ENZYMES IN THE FRACTIONS AFTER AMMONIUM SULPHATE FRACTIONATION AND HYDROPHOBIC INTERACTION CHROMATOGRAPHY AS % OF G6P-DH AND LDH ACTIVITIES

Enzymes	Fraction	
	After ammonium sulphate fractionation	After hydrophobic interaction chromatography
G6P-DH	(100)	(100)
Phosphoglucomutase	0.3	—
Phosphoglucose isomerase	8.3	0.4
Creatine phosphokinase	0.03	0.009
6-Phosphogluconate DH	0.3	0.006
NADH oxidase	0.06	0.001
NADPH oxidase	0.008	—
LDH	(100)	(100)
Alanine aminotransferase	0.0003	0.0002

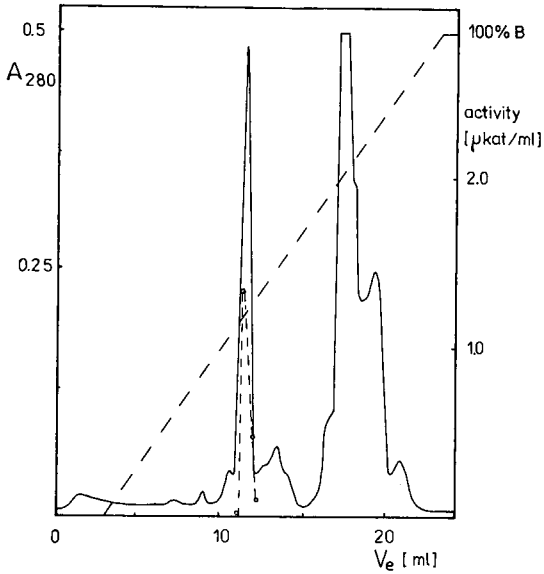


Fig. 2. Chromatography of partially purified G6P-DH on a Mono Q column. Buffers: (A) 0.05 *M* sodium phosphate (pH 7.4); (B) same as A but with 1 *M* sodium chloride; flow-rate, 1 ml/min. Lines symbol as in Fig. 1. Approximately 10 mg of protein were applied to the column.

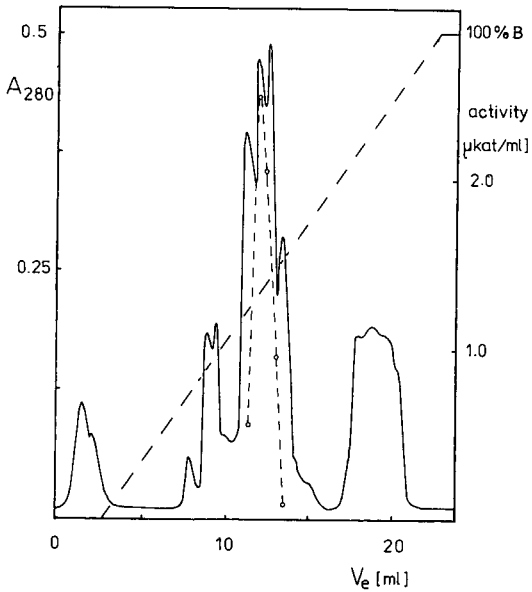


Fig. 3. Chromatography of partially purified LDH on a Mono Q column. Lines as in Fig. 2; (○) LDH activity.

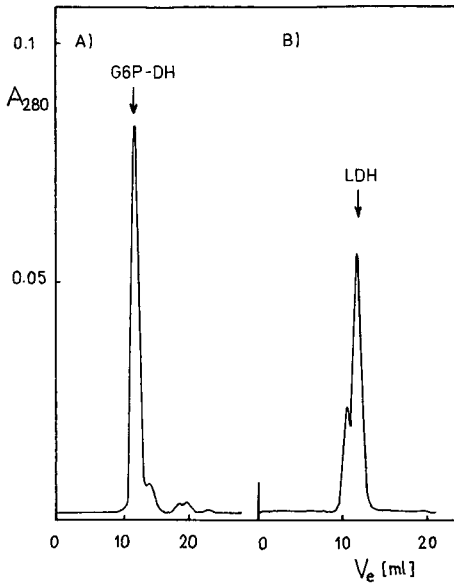


Fig. 4. Chromatography of (A) G6P-DH and (B) LDH on a Superose 12 column after ammonium sulphate fractionation, hydrophobic interaction chromatography and ion-exchange chromatography. Buffer: 0.05 M sodium phosphate (pH 7.4) with 0.15 M sodium chloride; flow-rate, 0.7 ml/min. Solid line as in Fig. 1.

This rapid chromatographic procedure is suitable for the preparation of several milligrams of G6P-DH and LDH. The chromatographic steps (see Table I) can be carried out in about 3 h, including the concentration with the ultrafiltration cell. Therefore, the whole procedure starting from the cell suspension of *Leuconostoc mesenteroides* can be performed in one working day. The purified G6P-DH and LDH

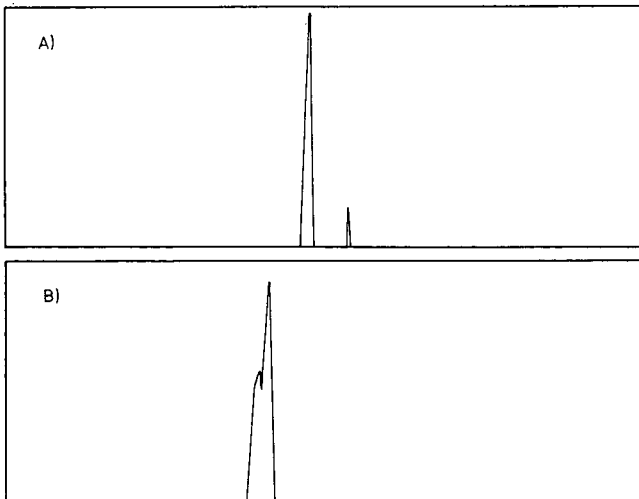


Fig. 5. SDS-PAGE densitograms of (A) G6P-DH and (B) LDH after ammonium sulphate fractionation, hydrophobic interaction chromatography and ion-exchange chromatography.

are suitable for enzymological studies and for analytical purposes. Their amounts are sufficient for *ca.* 1000 assays of glucose or 700 assays of creatine phosphokinase in the case of G6P-DH and for *ca.* 2500 assays of alanine aminotransferase in the case of LDH (under the conditions given in refs. 18–20). The method described can be easily modified for the preparation of both enzymes on a large scale.

ACKNOWLEDGEMENTS

The authors thank Drs. M. Smrž and P. Konečný for the gift of Spheron gels and for valuable suggestions and Prof. L. Skurský for useful discussions about the manuscript.

REFERENCES

- 1 E. A. Noltmann and S. A. Kuby, in P. D. Boyer (Editor), *The Enzymes*, Vol. 7, Academic Press, New York, 2nd ed., 1963, p. 223.
- 2 R. D. DeMoss, I. C. Gunsalus and R. G. Bard, *J. Bacteriol.*, 66 (1953) 1.
- 3 C. Olive and H. R. Levy, *Biochemistry*, 6 (1967) 730.
- 4 A. Ishaque, M. Milhausen and H. R. Levy, *Biochem. Biophys. Res. Commun.*, 59 (1974) 894.
- 5 *Biochemica Information*, Boehringer, Mannheim, 1973.
- 6 Y. D. Choi, M. H. Han and S. M. Byun, *Korean Biochem. J.*, 11 (1978) 12.
- 7 Y. Hey and P. D. G. Dean, *Biochem. J.*, 209 (1983) 363.
- 8 E. I. Garvie, *J. Gen. Microbiol.*, 58 (1969) 85.
- 9 H. W. Doelle, *J. Bacteriol.*, 108 (1971) 1284.
- 10 R. C. Garland, *Arch. Biochem. Biophys.*, 157 (1973) 36.
- 11 R. D. DeMoss, *Methods Enzymol.*, 1 (1955) 328.
- 12 H. U. Bergmeyer (Editor), *Methods of Enzymatic Analysis*, Vol. 1, Verlag Chemie, Weinheim, and Academic Press, New York, 2nd ed., 1974, p. 500.
- 13 A. S. Abramovitz and V. Massay, *J. Biol. Chem.*, 251 (1976) 5321.
- 14 H. U. Bergmeyer (Editor), *Methods of Enzymatic Analysis*, Vol. 1, Verlag Chemie, Weinheim, and Academic Press, New York, 2nd ed., 1974, p. 499.
- 15 H. U. Bergmeyer (Editor), *Methods of Enzymatic Analysis*, Vol. 1, Verlag Chemie, Weinheim, and Academic Press, New York, 2nd ed., 1974, p. 501.
- 16 H. A. Krebs, J. Mellanby and D. H. Williamson, *Biochem. J.*, 82 (1962) 96.
- 17 I. Matysková, J. Kovář and P. Racek, *Biochim. Biophys. Acta*, 839 (1985) 300.
- 18 *Glukose*, Boehringer, Mannheim, 1982.
- 19 *CK-NAC-Activated Monotest*, Boehringer, Mannheim, 1981.
- 20 *GPT Opt. Monotest*, Boehringer, Mannheim, 1980.

High-performance liquid chromatography of levomepromazine (methotrimeprazine) and its main metabolites

T. LOENNECHEN and S. G. DAHL*

Institute of Medical Biology, University of Tromsø, N-9001 Tromsø (Norway)

(First received June 14th, 1989; revised manuscript received October 16th, 1989)

SUMMARY

The phenothiazine drug levomepromazine (methotrimeprazine) has five metabolites which previously have been identified in plasma from psychiatric patients. These are formed by sulphoxidation, N-demethylation, O-demethylation and aromatic hydroxylation in two different positions. A high-performance liquid chromatographic system is described for the analysis of levomepromazine and its main metabolites on a Supelcosil C₁₈-DB column, based on ion-pair formation with sodium docecyl sulphate. The effects of variations in pH, buffer concentration, counter-ion concentration, temperature and concentration and composition of the organic solvent were examined. The six components may be analysed in 27.4 min at room temperature using 25 mM sodium dodecyl sulphate in 500 mM ammonium acetate buffer (pH 5.0)–5% v/v tetrahydrofuran in acetonitrile (50:50, v/v) as the mobile phase.

INTRODUCTION

The phenothiazine drug levomepromazine (methotrimeprazine) was introduced in 1959 as an agent with both neuroleptic¹ and analgesic² effects. Since then the drug has mainly been used in psychiatry, as a sedative adjuvant to other psychotropic drug treatment. Ten different levomepromazine metabolites have been identified in urine from psychiatric patients by nuclear magnetic resonance spectroscopy³ and combined gas chromatography–mass spectrometry^{4–6}. Five of these metabolites, all of which are formed by a single biotransformation step of the parent drug (Fig. 1), were found in the highest concentrations in urine. These metabolites, levomepromazine sulphoxide (LMSO), N-desmethyllevomepromazine (N-DLM), 3-hydroxylevomepromazine (3-OH-LM), 7-hydroxylevomepromazine (7-OH-LM) and O-desmethyllevomepromazine (O-DLM), have also been identified in plasma from patients treated with levomepromazine^{6,7}.

Their biological activities and plasma concentrations indicate that some levo-

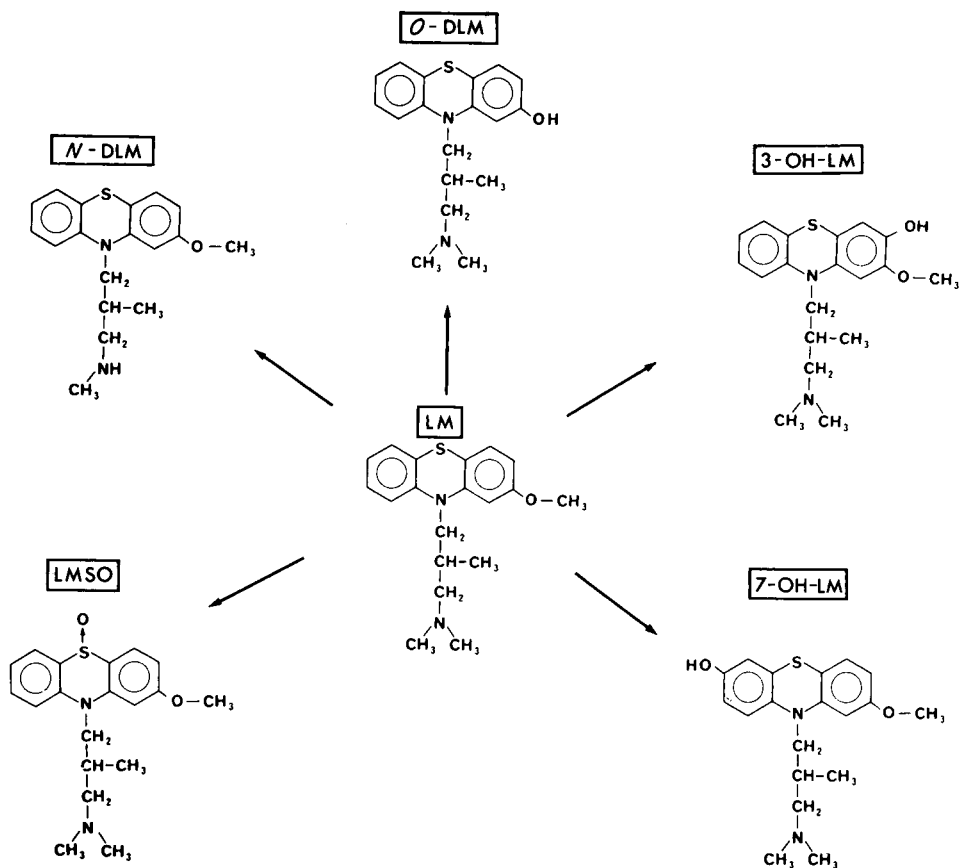


Fig. 1. Structures of levomepromazine (LM), levomepromazine sulphoxide (LMSO), N-desmethyllevomepromazine (N-DLM), 3-hydroxylevomepromazine (3-OH-LM), 7-hydroxylevomepromazine (7-OH-LM) and O-desmethyllevomepromazine (O-DLM).

mepromazine metabolites may contribute to the effects of the drug in man⁸. Phenothiazine neuroleptics show considerable between-patient variation in plasma drug levels and in metabolite-to-parent-drug plasma concentration ratios⁹. It may be expected that the contributions from metabolites to the effects of levomepromazine are subject to inter-individual variations. In order to examine this, it would be useful to have a chromatographic system that separates the six components in less than 30 min.

Normal-phase high-performance liquid chromatography (HPLC) has been reported to yield unsatisfactory results in the analysis of chlorpromazine, chlorpromazine sulphoxide and 7-hydroxychlorpromazine¹⁰. Similar results were obtained in our laboratory in attempts to analyse levomepromazine and its metabolites by normal-phase HPLC.

This paper describes an isocratic HPLC method for the analysis of LM and its five main metabolites (Fig. 1), based on reversed-phase ion-pair chromatography. The effects of variations in temperature and pH of the mobile phase and of the concentrations of the ion-pair forming agent, buffer and organic modifier on the retention and separation of the six compounds were examined.

EXPERIMENTAL

Chemicals

Levomepromazine hydrochloride, N-desmethylevomepromazine maleate, levomepromazine sulphoxide and methoxypromazine (MPZ) maleate were generously donated by Rhône-Poulenc Industries (Paris, France). O-Desmethylevomepromazine, 3-hydroxylevomepromazine and 7-hydroxylevomepromazine were synthesized from levomepromazine by a non-enzymatic method³. Stock solutions of levomepromazine and its metabolites were prepared at a concentration of 2 mM in methanol and stored at -20°C for up to 30 days.

Phenothiazine derivatives are prone to photodecomposition¹⁰, and exposure to light was therefore avoided throughout the experimental procedures. In order to minimize adsorptive losses, all glassware was silanized as described previously⁷, after initial cleaning with chromic acid-sulphuric acid. Solutions (0.01 mM) of levomepromazine and metabolites, which were used in the HPLC assay, were made by diluting stock solutions with mobile phase without tetrahydrofuran.

Analytical-reagent grade sodium dodecyl sulphate, which was used as a lipophilic counter ion, was obtained from Koch-Light Labs. (Colnbrook, U.K.). Ammonium acetate and acetic acid were obtained from Merck (Darmstadt, F.R.G.) and HPLC-grade tetrahydrofuran (THF), acetonitrile and methanol from Rathburn Chemicals (Walkerburn, U.K.).

Equipment

HPLC was carried out with a Rheodyne (Cotati, CA, U.S.A.) Model 7125 injector fitted with a 20- μ l loop, two pumps connected with a gradient master (Consta Metric; Laboratory Data Control, Riviera Beach, FL, U.S.A.) and an absorbance detector (Spectroflow Model 773 UV-VIS; Kratos, Ramsey, N.T., U.S.A.) operated at 254 nm and 0.001 a.u.f.s. Quantification was performed with an SP 4270 integrator (Spectra-Physics, San Jose, CA, U.S.A.).

The reversed-phase columns (analytical column, 250 nm \times 4.6 mm I.D.; pre-column, 20 mm \times 4.6 mm I.D.) were Supelcosil C₁₈-DB, 5 μ m particle size (Supelco, Bellefonte, OA, U.S.A.), and Supelguard LC₁₈-DB, 5 μ m particle size (Supelco). The analytical column had been alkylated by the manufacturer in order to optimize the separation of basic compounds.

Analysis

Two solutions, delivered to the chromatographic system by separate pumps, were prepared. The aqueous solution was prepared by adding 100 mM sodium dodecyl sulphate to a M ammonium acetate solution, followed by addition of concentrated acetic acid to the desired pH (37-38 ml in order to obtain pH 5.0) and distilled water to a total volume of 2 l. The organic solution consisted of acetonitrile or a mixture of THF and acetonitrile. The total flow-rate was kept constant at 1.5 ml/min and the effect of the concentration of organic modifier in the mobile phase was studied.

The dead volume of the system was measured as the first distortion of the baseline after injection of mobile phase. The capacity factor for each solute under the given experimental conditions was calculated by the equation $k' = (t_R - t_0)/t_0$, where

t_R and t_0 are the retention times for the solute and the solvent front, respectively.

Separation factors for two compounds are expressed as the ratio between the capacity factors of the last (k_2') and first (k_1') eluting peak, $\alpha = k_2'/k_1'$.

RESULTS AND DISCUSSION

Problems with separation from other components may arise in the analysis of levomepromazine and metabolites in biological extracts. We therefore examined how the capacity factors (k') and separation factors (α) of LM and its metabolites could be adjusted by changing the composition of the mobile phase.

Methanol alone as the mobile phase, at a flow-rate of 1 ml/min, produced retention times ranging from 43.67 to 11.65 min for LM and its metabolites and broad, tailing peaks. Acetonitrile alone as the mobile phase resulted in the elution of all components together with the solvent front within 1.45 min. Further experiments with acetonitrile and 50 mM ammonium acetate as the mobile phase demonstrated

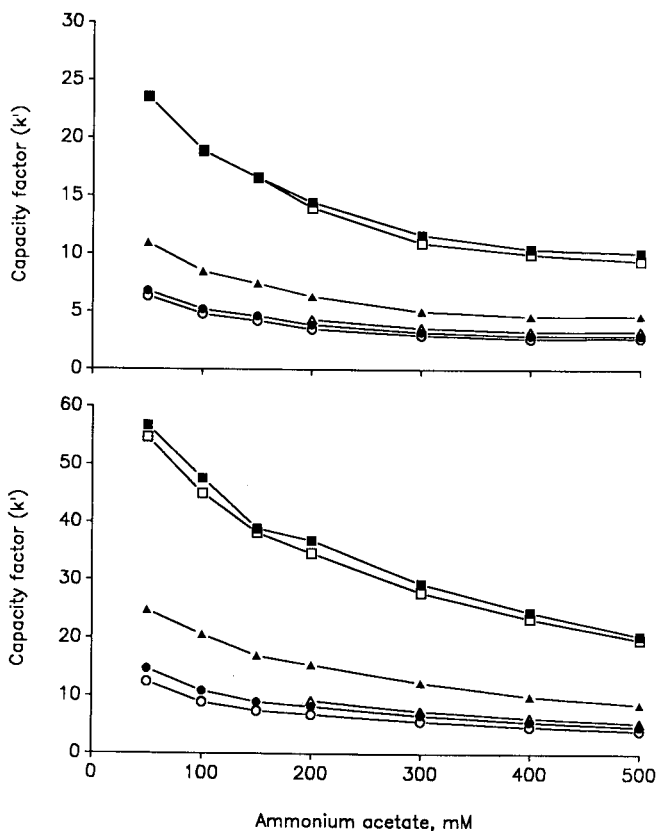


Fig. 2. Effect of buffer concentration on capacity factors (k') of levomepromazine and metabolites. Mobile phase: ammonium acetate buffer (pH 6.0) with 20 mM sodium dodecyl sulphate – acetonitrile, 45:55 (v/v) (upper curve) or 50:50 (v/v) (lower curve). (O) LMSO; (●) 7-OH-LM; (Δ) 3-OH-LM; (▲) O-DLM; (□) LM; (■) N-DLM.

TABLE I

EFFECT OF AMMONIUM ACETATE BUFFER CONCENTRATION ON SEPARATION FACTORS (α) OF LEVOMEPRMAZINE AND METABOLITES

Mobile phase: 20 mM sodium dodecyl sulphate in ammonium acetate buffer (pH 6.0) – acetonitrile (50:50, v/v). Flow-rate: 1.5 ml/min.

Compound	Ammonium acetate concentration (mM)						
	100	150	200	250	300	400	500
7-OH-LM/LMSO	1.18	1.21	1.20	1.20	1.18	1.17	1.16
3-OH-LM/7-OH-LM ^a	–	–	–	1.67	1.11	1.13	1.13
O-DLM/3-OH-LM ^a	–	–	–	2.25	1.66	1.18	1.59
LM/O-DLM	2.21	2.49	2.25	2.25	2.26	2.35	2.29
N-DLM/LM	1.04	1.06	1.02	1.07	1.06	1.05	1.03

^a 3-OH-LM could not be detected at buffer concentrations below 200 mM.

that increasing the amount of buffer from 10 to 50% (v/v) increased the capacity factors of all compounds except LMSO, for which it was virtually unchanged. However, this system also yielded peaks that were far too wide for analytical purposes. This problem was overcome by increasing the salt concentration in the aqueous solvent.

Ammonium acetate buffer concentration

As shown in Fig. 2, increasing ammonium acetate concentration in the range 50–500 mM decreased the capacity factors of the compounds by 55–70%. This may have been caused by decreased formation of ion pairs with the dodecyl sulphate counter ion, owing to competition from acetate ions.

As indicated in Fig. 2, 3-OH-LM could not be detected at ammonium acetate concentrations below 200 mM. At lower buffer concentrations the 3-OH-LM peak was replaced by two other unidentified peaks in the chromatogram, indicating that the metabolite had decomposed.

Owing to the apparent instability of 3-OH-LM, ammonium acetate concentrations ranging from 400 to 500 mM were used in further experiments. As shown in Table I, the separation factors did not differ significantly with different ammonium acetate concentrations in the range 200–500 mM.

Concentration of ion-pair forming agent

Addition of sodium dodecyl sulphate to the mobile phase was intended to produce ionic associations between negatively charged dodecyl sulphate ions and protonated amino groups in the phenothiazine derivatives. This method would be expected to produce complexes with lower polarities than the analysed compounds alone. As expected, increased retention times of levomepromazine and metabolites were observed on addition of sodium dodecyl sulphate to the mobile phase.

As shown in Fig. 3, increasing the sodium dodecyl sulphate concentrations from 5 to 50 mM resulted in a slight increase in the capacity factors of 3-OH-LM, 7-OH-LM and O-DLM, a 2- to 3-fold increase in the capacity factors of O-DLM and

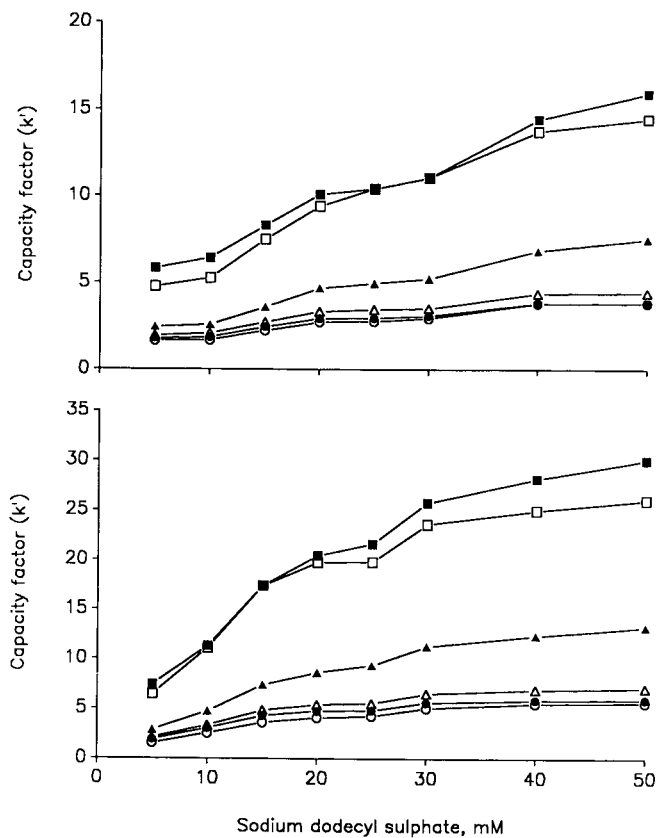


Fig. 3. Effect of sodium dodecyl sulphate concentration on capacity factors (k') of levomepromazine and metabolites. Mobile phase: 500 mM ammonium acetate buffer (pH 6.0) with sodium dodecyl sulphate – acetonitrile, 45:55 (v/v) (upper curve) or 50:50 (v/v) (lower curve). Symbols as in Fig. 2.

substantial increases in the capacity factors of levomepromazine and N-DLM. The difference between the effect of counter ion formation on the capacity factors of the compounds might be due to their different pK_a values (Table II). At pH 6.0, LM and

TABLE II

pK_a VALUES OF LEVOMEPRMAZINE AND METABOLITES

pK_a values were determined by titration of aqueous solutions of the compounds.

Compound	pK_{a_1}	pK_{a_2}
LM	8.8	–
N-DLM	8.1	–
LMSO	5.9	–
O-DLM	5.4	9.8
3-OH-LM	5.5	10.0
7-OH-LM	5.5	9.7

TABLE III

EFFECT OF SODIUM DODECYL SULPHATE CONCENTRATION ON SEPARATION FACTORS (α) OF LEVOMEPRMAZINE AND METABOLITES

Mobile phase: sodium dodecyl sulphate in 500 mM ammonium acetate buffer (pH 6.0) – acetonitrile (50:50, v/v). Flow-rate: 1.5 ml/min.

Compound	Sodium dodecyl sulphate concentration (mM)							
	5	10	15	20	25	30	40	50
7-OH-LM/LMSO	1.24	1.20	1.18	1.16	1.13	1.11	1.06	1.05
3-OH-LM/7-OH-LM	1.10	1.09	1.13	1.13	1.15	1.16	1.18	1.20
O-DLM/3-OH-LM	1.36	1.42	1.52	1.59	1.73	1.78	1.78	1.87
LM/O-DLM	2.23	2.33	2.36	2.29	2.12	2.09	2.03	1.97
NDLM/LM	1.15	1.02	1.00	1.03	1.10	1.09	1.13	1.15

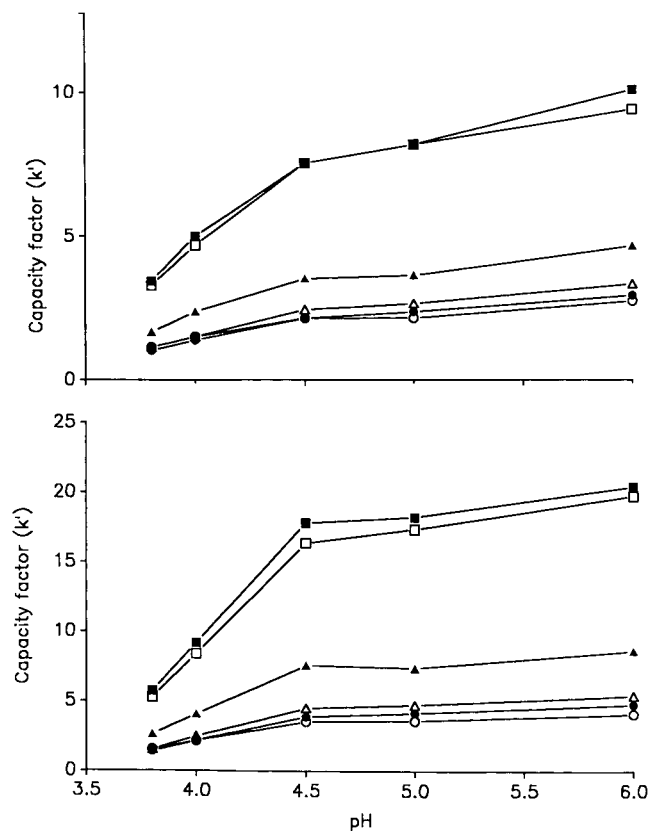


Fig. 4. Effect of pH on capacity factors (k') of levomepromazine and metabolites. Mobile phase: 500 mM ammonium acetate buffer with 20 mM sodium dodecyl sulphate – acetonitrile 45:55 (v/v) (upper curve) or 50:50 (v/v) (lower curve). Symbols as in Fig. 2.

TABLE IV

EFFECT OF AQUEOUS PHASE pH ON SEPARATION FACTORS (α) OF LEVOMEPRMAZINE AND METABOLITES

Mobile phase: 20 mM sodium dodecyl sulphate in 500 mM ammonium acetate buffer – acetonitrile (50:50, v/v). Flow-rate: 1.5 ml/min.

Compound	pH				
	6.0	5.0	4.5	4.0	3.8
7-OH-LM/LMSO	1.16	1.16	1.10	1.0	0.91
3-OH-LM/7-OH-LM	1.13	1.14	1.16	1.14	1.10
O-DLM/3-OH-LM	1.59	1.56	1.68	1.64	1.69
LM/O-DLM	2.29	2.38	2.17	2.06	2.01
N-DLM/LM	1.03	1.05	1.09	1.09	1.09

TABLE V

EFFECT OF TEMPERATURE ON CAPACITY FACTORS (k') OF LEVOMEPRMAZINE AND METABOLITES

Mobile phase: 25 mM sodium dodecyl sulphate in 500 mM ammonium acetate buffer (pH 5.0) – acetonitrile (50:50, v/v). Flow-rate: 1.5 ml/min.

Compound	Temperature (°C)	
	20	50
LMSO	3.82	3.40
7-OH-LM	4.31	3.70
3-OH-LM	5.00	4.30
O-DLM	8.65	6.87
LM	19.33	14.52
N-DLM	21.33	15.76

TABLE VI

EFFECT OF THF CONCENTRATION IN THE ORGANIC SOLVENT ON SEPARATION FACTORS (α) OF LEVOMEPRMAZINE AND METABOLITES

Mobile phase: 25 mM sodium dodecyl sulphate in 500 mM ammonium acetate buffer (pH 5.0) – acetonitrile with THF (50:50, v/v). Flow-rate: 1.5 ml/min.

Compound	THF concentration in acetonitrile (%)								
	0	2	3	4	5	8	12	20	25
7-OH-LM/LMSO	1.13	1.17	1.18	1.20	1.21	1.27	1.35	1.46	1.56
3-OH-LM/7-OH-LM	1.16	1.14	1.15	1.15	1.14	1.13	1.12	1.11	1.09
O-DLM/3-OH-LM	1.73	1.65	1.67	1.66	1.64	1.63	1.60	1.51	1.46
LM/O-DLM	2.23	2.10	2.02	2.00	1.98	1.91	1.84	1.74	1.66
N-DLM/LM	1.10	1.12	1.12	1.12	1.13	1.13	1.14	1.13	1.13

N-DLM are almost completely protonated, whereas the other compounds are approximately 50% protonated and thus have fewer amino groups available for ion-pair formation.

With a mobile phase of sodium dodecyl sulphate in 500 mM ammonium acetate buffer (pH 6.0)–acetonitrile (45:55, v/v), the highest separation factors were obtained with sodium dodecyl sulphate concentrations in the range 5–20 mM. With a 50:50 (v/v) mixture of aqueous and organic solvents, the highest separation factors of levomepromazine and metabolites were obtained with sodium dodecyl sulphate concentrations from 25 to 30 mM (Table III).

pH in the aqueous phase

As shown in Fig. 4, the capacity factors of all the six compounds decreased with decreasing pH. This effect was most pronounced at pH values below 4.5. With a mobile phase of 20 mM sodium dodecyl sulphate in 500 mM ammonium acetate buffer–acetonitrile (45:55 v/v), the highest separation factors of levomepromazine and metabolites were obtained at pH 6.0. With a 50:50 (v/v) mixture of aqueous and organic solvents the highest separation factors were observed at pH 5.0–6.0 (Table IV).

As indicated in Table IV, LMSO eluted after 7-OH-LM at pH values below 4.0. The LMSO peak in the chromatogram also overlapped with the 3-OH-LM peak at pH 3.8.

Effect of temperature

Elevated temperatures are sometimes used in HPLC in order to improve the separation of small molecules or control t values. As shown in Table V, the capacity factors of levomepromazine and metabolites decreased on increasing the column and mobile phase temperature from 20 to 50°C. It also seems likely that levomepromazine and its metabolites would be even more vulnerable to oxidation or decomposition at

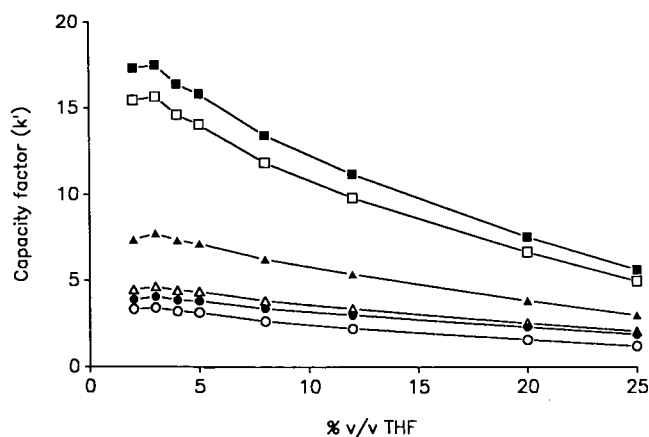


Fig. 5. Effect of THF concentration in the organic solvent on capacity factors (k') of levomepromazine and metabolites. Mobile phase: 500 mM ammonium acetate buffer (pH 5.0) with 25 mM sodium dodecyl sulphate – acetonitrile with THF (50:50, v/v). Symbols as in Fig. 2.

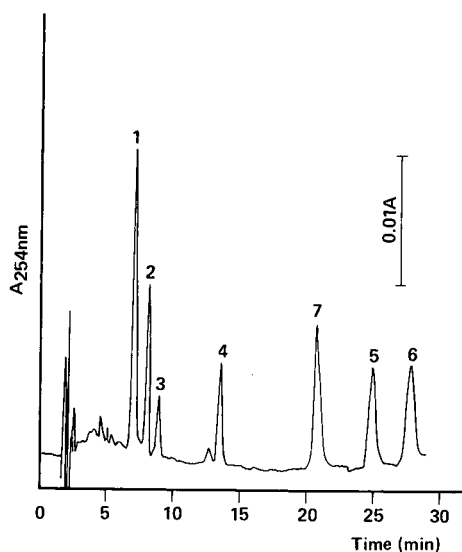


Fig. 6. Elution profile of a mixture containing 0.01 mM of levomepromazine and metabolites: 1 = LMSO (6.71 min); 2 = 7-OH-LM (7.80 min); 3 = 3-OH-LM (8.68 min); 4 = O-DLM (13.22 min); 5 = LM (24.53 min); 6 = N-DLM (27.43 min); 7 = methoxypromazine, internal standard (20.41 min). Mobile phase: 500 mM ammonium acetate with 25 mM sodium dodecyl sulphate (pH 5.0) – 5% (v/v) THF in acetonitrile (50:50, v/v).

elevated temperatures. For these reasons, all subsequent experiments were performed at 20°C.

Organic modifier

It has been shown that the addition of small amounts of tetrahydrofuran may improve the separation of non-polar components when acetonitrile is used as the organic modifier¹¹. In order to improve the separation of LM and its metabolites, various concentrations of THF were added to the organic solvent.

THF concentrations of up to 25% (v/v) in acetonitrile did not increase the separation factors of 3-OH-LM–7-OH-LM and N-DLM–LM. The separation factor of 7-OH-LM–LMSO, on the other hand, increased from 1.1 to 1.6 (Table VI). However, addition of up to 25% (v/v) THF to acetonitrile resulted in a pronounced decrease in the capacity factors of LM and N-DLM, a smaller decrease in the capacity factor of O-DLM and a slight decrease in the capacity factors of the other three compounds (Fig. 5).

On addition of 5% (v/v) THF to acetonitrile, the capacity factor of the last-eluting compound, N-DLM, was reduced from 21.2 to 15.8, which reduced the retention time from 38 to 27.4 min. As a compromise between distinct separation and reasonably short retention times, a mobile phase composition of 500 mM ammonium acetate buffer (pH 5.0) with 25 mM sodium dodecyl sulphate – 5% (v/v) THF in acetonitrile (50:50, v/v) was chosen. This system produced the chromatogram shown in Fig. 6.

Internal standard

In order to apply the method to quantitative analysis, a suitable internal standard would be required. Among several phenothiazine drugs and metabolites which were examined, methoxypromazine, which elutes between O-DLM and LM in this system (Fig. 6), was found to have the most suitable retention time.

REFERENCES

- 1 J. M. Huot and A. C. Kristof, *Can. Med. Assoc. J.*, 81 (1959) 546.
- 2 B. Paradis, *Anesthésie*, 16 (1959) 185.
- 3 S. G. Dahl, E. Kaufmann, B. Mompon and T. Purcell, *J. Pharm. Sci.*, 76 (1987) 541.
- 4 S. G. Dahl and M. Garle, *J. Pharm. Sci.*, 66 (1977) 190.
- 5 H. Johnsen and S. G. Dahl, *Drug Metab. Dispos.*, 10 (1982) 63.
- 6 S. G. Dahl, H. Johnsen and C. R. Lee, *Biomed. Mass Spectrom.*, 9 (1982) 534.
- 7 S. G. Dahl, T. Bratlid and O. Lingjærde, *Ther. Drug Monit.*, 4 (1982) 81.
- 8 S. G. Dahl, *Ther. Drug Monit.*, 4 (1982) 33.
- 9 S. G. Dahl, *Clin. Pharmacokinet.*, 11 (1986) 36.
- 10 D. Stevenson and E. Reid, *Anal. Lett.*, 14 (1981) 741.
- 11 W. S. Hancock and J. T. Sparrow, *HPLC Analysis of Biological Compounds (Chromatographic Science Series, Vol. 26)*, Marcel Dekker, New York, 1984.

High-performance liquid chromatography of clindamycin and clindamycin phosphate with electrochemical detection

A. HORNEDO-NUÑEZ^a, T. A. GETEK* and W. A. KORFMACHER^a

National Center for Toxicological Research, HFT-223, Jefferson, AR 72079 (U.S.A.)

and

F. SIMENTHAL

Food and Drug Administration, Washington, DC 20204 (U.S.A.)

(First received August 31st, 1989; revised manuscript received November 28th, 1989)

SUMMARY

The high-performance liquid chromatographic analysis of clindamycin phosphate and clindamycin hydrochloride was accomplished by using a mobile phase consisting of the ion pair reagent, sodium pentane sulfonate, and a reversed-phase ODS-II column. Detection was performed with a dual electrochemical cell at a screening potential of +0.7 V and a detecting potential of +0.9 V. Limits of detection for clindamycin were 100 pg injected on-column utilizing a pulse-free syringe pump. Bulk preparations of clindamycin hydrochloride were analyzed by high-performance liquid chromatography (HPLC) with electrochemical detection and compared to an HPLC technique utilizing ultraviolet detection at 214 nm.

INTRODUCTION

The official methods of analysis of the antibacterial antibiotics clindamycin (I) and clindamycin phosphate (II) (structures shown in Fig. 1) involve either a gas chromatographic separation after derivatization or a microbiological assay^{1,2}. In order to eliminate the time needed for derivatization in the gas chromatographic protocol, the analysis of clindamycin (in the hydrochloride form) and the associated phosphate ester has been performed by high-performance liquid chromatography (HPLC) using a refractive index (RI) detector³. The separation of clindamycin by HPLC followed by RI detection was accomplished by using an aqueous solution of dioctyl sodium sulfosuccinate and methanol as the mobile phase, which gave good chromatographic separation, but the quantity at which the samples were analyzed had to be approximately 100 µg injected on-column due to the low detection limits and insensitivity of the RI detector. Extensive sample preparation was also needed, which

^a Present address: Department of Chemistry, University of Puerto Rico, San Juan, PR 00931, U.S.A.

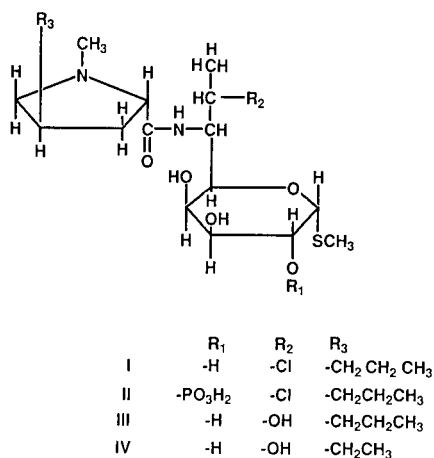


Fig. 1. Structures of clindamycin (I), clindamycin phosphate (II), lincomycin (III) and lincomycin B (IV).

added to the overall analysis time. Landis *et al.*⁴ utilized RI and ultraviolet (UV) detection at 214 nm with a reversed-phase ion pair mobile phase consisting of D,L-10-sodium camphorsulfonate or sodium pentane sulfonate for RI or UV detection, respectively. These mobile phases were applied for the analysis of clindamycin and bulk impurities. Minimal sample quantities for RI detection were at levels of 375 μg injected on-column and for UV detection a detection limit of approximately one fourth of RI limits was achieved. Analysis of the clindamycin phosphate ester and its degradation products was accomplished by HPLC with UV detection at 210 nm⁵ and a mobile phase containing aqueous potassium phosphate and acetonitrile. The impurities lincomycin (III) and lincomycin B (IV), which may exist in bulk preparations of clindamycin, were also detected. The amount of clindamycin phosphate injected was approximately 4 μg on-column. Recently, determination of clindamycin in plasma or serum was accomplished with UV detection at 198 nm at a detectable level of 0.17 $\mu\text{g}/\text{ml}$ after minimal sample preparation⁶.

During the course of evaluating the utility of HPLC with electrochemical detection (ED) for the assay of the aminoglycoside antibiotic gentamicin⁷, it was found that clindamycin generated an electrochemical response at an oxidizing potential⁸. This report describes the HPLC-ED determination of clindamycin and clindamycin phosphate, as well as its applicability for assaying bulk preparations of clindamycin hydrochloride.

EXPERIMENTAL

Electroanalytical measurements by differential pulse voltammetry (DPV) and cyclic voltammetry (CV) were made on a BAS-100A (Bioanalytical Systems, West Lafayette, IN, U.S.A.) with a glassy carbon working electrode (GCE), a Ag/AgCl reference electrode and a platinum wire as the counter electrode. Electrolyte was 0.04 M aqueous phosphate buffer for compound I and 0.025 M aqueous phosphate buffer for compound II. Phosphate buffer was composed of $\text{Na}_2\text{HPO}_4 \cdot 7\text{H}_2\text{O}$ and KH_2PO_4 at a pH of *ca.* 7. The DPV conditions were scan-rate 5 mV/s and pulse amplitude of 50 mV; CV was performed at scan-rates of 200 mV/s.

HPLC employed an Isco LC-5000 (Lincoln, NB, U.S.A.) syringe pump at a flow-rate of 1.0 ml/min. The mobile phase was similar to that used by Landis *et al.*⁴ and consisted of methanol-water (60:40) with 0.1 M phosphate buffer (pH 6) and 0.002 M sodium pentane sulfonate (Regis, Morton Grove, IL, U.S.A.). The phosphate buffer was prepared by using $\text{Na}_2\text{HPO}_4 \cdot 7\text{H}_2\text{O}$ and KH_2PO_4 and adjusted to pH 6, if necessary. A Spherisorb ODS-II C_{18} reversed-phase column (10 cm \times 4.6 mm I.D., 3 μm ; Custom LC, Houston, TX, U.S.A.) was used. The electrochemical cell was an ESA (Bedford, MA, U.S.A.) high-sensitivity cell, Model 5011, with an ESA Model 5100A Coulochem potentiostat. The cell utilized a dual-electrode configuration whereby the first electrode was set at a screening potential to diminish any electroactive species present in the mobile phase, and the second electrode detected the solute of interest. In the case of clindamycin, the screening potential was set at +0.7 V vs. Pd reference electrode and the detecting potential was +0.9 V vs. Pd reference electrode. The output from the detector was connected to a Shimadzu C-R3A integrator (Kyoto, Japan). Injections were made with a Rheodyne Model 7125 (Cotati, CA, U.S.A.) injector with a 20- μl loop.

Clindamycin, as it is referred to in the text, was used as the hydrochloride salt form. A standard for clindamycin with a microbiological potency of 837 mcg/mg was compared with the bulk preparations by HPLC-ED. The nominal concentrations for assay purposes of clindamycin were 0.01 mg/ml.

The HPLC-UV method used for comparison in this study is similar to that reported by Munson and Kubiak⁵. Detection was performed at a wavelength of 214 nm and with a flow-rate of 1.5 ml/min. Nominal concentrations of standard and samples were 0.8 mg/ml utilizing a 20- μl loop. The mobile phase consisted of phosphate buffer-acetonitrile (77:23). The phosphate buffer was prepared from potassium dihydrogen phosphate by dissolving 10.54 g into 1 l deionized water and adjusting the pH to 2.5 with 90% phosphoric acid.

Two mass units were used to describe clindamycin throughout the text. One mass unit, μg , refers to the mass of antibiotic injected on-column. The other mass unit, mcg/mg, where mc stands for micro, refers to the microbiological potency. When the bulk preparations were compared to the standard, the final value is related to the microbiological potency of the standard and has the unit mcg/mg.

RESULTS AND DISCUSSION

The electrochemistry of clindamycin (I), as determined by DPV, is shown in Fig. 2. An initial oxidation is observed at +0.92 V with a subsequent oxidation at +1.59 V, which was near the start of oxidation of the background solvent. In Fig. 3, the DPV of clindamycin phosphate (II) gave an initial oxidation at +0.99 V and a broad hump near the background oxidation at +1.70 V. CV on a GCE for clindamycin and its phosphate ester did not produce sharp waves; however, CV did indicate that the electrochemistry was irreversible in aqueous phosphate buffer.

An example of HPLC-ED of clindamycin is shown in Fig. 4. The chromatogram by HPLC-ED is similar to that reported for UV detection of clindamycin^{4,5}. Clindamycin is prepared from lincomycin (III), which is also detectable by HPLC-ED, as illustrated in Fig. 4. It was found that the chromatographic retention time for clindamycin was highly pH dependent, as reported previously⁴.

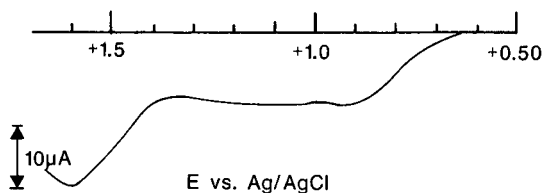


Fig. 2. Differential pulse voltammogram of clindamycin in 0.04 *M* aqueous phosphate buffer.

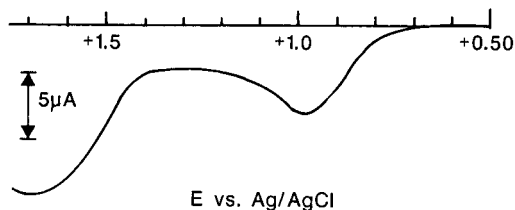


Fig. 3. Differential pulse voltammogram of clindamycin phosphate in 0.025 *M* aqueous phosphate buffer.

The linearity of the electrochemical signal *vs.* concentration of clindamycin as determined by on-column injections and the integrated peak area gave a correlation coefficient (*r*) of 0.99990 as indicated in Table I. The linear regression produced an equation with the slope being normalized to the *y*-intercept of $y = 142x + 1$ signal/ μg . The dynamic range of this analysis was *ca.* 0.05–1 μg injected on-column. The linearity study for clindamycin phosphate gave an *r* of 0.9990 for a range of approximately 0.06 to 1.2 μg injected on-column as shown in Table II. The result of linear regression, with normalization to the *y*-intercept, was $y = 153x + 1$. At approximately 1.5 μg injected on-column and above, the linear relationship for clindamycin and clindamycin phosphate was not maintained.

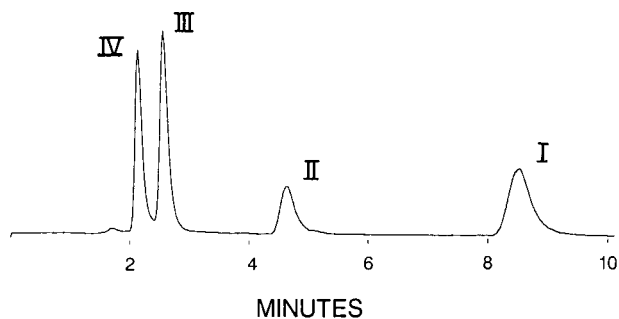


Fig. 4. Typical HPLC-ED of clindamycin and structurally related compounds. Roman numerals refer to structures shown in Fig. 1. Concentrations of all four compounds were 0.01 mg/ml each with 20- μl loop injection.

TABLE I

LINEARITY OF CLINDAMYCIN ANALYSIS BY HPLC-ED PERFORMED FOR TRIPLICATE ASSAYS

A clindamycin standard was used at a potency of 837 $\mu\text{g}/\text{mg}$.

<i>Amount injected on-column^a (μg)</i>	<i>Mean peak area</i>	<i>S.D.</i>	<i>R.S.D. (%)</i>
0.045	$7.6 \cdot 10^5$	$3.70 \cdot 10^4$	4.7
0.090	$1.53 \cdot 10^6$	$3.03 \cdot 10^2$	0.02
0.450	$7.37 \cdot 10^6$	$5.14 \cdot 10^4$	0.6
0.900	$1.43 \cdot 10^7$	$1.17 \cdot 10^5$	0.8
4.50	$3.78 \cdot 10^7$	$6.53 \cdot 10^5$	1.7

^a Correlation coefficient for the range 0.045–0.900 μg was 0.99990.

The standard deviation for these linearity studies is indicated in Tables I and II. As shown in Table I, the relative standard deviation (R.S.D.) in the range of 4.5 to 0.09 μg injected on-column was less than 2% for all levels. At the lowest level of 0.045 μg , R.S.D. for triplicate assays was 4.7%. These values for the R.S.D. compare favorably to those reported previously for HPLC with UV detection at 214 nm⁴ where the approximate amount of clindamycin was 90 μg and the R.S.D. was in the 0.5–2% range. For clindamycin phosphate, as shown in Table II, the R.S.D. for triplicate assays was 3.3% or less in the 0.12–5.8 μg range; and R.S.D. of 5.9% was obtained at the 0.058- μg injected level. Again, the R.S.D. values for clindamycin phosphate by HPLC-ED were comparable to those values reported by Munson and Kubiak⁵ employing UV detection at 210 nm, where quantities were approximately 4 μg ⁵. The linearity for the HPLC-UV analysis of clindamycin as described in this paper is shown in Table III. The R.S.D. values in Table III are comparable to those for the HPLC-ED method (Table I); however, the levels injected are *ca.* 100-fold less for the HPLC-ED technique.

TABLE II

LINEARITY OF CLINDAMYCIN PHOSPHATE ANALYSIS BY HPLC-ED PERFORMED FOR TRIPLICATE ASSAYS

Phosphate ester sample diluted from bulk sample solution rated at 150 mg/ml.

<i>Amount injected on-column^a (μg)</i>	<i>Mean peak area</i>	<i>S.D.</i>	<i>R.S.D. (%)</i>
0.058	$3.33 \cdot 10^5$	$1.98 \cdot 10^4$	5.9
0.12	$6.19 \cdot 10^5$	$1.03 \cdot 10^4$	1.6
0.58	$3.43 \cdot 10^6$	$6.91 \cdot 10^4$	2.0
1.17	$6.42 \cdot 10^6$	$4.13 \cdot 10^4$	0.7
5.84	$2.09 \cdot 10^7$	$6.86 \cdot 10^5$	3.3

^a Correlation coefficient for the range 0.058–1.17 μg was 0.9990.

TABLE III

LINEARITY OF CLINDAMYCIN ANALYSIS BY HPLC-UV FOR TRIPLICATE ASSAYS

A clindamycin standard was used at a potency of 966 $\mu\text{g}/\text{mg}$.

<i>Amount injected on-column^a</i> (μg)	<i>Mean peak area</i>	<i>S.D.</i>	<i>R.S.D.</i> (%)
4.2	$2.21 \cdot 10^5$	$8.34 \cdot 10^2$	0.4
10.0	$5.04 \cdot 10^5$	$4.83 \cdot 10^3$	1.0
16.0	$7.74 \cdot 10^5$	$4.38 \cdot 10^3$	0.6
20.0	$9.77 \cdot 10^5$	$2.21 \cdot 10^3$	0.2

^a Correlation coefficient was 0.9997.

As a test for the limit of detection for clindamycin by HPLC-ED, a 100-pg (*ca.* 240-fmol) injection on-column was made. Although the background trace was sloping, the chromatographic peak was easily observed as demonstrated in Fig. 5. This detection limit was highly dependent on the background noise encountered and the preconditioning of the electrochemical detector. The limit of detection for clindamycin phosphate was approximately an order of magnitude higher due to the operating parameters of the cell and potentiostat. As determined by CV and DPV, the oxidation potential for clindamycin phosphate is more anodic than that of clindamycin. In order to attain limits of detection of 100 pg for the phosphate ester, the detection potential would have to be set at a higher potential than +0.9 V. Unfortunately, background current at higher potentials due to the oxidation of the mobile phase, severely limited the analyte current that could be observed. The +0.9 V detection potential was a compromise between a good analyte signal for clindamycin phosphate and low background noise.

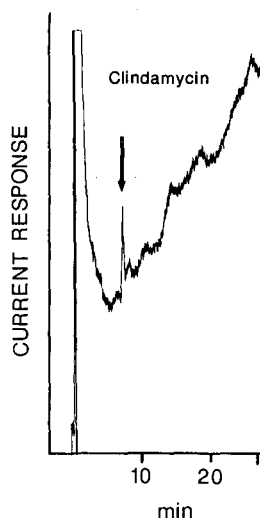


Fig. 5. Test for detection limit of clindamycin (I) by HPLC-ED with 100 pg injected on-column.

Three bulk preparations of clindamycin were assayed by HPLC-ED by comparison to a standard of clindamycin hydrochloride which had a potency of 837 mcg/mg. Nominal sample solutions of 0.01 mg/ml for the bulk preparations were prepared and assayed in triplicate. A linear calibration curve for the standard over the concentration range of the prepared bulk sample solutions was generated. Table IV illustrates the values obtained by HPLC-ED for these bulk preparations of clindamycin on two different days, as well as the average value measured by HPLC using UV detection at 214 nm. On each day, a new calibration curve was generated and new sample and standard solutions were prepared.

The variability of the mean potency from day one to day two for the bulk samples analyzed by HPLC-ED (Table IV) was calculated by taking the difference between the mean potencies and the average mean potencies. This variability ranged from 5.6% for bulk sample A to 2.2% for bulk sample C. The final two columns in Table IV indicate the R.S.D. for six measurements using day one and two combined. The R.S.D. for this HPLC-ED analysis of clindamycin ranged from 4.3% to 1.5%, which compares to an R.S.D. of less than 2% reported for the HPLC-UV analysis of clindamycin phosphate⁵. It should be stated that the typical amount injected on-column for HPLC-ED was *ca.* 20-fold less than the amount injected for the HPLC-UV analysis of clindamycin phosphate⁵. The R.S.D. for the HPLC-UV potencies shown in Table IV was less than 1%. From Table IV, it is noted that all potencies determined by HPLC-ED are less than the HPLC-UV potency. The clindamycin standard used for the evaluation of the bulk samples was not a United States Pharmacopia (USP) standard. It was observed with the non-USP standard that several additional chromatographic peaks, which included compounds III and IV, were observed. Subsequent HPLC-ED of a USP standard rated at a potency of 866 mcg/mg did not have the same quantity or magnitude of these additional chromato-

TABLE IV

COMPARISON OF ASSAY BY HPLC-ED AND HPLC-UV FOR BULK PREPARATIONS OF CLINDAMYCIN ON TWO DIFFERENT DAYS

Potencies in mcg/mg.

Bulk sample	HPLC-UV ^a potency	Day one			Day two			Day one and two combined ^b	
		Potency	Mean	R.S.D. (%)	Potency	Mean	R.S.D. (%)	Mean	(%)
A	820	800	768	4.2	805	812	2.5	790	4.3
		768			796				
		735			835				
B	825	765	775	1.5	755	803	3.7	786	3.7
		772			799				
		789			835				
C	822	789	788	0.5	765	771	0.9	780	1.4
		785			768				
		792			779				

^a Potency determined by HPLC with UV detection at 214 nm for one day only.

^b Total of six samples from day one and day two

graphic peaks. The difficulties in assaying antibiotics by HPLC and correlating the assays to the determined microbiological potency have been discussed by Thomas⁹. In this particular study, the compounds associated with the additional peaks observed in the non-USP standard may affect the specific potency indicative of the amount of clindamycin in the non-USP standard.

In the course of developing this analysis for clindamycin by HPLC-ED, several precautions had to be taken. The mixing of methanol and aqueous phosphate buffer generated a sufficient heat of mixing that resulted in retention times for clindamycin that were decreasing continually during the course of the day as the mobile phase cooled. This heating effect also perturbed the reproducibility of integrated peak areas. In order to alleviate this difficulty, the mobile phase was mixed and filtered several hours before use. Thermostating the HPLC-ED system may be helpful in diminishing this heating effect. The retention time for clindamycin, as reported earlier⁴, is highly pH dependent above pH 7; care must be taken to be sure that the pH of the mobile phase is 6. The dual electrochemical cell, as is the case for many cells used for HPLC-ED, required cleaning of adsorbed materials from the carbon electrode. This cleaning was performed by flushing the cell with diluted nitric acid. This study used a syringe pump for HPLC. Thorough flushing of the syringe pump and complete filling with the mobile phase is a requirement for reproducible retention times. It was subsequently found that for concentrations of 0.01 mg/ml and above, a conventional dual-head reciprocal HPLC pump may be employed. Furthermore the use of an ion pair reagent in the mobile phase for clindamycin may not be necessary. Varying the concentration of sodium pentane sulfonate did not have a profound effect on the retention times. As in the case with Munson and Kubiak⁵ and the HPLC-UV method used in this study, good reversed-phase HPLC with only aqueous phosphate buffer and acetonitrile was possible. Further work will establish the feasibility and reproducibility of HPLC-ED for assaying injectables of clindamycin phosphate.

CONCLUSIONS

The HPLC-ED method is an effective means to detect and analyze clindamycin and clindamycin phosphate. The low detection limits that are possible with HPLC-ED may make this technique viable for metabolite investigations of clindamycin and its phosphate ester. Because lincomycin and lincomycin B were also detected by HPLC-ED, the HPLC-ED method allowed analysis of several possible bulk impurities. The detection of clindamycin B and 7-epiclindamycin by HPLC-ED was not established due to a lack of representative samples for these compounds, which may also exist as bulk impurities in clindamycin⁴. Future work will develop a similar HPLC-ED procedure for the antibiotic lincomycin.

ACKNOWLEDGEMENTS

The authors would like to acknowledge helpful discussions with E. Hansen, Jr. of the National Center for Toxicological Research (NCTR), Thomas G. Alexander of the Food and Drug Administration (FDA) and Dr. Ali Shaikh of University of Arkansas at Little Rock for the use of BAS-100A. We also thank C. Hartwick for typing the manuscript. One of us (T.A.G.) was supported by an appointment to the

Oak Ridge Associated Universities Postgraduate Research Program at the NCTR administered by the Oak Ridge Associated Universities through an interagency agreement between the U.S. Department of Energy and the FDA. A.H.-N. was supported by a summer appointment at the NCTR through the COSTEP program. The authors acknowledge the aid of Jingzuo Xiang and Dr. Aszalos at the FDA, Wasington, DC for their HPLC-UV work. This research was presented in part at the *American Chemical Society Southwest Regional Meeting, Corpus Christi, TX, 1988.*

REFERENCES

- 1 L. W. Brown, *J. Pharm. Sci.*, 63 (1974) 1597.
- 2 *Code of Federal Regulations, Title 21, Part 436.304, 453.22, 453.22a*, April 1, 1984, U.S. Government Printing Office, Washington, DC, 1984.
- 3 L. W. Brown, *J. Pharm. Sci.*, 67 (1978) 1254.
- 4 J. B. Landis, M. E. Grant and S. A. Nelson, *J. Chromatogr.*, 202 (1980) 99.
- 5 J. W. Munson and E. J. Kubiak, *J. Pharm. Biomed. Anal.*, 3, 523 (1985).
- 6 G. LaFollette, J. Gambertoglio, J. A. White, D. W. Knuth and E. T. Lin, *J. Chromatogr.*, 431 (1988) 379.
- 7 T. A. Getek, A. C. Haneke and G. B. Selzer, *J. Assoc. Off. Anal. Chem.*, 66 (1983) 172.
- 8 T. A. Getek, unpublished results.
- 9 A. H. Thomas, *J. Pharm. Biomed. Anal.*, 5 (1987) 319.

High-pH ion-exchange separation and electrochemical detection of alditols, carbohydrates and acidic sugars

SUNIL V. PRABHU and RICHARD P. BALDWIN*

Department of Chemistry, University of Louisville, Belknap Campus, Louisville, KY 40292 (U.S.A.)

(First received September 12th, 1989; revised manuscript received November 14th, 1989)

SUMMARY

Recent advances in electrochemical detection of carbohydrates and related compounds have produced a need for chromatographic procedures which can effectively carry out the separation of these compounds under strongly alkaline conditions. Accordingly, the retention properties of commercially available, high-pH anion-exchange and ligand-exchange columns were evaluated for alditols, carbohydrates and aldonic, uronic and aldaric acids. It was shown that anion-exchange techniques were able to retain and resolve these groups from one another in a straightforward fashion by managing the mobile phase ionic strength. Separations involving mixtures of compounds belonging to any one family were difficult only for the alditols, which are only weakly retained under these conditions. For this specific case, ligand-exchange columns were found to be able to resolve most mixtures.

INTRODUCTION

In recent years, several electrochemically based approaches have been reported for the detection and quantitation of carbohydrates following liquid chromatography^{1–5}. The most widely used of these to date has undoubtedly been the pulsed amperometric detection (PAD) scheme developed by Johnson^{1,2}. This approach, which makes use of the adsorption of carbohydrate compounds onto platinum or gold electrodes to enable their oxidation at very low potentials, has evolved to a sufficient extent that instrumentation capable of generating the required sequence of applied potentials and current measurements is now commercially available. Very recently, a catalytic electrode system utilizing a copper-containing film deposited onto glassy carbon was shown to permit constant-potential detection of carbohydrates using conventional liquid chromatography (LC)–electrochemical detection (ED) equipment⁵. This approach is of interest because, by avoiding PAD's need to expose the platinum or gold electrode to regular cleaning and regeneration potentials, the copper-based chemically modified electrode's operation is simpler and appears to be slightly more sensitive. For example, glucose oxidation at the modified electrode gave an optimum detection limit of only 0.2 ng at +0.50 V vs. Ag/AgCl and was sufficient-

ly stable that 80–100 injections were reproducible to a relative standard deviation of 1–5%^{5,6}. In both cases, the electrochemical methodologies are extremely attractive because of the capability that they afford for direct monitoring of trace quantities of these compounds without the time-consuming or inefficient derivatization steps routinely required for the usual UV–visible absorption or fluorescence techniques to be applicable.

The principal drawback of all of the recommended electrode systems is that they uniformly require strongly alkaline conditions in order for optimum carbohydrate oxidation (and detection) to occur. Thus, LC–ED applications based on these electrode systems have typically employed mobile phases containing 0.001 *M* to 0.15 *M* OH[−]. Fortunately, this detector requirement, which drastically limits the stationary phase options available to carry out the carbohydrate separation, has not presented an insurmountable problem to the chromatographer. High-performance ion-exchange column packings which are stable at high pH conditions have conveniently become available within the last few years. This development, coupled with the fact that simple sugars possess *pK_a* values between 12 and 13 (ref. 7), has made anion-exchange chromatography in high pH solutions a viable choice for carbohydrate separation prior to ED^{3–5, 8–10}.

Very recently, we have shown that the copper-based chemically modified electrode (Cu–CME) initially used for oxidation and detection of simple carbohydrates⁵ exhibits similar activity toward a wide range of related compounds including, most notably, alditols and aldonic, uronic and aldonic acids¹¹. In order to realize the potential of electrochemical detection for these important classes of natural products, it is necessary to develop compatible chromatographic procedures for their separation. Previous liquid chromatography approaches for the acidic sugars have involved anion-exchange separations which are often coupled with a pre- or post-column derivatization step to enhance detectability^{12–14}. Alditols, which are ionized only in quite strong base, have been separated directly with aminoalkyl bonded phase columns¹⁵ and as their borate complexes with anion-exchange systems¹⁶. These and other chromatographic approaches have been reviewed by Honda¹⁷ and by Shaw¹⁸. However, in no cases of which we are aware have the strongly alkaline conditions required for efficient ED been employed. Thus, there is a need to develop high-pH chromatographic procedures suitable for the separation of alditols and acidic sugars. In this work, we have tried to meet this need by taking advantage of the compatibility of the new high-pH ion-exchange chromatography columns with the high-pH detection requirements of the Cu–CME in order to formulate direct and highly sensitive analysis procedures for these compounds.

EXPERIMENTAL

Reagents

Stock solutions of all alditols, carbohydrates and acidic sugars (purchased from Sigma and Aldrich) were prepared fresh daily in deionized water. Just prior to use, the stock solutions were adjusted to the desired concentration and pH by addition of the appropriate hydroxide-containing diluent. Mobile phases used for liquid chromatography were prepared from carbonate-free sodium hydroxide and thoroughly degassed deionized water. A.C.S. reagent grade sodium sulphate and sodium nitrate were obtained from Baker.

Electrodes

Electrode modification procedures were similar to those described previously^{5,11}. A freshly polished thin-layer glassy carbon electrode (Bioanalytical Systems, West Lafayette, IN, U.S.A.) was immersed at open circuit for 5 min in a 0.050 *M* CuCl₂ solution. At this point, a white deposit appeared on the glassy carbon surface; and the CME was ready for use. During exposure to the CuCl₂, it was necessary to immerse the entire electrode assembly, including the metallic leads, in order for the catalytically active deposit to develop. Subsequent investigations, to be reported separately⁶, have indicated the most likely source of the deposit to be the galvanic formation of a CuCl₂ species. The activity of the modified electrode could be restored to that of the original glassy carbon by polishing with alumina.

Apparatus

Liquid chromatography experiments were carried out with either a Waters Model M-45 or a Beckman Model 110B pump, a Rheodyne (Berkeley, CA, U.S.A.) Model 7125 injector with a 20- μ l sample loop, an SSI Model LP-21 pulse dampener and a Bioanalytical Systems Model LC-4B electrochemical detector maintained at +0.50 V vs. Ag/AgCl. The chromatographic columns employed were either a 25 cm \times 4 mm I.D. Dionex (Sunnyvale, CA, U.S.A.) CarboPac PA1 column or a 30 cm \times 4.6 mm I.D. Supelco (Bellefonte, PA, U.S.A.) C611-SP ion-exchange column. The mobile phase flow-rate was always 0.1 ml/min.

RESULTS AND DISCUSSION

Electrochemical detection

The construction and electrocatalytic response of the Cu-CME toward carbohydrates, alditols and acidic sugars has been described at length in our earlier reports^{5,11}. Briefly, the CME, which was produced by deposition of a Cu/Cl-containing film onto an ordinary glassy carbon surface, exhibited broad anodic waves for these compounds in both cyclic voltammetry and flow injection analysis experiments. These oxidations, which were centered at +0.5 V vs. Ag/AgCl and occurred to an appreciable extent only at hydroxide concentrations of 10⁻³ *M* or higher, were well suited for use in LC-ED and provided detection limits in the nanomole-to-picomole range in the applications considered. In principle, the chromatographic work described here could have been carried out with Au or Pt electrodes using the PAD approach^{1,2} or, in fact, with any of the other electrode systems previously recommended for carbohydrate detection. However, because of its ease of operation and its somewhat greater tolerance for lower hydroxide concentrations, the Cu-CME was utilized for all experiments that form the basis of this work.

Liquid chromatography

In view of the very weak acidities of simple carbohydrates, it is expected that anion-exchange chromatography in strongly basic solution might present a reasonable separations approach for sugar-containing samples. In fact, several successful high pH anion-exchange procedures have been developed and reported for mono- and oligosaccharides⁸⁻¹⁰. Analogous procedures for alditols, the p*K*_a values of which fall approximately from 13 to 14 (ref. 19) and acidic sugars, the p*K*_a values of which

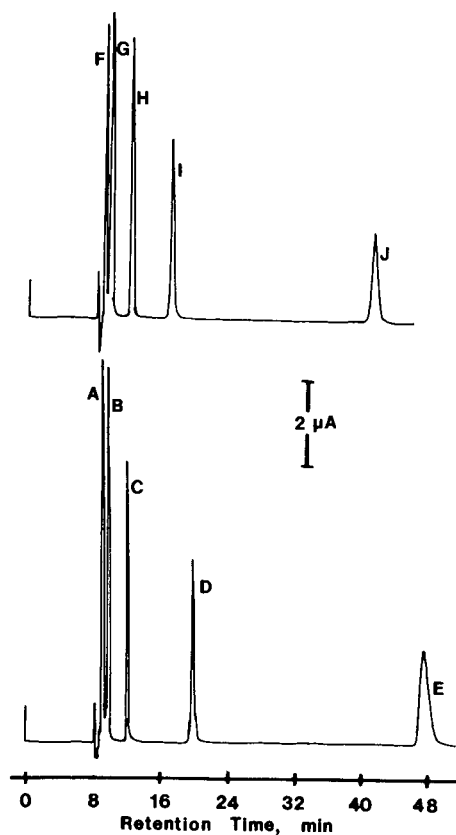


Fig. 1. Chromatograms of glucose and galactose families. Stationary phase, Dionex Carbowac PA1; mobile phase, 0.020 *M* sodium sulfate–0.134 *M* sodium hydroxide. Labeled peaks correspond to glucitol (A); glucose (B), gluconic acid (C, $8 \cdot 10^{-6}$ *M*); glucuronic acid (D); glucaric acid (E); galactitol (F); galactose (G), galactonic acid (H, $2.5 \cdot 10^{-5}$ *M*); galacturonic acid (I); and galactaric acid (J); all concentrations were $4 \cdot 10^{-5}$ *M* unless indicated otherwise.

are generally between 3 and 4 (ref. 7), should also be feasible under the appropriate mobile phase conditions. To our knowledge, however, such separations have not been reported previously.

TABLE I

CAPACITY FACTORS FOR GLUCOSE AND GALACTOSE DERIVATIVES

Chromatographic conditions as in Fig. 1.

Compound	k'	Compound	k'
Glucitol	0.09	Galactitol	0.08
Glucose	0.17	Galactose	0.17
Gluconic acid	0.45	Galactonic acid	0.45
Glucuronic acid	1.4	Galacturonic acid	1.0
Glucaric acid	4.8	Galactaric acid	3.9

The chromatograms shown in Fig. 1 for sample mixtures containing glucose and galactose as well as their alditol and acidic sugar derivatives illustrate the nature of the separations that can be achieved by means of the high pH anion-exchange approach. The isocratic mobile phase employed consisted of a mixture of 0.13 *M* sodium hydroxide and 0.02 *M* sodium sulfate. The former was present in order to ensure optimum electrode performance while the latter was used as the principal means of adjusting solvent strength. In both cases, the order of elution observed (alditol, aldose, aldonic acid, uronic acid, aldaric acid) was exactly that expected on the basis of the compounds' pK_a values and ionic character. Under the conditions shown, the retention of the column varied widely for the different analytes as reflected in the capacity factors (k') which, as shown in Table I, varied from 0.1 for the alditols to 4–5 for the aldaric acids.

Close comparison of the two chromatograms in Fig. 1 supports our general observation that different members of the same carbohydrate families exhibit roughly similar retention properties. Thus, it is relatively easy to resolve complex samples on the basis of functional group or family, *e.g.*, alditols from aldonic acids and so on. Furthermore, our work here, as well as that reported earlier²⁰, indicated that, for the more highly retained acidic sugars, resolution of individual members of each group can usually be accomplished quite easily by simply adjusting concentration of sodium sulfate (or other salt) to an optimum level for retention of that group. It is apparent from Fig. 1, for example, that glucuronic and galacturonic acids and glucaric and galactaric acids would be baseline-resolved by the mobile phase composition already in effect. The most challenging separation problems appear to be those involving the carbohydrates themselves and the alditols, both of which are practically unretained under the mobile phase conditions in effect in the Fig. Several studies^{3–5,8–10} have shown that acceptable carbohydrate separations can be achieved largely by using mobile phases containing sodium hydroxide only. By so doing, the solvent strength is decreased sufficiently that enough retention of the carbohydrates occurs that careful adjustment of the sodium hydroxide concentration can produce a reasonable degree of selectivity.

TABLE II

EFFECT OF HYDROXIDE CONCENTRATION ON CAPACITY FACTORS OF ALDITOLS IN ANION-EXCHANGE CHROMATOGRAPHY

Stationary phase, Dionex Carbopac PA1 column; mobile phase, sodium hydroxide concentration indicated; other conditions as in Fig. 2.

$[OH^-]$ (<i>M</i>)	<i>Glycerol</i>	<i>Threitol</i>	<i>Erythritol</i>	<i>Ribitol</i>	<i>Galactitol</i>	<i>Glucitol</i>	<i>Mannitol</i>	<i>Inositol</i>
0.50	0.20	0.28	0.30	0.47	0.46	0.50	0.58	0.17
0.45	0.20	0.27	0.27	0.51	0.48	0.55	0.60	0.20
0.40	0.24	0.28	0.23	0.55	0.55	0.58	0.65	0.18
0.30	0.21	0.30	0.29	0.62	0.62	0.63	0.72	0.22
0.15	0.25	0.33	0.31	0.72	0.72	0.72	0.93	0.25
0.075	0.25	0.33	0.31	0.75	0.75	0.75	1.0	0.29
0.010	0.24	0.32	0.32	0.82	0.75	0.82	1.1	0.32
0.005	0.27	0.38	0.29	0.90	0.90	0.98	1.3	0.29
0.001	0.27	0.40	0.29	0.97	1.6	1.6	1.6	0.29

By far the most difficult separation to achieve is that involving the alditols. For these compounds, decreases in solvent strength produced by elimination of the sodium sulfate employed above were not able by themselves to allow the alditols to be retained strongly enough for separation to be practical. Thus, further reductions in solvent strength could only be accomplished by decreasing the concentration of sodium hydroxide in the mobile phase. However, given the extremely weak acidity of the alditols and the changes in ionization likely to accompany a substantial OH^- decrease, it was unlikely that the resulting effects on retention would be straightforward. As shown in Table II, this was in fact the case. In general, increases in k' were observed as the sodium hydroxide concentration was decreased. But for many of the alditols examined (in particular, glycerol, threitol, erythritol and inositol) the changes in k' were quite minor even over a 500-fold sodium hydroxide concentration range. The best separations able to be achieved by this approach occurred at the lowest OH^- concentrations and for mixtures of different size alditols. For example, there was a nearly baseline separation (see Fig. 2) of a homologous series including glycerol, threitol, ribitol and glucitol for a 0.0010 M sodium hydroxide mobile phase.

An alternative approach for carbohydrate separations involves the use of a "fixed-cation" or "ligand-exchange" stationary phase in place of the direct anion-exchange column used above¹⁸. Ligand-exchange columns usually contain strongly cationic sulfonic acid type resins which have been permanently loaded with one or more cationic counterions such as Ca^{2+} , Ag^+ , Pb^{2+} or H^+ . The retention mechanism for carbohydrates on these columns is based on a chelation process in which the hydroxyl groups of the carbohydrate displace water molecules from the cation coordination sphere and form a complex with it. The selectivity of the resulting column is determined largely by the nature of the cation employed, with Ca^{2+} -loaded columns showing particular affinity for alditols as well as carbohydrates. Ordinarily, the carbohydrate separations with these columns have employed water or simple water-organic mobile phases at near neutral pH values. However, as such ligand-exchange systems have become commercially available in forms stable in relatively strong base, it seemed reasonable to investigate their utility for LC-ED under these conditions.

Initial experiments with such a column attempted to characterize the dependence of alditol retention on factors such as mobile phase pH and ionic strength. This was done by examining the effects that such changes exercised on the retention of

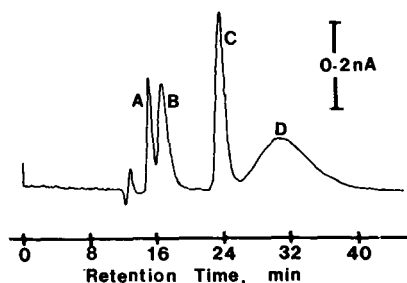


Fig. 2. Chromatogram of alditol test mixture on anion-exchange column. Stationary phase, Dionex Carbopac PA1; mobile phase, 0.0010 M sodium hydroxide. Labeled peaks correspond to glycerol (A, $6 \cdot 10^{-5} M$), threitol (B, $6 \cdot 10^{-5} M$), ribitol (C, $5 \cdot 10^{-5} M$) and glucitol (D, $5 \cdot 10^{-5} M$).

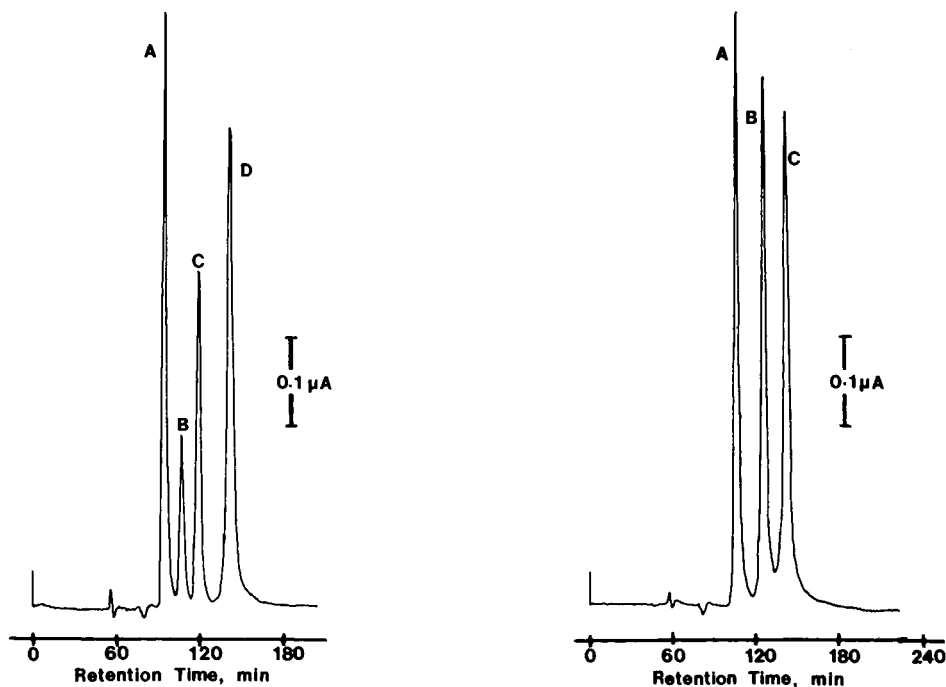


Fig. 3. Chromatogram of alditol test mixture on ligand exchange column. Stationary phase, Supelco C611-SP; mobile phase, 0.040 *M* sodium nitrate–0.0020 *M* sodium hydroxide. Labeled peaks correspond to ribitol (A, $1 \cdot 10^{-5}$ *M*), glycerol (B, $2 \cdot 10^{-5}$ *M*), threitol (C, $1 \cdot 10^{-5}$ *M*) and glucitol (D, $1 \cdot 10^{-5}$ *M*).

Fig. 4. Chromatogram of hexitol test mixture on ligand-exchange column. Stationary phase, Supelco C611-SP; mobile phase, 0.040 *M* sodium nitrate–0.0020 *M* sodium hydroxide. Labeled peaks correspond to mannitol (A), galactitol (B) and glucitol (C); all concentrations were $1 \cdot 10^{-5}$ *M*.

glycerol, threitol, ribitol and glucitol. The effect of pH changes was determined by systematically varying the sodium hydroxide concentration while maintaining ionic strength constant at 0.01 by adjusting the sodium nitrate concentration. Unfortunately, with the particular column used here, the pH could be usefully varied only from 10.5 to 11.6. At more acidic conditions, the response of the Cu-CME was far out of its optimum range while the ligand-exchange column was unstable and showed signs of deterioration at higher OH^- levels. Over the narrow pH range examined, however, the retention properties of the alditols were practically constant.

Fortunately, variations in ionic strength proved to be much more chromatographically useful. Such changes, achieved here by varying the salt concentration while holding the pH constant, produced the expected changes in retention: decreases in ionic strength always resulted in increased retention. Although retention of the alditols was never extremely strong (*i.e.*, $k' < 2$), acceptable separations, illustrated in Fig. 3 for the four test compounds and in Fig. 4 for the hexitols mannitol, galactitol and glucitol, were usually able to be obtained. Typical capacity factors, corresponding to various sodium nitrate concentrations at pH 11.2, are shown in Table III for eight alditols. Clearly, some individual pairs of compounds (*e.g.*, erythritol–inositol and glycerol–mannitol) would be extremely difficult to resolve by this approach; but suffi-

TABLE III

EFFECT OF SODIUM NITRATE CONCENTRATION ON CAPACITY FACTORS OF ALDITOLS IN LIGAND-EXCHANGE CHROMATOGRAPHY

Stationary phase, Supelco C611-SP column; mobile phase, 0.002 *M* sodium hydroxide plus the sodium nitrate concentration indicated; other conditions as in Figs. 3 and 4.

<i>NaNO</i> ₃ (<i>M</i>)	<i>Glycerol</i>	<i>Threitol</i>	<i>Erythritol</i>	<i>Ribitol</i>	<i>Galactitol</i>	<i>Glucitol</i>	<i>Mannitol</i>	<i>Inositol</i>
0.001	1.3	1.5	1.2	1.0	1.6	2.0	1.2	1.2
0.003	1.2	1.4	1.1	0.96	1.5	1.9	1.2	1.1
0.005	1.2	1.4	1.0	0.91	1.5	1.9	1.1	1.0
0.007	1.1	1.4	1.0	0.89	1.5	1.8	1.1	1.0
0.010	1.1	1.4	0.97	0.88	1.5	1.8	1.1	0.97
0.015	1.1	1.3	0.95	0.85	1.4	1.8	1.0	0.95
0.020	1.1	1.3	0.94	0.81	1.4	1.8	1.0	0.94
0.030	0.96	1.2	0.89	0.76	1.3	1.6	0.95	0.89
0.040	0.88	1.1	0.77	0.66	1.2	1.5	0.86	0.77

cient differences in retention exist that most mixtures could be reasonable well resolved.

The most troublesome aspect of the separations carried out on the ligand-exchange columns was undoubtedly the very long times often required. These times, which exceeded two hours for the mixtures in Figs. 3 and 4, were dictated by the very low flow-rates used in order to obtain good retention and resolution. For more favorable cases involving some of the more easily resolved alditols, much higher flow-rates and shorter retention times could certainly be achieved. Additional improvements might also be expected to accrue from operation of the column at higher temperature or under gradient elution conditions; if successful, this would likely produce greater resolution and allow the use of higher mobile phase flow-rates as well. Furthermore, as a greater variety of ligand-exchange columns becomes available, marked changes in the retention properties of the alditols might well be possible.

CONCLUSIONS

The separation and quantitation of carbohydrates and related compounds remains a challenging analytical problem for which the combination of high-pH ion-exchange chromatography and ED offers interesting and useful possibilities. In particular, anion-exchange techniques compatible with most suggested electrochemical monitoring systems are able to retain and resolve carbohydrates, alditols, aldonic acids, uronic acids and aldaric acids in a straightforward fashion by managing the mobile phase ionic strength. Separations involving mixtures of compounds belonging to any one family are difficult only for the alditols which are only weakly retained on simple anion-exchange columns. For this specific case, ligand-exchange columns provide an attractive ancillary approach. Thus, LC-ED clearly can be considered to offer not only extremely sensitive direct detection for carbohydrate-related compounds but also versatile and effective separations capabilities as well.

ACKNOWLEDGEMENT

This work was supported by the National Science Foundation through EPS-CoR Grant 86-10671-01.

REFERENCES

- 1 S. Hughes and D. C. Johnson, *Anal. Chim. Acta*, 132 (1981) 11.
- 2 G. G. Neuberger and D. C. Johnson, *Anal. Chem.*, 59 (1987) 150.
- 3 R. E. Reim and R. M. Van Effen, *Anal. Chem.*, 58 (1986) 3203.
- 4 L. M. Santos and R. P. Baldwin, *Anal. Chem.*, 59 (1987) 1766.
- 5 S. V. Prabhu and R. P. Baldwin, *Anal. Chem.*, 61 (1989) 852.
- 6 P. Luo, S. V. Prabhu and R. P. Baldwin, *Anal. Chem.*, in press.
- 7 J. A. Dean (Editor), *Lange's Handbook of Chemistry*, McGraw-Hill, New York, 10th ed., 1979, Ch. 5, pp. 17-41.
- 8 R. D. Rocklin and C. A. Pohl, *J. Liq. Chromatogr.*, 6 (1983) 1577.
- 9 P. Edwards and K. K. Haak, *Am. Lab. (Fairfield, Conn.)*, April (1983) 78.
- 10 J. D. Olechno, S. R. Carter, W. T. Edwards and D. G. Gillen, *Am. Biotechnol. Lab.*, Sept.-Oct. (1987) 38.
- 11 S. V. Prabhu and R. P. Baldwin, *Anal. Chem.*, 61 (1989) 2258.
- 12 S. Honda, S. Suzuki, M. Takahashi, K. Kakehi and S. Ganno, *Anal. Biochem.*, 134 (1983) 34.
- 13 P. Gacesa, A. Squire and P. J. Winterburn, *Carbohydr. Res.*, 118 (1983) 1.
- 14 P. J. M. Dijkgraaf, L. A. Th. Verhaar, W. P. T. Groenland and K. Van Der Wiele, *J. Chromatogr.*, 328 (1985) 371.
- 15 R. Schwarzenbach, *J. Chromatogr.*, 140 (1977) 304.
- 16 S. Honda, M. Takahashi, S. Shimada, K. Kakehi and S. Ganno, *Anal. Biochem.*, 128 (1983) 429.
- 17 S. Honda, *Anal. Biochem.*, 140 (1984) 1.
- 18 P. E. Shaw, *Handbook of Sugar Separations in Food by HPLC*, CRC Press, Boca Raton, FL, 1988, pp. 27-80.
- 19 H. S. Isbell, *Carbohydrates in Solution (Advances in Chemistry Series, No. 117)*, American Chemical Society, Washington, DC, 1973, Ch. 7.
- 20 A. M. Tolbert and R. P. Baldwin, *Electroanalysis*, 1 (1989) 389.

CHROM 22 137

Determination of iron(III) ion using ion chromatography with electrochemical detection and its application to the assay of the ferroxidase activity of ceruloplasmin

NANA KAWASAKI*, AKIKO ISHIGAMI, TSUYOSHI TANIMOTO and AKIRA TANAKA

Division of Biological Chemistry and Drugs, National Institute of Hygienic Sciences, 1-18-1, Kamiyoga, Setagaya-ku, Tokyo 158 (Japan)

(First received July 28th, 1989; revised manuscript received October 2nd, 1989)

SUMMARY

A simple, rapid and sensitive method for the determination of iron(III) ion by ion chromatography coupled with electrochemical detection was developed. The method reduced the interferences of iron(II) ions and enabled more than 5 pmol of iron(III) to be determined with an injection volume of 10 μ l. The method was applied to the determination of ferroxidase activity of ceruloplasmin with good reproducibility. The production of iron(III) ion by ceruloplasmin was found to be linear with respect to reaction time and protein concentration.

INTRODUCTION

Iron is an essential element in biological systems. It exists in an aqueous solution in two oxidation states, Fe^{II} and the Fe^{III}, on which the transport and storage of iron in biological systems is based¹.

Most methods now used for determination of Fe^{II} are spectrophotometric, using, for instance, bathophenanthroline as a reagent², but the determination of Fe^{III} is complicated as it must first be reduced to Fe^{II} and the total iron is determined, making the trace determination of Fe^{III} in the presence of excess Fe^{II} difficult. Osaki³ developed an assay method for ferroxidase activity of ceruloplasmin which catalyses the oxidation of Fe^{II} to Fe^{III} in the presence of oxygen⁴ and apparently detects ferroxidase-generated Fe^{III} by spectrophotometric measurement following Fe^{III}-transferrin formation. However, in this process, the form in which iron is incorporated into the apotransferrin molecule is unknown, and it is often influenced by the presence of contaminating substrates.

An ion chromatographic method was introduced for use in the separation and determination of some metal cations, the cations separated with an ion-exchange column being detected with a conductivity detector⁵ or a spectrophotometric detector^{6–8}. Recently, there has been increasing interest in the use of electrochemical

detectors for the trace determination of electroactive compounds⁹, as this method usually enhances both selectivity and sensitivity. However, few methods for the determination of Fe^{III} with an electrochemical detector have been reported^{10,11}, as it must be determined via a reduction step which introduces problems associated with oxygen interference.

In this work we attempted to develop a selective and sensitive method for the determination of Fe^{III} by combining an ion-exchange column with electrochemical detection. This method may be useful for determining the ferroxidase activity of ceruloplasmin.

EXPERIMENTAL

Materials

Lactic acid, lithium hydroxide, Fe(NH₄)₂(SO₄)₂ · 6H₂O and FeNH₄(SO₄)₂ · 12H₂O were obtained from Wako (Osaka, Japan), trichloroacetic acid from Nacalai Tesque (Kyoto, Japan) and ceruloplasmin from Green Cross (Osaka, Japan).

Chromatographic conditions

The chromatographic system consisted of a Hitachi (Tokyo, Japan) Model L-6000 pump and a Rheodyne Model 7125 injector (Tosoh, Tokyo, Japan). An HPIC-CS5 separation column with an HPIC-GS5 guard column (Dionex, Sunnyvale, CA, U.S.A.) was used to separate Fe^{III}. The latter was detected with an Irica Σ-875 amperometric detector with a glassy carbon working electrode and Ag/AgCl reference electrode (Irica Kogyo, Kyoto, Japan), and the detector output was recorded on a Hitachi Model D-2000 chromato-integrator.

The eluent was 250 mM lactic acid adjusted to pH 3.2 with lithium hydroxide and purged with nitrogen. The flow-rate was 1.0 ml/min.

Before the beginning of operation, 0.1 M sodium sulphite solution was pumped through the column at 1.0 ml/min for 1 h every day to remove oxygen from the system.

Samples were injected into a 10-μl PTFE sample loop with a plastic syringe.

Determination of Fe^{III}

A standard solution of Fe^{III} was prepared by dissolving FeNH₄(SO₄)₂ · 12H₂O in 50 mM hydrochloric acid just prior to use.

Determination of ferroxidase activity

A mixture of 530 μl of 0.2 M acetate buffer (pH 5.0) and 70 μl of 20 mM iron(II) ammonium sulphate solution was preincubated at 30°C for 3 min. A 100-μl volume of solution containing various amounts of ceruloplasmin (0.5–100 μg) was added to the mixture and mixed well. After incubation for 3 or 20 min at 30°C, the reaction was terminated by the addition of 300 μl of 12.5% trichloroacetic acid. The mixture was centrifuged at 6500 g for 10 min to remove the precipitated proteins and 10 μl of the supernatant were used for analysis. The enzyme activity was determined as the amount of Fe^{III} produced per minute.

RESULTS

Determination of Fe^{III}

The separation and detection of Fe^{III} was performed by ion chromatography with electrochemical detection as the lactic acid-chelated complex formed directly on the chromatographic column. In order to establish the optimum conditions for the rapid and sensitive determination of Fe^{III}, we investigated the effect of different factors on the chromatographic behaviour of the Fe^{III}-lactic acid complex.

The pH of the mobile phase was varied from 3.0 to 4.5. The retention times of Fe^{III} at pH 3.5 and 3.0 were 2.1 and 3.6 min, respectively. Hydrodynamic voltammograms of Fe^{III} in lactic acid at various pH are shown in Fig. 1. As the pH increased, the hydrodynamic voltammogram shifted to the negative side, and therefore it was found that the peak area increased with decreasing pH at a certain potential. However, when a more acidic mobile phase was used, the peak shape was broadened considerably, and the retention time was prolonged. Therefore, lactic acid at pH 3.2 was found to be most suitable with respect to both sensitivity and separation.

Another important factor is the applied potential of the working electrode to detect the Fe^{III} complex. The maximum peak area for Fe^{III} in lactic acid at pH 3.2 is obtained at a potential near -0.5 V, but this potential is unfavourable from the standpoint of interference by oxygen. A potential of -0.2 V was chosen to obtain an optimum balance between the sensitivity and stability of the electrode.

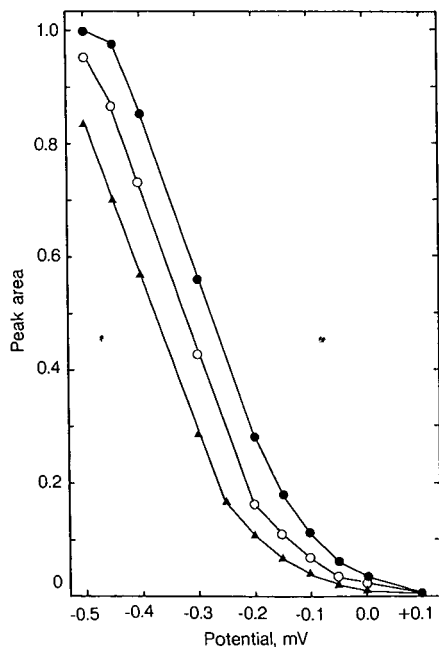


Fig. 1. Hydrodynamic voltammograms of Fe^{III} in 250 mM lactic acid at (●) pH 3.2, (○) pH 3.6 and (▲) pH 4.0. The peak area at pH 3.2 at a potential of -0.5 V was taken as 1.0.

Peak-area calibration was superior to peak-height calibration. The calibration graph for Fe^{III} obtained for a 10- μl injection was linear at concentrations of more than 5 pmol, and the correlation coefficient between 1000 and 5 pmol was 0.9997.

Determination of ferroxidase activity

The proposed method for the determination of Fe^{III} was applied to the determination of ferroxidase activity. Fig. 2 shows chromatograms of the reaction mixture consisting of ceruloplasmin and substrate Fe^{II} . Under the condition described, Fe^{III} was eluted with a retention time of 2.2 min, and a minor peak associated with trichloroacetic acid was detected at 4.3 min. The presence of a large excess of the substrate Fe^{II} did not interfere with the measurement of the product.

The enzymatic reaction proceeded linearly for 20 min up to 10 μg of ceruloplasmin. In the range from 10 to 100 μg of ceruloplasmin, the maximum rate of Fe^{III} production was obtained with incubation for 3 min (Fig. 3). Increasing the time of incubation lowered the detection limit.

In order to examine the stability of Fe^{III} , Fe^{III} solutions containing Fe^{II} or ceruloplasmin were incubated as described in Table I. Fe^{III} could be recovered quantitatively even if the mixtures were incubated for 20 min (Table I). Moreover, no over-recovery of Fe^{III} was found so that the non-enzymatic oxidation of excess Fe^{II} to Fe^{III} could be neglected under these conditions.

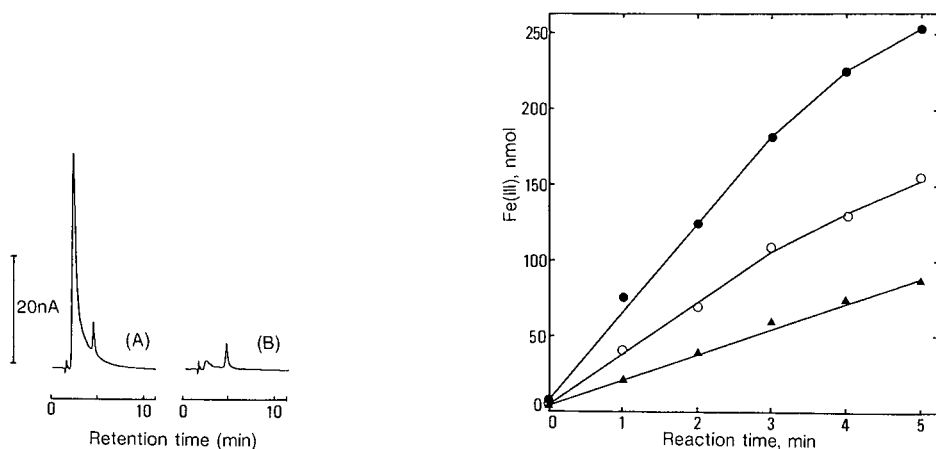


Fig. 2. Chromatograms of reaction mixtures consisting of ceruloplasmin and Fe^{II} . (A) Ceruloplasmin (50 μg) in acetate buffer (pH 5.0) containing 2 mM Fe^{II} was incubated for 3 min at 30°C. The reaction was stopped by addition of trichloroacetic acid. (B) Ceruloplasmin (50 μg) was added to a solution of trichloroacetic acid and acetate buffer containing 2 mM Fe^{II} and incubated for 3 min at 30°C. Each sample was centrifuged at 6500 g for 10 min, and 10 μl of sample were injected for ion chromatography.

Fig. 3. Time course of the generation of Fe^{III} with ceruloplasmin. Assay mixture containing (●) 100, (○) 50 or (▲) 25 μg of ceruloplasmin was incubated for the indicated time at 30°C, then the reaction was terminated by addition of 12.5% trichloroacetic acid.

TABLE I

RECOVERY OF IRON(III) ADDED TO THE INCUBATION MEDIUM

Iron(II) salt was added to acetate buffer (pH 5.0) containing Fe^{II} or ceruloplasmin, and the mixture was incubated for 3 or 20 min at 30°C. After incubation, trichloroacetic acid was added to the mixture. A 10- μl volume of each sample was used for analysis, and the appropriate blanks for correction were prepared. The peak areas of Fe^{III} in these samples were compared with that obtained from a 10- μl injection of 120 or 70 μM Fe^{III} standard solution.

Final concentration of Fe^{III} (μM)	Incubation medium		Time (min)	n	Recovery (%)	Reproducibility (R.S.D. ^a , %)
	Fe^{II} (mM)	Ceruloplasmin (μg)				
120	2	0	3	6	100	1.1
120	0	50	3	6	98	0.67
70	2	0	20	6	99	1.4
70	0	5	20	6	97	2.4

^a Relative standard deviation.

The method allowed the measurement of the activity of 0.5 μg of ceruloplasmin. The oxidation rate was proportional to the amount of the enzyme from 0.5 to 100 μg with a correlation coefficient of 0.9999 when the peak areas were measured at -0.2 V (Fig. 4).

The reproducibility of ferroxidase assay was determined by measuring the ferroxidase-generated Fe^{III} six times. The relative standard deviations for amounts of enzyme of 50 and 5 μg were 1.3 and 2.9%, respectively.

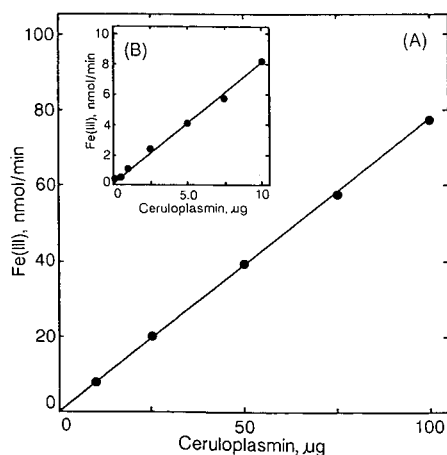


Fig. 4. Relationship between the rate of Fe^{III} generation and ceruloplasmin concentration. The reaction time was (A) 3 min or (B) 20 min.

DISCUSSION

The determination of Fe^{III} by electrochemical detection must necessarily be via the reduction step. However, the reduction process frequently introduces problems associated with oxygen interference. In addition, it is occasionally difficult to obtain the maximum response for the determination of Fe^{III} because the negative shift of the potential required for reduction is often dependent on the type of chelating agents used. Bond and Nagaosa¹¹ reported the determination of Fe^{III} as the Fe^{III}-8-hydroxyquinoline complex by reversed-phase high-performance liquid chromatography (HPLC) with electrochemical detection. To determine more than 1 ng of Fe^{III}, they had to select a potential of -0.5 V, which is unfavourable for routine analysis. Compared with their method, the use of lactic acid as the chelating agent enabled us to determine more than 0.3 ng of Fe^{III} even at -0.2 V, which is a practical and stable potential for the electrode.

Most HPLC methods for the determination of Fe^{III} are based on spectrophotometric detection, in which the eluted metal ions are detected after a post-column reaction with a chelating agent such as 4-(2-pyridylazo)resorcinol¹². Compared with this detection method, electrochemical detection is selective and simple as the separated Fe^{III} can be detected directly without a post-column reaction. This method is approximately ten times more sensitive than ion chromatography with spectrophotometric detection¹³.

Another HPLC method for the assay of ferroxidase activity based on the determination of ferroxidase-generated Fe^{III} was reported by Shioiri *et al.*¹⁴, who used an ion-exchange HPLC system connected with a UV detector, using sulphuric acid containing acetonitrile as the mobile phase. This procedure was 100 times less sensitive for the determination of Fe^{III} than our method and the measurement of the activity was limited to a narrow range of ceruloplasmin concentrations.

Takayanagi and Yashiro¹⁵ reported a ferroxidase assay procedure based on the measurement of the decrease in substrate Fe^{II} by ion chromatography coupled with spectrophotometric detection. However, this method was unsuitable for the micro-assay of iron species, as Fe^{II} was gradually oxidized to Fe^{III} under their conditions, and ferroxidase activity could not be measured accurately. In the method described here, this problem was overcome by using lactic acid at pH 3.2. This eluent reduced the blank value so that good reproducibility was obtained and over-recovery of Fe^{III} was not observed.

The ion chromatographic method coupled with electrochemical detection not only enhanced the sensitivity for the determination of Fe^{III} but also provided rapid, simple and sufficient reproducibility and recovery. This method was applicable to the determination of the ferroxidase activity of ceruloplasmin, and may be suitable for the investigation of other biological reactions associated with Fe^{III}.

REFERENCES

- 1 R. R. Crichton and M. Charlotiaux-Wauters, *Eur. J. Biochem.*, 164 (1987) 485.
- 2 V. M. Samokyszyn, D. M. Miller, D. W. Reif and S. D. Aust, *J. Biol. Chem.*, 264 (1989) 21.
- 3 S. Osaki, *J. Biol. Chem.*, 241 (1966) 5053.
- 4 S. Osaki, D. A. Johnson and E. Frieden, *J. Biol. Chem.*, 241 (1966) 2746.
- 5 F. R. Nordmeyer, L. D. Hansen, D. K. Eatough and J. D. Lamd, *Anal. Chem.*, 52 (1980) 852.

- 6 R. M. Cassidy and S. Elchuk, *Anal. Chem.*, 54 (1982) 1558.
- 7 A. M. Wang, Y. Chen and M. Wo, *Analyst (London)*, 109 (1984) 281.
- 8 H. Saito and K. Oikawa, *J. Chromatogr.*, 329 (1985) 247.
- 9 P. T. Kissinger, *Anal. Chem.*, 49 (1977) 447A.
- 10 D. C. Johnson and J. H. Larochele, *Talanta*, 20 (1973) 959.
- 11 A. M. Bond and Y. Nagaosa, *Anal. Chim. Acta*, 178 (1985) 197.
- 12 R. M. Cassidy and S. Elchuk, *Anal. Chem.*, 51 (1979) 1434.
- 13 C. O. Moses, A. T. Herlihy, J. S. Herman and A. L. Mills, *Talanta*, 35 (1988) 15.
- 14 T. Shioiri, S. Tanabe and T. Imanari, *Bunseki Kagaku*, 30 (1981) 631.
- 15 M. Takayanagi and T. Yashiro, *J. Chromatogr.*, 374 (1986) 378.

Feasibility of capillary zone electrophoresis with suppression of electroosmotic flow in completely closed systems

Th. P. E. M. VERHEGGEN, A. C. SCHOOTS and F. M. EVERAERTS*

Laboratory for Instrumental Analysis, Faculty of Chemical Technology, Eindhoven University of Technology, Eindhoven (The Netherlands)

(First received September 26th, 1989; revised manuscript received October 31st, 1989)

SUMMARY

Instrumental aspects of capillary zone electrophoresis in closed systems are reported. The combination of fixed-volume sample introduction, utilization of double-beam UV absorbance detection and the use of fixed membranes for the separation of the electrode reservoirs from the separation capillary proved to be a reliable instrumental configuration for capillary zone electrophoresis. Dispersion of eluted zones was studied as a function of capillary length. Repeatabilities of migration times and peak areas were determined. Several examples of separations of mixtures of organic acids and nucleotides are given. The separation of diluted and ultrafiltrated serum from patients with chronic renal failure proved to be promising.

INTRODUCTION

High-performance capillary electrophoresis (HPCE) 1–4, which includes various modes of capillary electrophoresis, has grown in popularity during the last decade⁵. Although electrophoretic techniques have been applied for many decades, the importance of using capillaries of, *e.g.*, Pyrex, glass, PTFE and fused silica was readily understood as evaporation of solvent is eliminated, dispersion is minimal and the development of detectors suitable for capillary systems makes it easy for researchers to start with HPCE.

Sometimes electroosmotic flow (EOF) is suppressed and in some experiments EOF is used as a pumping mechanism, especially because chromatographers show interest in these techniques^{6,7}. Therefore, stationary phases and quasi-stationary phases are used^{8–10} and a link is made between chromatography and electrophoresis. As a rule of thumb, it should be remembered that “chromatographic” interaction is generally suppressed in classical electrophoretic experiments. In this paper, capillary zone electrophoresis (CZE) with suppression of electroosmotic effects, as a specific mode of high-performance capillary electrophoresis, is described.

TABLE I
OPERATIONAL SYSTEMS USED IN CAPILLARY ZONE ELECTROPHORESIS

<i>Parameter</i>	<i>System I</i>	<i>System II</i>
Carrier electrolyte	β -Alanine (0.01 M) Acetate (pH 3.8)	MES ^a (0.01 M) Histidine (pH = 6.05)
Additive	0.05% MHEC ^b	0.05% MHEC
Capillary	PTFE, 0.2 mm I.D. ^c	PTFE, 0.2 mm I.D.
Driving current	50 μ A	35 μ A

^a MES = 2-(N-Morpholino)ethanesulphonic acid.

^b MHEC = Methylhydroxyethylcellulose.

^c Various lengths.

EXPERIMENTAL

Zone electrophoresis

The equipment used is described in detail under Results and Discussion. The separation capillary (I.D. 0.2 mm, O.D. 0.35 mm) was made of PTFE (Habia, Breda, The Netherlands). Cuprophane membranes were used in the electrode compartments. The UV absorbance detector used was a Model UV-M (Pharmacia, Uppsala, Sweden). Loading of the sample "loop" was done with a 2-ml Luer-lock syringe. A modified alpha-series (Model 807R) power supply (Brandenburg, Thornton Heath, U.K.) was used in the constant-current mode. The operational systems used are given in Table I.

Data acquisition

This was done with a Model 761S data interface and Model 2600 chromatography software (Perkin-Elmer-Nelson, Cupertino, CA, U.S.A.), running on an IBM PC/XT computer. Sampling frequencies used were 10 and 20 Hz.

Chemicals and sera

With the operational systems used, the voltage was approximately 10 kV in the constant-current mode. 2-(N-morpholino)ethanesulphonic acid (MES), histidine, β -alanine, acetic acid, picric acid, sulphanilic acid, 2,4-dihydroxybenzoic acid and *p*-nitrobenzoic acid (all of analytical-reagent grade) were purchased from Merck (Darmstadt, F.R.G.) and methylhydroxyethylcellulose (MHEC) from Serva (Heidelberg, F.R.G.). Uraemic sera were kept frozen at -20°C until use. Serum proteins were removed prior to zone electrophoretic analysis by ultrafiltration through centrifugation in Centrifree micropartition units (Amicon, Danvers, MA, U.S.A.) at 1800 *g*. Ultrafiltered serum samples were diluted 8-fold prior to injection.

RESULTS AND DISCUSSION

Instrumentation

The basic unit is shown schematically in Fig. 1. A₁ and A₂ are the electrode compartments, B is the sampling device, C the separation compartment and D the detector device.

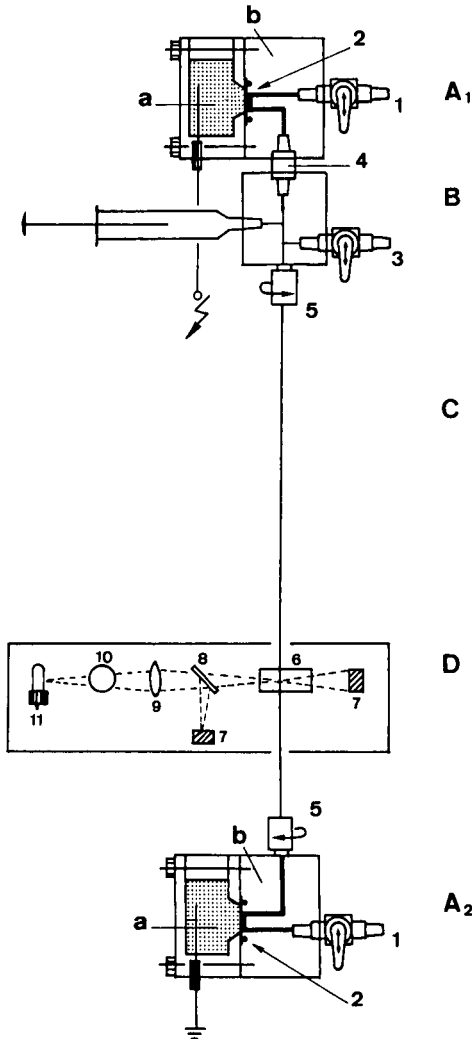


Fig. 1. Schematic diagram of electrophoretic equipment used for capillary zone electrophoresis. A_1 and A_2 = electrode blocks; B = sampling device; C = separation compartment (PTFE tubing); D = UV absorbance detector; a = electrode vessels; b = blocks used for rinsing and refilling the system; 1 = tap for rinsing and refilling the system; 2 = cuprophane semipermeable membranes; 3 = drain valve; 4 = connector of electrode block with injection system; 5 = screw connections; 6 = UV cell; 7 = photodetectors; 8 = beam splitter; 9 = lens; 10 = filter; 11 = UV source.

The electrode vessels (a) are filled with ultra pure water. The blocks (b) are provided with a channel, via which the system can be filled with electrolyte or rinsed with water via the valves 1. This channel connects the electrode vessel (a) with the sampling device and the separation compartment. Between the electrode vessels (a) and the blocks (b), flat membranes (2) are clamped by two screws and an O-ring. This means that the separation compartment is closed at both ends. If any gas is produced

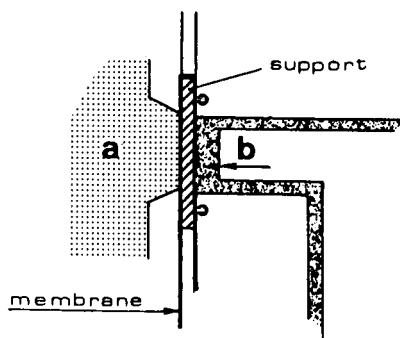


Fig. 2. Fixation of semi-permeable membrane to avoid movement during filling and rinsing. The membrane is folded around the solid support. (a) Water; (b) electrolyte.

by the electrodes, it cannot influence the analysis. Liquid applied via valves (1) passes and rinses the membranes. The volumes of the channels in the blocks (b) are large compared with the volume of the separation compartment. The potential drop in this channel, over and nearby the membrane, is small because the amount of buffer per unit length is high compared with the amount in the separation capillary. Therefore, it takes a long time before the pH jumps, which occur across the membranes owing to both the Donnan potential and electrode reactions, will enter the separation capillary and hence influence the analysis.

Movements of the membranes will affect the reproducibilities of injection and migration times. Therefore, the wetted membranes are folded and fixed around a solid support (Fig. 2). Sample solution is introduced into the sampling device through a feeder using a Luer-type syringe. This feeder and another one, which leads to waste (valve 3), are placed perpendicular to the injection channel. For a more detailed description, see ref. 11. The separation compartment is screw-connected (5) between the sampling device (B) and the electrode compartment A_2 . The volume of the sampling device is *ca.* $0.6 \mu\text{l}$. It has been reported previously that a sampling repeatability of less than 2% (relative standard deviation, R.S.D.) can be obtained, including day-to-day variation¹¹.

The separation compartment is a PTFE tube (I.D. 0.2 mm, O.D. 0.35 mm). A Model UV-M UV absorbance detector (Pharmacia) was used in the zone electrophoretic experiments. This detector was originally developed for various liquid chromatographic applications. By measuring UV absorbance with use of a beam splitter and two photodetectors instead of UV absorption, as in our isotachopheresis detector¹², the signal-to-noise ratio could be increased by a factor of at least ten. An advantage of this detector is the small optical unit, which is physically separated from the electronic control unit. Hence the optical unit can be placed easily at any position along the separation capillary, which permits monitoring the separation process. A quartz flow cell designed for high-performance liquid chromatography (HPLC) (18.0684.01; Pharmacia), which focuses the UV light in the centre of the separation capillary, is used. The flow cell is a straight flow-through cuvette. The separation capillary is drawn through the flow cell, and is consequently uninterrupted. The light from the UV source passes through the quartz wall of the cell and through the PTFE wall of the separation capillary. Therefore, the actual optical path length will be *ca.* 0.2 mm.

TABLE II

REPRODUCIBILITIES OF MIGRATION TIME AND PEAK HEIGHTS OF TEST ANIONS IN CLOSED-SYSTEM ZONE ELECTROPHORESIS ($n = 8$)

Solute	Migration time (sec)		Peak height (mm)	
	Mean	R.S.D. (%)	Mean	R.S.D. (%)
Picric acid	259.2	0.75	58.34	5.4
Sulphanilic acid	287.5	0.62	138.6	2.4
2,4-Dihydroxybenzoic acid	335.1	0.52	80.73	3.4
4-Nitrobenzoic acid	349.4	0.60	81.73	3.1

Performance of the system

For the zone-electrophoretic experiments we used operational systems I and II (see Table I). EOF was suppressed by adding MHEC to the carrier electrolyte. Assuming a zeta potential of approximately -1 mV (which is the value for HEC in PTFE tubing¹³), it can be calculated that the EOF "velocity" is only about 1% of the zone-electrophoretic velocity, and can be considered negligible. The repeatability of migration time and peak height was tested in system I using an anionic test mixture consisting of picric acid, sulphanilic acid, 2,4-dihydroxybenzoic acid and *p*-nitrobenzoic acid (all solutes of concentration 10^{-5} M). The results are given in Table II. The reproducibility of the migration time was *ca.* 0.6% (R.S.D., $n = 8$) for all components. Peak heights of the compounds in repeated injections varied between 2.4 and 5.4% (R.S.D.). These results demonstrate the possibilities of the sampling device and the usefulness of the present fixed-membrane configuration.

We determined the number of theoretical plates for the test compound sulphanilic acid at different lengths of the separation compartment. This was done by mounting a capillary of 60 cm length and moving the UV detector along the capillary. The resulting electropherograms are shown in Fig. 3. Plate numbers and plates per metre are plotted as a function of capillary length in Fig. 4. At a capillary length of *ca.* 15 cm the number of plates per metre becomes relatively independent of length (*i.e.*, 110 000 plates/m). Evidently, with shorter capillaries the contribution of instrumental factors to total band broadening becomes significant. Such factors can be related to the method of injection, *e.g.*, the shape and stability of the voltage-time curve when switching on the power supply, or diffusive wash-out of sample from "dead volumes", *e.g.*, the feeders to the injection channel. Moreover, the behaviour of the electrode compartment membranes during application of the voltage and during the analysis may be of importance. The influence of these factors may be diminished, *e.g.*, by computer control of voltage switching, choosing optimum membranes and improving the design of the sampling device and electrode blocks.

In order to estimate the smallest detectable amount of the test mixture in this equipment and electrolyte system, various dilutions of this mixture were injected. Fig. 5 shows an electropherogram of $0.6 \mu\text{l}$ injected from a $1 \mu\text{mol/l}$ solution of the test components. Each peak represents 0.6 pmol . This means that for sulphanilic acid *ca.*

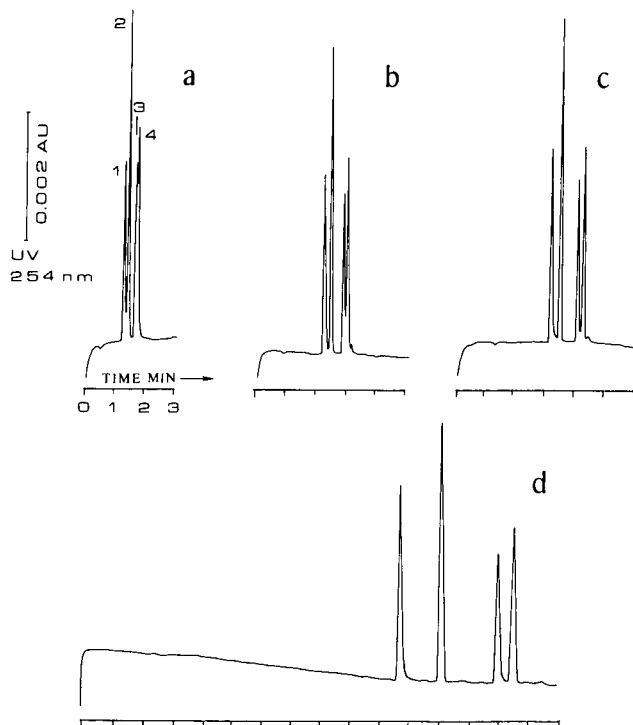


Fig. 3. Zone electropherograms of a test mixture of acids (electrolyte system I, Table I). The UV detector was placed at different positions along a separation capillary of 60 cm length. (a) 8 cm; (b) 13 cm; (c) 18 cm; (d) 58 cm. Peaks: 1 = picric acid; 2 = sulphanilic acid; 3 = 2,4-dihydroxybenzoic acid; 4 = *p*-nitrobenzoic acid.

10 pg (0.1 $\mu\text{mol/l}$), present in the original injection volume, can be detected. However, when diffusion coefficients of the test solutes are smaller, *i.e.*, with larger molecules, the plate number is expected to increase^{14,15} and consequently lower detection limits can be obtained, assuming these solutes have UV absorption in the range selected. By using a capillary that is more transparent for UV light, the signal-to-noise ratio will increase, and consequently lower detection limits are possible.

A calibration line of peak area *versus* amount injected was obtained for aqueous solutions of hippuric acid. Constant volumes (0.6 μl) of solutions with different concentrations were injected. The calibration line is shown in Fig. 6. The following linear model was fitted to the data: $\text{area} = (19.738 \cdot \text{amount}) - 27.2$. The correlation coefficient was $r = 0.998$ ($P < 0.0001$). This demonstrates a very good fit of peak area *versus* concentration. It should be noted, however, that these results cannot be extrapolated to the quantification of specific solutes in complex samples, *e.g.*, blood serum.

In Fig. 7 a zone electropherogram is shown of the test mixture. On the left the concentrations of the components are all $2 \cdot 10^{-5} \text{ M}$. On the right the concentration of sulphanilic acid is 100 times that of the other solutes. The migration times of components 3 and 4 changed by *ca.* 3%. The high concentration difference of sulphanilic acid causes a sharpening of the zone boundaries of the ionic solutes migrating with a lower effective mobility.

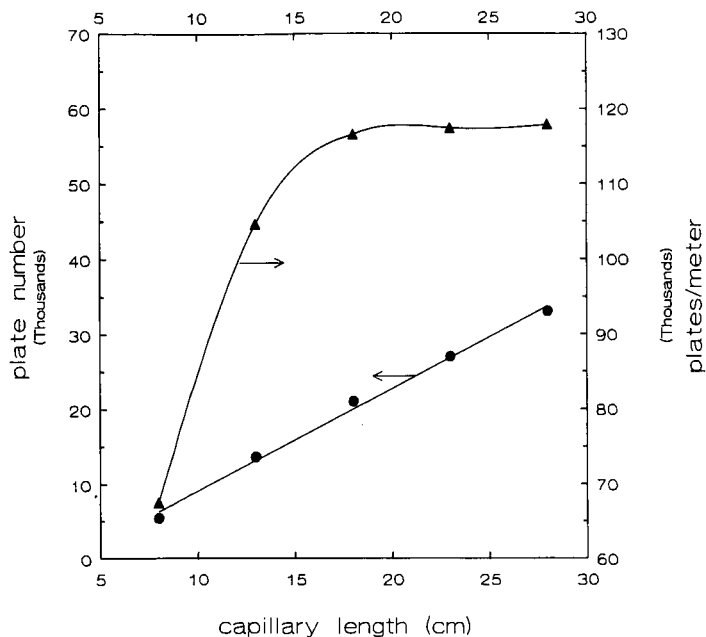


Fig. 4. Plots of number of theoretical plates and plates per metre as a function of length of separation compartment. Test compound, sulphanilic acid.

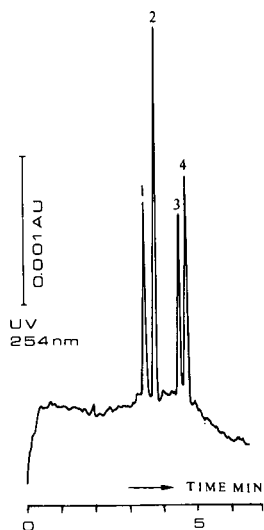


Fig. 5. Zone electropherogram of a standard test mixture at low concentration (electrolyte system I, Table I). Peaks as in Fig. 3. Each peak represents 0.6 pmol injected.

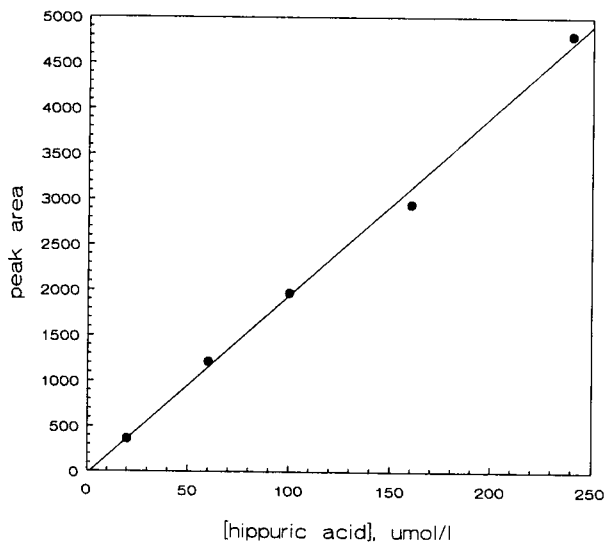


Fig. 6. Calibration line of hippuric acid concentration in aqueous solution *versus* peak area in CZE analysis. For statistics see text.

Applications

Nucleotides. In order to illustrate the difference in selectivity between the closed system with CZE (and no EOF) and that with CZE with EOF, a mixture of the nucleotides ATP, ADP, UMP, GMP, and AMP was analysed in system I (see Table

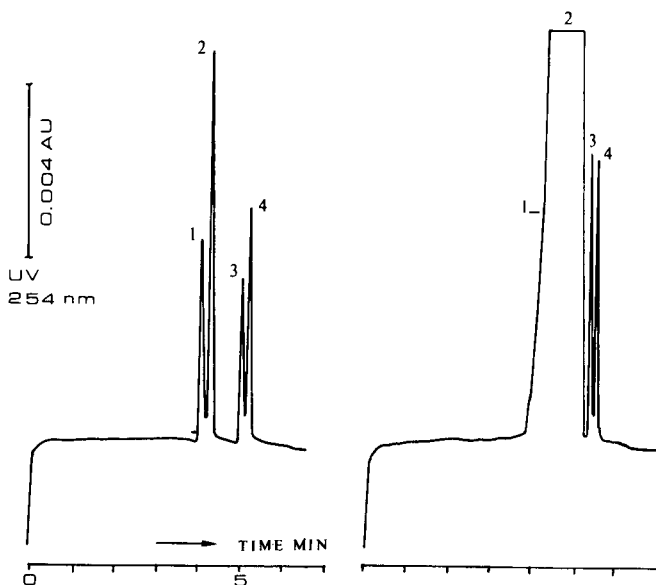


Fig. 7. Zone electropherograms of the test mixture, as shown in Fig. 3 (electrolyte system I, Table I). The concentration of sulphanic acid is 100 times that of the other solutes. Peaks as in Fig. 3.

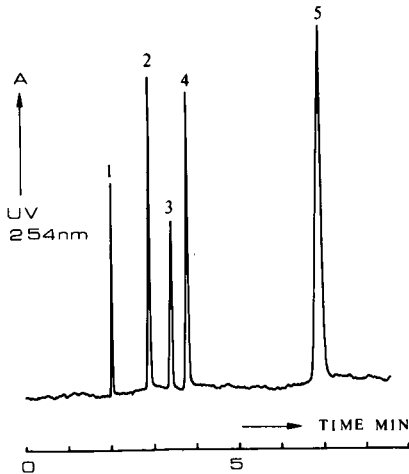


Fig. 8. Zone electropherogram of nucleotides analysed in electrolyte system I (Table I). Peaks: 1 = ATP; 2 = ADP; 3 = UMP; 4 = GMP; 5 = AMP. Length of separation capillary, 16 cm.

D). The concentrations injected were $2 \cdot 10^{-5} M$ for all solutes. The results are shown in Fig. 8. The elution order in this zone-electrophoretic experiment is opposite to that reported by Tsuda *et al.*¹⁶, which is explained by the fact that the latter workers used EOF in addition to differences in electrophoretic mobility¹⁷.

Anions in uraemic sera. Blood levels of many substances are raised in patients with chronic renal failure. They include nitrogenous waste products such as urea, creatinine, uric acid and methylguanidine, organic (aromatic) acids, polyols, aluminium, the hypothetical "middle molecules", parathormone, β_2 -microglobulin and many others^{18,19}. We studied the kinetic behaviour and distribution between patients of a range of accumulated solutes by HPLC^{20,21}. This HPLC profiling technique was designed to monitor UV-absorbing and fluorescent solutes from different solute classes. Both anionic and cationic substances were analysed. Especially the organic (aromatic) acids may play an important role in the etiology of the uraemic manifestations. Therefore, it is of importance to determine the aromatic acids in uraemic sera. This can be achieved by sample pretreatment prior to HPLC, *e.g.*, solid-phase extraction or isotachophoretic preseparation of anions²². However, capillary zone electrophoresis seems to be promising for the one-step analysis of these solutes in uraemic sera.

Ultrafiltered serum from an uraemic patient was analysed using operational system II (Table I). The elution pattern shown in Fig. 9 was obtained. Duplicate profiles from two separate injections are shown. As can be seen, they are highly reproducible. Peak identification was effected by co-elution of the respective compounds with the serum samples, and by comparison with the earlier described HPLC profiles in which these compounds were also detected by UV absorbance at 254 nm. Repeatabilities of peak height, peak area and migration time of uric acid in this complex mixture are listed in Table III. The determination of hippuric acid in uraemic sera by capillary zone electrophoresis will be compared with HPLC in another publication²³. In the electropherograms it can be seen that some early eluting peaks are very sharp. The number of theoretical plates, as defined by Giddings¹⁴, was calculat-

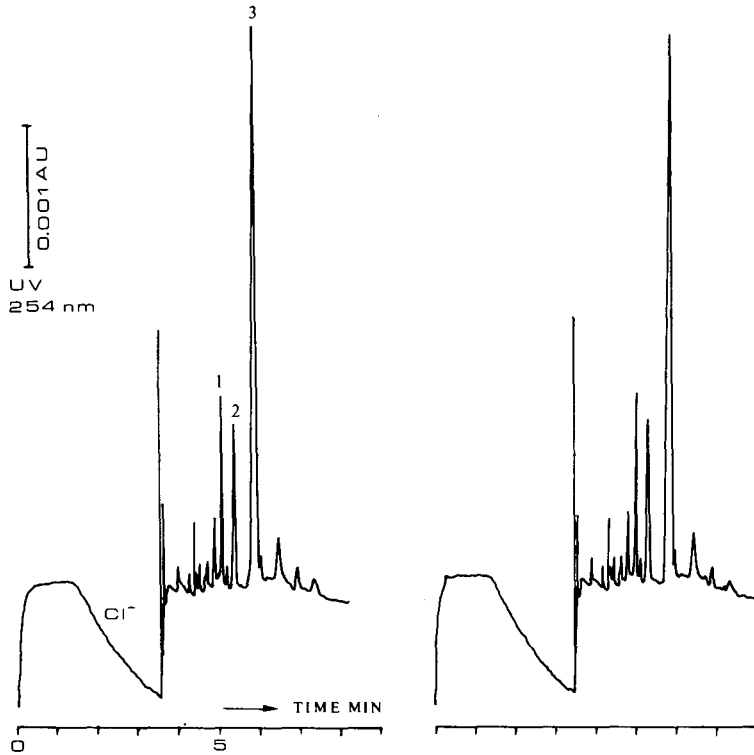


Fig. 9. Duplicate analyses, demonstrating repeatability, of zone electrophoretic separation of UV-absorbing anions in ultrafiltered uraemic sera (electrolyte system II, Table I). Peaks: (tentative): 1 = hippuric acid; 2 = *p*-hydroxyhippuric acid; 3 = uric acid. Length of separation capillary, 25 cm.

ed for these peaks and amounted over 10^6 (see also Fig. 8). This phenomenon will be described elsewhere, because it is rather complex, but Kohlrausch' law²⁴ must be obeyed. This results in a sharpening up after a large concentration "disturbance". The large negative peak observed in the electropherograms originates from chloride present in the serum samples (at approximately 110 mmol/l in the undiluted sample).

TABLE III

REPRODUCIBILITY OF MIGRATION TIME, PEAK AREA AND PEAK HEIGHT OF URIC ACID IN ULTRAFILTRATED URAEMIC SERUM, AFTER REPEATED INJECTION ($n = 5$)

Parameter	Mean	R.S.D. (%)
Migration time (s)	403	0.73
Peak area (μ Vs)	44 741	6.5
Peak height (μ V)	8294	4.5

CONCLUSION

It has been shown that zone electrophoresis in PTFE capillaries (I.D. 0.2 mm) with the described instrumental set-up is reliable with respect to migration time and peak area for several samples. Suppression of electroosmotic effects could be achieved by separating the electrode compartments from the separation compartment, and by adding a surface-active agent to the carrier electrolyte. Any hydrodynamic movement of the background electrolyte was avoided with the closed system. It was shown that the distance between injection compartment and detector should be at least 15 cm in order to avoid instrumental factors of dispersion. Experiments have shown that injections of solutes both in distilled water and in salt gradients gave a sharpening up of the zone boundaries. Plate numbers as large as 10^6 could be achieved.

ACKNOWLEDGEMENT

The authors thank Pharmacia Nederland (Woerden, The Netherlands) for their instrumental support with respect to UV detection.

REFERENCES

- 1 F. M. Everaerts and W. M. L. Hoving-Keulemans, *Sci. Tools*, 17 (1970) 25.
- 2 R. Virtanen, *Acta Polytech. Scand.*, 123 (1974) 1.
- 3 F. E. P. Mikkers, F. M. Everaerts and Th. P. E. M. Verheggen, *J. Chromatogr.*, 169 (1979) 1.
- 4 F. E. P. Mikkers, F. M. Everaerts and Th. P. E. M. Verheggen, *J. Chromatogr.*, 169 (1979) 11.
- 5 A. G. Ewing, R. A. Wallingford and T. M. Olefirowicz, *Anal. Chem.*, 61 (1989) 292A.
- 6 J. W. Jorgenson and K. DeArman Lukacs, *J. Chromatogr.*, 218 (1981) 209.
- 7 J. H. Knox and I. H. Grant, *Chromatographia*, 24 (1987) 135.
- 8 A. S. Cohen and B. L. Karger, *J. Chromatogr.*, 397 (1987) 409.
- 9 S. Terabe, K. Otsuka, K. Ichokawa, A. Tsuchiya and T. Ando, *Anal. Chem.*, 56 (1984) 111.
- 10 J. Snopek, I. Jelinek and E. Smolková-Keulemansová, *J. Chromatogr.*, 452 (1988) 571.
- 11 Th. P. E. M. Verheggen, J. L. Beckers and F. M. Everaerts, *J. Chromatogr.*, 452 (1988) 615.
- 12 F. M. Everaerts, J. L. Beckers and Th. P. E. M. Verheggen, *Isotachopheresis—Theory, Instrumentation and Applications*, Elsevier, Amsterdam, 1976.
- 13 J. C. Reijenga, G. Aben, Th. P. E. M. Verheggen and F. M. Everaerts, *J. Chromatogr.*, 260 (1983) 241.
- 14 J. C. Giddings, *Sep. Sci.*, 4 (1969) 181.
- 15 F. Foret, M. Deml and P. Boček, *J. Chromatogr.*, 452 (1988) 601.
- 16 T. Tsuda, G. Nakagawa, N. Sato and K. Yagi, *J. Appl. Biochem.*, 5 (1983) 330.
- 17 F. M. Everaerts, A. A. A. M. van de Goor, Th. P. E. M. Verheggen and J. L. Beckers, *J. High Resolut. Chromatogr.*, 12 (1989) 28.
- 18 M. R. Wills, *Clin. Chem.*, 31 (1985) 5.
- 19 A. Schoots, F. Mikkers, C. Cramers, R. De Smet and S. Ringoir, *Nephron*, 38 (1984) 1.
- 20 A. C. Schoots, J. B. Dijkstra, S. M. G. Ringoir, R. Vanholder and C. A. Cramers, *Clin. Chem.*, 34 (1988) 1022.
- 21 A. C. Schoots, P. G. G. Gerlag, A. W. Mulder, J. A. G. Peeters and C. A. M. G. Cramers, *Clin. Chem.*, 34 (1988) 91.
- 22 A. C. Schoots and F. M. Everaerts, *J. Chromatogr.*, 277 (1983) 328.
- 23 A. C. Schoots, Th. P. E. M. Verheggen, P. M. J. M. de Vries and F. M. Everaerts, *Clin. Chem.*, in press.
- 24 F. Kohlrausch, *Ann. Phys. Chem.*, 62 (1897) 209.

Note

Enantiomer separation of chiral barbiturates and of α -lipoic acid by capillary gas chromatography with modified cyclodextrins as chiral stationary phases

WILFRIED A. KÖNIG*, SABINE LUTZ and PETRA EVERS

Institut für Organische Chemie, Universität Hamburg, Martin-Luther-King-Platz 6, D-2000 Hamburg 13 (F.R.G.)

and

JOACHIM KNABE

Fachrichtung Pharmazeutische Chemie, Universität des Saarlandes, D-6600 Saarbrücken (F.R.G.)

(First received September 6th, 1989; revised manuscript received October 26th, 1989)

Knowledge of the difference in activity of stereoisomeric drugs has initiated the development of new methods for enantiomer separation and stereochemical analysis¹. Sensitive and accurate procedures for the determination of the enantiomeric composition of chiral drugs are not only important in cases where one of the enantiomers has toxic properties (*e.g.*, DOPA, penicillamine) but may also be utilized to study pharmacokinetics and the enantioselective metabolism of a chiral drug.

In previous investigations we have demonstrated the gas chromatographic enantiomer separation of pharmaceuticals of the amino alcohol type^{2–4} (β -blockers, adrenergic drugs), some barbiturates², panthenol⁵, penicillamine⁶ and some others¹ using chiral polysiloxanes, *e.g.*, XE-60-L-valine-(*R*)- α -phenylethylamide, as stationary phases. More recently we have shown that hydrophobic derivatives of cyclodextrins can also be applied for the separation of pharmaceuticals (succinimides⁷, drugs of the amine⁸ and amino alcohol⁹ type).

In this work, improved resolutions of racemic barbiturates and the first separation of the enantiomers of α -lipoic acid are demonstrated.

EXPERIMENTAL

The preparation of hexakis(2,3,6-tri-O-pentyl)- α -cyclodextrin¹⁰ (Lipodex A) and of heptakis(3-O-acetyl-2,6-di-O-pentyl)- β -cyclodextrin⁸ (Lipodex D) has been described previously (Pyrex glass capillary columns containing Lipodex cyclodextrin derivatives are available from Macherey, Nagel & Co., Düren, F.R.G.). Pyrex glass capillaries were coated according to the static procedure¹¹ using a Silanox interlayer².

Carlo Erba Model 2101 gas chromatographs with split injection and flame ionization detection were used for gas chromatographic investigations.

The optically active barbiturates were prepared by the separation of racemic

intermediates according to the procedure described by Knabe *et al.*¹². Racemic α -lipoic acid and both enantiomers were kindly supplied by B. Büchele (Kirchberg, F.R.G.).

RESULTS AND DISCUSSION

About 40% of the pharmaceuticals which are obtained synthetically are chiral but only about 10% of them are applied as pure enantiomers, 90% being used in the racemic form, in spite of the fact that in many instances the enantiomers show distinct differences in their pharmacological effects. With barbiturates, it was proved by Knabe *et al.*¹² that the narcotic effects of the enantiomers of N-alkylated barbiturates differ markedly. In some instances one of the enantiomers even displays convulsive properties. The enantiomers also show different pharmacokinetic properties. The enantiomeric purity of barbiturates has been determined by the isotope dilution method or, more efficiently, by NMR spectroscopy using chiral lanthanide shift reagents. The precision of these methods for small amounts of enantiomeric impurities is far from satisfactory.

We have found that alkylated or selectively alkylated and acylated derivatives of cyclodextrins are highly enantioselective chiral stationary phases and can be used to separate a wide variety of compounds by capillary gas chromatography¹³. These separations are independent of hydrogen-bonding interactions and are therefore possible also with substrates of medium or low polarity (saturated and unsaturated

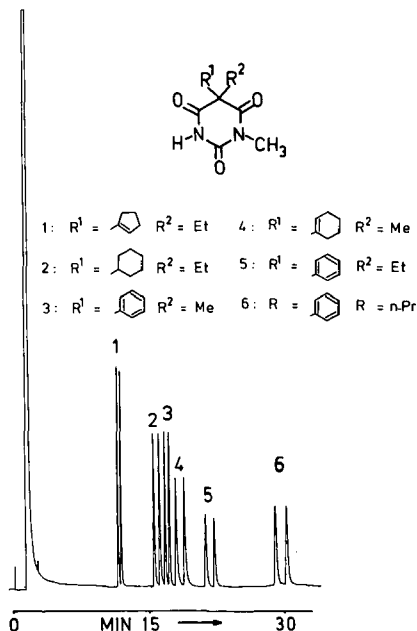


Fig. 1. Enantiomer separation of some N-alkylated barbiturates; (*R*)-enantiomers are eluted before (*S*)-enantiomers. Pyrex glass capillary column (36 m) with hexakis(2,3,6-tri-*O*-hexyl)- α -cyclodextrin; column temperature 180°C; carrier gas, hydrogen at 1 bar. Et = Ethyl; Me = methyl; Pr = propyl.

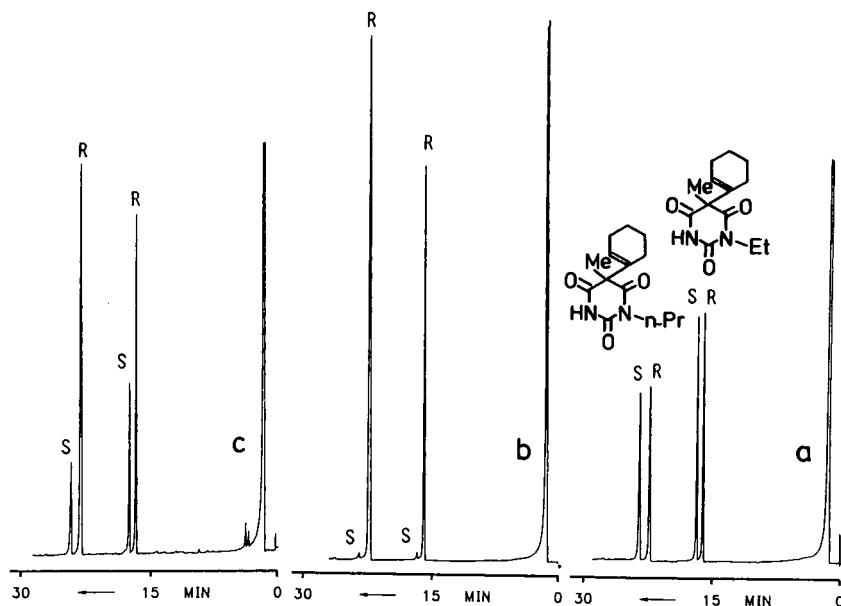


Fig. 2. (a) Enantiomer separation of *N*-alkyl-*nor*-hexobarbitals, (b) investigation of enantiomeric purity of (*R*)-enantiomers and (c) assignment of the order of elution. Column temperature, 195°C; for other details see Fig. 1.

hydrocarbons, alkyl halides, spiroacetals, lactones, ketones, etc.) that cannot be separated on columns with chiral polysiloxanes¹⁴. The enantiomers of *N*-alkylated barbiturates can be resolved on peralkylated cyclodextrins (e.g., perpentylated α -cyclo-

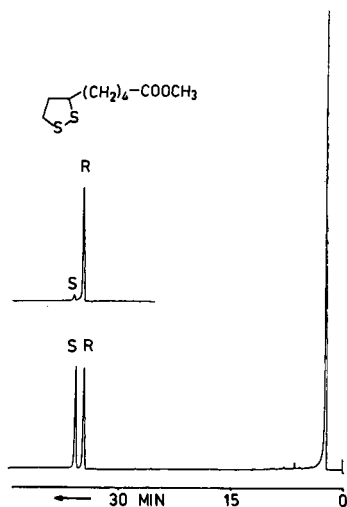


Fig. 3. Enantiomer separation of α -lipoic acid methyl ester (esterification with diazomethane) and determination of enantiomeric purity of the (*R*)-enantiomer. Pyrex glass capillary column (40 m) with Lipodex D; column temperature, 180°C; carrier gas, hydrogen at 1 bar.

dextrin, Lipodex A or perhexylated α -cyclodextrin) at column temperatures between 180 and 220°C, as shown in Figs. 1 and 2. Even minute contributions of enantiomeric impurities can be detected. In Fig. 2b the ratio of (*R*)- to (*S*)-enantiomers is 97.99:2.01 for the N-ethyl derivative and 98.64:1.36 for the N-*n*-propyl derivative. It can be assumed that enantiomeric contributions of less than 1% could be quantified in this instance. The smallest precisely detectable contribution may be even smaller if the order of elution of the enantiomers is reversed. The detection limit greatly depends, however, on the separation factor (α -value) and may be as low as 0.1% in favourable instances. In all separations the (*R*)-enantiomers are eluted prior to the (*S*)-enantiomers. Compounds substituted at the chiral centre by two alkyl groups differing by only one CH₂ group were separated incompletely or not at all.

Some chiral barbiturates have also been separated by liquid chromatography. Thus hexobarbital was resolved on triacetylcellulose by Koller *et al.*¹⁵ and the same compound together with other barbiturates by Yang *et al.*¹⁶ on a Pirkle-type phase.

α -Lipoic acid (Fig. 3) is involved in the oxidative decarboxylation of pyruvic acid to activated acetaldehyde, which is bound to α -lipoic acid and transferred to coenzyme A to form acetyl coenzyme A. It is also claimed to be an efficient detoxicant and is administered as its racemate (thioctacid) in the treatment of liver diseases. Although natural (+)- α -lipoic acid has the (*R*)-configuration, it is not known if the unnatural (*S*)-enantiomer has equivalent activity. As shown in Fig. 3, the enantiomers can be easily separated on heptakis(3-O-acetyl-2,6-di-O-pentyl)- β -cyclodextrin (Lipodex D), and it would be interesting to study the relationship between the stereochemistry and pharmacological activity of this compound.

ACKNOWLEDGEMENTS

This work was supported in part by the Bundesminister für Forschung und Technologie (project No. 0319134 A) and by the Fonds der Chemischen Industrie.

REFERENCES

- 1 W. A. König, in I. W. Wainer and D. E. Drayer (Editors), *Drug Stereochemistry*, Marcel Dekker, New York, Basle, 1988, p. 113.
- 2 W. A. König and K. Ernst, *J. Chromatogr.*, 280 (1983) 135.
- 3 W. A. König, K. Ernst and J. Vessman, *J. Chromatogr.*, 294 (1984) 423.
- 4 W. A. König, O. Gyllenhaal and J. Vessman, *J. Chromatogr.*, 356 (1986) 354.
- 5 W. A. König and U. Sturm, *J. Chromatogr.*, 328 (1985) 357.
- 6 W. A. König, E. Steinbach and K. Ernst, *J. Chromatogr.*, 301 (1984) 129.
- 7 W. A. König, S. Lutz, C. Colberg, N. Schmidt, G. Wenz, E. von der Bey, A. Mosandl, C. Günther and A. Kustermann, *J. High Resolut. Chromatogr. Chromatogr. Commun.*, 11 (1988) 621.
- 8 W. A. König, S. Lutz, G. Wenz and E. von der Bey, *J. High Resolut. Chromatogr. Chromatogr. Commun.*, 11 (1988) 506.
- 9 W. A. König, *Carbohydr. Res.*, 192 (1989) 51.
- 10 W. A. König, S. Lutz and G. Wenz, *Angew. Chem.*, 100 (1988) 989; *Angew. Chem., Int. Ed. Engl.*, 27 (1988) 979.
- 11 J. Bouche and M. Verzele, *J. Gas Chromatogr.*, 6 (1968) 501.
- 12 J. Knabe, W. Rummel, H. P. Büch and N. Franz, *Arzneim.-Forsch./Drug Res.*, 28 (1978) 1048.
- 13 W. A. König, *Nachr. Chem. Tech. Lab.*, 37 (1989) 471.
- 14 W. A. König, *The Practice of Enantiomer Separation by Capillary Gas Chromatography*, Hüthig, Heidelberg, 1987.
- 15 H. Koller, K. H. Rimbock and A. Mannschreck, *J. Chromatogr.*, 282 (1983) 80.
- 16 Z. U. Yang, S. A. Barkan, C. Brunner, J. D. Weber, T. D. Doyle and I. W. Wainer, *J. Chromatogr.*, 324 (1985) 444.

Note

Capillary gas chromatographic determination of sulphadimidine in pork tissues

SVATOMÍR KMOŠŤÁK* and MIROSLAV DVOŘÁK

Research Institute of Feed Supplements and Veterinary Drugs, Pohoři-Chotouň, 254 49 Jilové near Prague (Czechoslovakia)

(First received July 7th, 1989; revised manuscript received October 27th, 1989)

Sulphonamides are important drugs in veterinary practice for the prevention and treatment of diseases and for promotion of animal growth. Therefore, it is essential to monitor human foodstuffs for drug residues resulting from both the promotion and treatment. Many chromatographic methods, such as thin-layer chromatography (TLC), high-performance liquid chromatography (HPLC) and gas-liquid chromatography (GLC) have been utilized for the determination of residual sulphonamides in animal tissues and comparisons of these methods have been published^{1–3}. Owing to the large number of samples that must be tested for sulphonamides it is of the utmost importance that the method utilized should be rapid and practical with a sensitivity below 100 ppb. HPLC methods are now preferred⁴, because in contrast to GLC^{5,6} no derivatization steps are required and it is less complicated than TLC separations⁷.

For the GLC procedure it is necessary to convert sulphonamides into suitable derivatives with good chromatography behaviour that are highly electronegative and amenable to sensitive electron-capture detection (ECD). The most common derivatization involves either a single-stage N¹-methylation of the polar acidic sulphamoyl group with diazomethane^{8–10} or N¹-methylation followed by acylation of the N⁴-primary amino function with pentafluoroalkane carboxylic anhydride^{11,12}. Our method uses sorption of the residual sulphadimidine N¹-(4,6-dimethyl-2-pyrimidyl) sulphanilamide from an organic extract on activated alumina¹³ and N¹-extractive methylation¹⁴, followed by N⁴-acetylation with trifluoroacetic anhydride. This method should prove convenient for the determination of residual levels of sulphadimidine (SDM) with rapid derivatization steps by means of high-resolution capillary gas chromatography with ECD and the possibility of the gas chromatographic-mass spectrometric (GC-MS) confirmation of sulphonamide residues.

EXPERIMENTAL

Chemicals and reagents

The solvents chloroform, dichloromethane, toluene (analytical-reagent grade) (Chemapol, Prague, Czechoslovakia) and acetonitrile (VEB-Laborchemie, GDR) were doubly distilled in an all-glass apparatus with added P₂O₅ and cleaned on a

chromatographic column filled with activated silica (70–230 mesh) (Merck, Darmstadt, F.R.G.) and basic alumina (Lachema, Brno, Czechoslovakia). *n*-Heptane (spectroscopic grade) from Chemapol was dried for 48 h with LiAlH_4 , distilled and cleaned on a chromatographic column filled with activated silica (Merck). Carbonate buffers, 0.2 *M* (pH 11) and 0.5 *M* (pH 9.5), were prepared from 0.2 *M* and 0.5 *M* solutions of NaCO_3 and NaHCO_3 . Acetate buffer 1 *M* (pH 5.5), was prepared from 1 *M* acetic acid and 1 *M* sodium acetate solutions. Tetrabutylammonium hydroxide (TBAH) buffer (0.1 *M*) was prepared from tetrabutylammonium bromide (Fluka, Buchs, Switzerland) by neutralization with 0.1 *M* NaOH, diluted to volume in a volumetric flask with 0.5 *M* carbonate buffer (pH 5.5) and cleaned by extraction with 50 ml of dichloromethane and 2×50 ml of *n*-heptane. Neutral activated alumina (Brockman activity 1) was prepared from chromatographic-alumina (100–200 mesh) (Reanal, Budapest, Hungary) by activation for 6 h at 450°C. The reagents methyl iodide (gold label; Aldrich, F.R.G.) as a 0.16 *M* solution in dichloromethane, 4-dimethylaminopyridine (4-DMAP) (Sigma, F.R.G.) as a 2 mg/ml solution in toluene–acetonitrile (95:5), trifluoroacetic anhydride (TFAA) and octamethylcyclotetrasiloxane (D_4) were obtained from Fluka, hexamethyldisilazane (HMDS) from Lachema and sulphadimidine base from Spofa (Czechoslovakia).

Sample preparation and purification

To 5 g of homogenized tissue sample in a 50-ml glass centrifuge tube, 5 ml of acetate buffer (pH 5.5) and 10 ml of ethyl acetate–chloroform (1:1) were added. The mixture was stirred on an Ultra-Turrax at low speed. After a second addition of 10 ml of the extraction mixture to the sample, centrifugation was carried out at 250 *g*. The organic layer was dried by passage through a 3-cm layer of anhydrous Na_2SO_4 in a 5-ml pipette tip and transferred to a 60×8 mm sorption microcolumn with layers of 0.2 g of sea sand at the bottom, 0.3 g of activated alumina and 0.2 g of sea sand at the top, in a vacuum manifold flow-rate (*ca.* 2 ml/min). After application of 2×1 ml of chloroform to each microcolumn, the vacuum was increased. When the moisture on the outside walls disappeared, the column was eluted with 500 μl of carbonate buffer (pH 11).

Derivatization

*N*¹-Extractive alkylation. To a 100 μl of buffered effluent in 1-ml amber-colored Reacti-Vials, 100 μl of TBAH solution in 0.5 *M* carbonate buffer was added. After the addition of 200 μl of 0.16 *M* methyl iodide solution in dichloromethane, the Reacti-Vials were firmly capped and heated for 10 min at 70°C in a dry-heated block, then thoroughly shaken in shaker for 20 min. Phase separation was effected by centrifugation at 250 *g*. A 100- μl bottom organic layer was withdrawn in to 3 ml Reacti-Vials and evaporated at 40°C under gentle stream of nitrogen.

*N*⁴-Trifluoroacetylation. A 1-ml volume of mixture of 4-DMAP in toluene–acetonitrile (95:5) and 50 μl of TFAA were added to each dry residue. The vials were heated for 20 min at 70°C. After the reaction was completed¹⁵, the vials were cooled to room temperature, 1 ml of 3% NaHCO_3 was added and the vials were shaken. After centrifugation at 50 *g*, 100 μl of the organic layer were withdrawn into 900 μl of *n*-heptane and 3 μl of each sample were then injected by an autosampler (ALS) into the capillary column in the splitless mode.

Calculations

A calibration graph was obtained using 12.5, 25.0, 125.0 and 250.0 ng/ml of underivatized SDM solution in the extraction mixture to give 50, 100, 500 and 1000 ppb levels for raw tissue samples. After the sorption and derivatization steps with 20 ml of this mixture four calibration measurements were made at each level. The equation for the resulting line ($P \leq 0.05$) was $y = 1.9845 \cdot 10^{-5}x - 0.1011$ ($r = 0.9975$). The external standard method on the peak area of SDM in unknown samples was employed to calculate their concentrations from the calibration graph.

Instrumental

Analyses were performed on a Hewlett-Packard 5880A level IV gas chromatography with split-splitless injection, a Model 7671A autosampler and a ^{63}Ni electron-capture detector. An Ultra 1 capillary column (25 mm \times 0.2 mm I.D., 0.33 μm film thickness (Hewlett-Packard, Avondale, PA, U.S.A.) was connected to a 1 m \times 0.2 mm I.D. deactivated retention gap by a butt connector (all from Supelco, Bellefonte, PA, U.S.A.) to the injection port. Data collection and integration were performed for a set 0.02-min peak width, attenuation 2×10 , threshold 9 and chart speed 0.5 cm/min.

Instrumental conditions

The injection port and detector temperature were set at 200 and 350°C, respectively. The oven temperature programme was 80°C initial temperature, 1-min hold; 30°C/min to 290°C; 20°C/min to 320°C, 1-min hold; and post-column 325°C, 1-in hold.

The carrier gas was Ultra-pure helium (Messer and Griesheim, Austria) at a flow-rate of 0.3 ml/min, cleaned via an oxygen filter and molecular sieve 5A, head pressure 200 kPa, splitting ratio 1:50, septum purge 1 ml/min and splitless delay 1 min. The make-up gas was argon-methane (95:5) (Messer and Griesheim) at a flow-rate of 50 ml/min, regulated through a base flow unit (BFU 101; Chrompack, Middelburg, The Netherlands), inlet pressure 70 kPa, cleaned over activated charcoal and molecular sieve 5A in series.

The capillary column was conditioned at 300°C for 24 h, $5 \times 80^\circ\text{C}$ for 1 h and $5 \times 320^\circ\text{C}$, 1-h hold. The solvent effect was determined with five 3- μl *n*-heptane injections with the model 7671A autosampler. The retention time for derivatized SDM under these conditions was 8.43 ± 0.00 min for base-horizontal separation.

RESULTS AND DISCUSSION

The accuracy and precision of the method for the determination of SDM in standard samples at two sensitivity levels are presented in Table I. The results for the retention time repeatability and chromatograms for real samples (Fig. 1) indicate that the method is selective and sensitive. The splitless injection mode is a suitable technique for the determination of residual SDM in pork tissues. The source of errors arises from the separation and derivatization procedures. For separation we used solvent extraction from buffered samples excluding the influence of other endogenous substances from tissue matrix^{16,17} on the accuracy and precision of the method.

The extraction recovery from tissues was determined by quadruplicate addition of SDM solvent solution to each homogenized tissue sample. The absolute recovery

TABLE I

ACCURACY AND PRECISION OF DETERMINATION OF SULPHADIMIDINE IN STANDARD SAMPLES

Results calculated as the means of six determinations.

Sensitivity for peak level (pg)	Retention time (min) (mean \pm S.D.)	Relative standard deviation (%)	
		Intra-	Inter- ^a
5	8.427 \pm 0.0013	1.01	7.99
100	8.426 \pm 0.0015	3.46	6.76

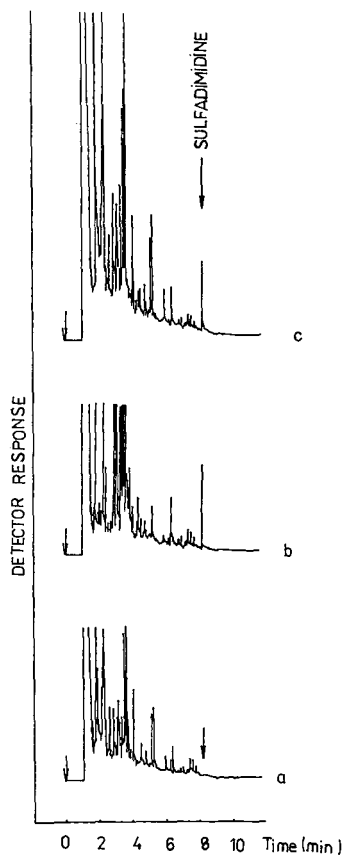
^a Calculated from four determinations.Fig. 1. Typical gas chromatograms of extracts carried through the procedure: (a) blank liver; (b) liver extract from 10th day after the end of 5 days treatment; (c) sulphadimidine standard, $0.05 \mu\text{g g}^{-1}$.

TABLE II
RECOVERIES OF SULPHADIMIDINE FROM PORK TISSUES

Results calculated as the means of four determinations.

<i>Sample</i>	<i>SDM added to 1 g of tissue (ng)</i>	<i>SDM recovered after extraction (ng) (mean ± S.D.)</i>	<i>Recovery (%)</i>	<i>R.S.D. (%)</i>
Flesh (ham)	50	43.21 ± 4.04	87.08	9.27
Kidney	50	34.63 ± 1.68	69.26	4.86
Liver	50	40.21 ± 2.02	80.42	5.02

was calculated by comparing the calibration graph for SDM with results obtained using the described procedure with spiked samples (Table II). Our results at a spiking level of 50 ppb were lower than those with the HPLC method only for kidney¹⁸. For liver at a spiking level of 100 ppb and the some solvent extraction system a recovery 50.8% has been achieved¹⁹ and for extraction with acetone-chloroform (1:1) a recovery of 84.3%⁸. The results of the recovery studies depend on the calibration procedure used and the polarity of the extraction system²⁰. The large variations in the recovery studies show a significant matrix effect as a result of the higher fats and glucuronide content of organ samples. The lower recovery from pig kidney is probably due to the high adsorption of free SDM in this organ²¹.

Our method, involving the sorption of residues on activated neutral alumina as a purification step, followed by rapid derivatization, is suitable for routine analysis. Under the operating conditions a detection limit of 10 ppb, corresponding to a minimum of 1 pg of derivatized SDM (at a signal-to-noise ratio > 10) was achieved. For this picogram detection limit its critical to have very pure solvents and a thoroughly deactivated injection liner. The method has been used for the determination of residual SDM in pork tissue after 5 days of continuous feeding with a dosage at the level of 50 mg of SDM per kilogram live weight (Table III). This method is rapid and enables

TABLE III
SULPHADIMIDINE RESIDUAL CONCENTRATION IN PORK TISSUES AFTER 5 DAYS OF CONTINUAL FEEDING WITH A DOSAGE AT THE LEVEL OF 50 mg OF SDM PER KILOGRAM LIVE WEIGHT

Results calculated as the means of two determinations, made 6, 10, 16 and 20 days after the end of 5 days treatment.

<i>Sample</i>	<i>SDM (ng/g) after day</i>			
	<i>6</i>	<i>10</i>	<i>16</i>	<i>20</i>
Liver	120	160	^a	N.D.
Kidney	180	110	N.D.	N.D.
Lungs	100	80	50	N.D.
Flesh (ham)	60	N.D.	N.D.	N.D.
Blood	80	N.D.	N.D.	N.D.

^a Below the detection limit of the method (10 ng/g).

ten samples to be prepared simultaneously. Over 100 injections of tissue extracts have been performed without changing the splitless liner.

REFERENCES

- 1 A. J. Malanovski, Ch. J. Barnes and T. Fazio, *J. Assoc. Off. Anal. Chem.*, 67 (1981) 1386.
- 2 J. E. Matusik, Ch. J. Barnes, D. R. Newkirk and T. Fazio, *J. Assoc. Off. Anal. Chem.*, 65 (1982) 566.
- 3 M. Petz, *Z. Lebensm.-Unters.-Forsch.*, 176 (1983) 289.
- 4 N. Haagsma, R. J. Nooteboon, B. G. Gotemarker and M. J. Maas, *Z. Lebensm.-Unters.-Forsch.*, 181 (1985) 194.
- 5 G. D. Paulson, A. D. Mitchel and R. G. Zaylski, *J. Assoc. Off. Anal. Chem.*, 68 (1985) 1000.
- 6 S. J. Stoud, W. A. Steller, A. J. Manuel, M. O. Poeppel and A. R. DaCunha, *J. Assoc. Off. Anal. Chem.*, 67 (1984) 142.
- 7 M. H. Thomas, K. E. Soroka, R. M. Simpson and R. L. Epstein, *J. Agric. Food Chem.*, 39 (1981) 621.
- 8 A. J. Manuel and W. A. Steller, *J. Assoc. Off. Anal. Chem.*, 64 (1981) 794.
- 9 F. J. Suhre, R. M. Simpson and J. W. Shafer, *J. Agric. Food Chem.*, 29 (1981) 727.
- 10 R. J. Munns and J. E. Roybal, *J. Assoc. Off. Anal. Chem.*, 65 (1982) 1048.
- 11 D. P. Goodspeed, R. M. Simpson, R. B. Ashworth, J. W. Shafer and H. R. Cook, *J. Assoc. Off. Anal. Chem.*, 61 (1978) 1050.
- 12 R. M. Simpson, F. J. Suhre and J. W. Shafer, *J. Assoc. Off. Anal. Chem.*, 68 (1985) 23.
- 13 O. W. Parks, *J. Assoc. Off. Anal. Chem.*, 68 (1985) 20.
- 14 O. Gyllenhaal, U. Tjarlund, H. Ehrsson and P. Hertvig, *J. Chromatogr.*, 156 (1978) 275.
- 15 G. M. Ware, O. J. Francis, A. S. Carman and S. Shia Kuann, *J. Assoc. Off. Anal. Chem.*, 69 (1988) 900.
- 16 V. Ascalone, *Boll. Chim. Farm.*, 117 (1978) 176.
- 17 D. P. Schartz, *J. Assoc. Off. Anal. Chem.*, 68 (1985) 214.
- 18 A. B. Vilim, L. Larocque and I. MacIntosh, *J. Liq. Chromatogr.*, 3 (1980) 1725.
- 19 O. W. Parks, *J. Assoc. Off. Anal. Chem.*, 65 (1982) 632.
- 20 W. J. Blanchflower and D. A. Rice, *J. Assoc. Off. Anal. Chem.*, 71 (1988) 302.
- 21 J. F. M. Nouws, T. B. Vree, M. Baakman, F. Driessens, L. Vellenga and D. J. Mevius, *Vet. Q.*, 8 (1986) 123.

Note

Direct liquid chromatographic separation of enantiomeric and diastereomeric terpenic alcohols as β -cyclodextrin inclusion complexes

ANGELA ITALIA*, MARCO SCHIAVI and PAOLO VENTURA^a

Analytical Chemistry Department, Camillo Corvi SpA, Stradone Farnese 118, 29100 Piacenza (Italy)

(First received May 8th, 1989; revised manuscript received October 26th, 1989)

Sobrerol¹, a fluidificant mucoregulatory drug widely used for the treatment of respiratory diseases as the *trans* racemate^{2,3} and a new more potent mucofluidifying terpenic alcohol, CO/1408⁴, exhibit two asymmetric centres on the cyclohexene ring. Therefore, each compound produces four isomers: two enantiomeric pairs derived from the two *cis* and *trans* diastereoisomers. Their absolute configurations are shown in Figs. 1 and 2.

The ability of cyclodextrins (CDs) to form inclusion complexes with many molecules and ions has been known for a long time. However, their utilization, especially for analytical purposes, started only a few years ago when CDs became available in larger amounts and at lower cost. The highly selective inclusion properties of CDs have been applied successfully in high-performance liquid chromatography (HPLC) in two different approaches, CDs being used either as a specific modifier of the mobile phase^{5–8} or as a chemically bonded stationary phase^{9–12}.

This paper describes the separation of the enantiomeric and diastereomeric pairs of sobrerol and CO/1408 by reversed-phase (RP) using β -CDs in the above two approaches.

EXPERIMENTAL

A Varian 2010 liquid chromatograph, equipped with a Model 2050 variable-wavelength UV detector, a Rheodyne 7125 sample injector with a 10- μ l loop and a Varian Model 9176 recorder, was used at a detection wavelength of 205 nm. Experiments were carried out with prepacked LiChrosorb RP-18 (10 μ m) and LiChrospher RP-18 (5 μ m) columns (250 \times 4.0 mm) (Merck, Darmstadt, F.R.G.) and with a Cyclobond I column (250 \times 4.6 mm I.D.) packed with 5- μ m silica gel with chemically bonded β -CD (ASTEC, Whippony, NJ, U.S.A.).

Chemicals used for buffer preparation were of analytical-reagent grade and

^a Present address: c/o Chiesi Farmaceutici SpA, Via Palermo 26/A, 43100 Parma, Italy.

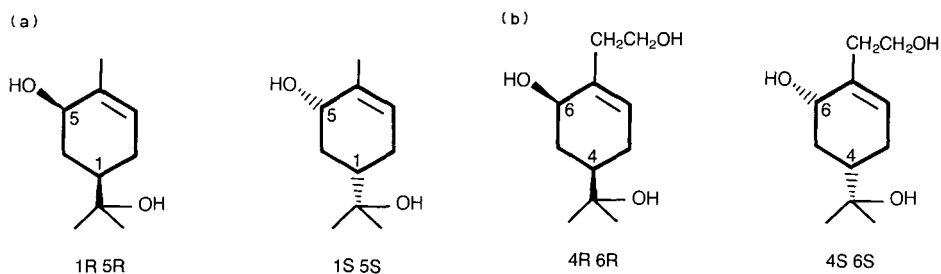


Fig. 1. (a) Enantiomeric pair of *cis*-sobrerol: (1*R*,5*R*)- and (1*S*,5*S*)-5-hydroxy- $\alpha,\alpha,4$ -trimethyl-3-cyclohexene-1-methanol. (b) Enantiomeric pair of *cis*-CO/11408: (4*R*,6*R*)- and (4*S*,6*S*)-6-hydroxy-4(1-hydroxy-1-methylethyl)-1-cyclohexene-1-ethanol.

obtained from Merck. The eluents were prepared with Merck HPLC-grade solvents and were degassed prior to use. β -Cyclodextrin was of analytical-reagent grade and supplied by Fluka (Buchs, Switzerland). Racemates and enantiomers of *cis*- and *trans*-sobrerol and CO/1408 were synthesized in our laboratories; their purity was checked by polarimetry and differential scanning calorimetry.

RESULTS AND DISCUSSION

HPLC allowed the partial separation of the diastereomeric *cis* and *trans* terpenic alcohol pairs using the conventional Rp mode phase but failed in the resolution of their enantiomers. The addition of β -CD to the mobile phase decreased the retention times of the diastereoisomers and improved their separation (see Table I and Fig. 3).

The use of α -CD instead of β -CD did not improve the two diastereomeric separations compared with those obtained with the conventional RP analysis, as shown in Table I. The results suggest that the α -CD cavity is too small to include these terpenic compounds whereas the cavity of β -CD is appropriate for the formation of inclusion complexes with these alcohols.

Another aim of this work was to determine whether β -CD might be a selective mobile phase modifier for the resolution of the two terpenic alcohol racemates by HPLC. From the structures of the two terpenic compounds, able to form inclusion complexes with the β -CD cavity (probably via the cyclohexene ring), enantiomeric separation could be expected according to the three-point interaction model originally proposed by Dalglish¹³ and later used by Hinze *et al.*¹⁴ to explain enantiomeric

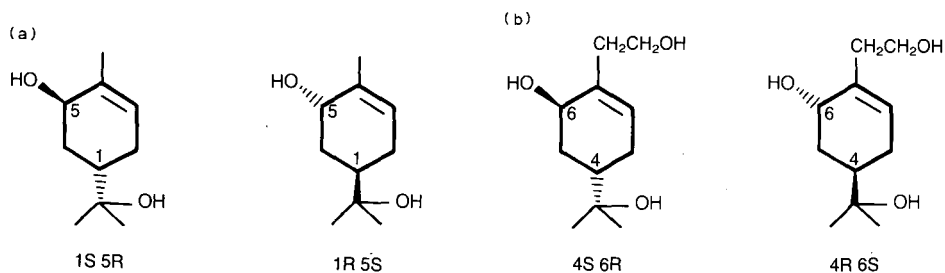


Fig. 2. (a) Enantiomeric pair of *trans*-sobrerol. (b) Enantiomeric pair of *trans*-CO/1408.

TABLE I

DIASTEREOMERIC SEPARATION OF *cis/trans*-TERPENIC ALCOHOLS USING DIFFERENT CD MOBILE PHASES

Mobile phase: potassium phosphate buffer solution (0.025 M; pH 7.25) with ethanol as organic modifier (20% for sobrerol and 10% for CO/1408). A flow-rate of 1 ml/min was used for the 250 × 4.0 mm I.D. (10 μm) LiChrosorb RP-18 column and the mobile phase was saturated with different CDs. Parameters: k' = capacity factor; α = separation factor; R_s = resolution

Diastereomeric pair	k'^a	α	R	Mobile phase
<i>cis/trans</i> -Sobrerol	6.00	1.07	0.89	Without CD
	6.00	1.07	0.89	α -CD
	3.44	1.36	2.44	β -CD
<i>cis/trans</i> -CO/1408	6.00	1.11	0.86	Without CD
	6.00	1.11	0.86	α -CD
	2.33	1.81	3.40	β -CD

^a Value for the first-eluting enantiomer (*cis*-sobrerol and *cis*-CO/1408).

separations with cyclodextrins. The possibility of this chiral recognition and subsequent chromatographic optical resolution are probably due, after inclusion with β -CD, to steric interactions with the outer rim of β -CD. These interactions may involve hydrogen bonding between the terpenic alcohols and β -CD hydroxyl groups and potential steric interactions between alkyl substituents of terpenic compounds and the outer rim of β -CD.

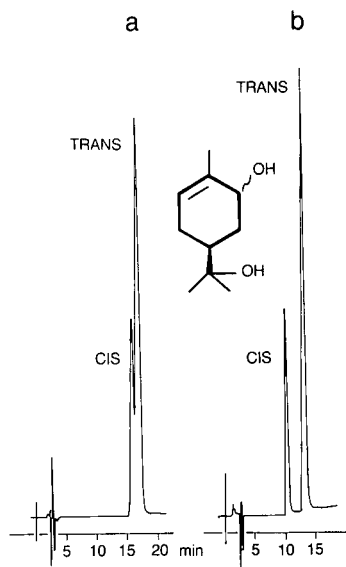


Fig. 3. Separation of *cis*- and *trans*-sobrerol on a LiChrosorb RP-18 (10 μm) column (250 × 4.0 mm I.D.). Mobile phase: 20% ethanol-potassium phosphate buffer solution (0.025 M; pH 7.25), (a) without β -CD and (b) saturated with β -CD. Flow-rate: 1 ml/min.

TABLE II

ENANTIOMERIC SEPARATION OF TERPENIC ALCOHOLS USING A β -CD MOBILE PHASE

Mobile phase: potassium phosphate buffer solution (0.025 M; pH 7.25) with ethanol as organic modifier. A flow-rate of 0.3 ml/min was used for the 250 \times 4.0 mm I.D. (5 μ m) LiChrospher 100 RP-18 column and the mobile phase was saturated with β -CD.

Enantiomeric pair	k'^a	α	R_s	Mobile phase ^b
(\pm)- <i>trans</i> -sobrerol	24.4	1.08	1.45	7.5 : 92.5
(\pm)- <i>cis</i> -sobrerol	Not resolved			
(\pm)- <i>trans</i> -CO/1408	20.6	1.08	1.46	0.8 : 99.2
(\pm)- <i>cis</i> -CO/1408	Not resolved			

^a Value for the first-eluting enantiomer [($-$)-*trans*-sobrerol and ($-$)-*trans*-CO/1408].

^b Numbers represent the volume percentage of ethanol added to buffer solution.

Table II gives separation data for *trans*-sobrerol and *trans*-CO/1408 racemates resolved on the LiChrospher 100 RP-18 column with aqueous ethanol-potassium phosphate buffer as the mobile phase, saturated with β -CD. The order of elution of enantiomers determined by injecting single antipodes and the chromatogram of CO/1408 is shown as an example in Fig. 4. Enantiomeric resolutions were obtained with a more efficient column, a smaller percentage of cosolvent (ethanol) and a lower flow-rate compared with the parameters used for *cis-trans* separations (see Tables I and II) according to the general concept that these factor changes can improve the resolution of inclusion complexes¹⁴.

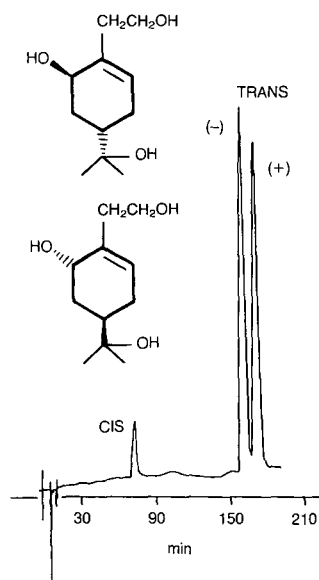


Fig. 4. Enantiomeric resolution of (\pm)-*trans*-CO/1408 on a LiChrospher 100 RP-18 (5 μ m column (250 \times 4.0 mm I.D.). Mobile phase: 0.8% ethanol-potassium phosphate buffer solution (0.025 M; pH 7.25) saturated with β -CD. Flow-rate: 0.3 ml/min.

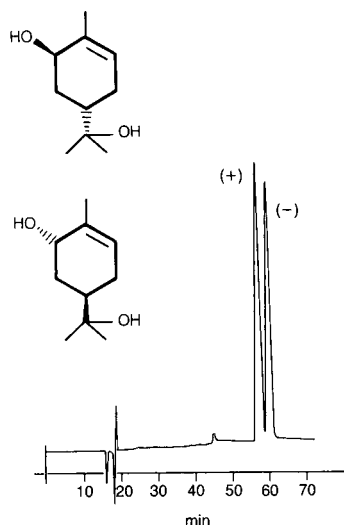


Fig. 5. Enantiomeric resolution of (\pm)-*trans*-sobrerol on a chiral β -CD Cyclobond I ($5 \mu\text{m}$) column ($250 \times 4.6 \text{ mm}$ I.D. Mobile phase: 7% acetonitrile–aqueous triethylammonium acetate (0.005 M ; pH 6.3). Flow-rate: 0.2 ml/min.

The enantiomeric separations of *cis*- and *trans*-sobrerol and CO/1408 were repeated with the Cyclobond I column. In this instance we were able not only to separate *trans*-sobrerol (Fig. 5) and *trans*-CO/1408 racemates faster than when using β -CD saturated eluents (compare Table III with Table II), but also to resolve the *cis*-sobrerol enantiomers (Table III). To obtain this separation within a reasonable elution time it was necessary to modify the chromatographic conditions used for the

TABLE III

ENANTIOMERIC SEPARATION OF TERPENIC ALCOHOLS USING A CHIRAL $250 \times 4.6 \text{ mm}$ I.D. ($5 \mu\text{m}$) β -CD CYCLOBOND I COLUMN AND DIFFERENT MOBILE PHASES

Enantiomeric pair	k'^a	α	R_s	Mobile phase ^b	pH
(\pm)- <i>trans</i> -sobrerol	2.67	1.08	1.55	Acetonitrile–buffer	4.40
	2.55	1.07	1.33	(7 : 93) ^c	5.25
	2.48	1.08	1.20		6.32
	2.43	1.08	1.09		7.30
(\pm)- <i>cis</i> -sobrerol	4.45	1.06	0.75	Acetonitrile–isopropanol–buffer (7 : 0.25 : 92.75) ^d	6.32
(\pm)- <i>trans</i> -CO/1408	2.06	1.04	0.75	Acetonitrile–buffer (7 : 93) ^c	6.32
(\pm)- <i>cis</i> -CO/1408	Not resolved				

^a Value for the first-eluted enantiomer [(+)-*trans*-sobrerol, (+)-*trans*-CO/1408 and (-)-*cis*-sobrerol].

^b Buffer: 0.005 M triethylammonium acetate of different pH.

^c Flow-rate: 0.2 ml/min.

^d Flow-rate: 0.3 ml/min.

separations of *trans*-sobrerol enantiomers by increasing the flow-rate and adding 0.25% of 2-propanol to the eluent. In fact, using the Cyclobond I column, *cis*-sobrerol and *cis*-CO/1408 are retained longer than their *trans* forms. Hence the elution order of the diastereoisomers is opposite to that observed with β -CD dissolved in the mobile phase. Further, an inversion of the elution order was also noted for the enantiomers. This HPLC retention behaviour has also been observed by other workers¹⁵ and it is in agreement with the inclusion mechanism generally proposed to rationalize chromatographic separations with cyclodextrins¹⁵.

The effect of mobile phase pH on the resolution was studied for sobrerol and the results are summarized in Table III. It is apparent that there was no significant change in the separation factor but an appreciable improvement in resolution was observed as the pH was reduced.

REFERENCES

- 1 C. Corvi Mora, *U.S. Pat.*, 3 592 908 (1971).
- 2 P. C. Braga, L. Allegra, R. Bossi, R. Scuri, C. L. Castiglioni and S. Romandini, *Int. J. Clin. Pharm. Res.*, 7 (1987) 381.
- 3 R. Bossi, C. Rampoldi, F. Colombo, G. Caminiti, S. Romandini, L. Allegra and P. C. Braga, *Clin. Trials J.*, 24 (1987) 131.
- 4 C. Corvi Mora, *U.S. Pat.*, 4 644 087 (1987).
- 5 J. Zukowsky, D. Sybilska and J. Bojarski, *J. Chromatogr.*, 364 (1986) 225.
- 6 M. Gazdag, G. Szepesi and L. Huszar, *J. Chromatogr.*, 351 (1986) 128.
- 7 J. Debowski, J. Jurczak and D. Sybilska, *J. Chromatogr.*, 282 (1983) 83.
- 8 K. Uekama, F. Hirayama, K. Ikeda and K. Inaba, *J. Pharm. Sci.*, 66 (1977) 706.
- 9 D. W. Armstrong, A. Alak, K. Bui, W. De Mond, T. Ward, T. E. Riehl and W. L. Hinze, *J. Inclusion Phenom.*, 2 (1984) 533.
- 10 D. W. Armstrong, *J. Liq. Chromatogr.*, 7 (S-2) (1984) 353.
- 11 J. H. Maguire, *J. Chromatogr.*, 387 (1987) 453.
- 12 S. M. Han, Y. I. Han and D. W. Armstrong, *J. Chromatogr.*, 441 (1988) 376.
- 13 E. E. Dalglish, *J. Chem. Soc.*, 137 (1952) 3940.
- 14 W. L. Hinze, T. E. Riehl, D. W. Armstrong, W. De Mond, A. Alak and T. Ward, *Anal. Chem.*, 57 (1985) 237.
- 15 E. Smolková-Keulemansová, in D. Duchène (Editor), *Cyclodextrins and Their Industrial Uses*, Editions de Santé, Paris, 1987, ch. 7, p. 261.

Note

Immobilized mucin : an affinity matrix for the isolation of winged bean acidic and basic lectins

SUSHMA Y. SAWHNEY and SHOBHANA V. BHIDE*

Department of Chemistry, Division of Biochemistry, University of Poona, Pune 411 007 (India)

(First received June 15th, 1989; revised manuscript received October 26th, 1989)

Lectins, sugar binding and cell agglutinating proteins, are predominantly present in the seeds of legumes. They show a wide diversity in their sugar specificities and have proved to be useful for probing the structural features of cell surface glycoconjugates. As a result, lectins have widespread applications in various fields of research in biochemistry, medicine and cell biology¹⁷⁻²⁰.

A lectin with a molecular weight (M_r) of 46 000 and a pI of 5.5 was first isolated from winged bean (*Psophocarpus tetragonolobus* LDC) seeds by Pueppke²¹. The lectin agglutinated only trypsinized and desialysed human erythrocytes of A, B and O types. Appukuttan and Basu²² reported the isolation of a lectin from winged beans by affinity chromatography on Sepharose-N-caproyl-D-galactosamine, which has an M_r of 38 000 and agglutinated untreated human A, B and O erythrocytes. Recently, two types of lectins with different pI s and erythrocyte-agglutinating specificities have been reported. Kortt^{3,4} reported the isolation of three acidic lectins ($pI \approx 5.5$)⁴ and three basic lectins ($pI > 9.5$)³. Higuchi *et al.*¹² reported the isolation of a single acidic lectin ($pI \approx 5.5$)¹⁴ and a single basic lectin ($pI \approx 8.6$)¹³ from winged beans. Acidic lectin(s) agglutinate human A, B and O erythrocytes strongly but not rabbit, whereas the basic lectin(s) agglutinate rabbit and human A and B but not O erythrocytes. The specificity of the acidic lectins was directed towards β -D-galactosides, whereas that of the basic lectins was directed towards α -D-galactosides.

Here, we describe a simple, one-step preparative method for the isolation of acidic and basic lectins from seeds of winged beans by affinity chromatography.

EXPERIMENTAL

Porcine gastric mucin and glutaraldehyde were obtained from Sigma. All other chemicals were of analytical-reagent grade. Winged bean seeds (*Psophocarpus tetragonolobus*) were obtained locally.

Protein concentrations were determined by absorbance measurements at 280 nm using bovine serum albumin as standard ($A_1^{1\%} = 7.45 \text{ cm}^{-1}$, 1%). Haemagglutination assays were carried out as reported earlier¹. Centrifugation was carried out in Sorwall SS-3 automatic centrifuge using an SS-34 rotor (capacity $8 \times 50 \text{ ml}$, 12 080 g)

at room temperature (26–28°C) and in a refrigerated centrifuge (capacity 2×180 ml, 2412 g) at 4°C. Saline solutions I (0.145 M sodium chloride) and II (1.0 M sodium chloride) were used.

The preparation of delipidated acetone dried powder from dry winged bean seeds, the extraction of acetone dried powder with saline solution I and ammonium sulphate fractionation were carried out as described previously¹. The protein fraction precipitating between 30 and 80% ammonium sulphate saturation was dissolved in the minimum amount of water and extensively dialysed against water and finally against saline solution II. On dialysis the solution containing lectin activity was clarified by centrifugation at 12 080 g and then stored at –20°C. This solution (fraction A) was used to isolate lectin by affinity chromatography.

Preparation of affinity matrix

Porcine gastric mucin was partially desialylated (by gentle acid treatment) according to the procedure of Svennerholm². Desialomucin was then immobilized by entrapment in glutaraldehyde-cross-linked gelatin gel granules as follows. Desialomucin (1.0 g) was suspended in borate buffer (pH 8.0, 0.2 M, 30 ml) to give a uniform suspension. Gelatin solution was prepared by suspending skin gelatin (6.0 g) in 70 ml of borate buffer (pH 8.0, 0.2 M) and warming on a hot waterbath (70–80°C), to give a clear solution. It was then cooled to room temperature, mixed with mucin suspension and the mixture was allowed to set in the form of a gel (5 mm thick) in a tray at 4°C. Next day, the gel was cut into pieces (1 × 1 cm), suspended in glutaraldehyde solution [8% (v/v), 250 ml] and the pH was adjusted to 9.0 with 1.0 M sodium hydroxide solution. After allowing it to stand at 4°C overnight, the cross-linked gel was blended in a blender and the gel granules were collected by centrifugation (2418 g). It was then washed free of glutaraldehyde by repeated washing with distilled water (4°C). The fines, removed by decantation, were discarded. The gel granules were then suspended in saline solution I containing glycine (0.1 M) overnight, to block the unreacted aldehyde groups. After washing with borate buffer (pH 8.0, 0.2 M), the gel was preserved in saline solution I containing sodium azide (0.02%, w/v) at 4°C. The amount of sedimented gel obtained was 150 ml.

RESULTS AND DISCUSSION

Winged bean seeds contain two distinct groups of D-galactose/N-acetyl-D-galactosamine-specific lectins, the acidic and the basic, which differ in their erythrocyte agglutination specificities and isoelectric points. The acidic lectins agglutinate human A, B and O erythrocytes, but not rabbit erythrocytes, and their sugar specificity is directed towards β -D-galactosides. The basic lectins, specific for α -D-galactopyranosides, agglutinate human A and B erythrocytes and rabbit erythrocytes, but not O erythrocytes^{3–5,12–14}.

Our preliminary results indicated the presence of both acidic and basic lectins in the local varieties of winged bean seeds.

When fraction A was loaded on a column packed with immobilized desialomucin, both lectins were retained on the column (as judged from the haemagglutinating assay). Fig. 1 shows the elution profile of the winged bean lectins on the desialomucin column, and Fig. 2 shows the polyacrylamide gel electrophoresis (PAGE) pattern at

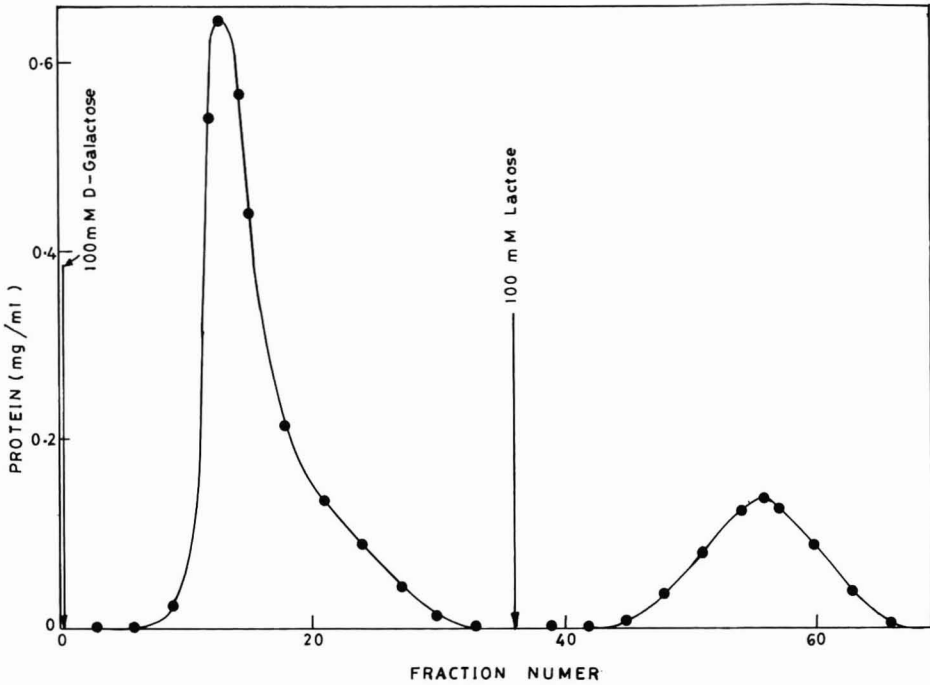


Fig. 1. Elution profile of winged bean seed basic and acidic lectins on an immobilized desialomucin column. Fraction A of winged bean seeds was applied on the immobilized desialomucin column (18.0 × 3.0 cm I.D., capacity 90 ml), equilibrated with saline solution II (1.0 M sodium chloride containing 0.02% sodium azide). The column was washed with saline solution II until free of unadsorbed proteins. The adsorbed lectins were first eluted with 100 mM D-galactose followed by elution with 100 mM lactose in saline solution II.

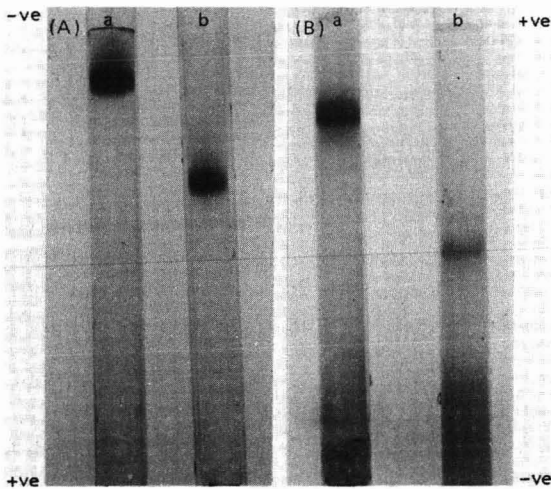


Fig. 2. PAGE pattern of winged bean lectins at (A) pH 8.3 and (B) pH 4.5. (a) D-Galactose-cluted peak protein (fraction 13); (b) lactose-eluted peak protein (fraction 56).

pH 4.5⁹ and 8.3⁶ of the D-galactose- and lactose-eluted protein peaks. Lectin eluted with D-galactose agglutinated normal human A and B erythrocytes in addition to normal and papain-treated rabbit erythrocytes, but not O erythrocytes, the property characteristic of the basic lectin. The protein eluted with lactose agglutinated human A, B and O erythrocytes but not rabbit erythrocytes, the property characteristic of acidic lectin. Hence a clear cut gross separation of acidic and basic lectins has been achieved. The yield of the lectins (acidic + basic) was 36 mg per 10 g of seeds with 80-fold purification and the ratio of acidic to basic lectins was 1:4.

Lectins are usually isolated by affinity chromatography using matrix-coupled monosaccharides, glycosides or water-insoluble polysaccharide derivatives⁷. The isolation of winged bean basic and acidic lectins has been reported by a number of workers. Kortt^{3,4} reported the separation of acidic and basic lectins from the seeds and tuberous roots of *Phosphocarpus tetragonolobus*^{3,4,8,10} and *Phosphocarpus scandens*¹¹ seeds, using a combination of gel filtration on Ultrogel AcA44, ion-exchange chromatography on SP-Sephadex C-25 and/or affinity chromatography. A single-step purification of winged bean acidic and basic lectins from tuber extracts by affinity chromatography on lactose-Sepharose 4B and melibiose-Bio-Gel P-150, respectively, has also been reported¹³. Higuchi *et al.*¹² reported the isolation of a single acidic¹⁴ ($pI = 5.5$) and a single basic lectin ($pI = 8.6$)¹³ by initial ion-exchange chromatography of the seed extract on DEAE-Sephadex A-50 followed by affinity chromatography on N-acetylgalactosamine-agarose and *p*-aminophenyl- β -D-galactopyranoside-bound Sepharose 4B, respectively. Khan *et al.*⁵ isolated winged bean basic and acidic lectins by affinity chromatography on Sepharose-6-aminocaproyl-D-galactosamine and lactosaminyl-Bio-Gel respectively. All the above methods involved either at least two steps of purification and/or use of separate affinity media for the basic and acidic lectins.

Many lectins bind only to complex oligosaccharide determinants on cell surfaces or naturally occurring glycoproteins, and special procedures have to be developed for the isolation of such lectins^{15,16}. Freier *et al.*¹⁶ reported the use of two easily available glycoproteins, *viz.*, hog gastric mucin and ovomucoid, by coupling to cyanogen bromide-activated Sepharose 4B as general affinity adsorbents for lectins. They isolated 30 lectins from 27 different plants.

In this work, desialyated porcine gastric mucin immobilized by entrapment in glutaraldehyde-cross-linked gelatin gel granules was used as an affinity matrix for the isolation of winged bean seed lectins. Both acidic and basic lectins from winged bean seeds were absorbed on the immobilized desialomucin column. Elution of the adsorbed lectins was carried out first with D-galactose, when only the basic lectin was eluted. The acidic lectin was eluted only when lactose was employed as an eluent. Hence gross separation of winged bean basic and acidic lectins from the crude seed extract can be achieved in one run on the same affinity matrix by simply changing the desorption conditions. The method is simple, rapid and reproducible.

Many plants are known to contain more than one lectin with only minor differences in their sugar specificity¹⁶. The use of an immobilized mucin column and elution of the adsorbent lectins with different sugars can be employed as a general method for the isolation of such lectins.

ACKNOWLEDGEMENT

We thank the Council of Scientific and Industrial Research, New Delhi, for the award of Research Fellowship to S.Y.S.

REFERENCES

- 1 U. N. Nandedkar, S. Y. Sawhney, S. V. Bhide and N. R. Kale, *J. Chromatogr.*, 396 (1987) 363.
- 2 L. Svennerholm, *Acta Chem. Scand.*, 12 (1958) 547.
- 3 A. A. Kortt, *Eur. J. Biochem.*, 138 (1984) 519.
- 4 A. A. Kortt, *Arch. Biochem. Biophys.*, 236 (1985) 544.
- 5 M. I. Khan, M. V. Sastry and A. Surolia, *J. Biol. Chem.*, 261 (1986) 3013.
- 6 D. E. Williams and R. A. Reisfeld, *Ann. N.Y. Acad. Sci.*, 121 (1964) 373.
- 7 H. Lis and N. Sharon, *J. Chromatogr.*, 215 (1981) 361.
- 8 A. A. Kortt and J. B. Caldwell, *J. Sci. Food Agric.*, 36 (1985) 863.
- 9 R. A. Reisfeld, Y. I. Lewis and D. E. Williams, *Nature (London)*, 195 (1962) 281.
- 10 A. A. Kortt and J. B. Caldwell, *J. Sci. Food Agric.*, 39 (1987) 47.
- 11 A. A. Kortt, *Phytochemistry*, 27 (1988) 2847.
- 12 M. Higuchi, K. Inoue and K. Iwai, *Agric. Biol. Chem.*, 48 (1984) 2177.
- 13 M. Higuchi and K. Iwai, *Agric. Biol. Chem.*, 49 (1985) 391.
- 14 M. Higuchi, Y. Ohtani and K. Iwai, *Agric. Biol. Chem.*, 50 (1986) 1847.
- 15 J. L. Ochoa and T. Kristiansen, *FEBS Lett.*, 90 (1978) 145.
- 16 T. Freier, G. Fleishman and H. Rudiger, *Biol. Chem., Hoppe Seyler*, 366 (1985) 1023.
- 17 I. J. Goldstein and C. E. Hayes, *Adv. Carbohydr. Chem.*, 35 (1978) 128-334.
- 18 H. Lis and N. Sharon, *Ann. Rev. Biochem.*, 55 (1986) 35-69.
- 19 I. E. Liener, *Ann. Rev. Plant Physiol.*, 27 (1976) 291-319.
- 20 M. E. Etzler, *Ann. Rev. Plant Physiol.*, 36 (1985) 209-234.
- 21 S. Pueppke, *Biochem. Biophys. Acta*, 581 (1979) 63.
- 22 P. S. Appukuttan and D. Basu, *Anal. Biochem.*, 113 (1981) 253.

CHROM 22 139

Note

Purification of mammalian tyrosyl-tRNA synthetase by high-performance liquid chromatography

A. D. WOLFSON*, Yu. A. MOTORIN

A. N. Bakh Institute of Biochemistry, Academy of Sciences of the U.S.S.R., Leninsky pr. 33, 117071 Moscow (U.S.S.R.)

and

T. I. RIBKINSKA and S. F. BERESTEN

Institute of Molecular Biology, Academy of Sciences of the U.S.S.R., Vavilova 32, 117984 Moscow (U.S.S.R.)

(Received September 12th, 1989)

Aminoacyl-tRNA synthetases catalyse the specific aminoacylation of cognate tRNA by amino acids. Aminoacyl-tRNA synthetases of higher eukaryotes, including mammals, have been less studied than the bacterial and yeast enzymes, mainly owing to difficulties in their purification. Usually the concentration of mammalian aminoacyl-tRNA synthetases in tissue is about 0.1 – 0.01% of total protein^{1,2}, and about 1000 – 10 000-fold purification is required in order to obtain homogeneous enzymes. In addition, aminoacyl-tRNA synthetases are very susceptible to endogeneous proteolysis and special precautions should be taken to obtain pure native enzyme. Normally, procedures for the purification of mammalian enzymes require stage(s) of affinity chromatography or numerous conventional chromatography stages^{1–5} and are time consuming. Recently we described the successful application fast protein liquid chromatography (FPLC) to the purification of mammalian valyl-tRNA synthetase⁶, which made the purification procedure rapid and reproducible.

Several attempts to purify tyrosyl-tRNA synthetase have been made^{7–9}. However, the reported molecular weights and properties of the enzyme vary significantly. Here we present a rapid method for the purification of mammalian tyrosyl-tRNA synthetase by FPLC.

EXPERIMENTAL

Materials

We used dithiothreitol (DTT), phenylmethylsulphonyl fluoride (PMSF) from Serva (Heidelberg, F.R.G.) diisopropyl fluorophosphate (DFP) from Merck (Darmstadt, F.R.G.) and ¹⁴C-labelled tyrosine from Chemapol (Prague, Czechoslovakia). All other reagents were of analytical-reagent grade.

Enzyme assay

Enzyme activity was measured in 50 μ l of a mixture containing 100 mM Tris-HCl (pH 7.5) (37°C), 5 mM MgCl₂, 25 mM KCl, 0.1 mM DTT, 3 mM ATP, 5 μ M [¹⁴C]tyrosine (400 Ci/mol) and 50 – 100 μ g of rabbit liver tRNA. Reaction was initiated by addition of the limiting amount of enzyme. Samples were incubated for 3 min at 37°C, reaction was stopped by the addition of 5% trichloroacetic acid, samples were filtered through GF/C glass-fibre filters (Whatman) and the filters were dried and counted in a toluene scintillator.

Purification procedure

Separation was effected with an FPLC system (Pharmacia, Uppsala, Sweden) on a DEAE-Toyopearl 650S (20 cm x 2 cm I.D.) prepacked column (Toyo Soda, Tokyo, Japan) and Mono S HR 5/5 and Mono Q HR 5/5 columns (5 cm x 5 mm I.D.) (Pharmacia). Chromatography was performed at room temperature.

Liver extract was obtained by homogenization of liver in a Waring blender for 60 s at 8000 rpm in two volumes of cold buffer [50 mM Tris-HCl (pH 7.5), 5 mM MgCl₂, 1 mM DTT, 10% glycerol] containing 1 mM of both PMSF and DFP. Protease inhibitors were added as 0.2 M acetone solutions just before homogenization. The homogenate was centrifuged for 20 min at 10 000 g, filtered through four layers of gauze and used for PEG-6000 fractionation.

Polyethylene glycol (PEG) 6000 (Merck) solution (50%, w/v) was slowly added to the extract up to the final concentration of 5%. Precipitated protein was removed by centrifugation at 10 000 g for 10 min and PEG solution was added to the supernatant to obtain a concentration of 9%. A pellet obtained as above was dissolved in buffer A [25 mM Tris-HCl (pH 7.5), 1 mM MgCl₂, 1 mM DTT, 10% glycerol], centrifuged for 10 min at 10 000 g and applied to the DEAE-Toyopearl 650S column at a flow-rate of 3 ml/min. The column was washed with two volumes of starting buffer and proteins were eluted by a linear 0–0.3 M KCl gradient in 200 ml of buffer A. Active fractions that eluted at 60–90 mM KCl concentration were pooled, diluted twice with buffer A and applied to the Mono S column. Chromatography was performed at a flow-rate of 1 ml/min. Proteins were eluted with 20 ml of a 0–0.4 M KCl gradient in buffer A. Active fractions that eluted at 80 mM KCl concentration were pooled, diluted twice with buffer A and applied to the Mono Q column. Chromatographic conditions for the Mono Q step were the same as for Mono S. Active fractions containing purified tyrosyl-tRNA synthetase were stored frozen in liquid nitrogen.

Sodium dodecylsulphate polyacrylamide gel electrophoresis (SDS-PAGE) was performed on a PhastSystem (Pharmacia) using Phast Gradient Gels 10–15. After separation the gels were stained according to Pharmacia recommendations¹⁰.

Protein was determined according to Bradford¹¹.

RESULTS AND DISCUSSION

A rapid four-step purification method has been developed for the isolation of mammalian tyrosyl-tRNA synthetase. The procedure consists of the PEG-6000 precipitation and three consecutive steps of high-performance ion-exchange chromatography on DEAE-Toyopearl, Mono S and Mono Q columns. Purification data are summarized in Table I.

TABLE I
PURIFICATION OF TYROSYL-tRNA SYNTHETASE

Purification starts from 95 g of rabbit liver.

Purification step	Protein (mg)	Total activity (U) ^a	Specific activity (U/mg) ^a	Yield (%)	Purification (fold)
Extract	7100	70.3	0.0099	100	1
PEG-6000 (5-9%) precipitation	2200	40.8	0.018	58.5	1.8
DEAE-Toyopearl	82	22.1	0.27	31.7	27.3
Mono S	0.51	15.9	31.7	22.6	3200
Mono Q	0.11	15.4	140	22.0	14140

^a 1 Unit (U) corresponds to the formation of 1 nmol of aminoacyl-tRNA per minute at 37°C.

The first step of the purification procedure is PEG-6000 precipitation. This method is better than the commonly used ammonium sulphate precipitation as it does not require dialysis or desalting prior to the ion-exchange chromatographic step. Tyrosyl-tRNA synthetase precipitates at high PEG-6000 concentrations (5-9%), which is characteristic of the 'soluble' cytoplasmic aminoacyl-tRNA synthetases.

The next step is chromatography on a DEAE-Toyopearl column. Tyrosyl-tRNA synthetase binds to this matrix and elutes at KCl concentrations of 60-90 mM as a single sharp peak [Fig. 1]. Active fractions after two-fold dilution are applied to the Mono S cation-exchange column [Fig. 2]. This step is extremely effective in the purification of tyrosyl-tRNA synthetase (see Table I) as more than 95% of the applied protein remains in the flow-through fraction, whereas tyrosyl-tRNA synthetase

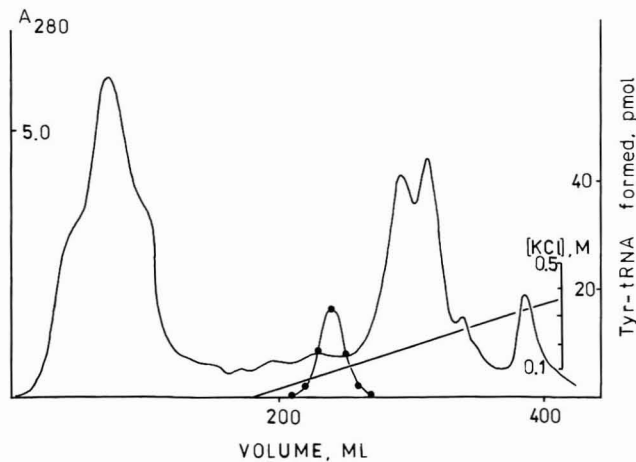


Fig. 1. Chromatography of tyrosyl-tRNA synthetase on the DEAE-Toyopearl 650S prepacked column (20 × 2 cm I.D.). Proteins from PEG-6000 (5-9%) precipitate were dissolved in buffer A and applied to the column at a flow-rate of 3 ml/min. Elution was performed with a linear KCl gradient from 0 to 0.3 M in 200 ml of buffer A. ● = Activity of tyrosyl-tRNA synthetase.

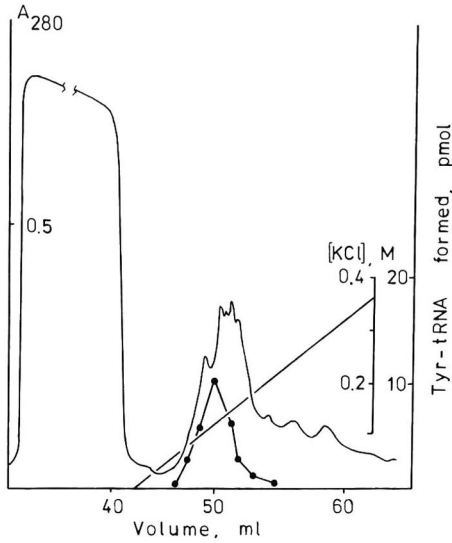


Fig. 2. Chromatography of tyrosyl-tRNA synthetase on the Mono S HR 5/5 column. Active fractions after DEAE-Toyopearl chromatography were applied to the Mono S column. Elution was performed with a linear KCl gradient from 0 to 0.4 M in 20 ml of the buffer A. Flow-rate, 1 ml/min. ● = Activity of tyrosyl-tRNA synthetase.

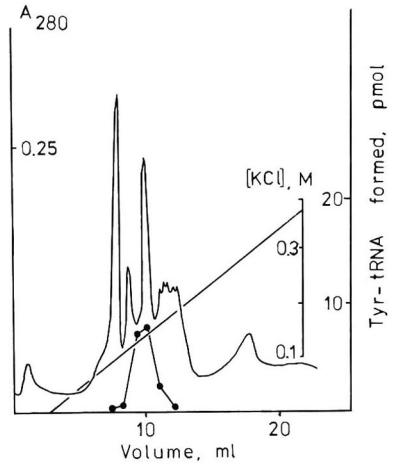


Fig. 3. Chromatography of tyrosyl-tRNA synthetase preparation on the Mono Q HR 5/5 anion-exchange column. Tyrosyl-tRNA synthetase preparation from the Mono S column was applied to the Mono Q column. Chromatographic conditions as in Fig. 2.

activity binds completely to the matrix. Enzyme elutes from the Mono S column at a KCl concentration of 80 mM. Tyrosyl-tRNA synthetase is finally purified by anion-exchange chromatography on a Mono Q column, where it elutes as a sharp peak well separated from the other protein peaks (Fig. 3).

SDS-PAGE of this fraction reveals a single polypeptide band with molecular weight M_r 70 000 (Fig. 4). Gel filtration of the purified enzyme also reveals a single peak corresponding to M_r 140 000 (data not shown), indicating that mammalian

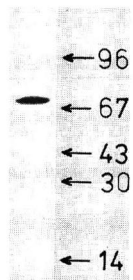


Fig. 4. SDS-page of the Mono Q tyrosyl-tRNA synthetase preparation. Arrows indicate the position of molecular weight markers: 96 = phosphorylase *b* (96 000 daltons); 67 = bovine serum albumin (67 000 daltons); 43 = ovalbumin (43 000 daltons); 30 = carboanhydrase (30 000 daltons); 14 = lactalbumin (14 000 daltons).

tyrosyl-tRNA synthetase has the same α_2 structure as all known tyrosyl-tRNA synthetases¹². The molecular weight of the enzyme is higher than that previously reported, which suggests that previously reported preparations may be degraded by proteolysis.

The method described allows 14 000-fold purification of the enzyme to be achieved with a yield of about 22% (Table I). Enzyme with the same properties was also obtained from beef liver by the same method.

Several points should be noted. First, the time required to complete the purification is a single working day and the same buffer system is used throughout the purification. Second, this method can be easily scaled up by increasing the dimensions of the DEAE-Toyopearl column only, as the protein loading of the Mono S HR 5/5 column may be increased up to 10-fold.

In our laboratory we have successfully purified tyrosyl-tRNA synthetase from 0.5 kg of rabbit liver using the described method within a single working day.

Easy purification makes mammalian tyrosyl-tRNA synthetase a suitable material for kinetic and structural studies.

ACKNOWLEDGEMENTS

We are grateful to Professor L. L. Kisselev and Dr. A. F. Orlovsky for their comments and suggestions.

REFERENCES

- 1 J. P. Pailliez and J. P. Waller, *J. Biol. Chem.*, 259 (1984) 15491.
- 2 T. Mizutani, T. Narihara and A. Hashimoto, *Eur. J. Biochem.*, 143 (1984) 9.
- 3 R. Rauchut, H.-J. Gabius and F. Cramer, *Biosystems*, 19 (1986) 173.
- 4 O. Kellerman, H. Tonetti, A. Brevet, M. Mirande, J.-P. Pailliez and J.-P. Waller, *J. Biol. Chem.*, 257 (1982) 11041.
- 5 D. E. Godar and D. C. H. Yang, *Biochemistry*, 27 (1988) 2181.
- 6 Y. A. Motorin, A. D. Wolfson, A. F. Orlovsky and K. L. Gladilin, *FEBS Lett.*, 220 (1987) 363.
- 7 Y. S. Prasada Rao and P. R. Srinivasan, *Nucl. Acid Res.*, 4 (1977) 3887.
- 8 F. Deak and G. Denes, *Biochem. Biophys. Acta*, 526 (1978) 626.
- 9 J. M. Clark and J. P. Eyzaguirre, *J. Biol. Chem.*, 237 (1962) 3698.
- 10 *PhastSystem Owners Manual*, Pharmacia, Uppsala, 1987.
- 11 M. M. Bradford, *Anal. Biochem.*, 72 (1976) 248.
- 12 L. L. Kisselev, O. O. Favorova and O. I. Lavrik, *Protein Biosynthesis from Amino Acids to Aminoacyl-tRNA*, Nauka, Moscow, 1984, p. 22.

CHROM 22 141

Note

High-performance liquid chromatographic determination of alterporriol D and E in fermentation of *Alternaria porri* (Ellis) Ciferri

R. SUEMITSU*

Department of Applied Chemistry, Faculty of Engineering, Doshisha University, Kamikyo-ku, Kyoto 602 (Japan)

K. HORIUCHI

Kyoto Chromato Co. Ltd., 54 Ohyakesawa Yamashina-ku, Kyoto 607 (Japan)

and

K. OHNISHI and M. KUBOTA

Department of Applied Chemistry, Faculty of Engineering, Doshisha University, Kamikyo-ku, Kyoto 602 (Japan)

(First received March 20th, 1989; revised manuscript received October 20th, 1989)

In the course of our investigation on pigments of *Alternaria porri* (Ellis) Ciferri, the causal fungus of black spot disease, we have isolated five modified bianthraquinone pigments from the culture liquid, named alterporriol A (Ap-A, **1**)¹, B (Ap-B, **1**)², C (Ap-C, **2**)³, D (Ap-D, **3**)⁴ and E (Ap-E, **3**)⁴, and determined their chemical structures. Of these pigments, Ap-A, -B and -C consist of macrosporin (Mac, **4**)⁵ and altersolanol A (As-A, **5**), both of which are metabolic pigments of *Alternaria solani*⁶ and *Alternaria porri*⁷ and Ap-A and -B are atropisomers of each other. Likewise, Ap-D and -E were found to be atropisomers of each other and their planar and spatial structures are shown in Fig. 1 (**3**). Recently, Lazarovits *et al.*⁸ reported the dimers of As-A from the culture liquid of *Alternaria solani* and presented their planar structures. Comparing the structures, spectral data and other physico-chemical properties of Ap-D and -E with those of the dimers of As-A just mentioned, they were found to be the same.

Previously, we reported the high-performance liquid chromatographic (HPLC) determination of As-A, Mac and Ap-A, Ap-B and Ap-C in the fermentation of *Alternaria porri* in order to explore the biosyntheses of Ap-A, Ap-B and Ap-C⁹. The structures of Ap-D and Ap-E show that they consist of two moieties of As-A. So far as the biosyntheses of Ap-D and -E are concerned, two pathways can be considered, namely, whether As-A is first metabolized and then two moieties of As-A bond to Ap-D and -E, or Ap-D and -E are first metabolized and then their C-C linkages connecting the monomeric halves are cleaved into two halves of the molecule, two moieties of As-A. This paper deals with the HPLC determination of Ap-D and -E during the period of fermentation in order to explore their metabolic pathways.

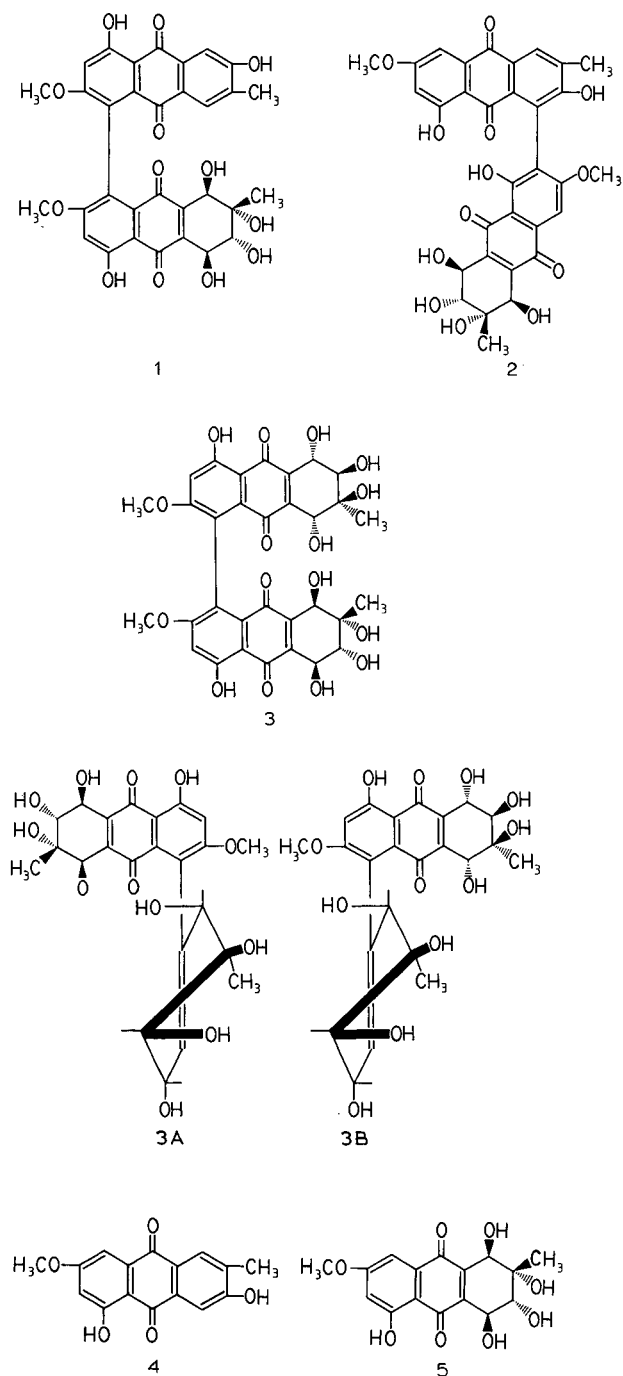


Fig. 1. Structure of pigments **1** = Alterporriol A and B; **2** = alterporriol C; **3** = alterporriol D and E; **3A** = spatial structure of alterporriol D (*R*-form); **3B** = spatial structure of alterporriol E (*S*-form); **4** = macrosporin; **5** = altersolanol A.

EXPERIMENTAL

Material

As-A, Ap-D and -E were isolated as metabolic pigments of *Alternaria porri* (IFO 9762), which was isolated and donated by the Institute for Fermentation, Osaka, Japan (IFO).

High-performance liquid chromatography

HPLC was performed on a Shimadzu LC-6A liquid chromatograph equipped with a UV detector operating at 254 nm for all assays. The solvent system used was 0.05 M ammonium dihydrogenphosphate (adjusted to pH 2.5 with phosphoric acid-acetonitrile (41:9). The column used was a YMC A-312 (Yamamura Chemical Labs.), commercially packed with reversed-phase octadecylsilica (5 μ m) (150 mm x 6.0 mm I.D.); the mobile phase flow-rate was 1.0 ml/min. Samples of 10 μ l were injected onto the column.

Fermentation and extraction of pigments

A 2% (w/v) sucrose solution of onion decoction was used as a culture medium. A number of 500-ml erlenmyer flasks containing 200 ml of the medium were sterilized in a autoclave for 20 min at 2.3 bar and 120°C. The fungi, cultured on agar for 7–10 days, were inoculated into the flasks, which were then kept at 25°C. After fermentation for 2 days, 10 ml of the culture liquid were taken and extracted with *n*-hexane (4 \times 10 ml) to remove lipids. The aqueous layer obtained was called S-2. By a similar procedure, the filtrates corresponding to fermentation periods of 5, 7, 14, 21 and 28 days were designated S-3, S-4, S-5, S-6 and S-7, respectively, plus S-1 for the blank.

RESULTS AND DISCUSSION

Determination of As-A, Ap-D and Ap-E during the fermentation period

The data obtained as mean values of nine experiments and those of one representative experiment are given in Tables I and II. The chromatograms of pigments

TABLE I

VARIATION OF PIGMENTS AT DIFFERENT STAGES OF FERMENTATION

Mean values of nine experimental results are shown. *A* = peak-area ratio to I.S.; *B* = weight ratio to I.S.; *C* = concentration (mg/ml), *S* = standard deviation (mg/ml).

Sample	<i>Altersolanol A</i>				<i>Alterporriol D</i>				<i>Alterporriol E</i>			
	<i>A</i>	<i>B</i>	<i>C</i>	<i>S</i>	<i>A</i>	<i>B</i>	<i>C</i>	<i>S</i>	<i>A</i>	<i>B</i>	<i>C</i>	<i>S</i>
S-1	—	—	—	—	—	—	—	—	—	—	—	—
S-2	0.783	0.610	0.061	0.013	0.274	0.013	0.001	0.0006	0.284	0.023	0.002	0.0015
S-3	5.469	4.354	0.435	0.14	0.917	0.132	0.013	0.0078	1.619	0.278	0.028	0.021
S-4	6.609	5.265	0.527	0.18	2.777	0.476	0.048	0.022	2.970	0.536	0.054	0.018
S-5	4.107	3.266	0.327	0.12	2.955	0.509	0.051	0.012	3.289	0.597	0.060	0.025
S-6	0.685	0.532	0.053	0.036	2.685	0.459	0.046	0.020	2.676	0.480	0.048	0.022
S-7	0.640	0.496	0.050	0.025	2.004	0.333	0.033	0.013	2.273	0.403	0.040	0.017

TABLE II.

VARIATION OF PIGMENTS OBSERVED IN ONE REPRESENTATIVE EXPERIMENT AT DIFFERENT STAGES OF FERMENTATION

Symbols as in Table I.

Sample	<i>Altersolanol A</i>				<i>Alterporriol D</i>				<i>Alterporriol E</i>			
	A	B	C	S	A	B	C	S	A	B	C	S
S-1	—	—	—	—	—	—	—	—	—	—	—	—
S-2	1.25	0.983	0.098	$1.1 \cdot 10^{-3}$	0.074	0.010	0.001	$1.7 \cdot 10^{-5}$	0.076	0.012	0.001	$3.1 \cdot 10^{-5}$
S-3	5.68	4.52	0.452	$5.9 \cdot 10^{-3}$	1.01	0.149	0.015	$1.8 \cdot 10^{-4}$	0.877	0.136	0.014	$2.8 \cdot 10^{-4}$
S-4	7.32	5.83	0.583	$1.7 \cdot 10^{-2}$	3.26	0.565	0.057	$1.1 \cdot 10^{-3}$	2.43	0.433	0.043	$5.3 \cdot 10^{-4}$
S-5	2.49	1.97	0.197	$2.9 \cdot 10^{-3}$	3.41	0.593	0.059	$1.1 \cdot 10^{-3}$	2.64	0.473	0.047	$1.0 \cdot 10^{-3}$
S-6	0.874	0.683	0.068	$2.1 \cdot 10^{-3}$	2.90	0.499	0.050	$5.6 \cdot 10^{-4}$	2.37	0.421	0.042	$1.4 \cdot 10^{-3}$
S-7	0.911	0.712	0.071	$2.4 \cdot 10^{-3}$	2.13	0.356	0.036	$7.5 \cdot 10^{-4}$	1.72	0.297	0.030	$3.1 \cdot 10^{-4}$

and the internal standard (I.S.) are shown in Fig. 2, in which the retention times (t_R) were 6.0 min (Ap-D, capacity factor, $k' = 1.71$), 7.8 min (As-A, $k' = 2.23$) and 9.6 min (Ap-E, $k' = 2.74$). We used the internal standard method for quantitation and benzoic acid ($t_R = 14$ min, $k' = 4.00$) was used as the internal standard for As-A, Ap-D and Ap-E. For example, methanolic solutions of As-A (1 mg/ml) (0.4, 0.6, 0.8, 1.0 and 1.2 ml) were placed in sample vials and 1-ml portions of methanolic solutions of benzoic acid (1 mg/ml) were added. After the volumes had been adjusted to 10 ml with methanol, 10- μ l portions of each were subjected to HPLC under the conditions mentioned above. By plotting the peak-area ratio against sample weight a calibration graph for As-A was obtained. The calibration graphs for Ap-D and Ap-E were

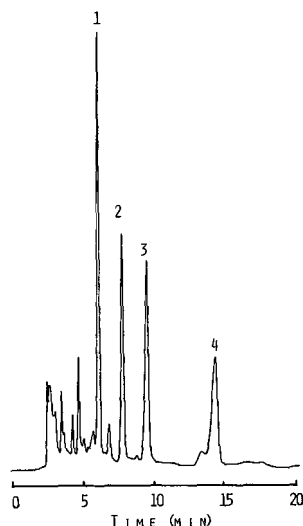


Fig. 2. Chromatograms of pigments and I.S. Peaks: 1 = alterporriol D (26.3%); 2 = altersolanol A (22.9%); 3 = alterporriol E (22.1%); 4 = benzoic acid (13.6%).

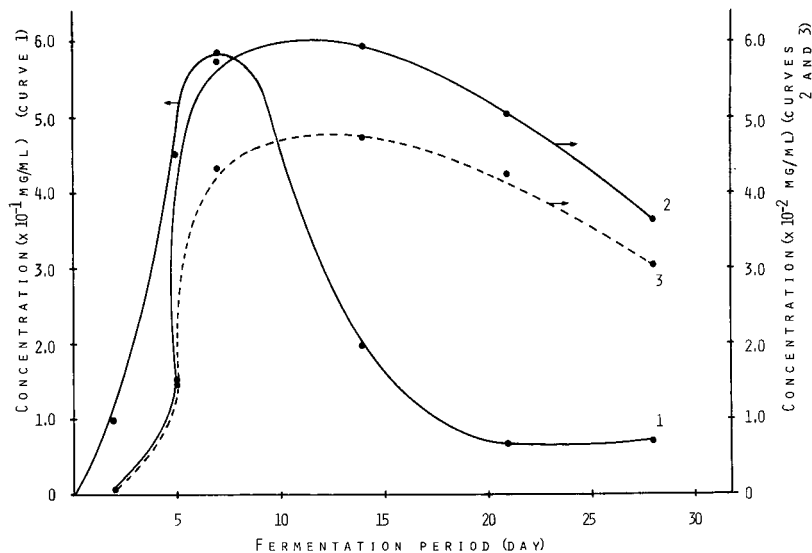


Fig. 3. Relationship between concentration of pigments and fermentation periods: 1 = altersolanol A; 2 = alterporriol D; 3 = alterporriol E.

obtained by using the same concentrations as that of As-A⁹. The limits of detection, based on a signal-to-noise ratio of 10 for As-A, Ap-D and Ap-E, were 0.1 $\mu\text{g/ml}$.

The concentrations of As-A, Ap-D and Ap-E were calculated from the detector responses (peak areas) by using the method of least squares:

$$\text{As-A: } y = (0.799x - 1.57 \cdot 10^{-2}) \cdot 0.1$$

$$\text{Ap-D: } y = (0.185x - 3.77 \cdot 10^{-2}) \cdot 0.1$$

$$\text{Ap-E: } y = (0.191x - 3.12 \cdot 10^{-2}) \cdot 0.1$$

where y is the concentration of the pigment (mg/ml) and x is the ratio of the peak area of the pigment to that of the internal standard (I.S.).

As a practical procedure, benzoic acid (1 mg) was dissolved in each of culture liquids S-1 to S-7 and then 10 μl of each were subjected to HPLC under the conditions given above.

The combined results obtained from nine fermentation experiments indicated that As-A was detected after fermentation for 2 days, Ap-D and Ap-E were not or only slightly detected at this time and the content of As-A was found to increase continuously for 7 days and then gradually to decrease, whereas those of Ap-D and Ap-E were found to increase continuously for up to 14 days and then gradually to decrease, as shown in Fig. 3. It is of interest that the amounts of Ap-D and Ap-E are similar throughout the fermentation period, as shown in Tables I and II.

We conclude that As-A is first formed in the early period of fermentation, and then two moieties of As-A are bonded to Ap-D and Ap-E when fungus is cultured on onion decoction medium.

REFERENCES

- 1 R. Suemitsu, T. Yamamoto, T. Miyai and T. Ueshima, *Phytochemistry*, 26 (1987) 3221.
- 2 R. Suemitsu, T. Sano, M. Yamamoto, Y. Arimoto, F. Morimatsu and T. Nabeshima, *Agric. Biol. Chem.*, 48 (1984) 2611.
- 3 R. Suemitsu, T. Yamamoto, T. Ueshima and S. Yanagawase, *Phytochemistry*, 27 (1988) 3251.
- 4 R. Suemitsu, Y. Sakurai, K. Nakachi, I. Miyoshi, M. Kubota and K. Ohnishi, *Agric. Biol. Chem.*, 53 (1989) 1301.
- 5 R. Suemitsu, M. Nakajima and M. Hiura, *Agric. Biol. Chem.*, 25 (1961) 100.
- 6 A. Stoessl, *Can. J. Chem.*, 47 (1969) 767.
- 7 R. Suemitsu and A. Nakamura, *Agric. Biol. Chem.*, 45 (1981) 2363.
- 8 G. Lazarovits, R. Steele and A. Stoessl, *Z. Naturforsch., C*, 43 (1988) 813.
- 9 R. Suemitsu, K. Horiuchi, K. Ohnishi and S. Yanagawase, *J. Chromatogr.*, 454 (1988) 406.

Note

Analysis of peramine in fungal endophyte-infected grasses by reversed-phase thin-layer chromatography

F.F. FANNIN, L.P. BUSH* and M.R. SIEGEL

University of Kentucky, Department of Agronomy and Plant Pathology, Lexington, KY 40546 (U.S.A.)
and

D.D. ROWAN

Biotechnology Division, Department of Scientific and Industrial Research, Private Bag, Palmerston North
(New Zealand)

(First received August 14th, 1989; revised manuscript received November 28th, 1989)

The presence of the fungal endophyte *Acremonium lolii* in perennial ryegrass (*Lolium perenne*) has been linked to resistance of infected plants to attack by the Argentine stem weevil (*Listronotus bonariensis*). Production in the infected plants of the alkaloid peramine, a feeding deterrent to adult weevils, is thought to be largely responsible for the resistance¹.

Isolation and identification of peramine was first reported by Rowan and co-workers^{1,2}, but the method used was too time-consuming and difficult for use in routine analysis. Tapper *et al.*³ recently reported an improved method for extraction, identification and measurement of peramine. Their procedure involved a two-stage extraction using methanol–chloroform (1:1, v/v); then hexane–water (1:1, v/v) followed by cleanup of the extract on small ion-exchange columns. Peramine was detected on silica gel layers using Ehrlich's reagent or quantified by a high-performance liquid chromatography (HPLC) procedure.

We report here the development of a rapid and sensitive reversed-phase (RP) thin-layer chromatography (TLC) procedure for detection and quantitation of peramine in crude extracts of endophyte-infected grasses.

EXPERIMENTAL

Peramine calibration curve

A solution of peramine bromide (derived from endophyte-infected *L. perenne*) containing 8.5 ng peramine per microliter of 80% aqueous ethanol was used in preparing a calibration curve. Portions of this solution were applied (in duplicate) with a microliter syringe to a Whatman LKC18F reversed-phase plate (10 cm × 16 cm; American Scientific) 2.5 cm from the long edge "A" of the plate. Development of the chromatogram was carried out in two stages. First the plate was immersed with edge A up in 60% aqueous methanol containing 0.1% phosphoric acid adjusted to pH 7.3

with potassium hydroxide (solvent A) to a depth such that the origin was about 1 cm above the solvent surface. When the solvent reached edge A of the plate the plate was removed and allowed to partially dry. The entire plate was covered with aluminum foil with the exception of two corner areas where the first and last samples of peramine standard had been applied. The exposed areas were sprayed with Van Urk's reagent (1 g *para*-dimethylaminobenzaldehyde in 50 ml concentrated hydrochloric acid plus 50 ml 95% ethanol) and after the color had developed, the foil was removed and a strip of adsorbent approximately 12 mm wide from edge A (approximately 3 mm from edge of spots) was removed. Two strips of adsorbent were also removed at right angles to edge A (first and last lanes which contained the stained peramine spots). The plate was allowed to thoroughly dry and was then developed in 50% methanol containing 0.5 M sodium chloride (solvent B) with edge A down until the solvent front had moved approximately 70 to 75 mm. The plate was allowed to partially dry and then sprayed with Van Urk's reagent. After thorough drying, the plate was scanned (could be stored in the freezer overnight) with a Shimadzu High-Speed Thin Layer Chromato Scanner Model CS-920 at 600 nm (reflectance mode). The R_F of peramine was approximately 0.6.

The external standard used in assays of extracts of grasses was purified from endophyte-infected ryegrass according to the methods of Rowan and Gaynor¹.

Extraction

Endophyte-infected grass leaf tissue, either dried at 60°C or freeze-dried, was ground in a Wiley mill to pass through a 40-mesh screen. To each of 3 tubes, 50 mg of dried ground leaves from endophyte-infected perennial ryegrass were added. Aliquots of 2.5 ml aqueous ethanol (80, 90 or 95% ethanol) were added and the tubes were capped and shaken at room temperature for 30 min. The solids were allowed to settle and 2 ml of extract were removed from each tube. To each tube containing the solids were added 2.5 ml 80% ethanol and the tubes were stored at -20°C overnight. The tubes were allowed to warm to room temperature with shaking and the solids were again allowed to settle and supernatant liquid removed. Portions of 0.5 ml of the first and second supernatants from each sample were dried with a stream of nitrogen and the residue was redissolved in 50 μ l of 80% ethanol.

"Two-directional" reversed-phase TLC for extracts

Portions of 10 μ l of each sample, two peramine standard samples (72 ng/spot), plus peramine in the outside lanes to determine distance for adsorbent removal after development in the first direction, were applied 2.5 cm from edge A of the RP-TLC plate and allowed to dry. Development of the chromatogram was then carried out in two stages as described for the peramine calibration curve. The purpose of the first stage was to remove materials which interfered with peramine measurement. The peramine concentration in samples was quantified by single point calibration using the peramine standards applied to the same plate.

RESULTS AND DISCUSSION

Calibration curve

The area of the stained peramine spots was not a linear function of the amount

of peramine applied to the TLC plate. However, a linear standard curve was obtained if the "linearizer" function of the scanner (position 1) was used. Absorbance measurements on thin-layer materials tend to deviate from the Beer-Lambert Law due to scattering by the adsorbent on the plate. The apparent non-linear relationship between absorbance and concentration is linearized by a microcomputer program in the Model CS-920 scanner⁴. The computer-corrected integration of absorbance (area) shows a linear dependence on weight of peramine in the range of 8.5 ng to 68 ng/spot with a regression equation of $y = 14x$ ($R^2 = 0.9946$; $P = 0.0000$). The detection limit for peramine with the TLC scanner was about 5 ng/spot though smaller quantities could be detected visually.

Extraction of peramine

In the original publication on the isolation of peramine from endophyte-infected perennial ryegrass, Rowan and Gaynor¹ used 95% ethanol for extraction. Some preliminary results of our work (data not shown) suggested that 95% ethanol did not completely extract peramine from freeze-dried ryegrass. Nearly complete peramine extraction (>90%) was possible with either 80% or 90% ethanol, but not with 95% ethanol. For example, when 2.5 ml of 80, 90 or 95% ethanol were used to extract 50 mg samples of infected ryegrass, the recovered alcoholic solvent (2 ml) contained 1201 ng, 1288 ng and 690 ng, respectively. Following a second extraction of each sample residue with 2.5 ml of 80% ethanol, the solvent contained 682 ng peramine when the first extractant was 95% ethanol but only 183 ng and 312 ng if the first extractant was 80% and 90% ethanol, respectively. These results indicate that the first extraction with either 80% or 90% ethanol released essentially all of the peramine in the sample. The second extraction recovered most of the peramine remaining in the void volume of the pelleted material. Using 95% ethanol as the extractant, only about 60% of the peramine was removed with the first solvent extraction. Our routine assay now involves shaking a 150 mg sample with 1.2 ml 80% ethanol for 1 h.

Peramine levels of 8 ppm or greater in tissue of fungal endophyte-infected grass could be measured in crude extracts. If the crude extracts were concentrated 5-fold, 1 ppm peramine on a dry-weight basis could be determined. Isolated peramine was confirmed by NMR and mass spectroscopy by procedures used by Rowan and Gaynor¹.

The use of the first chromatography step in the two-stage TLC procedure is a convenient alternative to preliminary cleanup of the crude extracts prior to TLC. It is especially important for eliminating materials that interfere with resolution and measurement in extracts containing small amounts of peramine. If the first step is not used, the peramine spot tends to become distorted and excessive streaking occurs (especially with highly concentrated extracts) which tends to obscure the peramine after treatment with Van Urk's reagent.

Recovery of peramine standard added to uninfected ryegrass

Purified peramine in 80% ethanol was added to a powdered sample of uninfected ryegrass to give a peramine concentration of 20 $\mu\text{g/g}$. The mixture was dried, extracted for 1 h at room temperature with 80% ethanol, and then analyzed by our RP-TLC method. Extraction of peramine was essentially complete as recovery values of 94% and 104% were found for two TLC assays on the same extract.

TABLE I
COMPARISON OF PERAMINE LEVELS DETECTED BY RP-HPLC AND RP-TLC METHODS

Grass species and cultivar	Endophyte	Peramine (ppm) ^a	
		RP-HPLC	RP-TLC
<i>Lolium perenne</i> Gator	<i>Epichloe typhina</i> ^d	<0.6	n.d. ^b
<i>L. perenne</i> Gator	<i>E. typhina</i> ^e	10	16.2
<i>L. perenne</i> Repel	<i>Acremonium lolii</i>	29.9	39.8 ± 2.2(3) ^c
<i>Festuca longifolia</i>	<i>E. typhina</i>	15.0	20.3 ± 1.7(12) ^c

^a RP-HPLC analyses carried out at DSIR in New Zealand and RP-TLC analyses carried out at the University of Kentucky.

^b Not detected.

^c Mean ± standard error; number in parentheses indicates number of replicate determinations.

^{d,e} *E. typhina* from *Festuca rubra commutata* (d), and from *F. longifolia* (e), respectively, were artificially transferred into *Lolium* seedlings by the method of Latch and Christensen⁶.

In another test, a powdered sample of infected ryegrass containing 20 µg/g peramine was mixed with powdered non-infected material in a ratio of one part infected ryegrass to nine parts non-infected grass. A value of 2.0 ppm in the mixture was determined by our extraction and RP-TLC quantitation procedure.

Analysis of peramine from endophyte-infected grasses

Analysis of samples that were freeze-dried, ground and then split for analysis by both the RP-HPLC method of Tapper *et al.*³ and by our RP-TLC method indicated that the two methods were of similar sensitivity but amounts determined with the RP-HPLC method were about 25–30% lower than those for the RP-TLC method (Table I). The reason for these differences is unknown.

The distribution of peramine between roots, stems and blades of some endophyte-infected grasses were checked by the RP-TLC method (Table II). While the

TABLE II
PERAMINE DISTRIBUTION IN ENDOPHYTE-INFECTED TALL FESCUE AND PERENNIAL RYEGRASS

Grass (species)	Plant part	Peramine (ppm), mean ± standard error (n)
<i>F. arundinacea</i> ^a	Root	n.d. ^c
	Stem	3.4 ± 0.4(3)
	Blade	3.1 ± 0.4(3)
<i>L. perenne</i> ^b	Root	3.7(1)
	Stem	10.2 ± 1.3(3)
	Blade	28.4 ± 2.3(3)

^a G1-320 tall fescue artificially infected with *Acremonium coenophialum*.

^b NK 79307 perennial ryegrass (Northrup King) naturally infected with *A. lolii*.

^c Not detected.

different pattern of peramine distribution between the two endophyte–host combinations may reflect the differences in endophyte distribution within the two different hosts, it also suggests a relatively greater translocation of peramine to the leaf blade in *L. perenne* compared to *F. arundinacea*. The endophyte is not found in roots and lesser amounts of endophyte are found in leaf blade than in stem of both hosts⁵.

Using the RP-TLC method, we determined the level of peramine from a number of different endophyte–host combinations. As indicated in Tables I and II, peramine is produced not only in *A. lolii*-infected perennial ryegrass¹, but also in *E. thypina*-infected perennial ryegrass (Table I) and in *A. coenophialum*-infected tall fescue (Table II). The *E. typhina* in infected perennial ryegrass originated from two different species of *Festuca* and were artificially inoculated into *L. perenne* cv. Gator. Rowan *et al.*² have shown that peramine is of fungal origin, and as expected, the *E. typhina* from *F. longifolia* produced similar levels in its own host (*F. longifolia*) and in *L. perenne* cv. Gator. On the other hand, the *E. typhina* isolate from *F. rubra*, when transferred to Gator, did not produce appreciable amounts of peramine.

ACKNOWLEDGEMENT

This paper (No. 89-3-11-167) is published with approval of the Director of the Kentucky Agricultural Experiment Station and was supported in part by U.S. Department of Agriculture Grant No. 88-37151-3860.

REFERENCES

- 1 D. D. Rowan and D. L. Gaynor, *J. Chem. Ecol.*, 12 (1986) 115.
- 2 D. D. Rowan, M.B. Hunt and D.L. Gaynor, *J. Chem. Soc. Chem. Commun.*, 12 (1986) 935.
- 3 B.A. Tapper, D.D. Rowan and G.C.M. Latch, *J. Chromatogr.*, 463 (1989) 133.
- 4 H. Yamamoto, T. Kurita, J. Suzuki, R. Hira, K. Nakano, H. Makabe and K. Shibata, *J. Chromatogr.*, 116 (1976) 29.
- 5 C.W. Bacon and M.R. Siegel, *J. Prod. Agric.*, 1 (1988) 45.
- 6 G.C.M. Latch and M.J. Christensen, *Ann. Appl. Biol.*, 107 (1985) 17.

PUBLICATION SCHEDULE FOR 1990

Journal of Chromatography and Journal of Chromatography, Biomedical Applications

MONTH	J	F	M	A	M	
Journal of Chromatography	498/1 498/2 499	500 502/1	502/2 503/1 503/2 504/1	504/2 505/1	505/2 506 507	The publication schedule for further issues will be published later
Cumulative Indexes, Vols. 451-500		501				
Bibliography Section		524/1		524/2		
Biomedical Applications	525/1	525/2	526/1	526/2 527/1	527/2	

INFORMATION FOR AUTHORS

(Detailed *Instructions to Authors* were published in Vol. 478, pp. 453-456. A free reprint can be obtained by application to the publisher, Elsevier Science Publishers B.V., P.O. Box 330, 1000 AH Amsterdam, The Netherlands.)

Types of Contributions. The following types of papers are published in the *Journal of Chromatography* and the section on *Biomedical Applications*: Regular research papers (Full-length papers), Notes, Review articles and Letters to the Editor. Notes are usually descriptions of short investigations and reflect the same quality of research as Full-length papers, but should preferably not exceed six printed pages. Letters to the Editor can comment on (parts of) previously published articles, or they can report minor technical improvements of previously published procedures; they should preferably not exceed two printed pages. For review articles, see inside front cover under Submission of Papers.

Submission. Every paper must be accompanied by a letter from the senior author, stating that he is submitting the paper for publication in the *Journal of Chromatography*. Please do not send a letter signed by the director of the institute or the professor unless he is one of the authors.

Manuscripts. Manuscripts should be typed in double spacing on consecutively numbered pages of uniform size. The manuscript should be preceded by a sheet of manuscript paper carrying the title of the paper and the name and full postal address of the person to whom the proofs are to be sent. Authors of papers in French or German are requested to supply an English translation of the title of the paper. As a rule, papers should be divided into sections, headed by a caption (*e.g.*, Summary, Introduction, Experimental, Results, Discussion, etc.). All illustrations, photographs, tables, etc., should be on separate sheets.

Introduction. Every paper must have a concise introduction mentioning what has been done before on the topic described, and stating clearly what is new in the paper now submitted.

Summary. Full-length papers and Review articles should have a summary of 50-100 words which clearly and briefly indicates what is new, different and significant. In the case of French or German articles an additional summary in English, headed by an English translation of the title, should also be provided. (Notes and Letters to the Editor are published without a summary.)

Illustrations. The figures should be submitted in a form suitable for reproduction, drawn in Indian ink on drawing or tracing paper. Each illustration should have a legend, all the legends being typed (with double spacing) together on a *separate sheet*. If structures are given in the text, the original drawings should be supplied. Coloured illustrations are reproduced at the author's expense, the cost being determined by the number of pages and by the number of colours needed. The written permission of the author and publisher must be obtained for the use of any figure already published. Its source must be indicated in the legend.

References. References should be numbered in the order in which they are cited in the text, and listed in numerical sequence on a separate sheet at the end of the article. Please check a recent issue for the layout of the reference list. Abbreviations for the titles of journals should follow the system used by *Chemical Abstracts*. Articles not yet published should be given as "in press" (journal should be specified), "submitted for publication" (journal should be specified), "in preparation" or "personal communication".

Dispatch. Before sending the manuscript to the Editor please check that the envelope contains three copies of the paper complete with references, legends and figures. One of the sets of figures must be the originals suitable for direct reproduction. Please also ensure that permission to publish has been obtained from your institute.

Proofs. One set of proofs will be sent to the author to be carefully checked for printer's errors. Corrections must be restricted to instances in which the proof is at variance with the manuscript. "Extra corrections" will be inserted at the author's expense.

Reprints. Fifty reprints of Full-length papers, Notes and Letters to the Editor will be supplied free of charge. Additional reprints can be ordered by the authors. An order form containing price quotations will be sent to the authors together with the proofs of their article.

Advertisements. Advertisement rates are available from the publisher on request. The Editors of the journal accept no responsibility for the contents of the advertisements.

The ideal combination:

BOOK, SOFTWARE and DATABASE

BASIC GAS CHROMATOGRAPHY- MASS SPECTROMETRY: Principles and Techniques

*F.W. Karasek and R.E. Clement,
Waterloo, Ont., Canada*

The book opens with the principles of both GC and MS necessary to understand and deal with the data generated in GC/MS analyses.

The focus then turns to the particular requirements created by a direct combination of these two techniques into a single instrumentation system. The data generated and their use are covered in detail. The role of the computer and its specific software, especially in compound identification via mass spectral search techniques, receives special attention.

Representative applications and results obtained with GC/MS-computer techniques are presented, permitting extrapolation of specific applications to similar problems encountered by the reader. Instructional, informative and application-oriented, the material will be useful to a wide range of people.

Designed to be used independently, the book is admirably complemented when used in conjunction with the software.

1988 viii + 202 pages
US\$ 79.00 / Dfl. 150.00
ISBN 0-444-42760-0

GAS CHROMATOGRAPHY- MASS SPECTROMETRY: A Knowledge Base

*F.A. Settle, Jr. and M.A. Pleva,
Lexington, VA, USA*

This electronic module, though an independent source of current information on GC/MS, can also be used as a helpful supplement to the book.

The module consists of a knowledge base and a retrieval program allowing the information to be presented in a user-friendly format. A number of special purpose files are included: an index, a glossary, and a list of keywords. The module is available for the IBM-PC and its compatibles as a set of three 5¹/₄" diskettes, requiring 128K RAM memory and two disk drives.

It is useful as an introduction to the operation of instrument components, data systems and the interpretation of resulting data. It aids workers requiring GC/MS analysis in the fields of medicine, pharmacy, environmental and forensic science and helps to acquaint potential purchasers with the different types of equipment available, along with a guide to manufacturers and prices.

3 Diskettes + manual:
US\$ 144.75 / Dfl. 275.00
ISBN 0-444-42761-9

A brochure giving full details is available from...

ELSEVIER SCIENCE PUBLISHERS

P.O. Box 211, 1000 AE Amsterdam, The Netherlands

P.O. Box 882, Madison Square Station, New York, NY 10159, USA

